CHEMICAL REVIEWS

Review

pubs.acs.org/CR

Wood-Derived Materials for Green Electronics, Biological Devices, and Energy Applications

Hongli Zhu,*[,†,‡,§] Wei Luo,[†,§] Peter N. Ciesielski,[∥] Zhiqiang Fang,[†] J. Y. Zhu,[⊥] Gunnar Henriksson,[#] Michael E. Himmel,[∥] and Liangbing Hu*[,†]

[†]Department of Materials Science and Engineering, University of Maryland, College Park, Maryland 20742, United States

[‡]Department of Mechanical and Industrial Engineering, Northeastern University, Boston, Massachusetts 02115, United States

[∥]Biosciences Center, National Renewable Energy Laboratory, 15013 Denver West Parkway, Golden, Colorado 80401, United States

[⊥]Forest Products Laboratory, USDA Forest Service, Madison, Wisconsin 53726, United States

[#]Division of Wood Chemistry and Pulp Technology, Department of Fiber and Polymer Technology, Royal Institute of Technology, KTH, Stockholm, Sweden

ABSTRACT: With the arising of global climate change and resource shortage, in recent years, increased attention has been paid to environmentally friendly materials. Trees are sustainable and renewable materials, which give us shelter and oxygen and remove carbon dioxide from the atmosphere. Trees are a primary resource that human society depends upon every day, for example, homes, heating, furniture, and aircraft. Wood from trees gives us paper, cardboard, and medical supplies, thus impacting our homes, school, work, and play. All of the above-mentioned applications have been well developed over the past thousands of years. However, trees and wood have much more to offer us as advanced materials, impacting emerging high-tech fields, such as bioengineering, flexible electronics, and clean energy. Wood naturally has a hierarchical structure, composed of well-oriented microfibers and tracheids for water, ion, and oxygen transportation during metabolism. At higher magnification, the walls of fiber cells have an interesting morphology—a distinctly mesoporous structure. Moreover, the walls of fiber cells are composed of thousands of fibers (or macrofibrils) oriented in a similar angle. Nanofibrils and nanocrystals can be further liberated from macrofibrils by mechanical, chemical, and enzymatic methods. The obtained nanocellulose has unique optical, mechanical, and barrier properties and is an excellent candidate for chemical modification and reconfiguration. Wood is naturally a composite material, comprised of cellulose, hemicellulose, and lignin. Wood is sustainable, earth abundant, strong, biodegradable, biocompatible, and chemically accessible for modification; more importantly, multiscale natural fibers from wood have unique optical properties applicable to different kinds of optoelectronics and photonic devices. Today, the materials derived from wood are ready to be explored for applications in new technology areas, such as electronics, biomedical devices, and energy. The goal of this study is to review the fundamental structures and chemistries of wood and wood-derived materials, which are essential for a wide range of existing and new enabling technologies. The scope of the review covers multiscale materials and assemblies of cellulose, hemicellulose, and lignin as well as other biomaterials derived from wood, in regard to their major emerging applications. Structure−properties−application relationships will be investigated in detail. Understanding the fundamental properties of these structures is crucial for designing and manufacturing products for emerging applications. Today, a more holistic understanding of the interplay between the structure, chemistry, and performance of wood and wood-derived materials is advancing historical applications of these materials. This new level of understanding also enables a myriad of new and exciting applications, which motivate this review. There are excellent reviews already on the classical topic of woody materials, and some recent reviews also cover new understanding of these materials as well as potential applications. This review will focus on the uniqueness of woody materials for three critical applications: green electronics, biological devices, and energy storage and bioenergy.

CONTENTS

Received: April 19, 2016

DOI: 10.1021/acs.chemrev.6b00225
Chem. Rev. XXXX, XXX, XXX−XXX

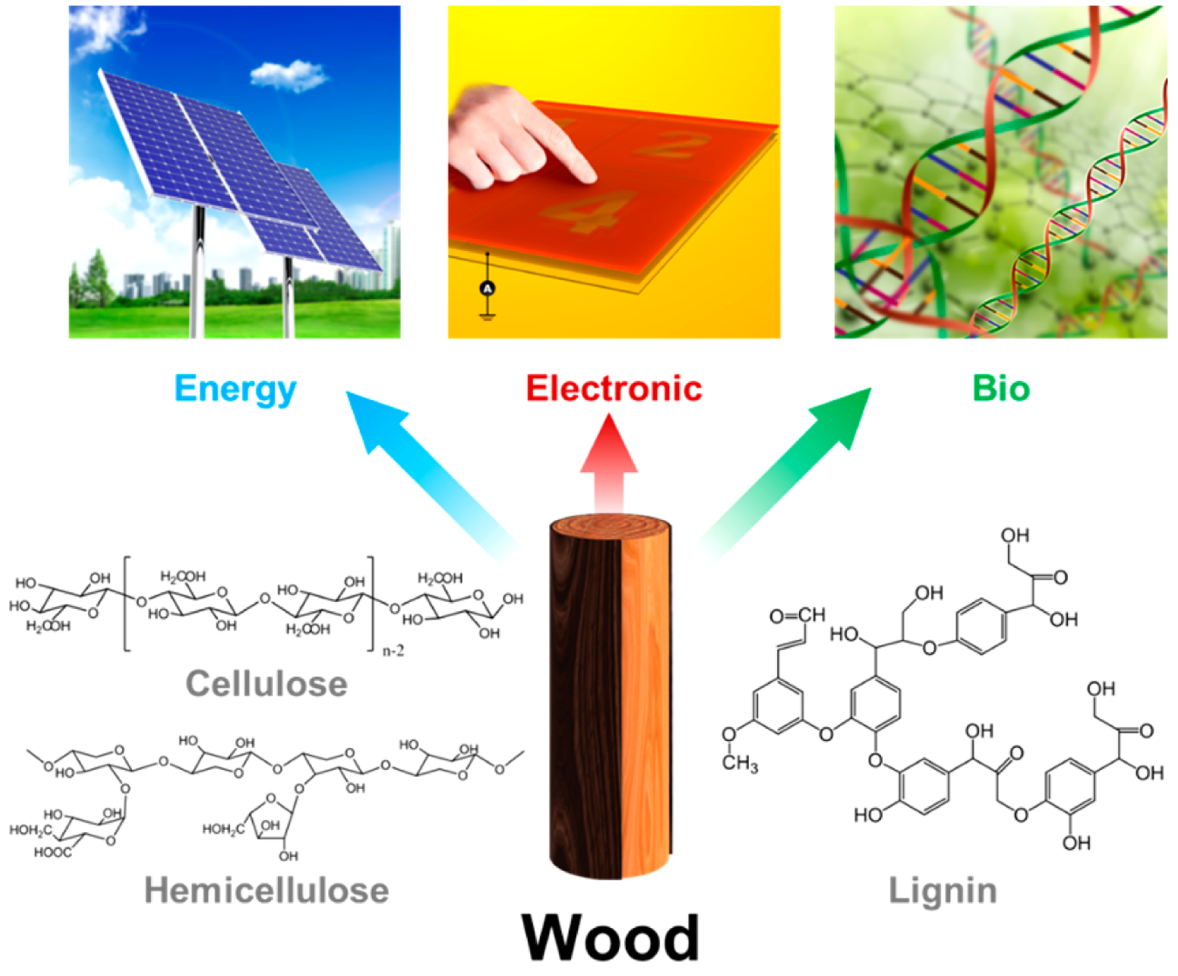

Figure 1. Schematic visually summarizes the topical focus of this review, wherein we cover the current development and outlook for renewable energy, green electronics, and biological devices using wood-derived biopolymers and nanomaterials. The chemistry, structure, materials properties, and rational functionalization of cellulose, hemicellulose, and lignin associated with these key applications will be discussed and summarized.

DOI: 10.1021/acs.chemrev.6b00225
Chem. Rev. XXXX, XXX, XXX−XXX

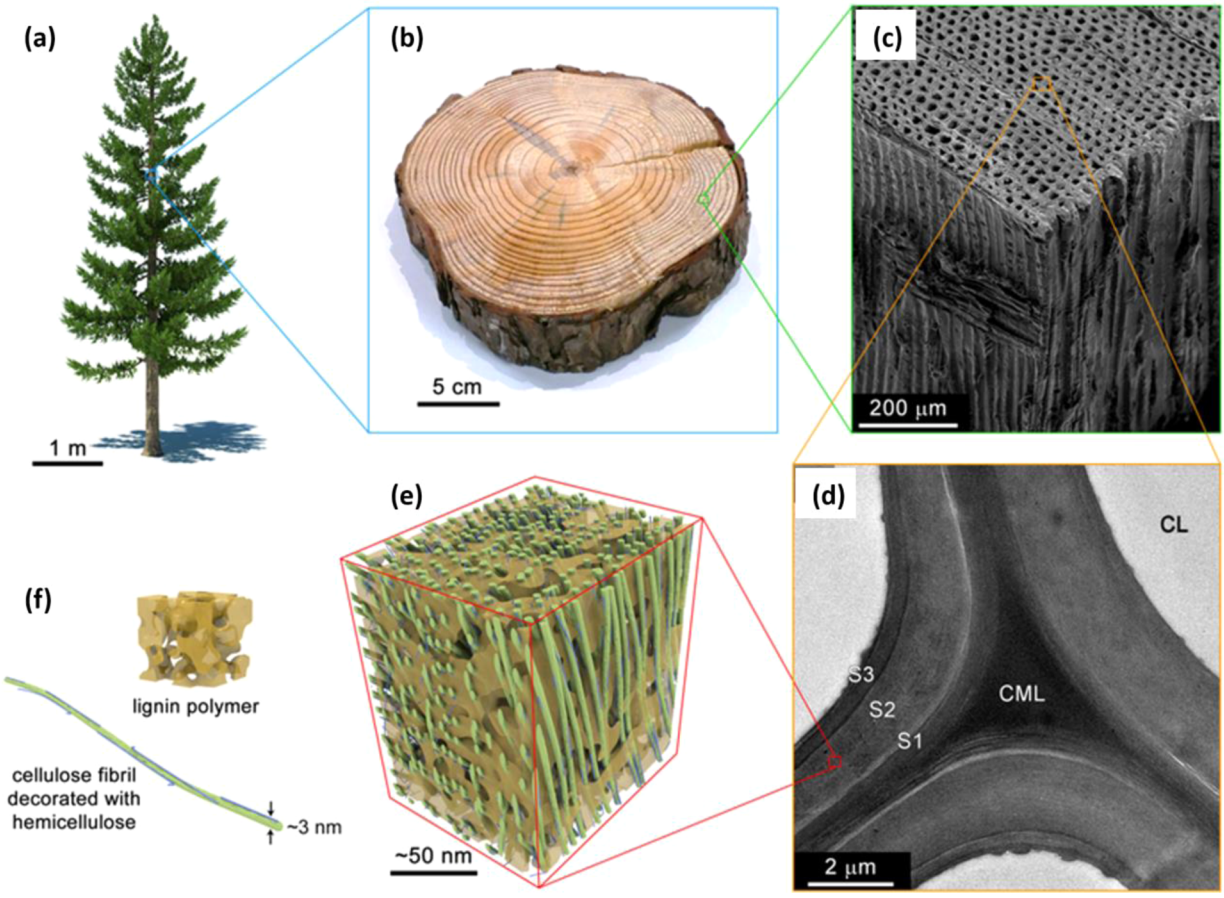

Figure 2. Hierarchal structure of wood. (a) Coniferous tree. (b) Photograph of trunk section from a pine tree. (c) SEM image of the tissue structure softwood (yellow pine). (d) TEM image showing the ultrastructure wood cell wall. CL, cell lumen; CML, compound middle lamella; S1, S2, and S3 denote layers of the secondary cell wall. (e) Schematic of the nanoscale architecture of lignocellulose. (f) Idealized depiction of an amorphous lignin polymer and a cellulose elementary fibril decorated with hemicellulose (microfibril). Images and schematics courtesy of National Renewable Energy Laboratory (NREL) Biomass Surface/Structure Characterization Lab, USA.

1. INTRODUCTION

With the arising of global climate change and resource shortage, in recent years, increased attention has been paid to environmentally friendly materials. Trees are sustainable and renewable materials, which give us shelter and oxygen and remove carbon dioxide from the atmosphere. Trees are a primary resource that human society depends upon every day, for example, homes, heating, furniture, and aircraft. Wood from trees gives us paper, cardboard, and medical supplies, thus impacting our homes, school, work, and play. All of the above-mentioned applications have been well developed over the past thousands of years. However, trees and wood have much more to offer us as advanced materials, impacting emerging high-tech fields, such as bioengineering, flexible electronics, and clean energy.

Wood naturally has a hierarchical structure, composed of well-oriented microfibers and tracheids for water, ion, and oxygen transportation during metabolism. At higher magnification, the walls of fiber cells have an interesting morphology—a distinctly mesoporous structure. Moreover, the walls of fiber cells are composed of thousands of fibers (or macrofibrils) oriented in a similar angle. Nanofibrils and nanocrystals can be further liberated from macrofibrils by mechanical, chemical, and enzymatic methods. The obtained nanocellulose has unique optical, mechanical, and barrier properties and is an excellent candidate for chemical modification and reconfiguration. Wood is naturally a composite material, comprised of cellulose, hemicellulose, and lignin. Wood is sustainable, earth-abundant, strong, biodegradable, biocompatible, and chemically accessible for modification; more importantly, multiscale natural fibers from wood have unique optical properties applicable to different kinds of optoelectronics and photonic devices. Today, the materials derived from wood are ready to be explored for applications in new technology areas, such as electronics, biomedical devices, and energy.

The goal of this study is to review the fundamental structures and chemistries of wood and wood-derived materials, which are essential for a wide range of existing and new enabling

DOI: 10.1021/acs.chemrev.6b00225
Chem. Rev. XXXX, XXX, XXX−XXX

technologies. As outlined in Figure 1, the scope of the review covers multiscale materials and assemblies of cellulose, hemicellulose, and lignin, as well as other biomaterials derived from wood, in regard to their major emerging applications. Structure−properties−application relationships will be investigated in detail. Understanding the fundamental properties of these structures is crucial for designing and manufacturing products for emerging applications. Today, a more holistic understanding of the interplay between the structure, the chemistry, and the performance of wood and wood-derived materials is advancing historical applications of these materials. This new level of understanding also enables a myriad of new and exciting applications, which motivate this review. There are excellent reviews already on the classical topic of woody materials, and some recent reviews also cover new understanding of these materials as well as potential applications.[1−5] This review will focus on the uniqueness of woody materials for three critical applications: green electronics, biological devices, and energy storage and bioenergy.

2. WOOD STRUCTURE AND CHEMISTRY

2.1. Multiscale Structure and Morphology of Wood and Wood-Derived Materials

Wood is a biopolymer composite that exhibits structural complexity spanning many orders of magnitude in length. Natural diversity further imparts substantial variability between the structures of wood for different species. The hierarchical structure of wood is visualized in Figure 2. At the macro-organism scale, interspecies differences in wood structure manifest as overall size and shape of the tree, branching patterns and frequencies, and bulk materials properties, such as density, thermal conductivity, strength, and elastic properties. The visually observable "wood grain", which results from the higher order arrangement and directionality of various cell types, also varies widely in appearance between species and contributes to the decorative value of the wood. Microscopic investigation of woody tissue reveals the highly ordered, interconnected network of pores formed by the cells during the growth of the tree. Interspecies differences in this microstructure are largely responsible for observed variations in aforementioned bulk thermal and mechanical properties. Wood cells generally resemble high-aspect ratio cylinders that run parallel to the axis of the trunk (axial tracheids and vessel cells) as well as cells that run radially from the heartwood to the bark (ray cells) to form a continuous network to transport and store water and nutrients throughout the organism. Several significant differences exist between the microstructure of hardwood and softwood species. First, the axial tracheid cells, which are commonly termed "fiber cells" or simply "fibers" in softwoods by the pulp and paper industry, range from 3 to 5 mm in length, whereas those cells in hardwoods are typically shorter and range from 0.75 to 1.5 mm in length.[6] Second, hardwoods contain vessel elements, which are an additional class of axially aligned cells with a significantly larger diameter than the axial tracheids. Both hardwood and softwood cells contain pits that connect adjacent cells. For example, axial tracheids of Loblolly Pine sample (Figure 2a and 2b) can be seen running vertically through the block in the scanning electron microscope (SEM) image shown in Figure 2c, and portions of ray cells can be seen on the left side of the block in the same image.

Unlike the microstructure of woody tissue, the ultrastructure of the cell walls in wood is largely similar between species and cell type. While the bulk density of wood can vary from ∼0.3 g/cm^3 to greater than 1 g/cm^3 at 12% moisture content[7] (likely due to differences in microstructure), the density of wood cell walls is quite similar between species, ranging from ∼1.46 to 1.56 g/cm^3.[8] Wood cell walls generally comprise three ultrastructural domains: the middle lamella, the primary wall, and the secondary wall. The middle lamella acts to adhere adjacent cells and is heavily lignified. In many cases, it is difficult to precisely delineate the primary cell wall from the middle lamella; thus, these two regions are often collectively termed the "compound middle lamella." The secondary wall contains the majority of the mass of wood and is typically composed of three distinct layers, denoted S1, S2, and S3. These various layers are indicated in the transmission electron microscopy (TEM) image of a Loblolly Pine cell wall shown in cross section in Figure 2d.

The nanostructure of wood cell walls is a robust assembly of three primary biopolymers: cellulose, which is present as semicrystalline elementary fibrils; hemicellulose, which acts to decorate and cross-link elementary fibrils and facilitate interactions between other biopolymers; and lignin, which is an amorphous polymer of phenylpropanoids that associates closely with hemicellulose. The fully hemicellulose-sheathed elementary fibrils are termed microfibrils. Microfibrils and higher order bundles thereof often termed "macrofibrils" form networks to physically support the cell wall. The molecular structure of each of these biopolymers will be described in greater detail in the following sections. A schematic depicting a cubic section of a lignocellulosic cell wall is shown in Figure 2e and 2f.

Much work has been devoted to determining the precise configuration of various biopolymers within plant cell walls. Investigations of the primary cell wall have attracted much attention from the plant biology community because of its importance to cell wall biosynthesis, and this effort has provided generally accepted models for primary wall nanostructure.[9,10] Furthermore, secondary cell walls have been the focus of the forest products industry because of their importance to engineering applications of wood.[11] Similarly, the biofuels community has also turned their attention to secondary cell walls, because the majority of the biomass by weight is found in these walls. Secondary cell walls are also more recalcitrant to biochemical conversion processes, probably due to the increased lignin content in these walls.[12] For an excellent resource regarding the structure and properties of many industrially relevant wood species, the reader is directed to the *Wood Handbook: Wood as an Engineering Material*, a publication of the USDA Forest Products Laboratory.[7] Great strides toward elucidating the nanostructure of secondary walls have been made using advanced imaging techniques. Transmission electron tomography is a powerful imaging tool that has been used to investigate the configuration of cellulose and lignin in wood samples.[13] Fernandes and co-workers used X-ray scattering to provide fundamental insights into the structure of elementary fibrils in spruce wood.[14] Recently, Ding et al. used atomic force microscopy (AFM) to visualize the arrangement of cellulose microfibrils on the surface of both primary and secondary cell walls.[15] Ciesielski and co-workers combined electron tomography, computational geometry, and atomic modeling to suggest atomistic models for cellulose microfibrils that exhibit realistic nanoscale architecture obtained from the volume reconstructions (Figure 3).[16] While many of the models for the cell wall and its biopolymer constituents found in the literature are essentially conceptual and qualitative in nature, models that incorporate quantitative structural parameters derived from imaging or other experimental measurements into a simulation environment, such

DOI: 10.1021/acs.chemrev.6b00225
Chem. Rev. XXXX, XXX, XXX−XXX

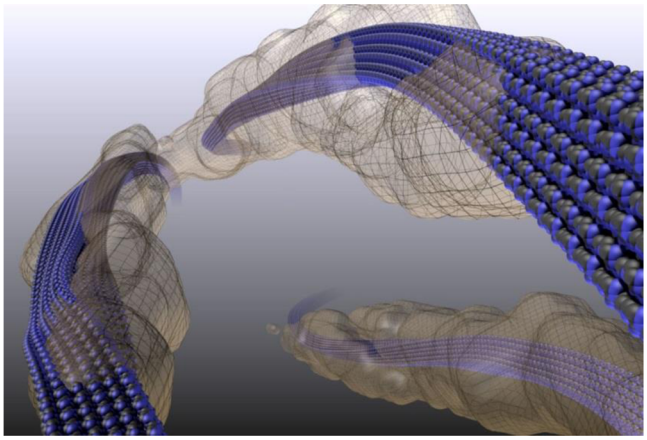

Figure 3. Atomic models of cellulose elementary fibrils exhibiting the nanostructural geometry obtained by computational analysis of transmission electron tomographic reconstructions. Blue black color indicates cellulose, and gray color indicates lignin. This model was constructed using methods adapted from Ciesielski et al.

as those shown in Figure 3, facilitate additional utility because they may be subjected to computational studies that probe the thermodynamics of the proposed biopolymer configurations. These more mathematically rigorous models will eventually elucidate quantitative relationships between structural features at multiple length scales and important process parameters, such as biofuel product yield or mechanical properties of bulk material.

The inherent mesoporosity of cell walls that arises from the assembly of their nanoscale constituents is of particular significance to energy applications of wood and other biomass. Applications such as energy storage, including capacitors and batteries, rely on the mobility of ions throughout the material,[17] whereas biofuels applications are based on liquid-phase, catalytic conversion requiring effective penetration of catalysts into the cell wall.[18] Bulk transport at the tissue scale is facilitated by the cellular network in wood (pores and pits), whereas the intracellular wall mesoporosity facilitates transport of ions and small molecules through the cell wall. This intracell wall porosity is visualized in Figure 4 by volume rendition (left) and isosurface rendition (right) of tomographic reconstruction of a native cell wall. The micro- and mesoporosity of the cell walls of various plant species have been measured by various techniques, including solvent exclusion,[19,20] cytochemical staining,[21] direct visualization by electron microscopy,[22] and mercury intrusion porosimetry.[23] The physiochemical mechanisms by which ions move through the cell wall have also come under study recently. Jakes and co-workers theorized that the onset of ionic mobility occurs when the hemicellulose undergoes a moisture-induced glass transition.[24] Subsequently, the same group has produced perhaps the best direct observation of intracell wall ionic transport to date using X-ray fluorescence spectroscopy of wood samples over a range of moisture contents.[25] These studies clearly highlight the importance of water within the cell wall to enable effective diffusion, and this should be an important consideration when designing wood- or biomass-based devices that rely on the transport of ions or small molecules.

Wood has long provided humans with many useful materials and chemicals. Historically, bulk wood has found utility as source materials for construction, papermaking, and fuels. Each of these applications of wood has experienced significant technological advances since their inception. Advances in wood treatment have improved the longevity of wood used in construction applications and allowed its utilization in more extreme environments.[11,12] Progress in biochemical and thermochemical deconstruction of wood has resulted in processes that produce sustainable, renewable liquid biofuels, which will be described later in this work. Papermaking is an ancient process; however, recent advances in processes by which wood may be selectively deconstructed to finer scales have given rise to a new class of nanomaterials derived from wood. Images of wood-derived products that range in size from millimeters to nanometers are shown in Figure 5. The majority of the processes that produce these materials begin with pulping of wood chips (Figure 5a) to remove lignin and liberate intact fiber cells (Figure 5b). At present, the most common industrial pulping processes are variations of kraft pulping, which employ alkaline thermochemical conditions to extract lignin from the wood tissue to facilitate its fiberization.[26] Wood pulp may then be subjected to additional chemical and mechanical treatments to produce cellulose microfibrils (Figure 5c).[27,28] Controlled hydrolysis of cellulosic fibers may be used to produce yet another class of cellulosic nanomaterials, termed cellulose nanocrystals (Figure 5d).[29] Note that cellulose nanofibrils and nanocrystals are terms used to describe cellulosic wall structures produced by chemical/mechanical processes. These materials are beginning to enable

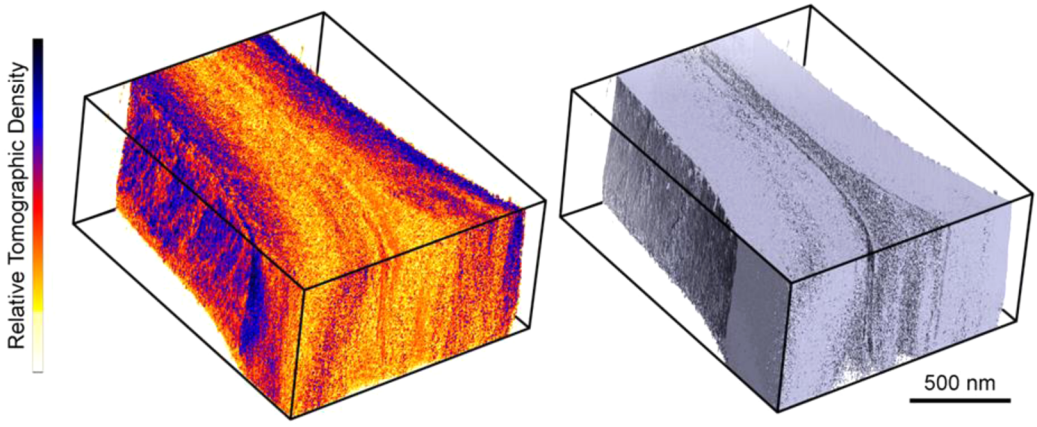

Figure 4. Tomographic reconstruction of a phloem cell wall in maize. (Left) Volumetric rendition reveals nanoscale variations in the density of the secondary wall and compound middle lamella. (Right) Isosurface rendition of the tomographic volume visualizing intracell wall mesoporosity. Tomographic data and visualization images courtesy of NREL Biomass Surface/Structure Characterization Lab.

DOI: 10.1021/acs.chemrev.6b00225
Chem. Rev. XXXX, XXX, XXX−XXX

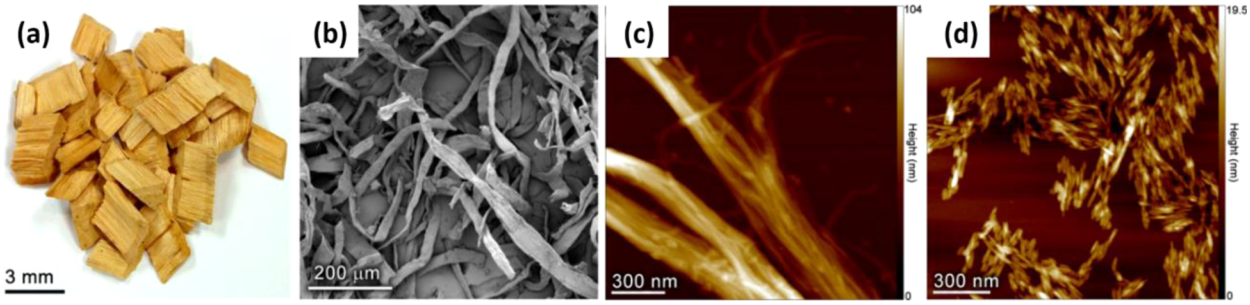

Figure 5. Wood-derived materials at multiple length scales. (a) Wood chips are the typical feedstock to downstream processes such as pulping. (b) SEM image of bleached kraft wood pulp showing individual fiber cells (c) AFM image of cellulose macro- and microfibrils. Individual microfibrils can be seen separating from larger bundles. (d) AFM image of cellulose nanocrystals produced by controlled acid hydrolysis. CNF and CNC were produced by the USDA Forest Products Lab. Images courtesy of NREL Biomass Surface/Structure Characterization Lab.

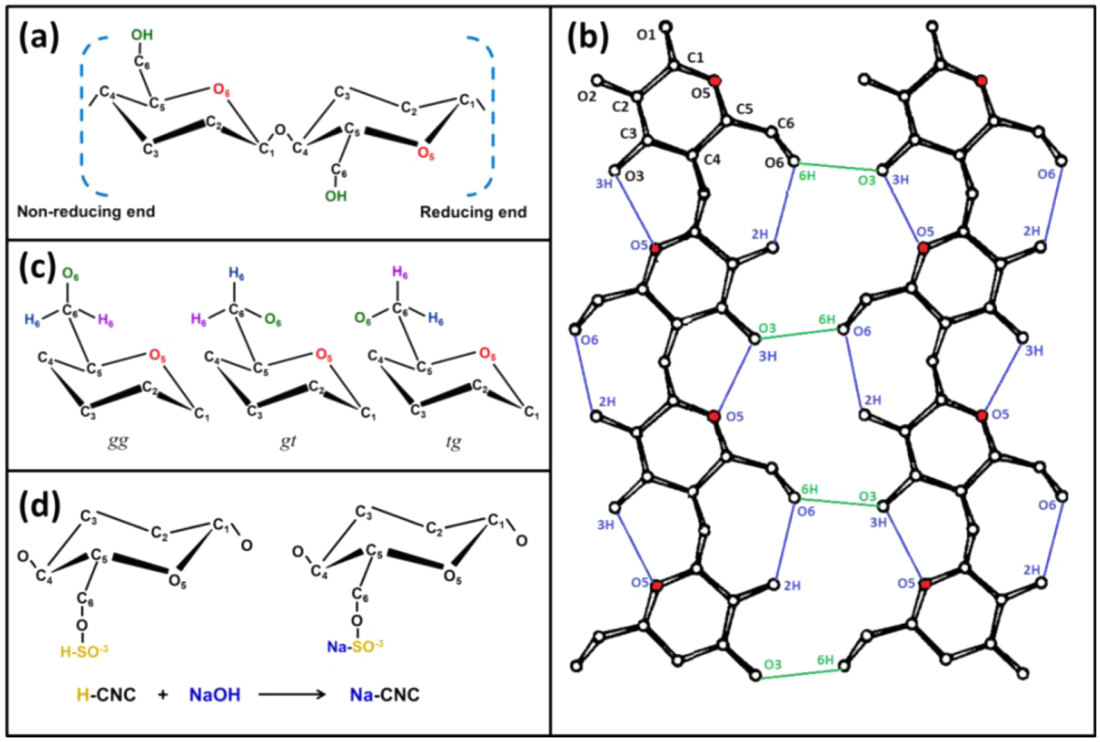

Figure 6. Schematics of cellulose molecular structure. (a) Cellobiose: basic cellulose chain unit. (b) Intra- and interchain hydrogen bonding. Reprinted with permission from ref 44. Copyright 1974 from Elsevier. (c) Local conformations of the cellulose C(6)H_2OH group. (d) Conversion of H−CNC to Na−CNC to improve thermal stability.

more concise control over the properties of cellulosic assemblies that are finding utility in many new and exciting applications described in this review.

2.2. Wood Chemistry: Molecular and Macromolecular Structure of Cell Wall Biopolymers

2.2.1. Cellulose and Nanocellulose. Cellulose is the major component in lignocellulosic plant biomass and is approximately 40−45% of wood by weight,[30,31] depending on wood species. It is the most abundant natural polymer on earth. Approximately 75−100 billion tons of cellulose can be produced annually worldwide.[32,33] Cellulose was first isolated by Anselme Payen in 1938 when he treated wood with nitric acid.[34] Cellulose consists of chains of thousands of D-glucan units connected by the β-1−4 linkage (Figure 6a). An elementary cellulose fibril in plant biomass consists of multiple (16−36) cellulose chains.[35−37] The chain length or degree of polymerization of cellulose is on the order of 10 000 in wood cellulose.[38] As described in textbooks and reviews,[2,38] cellulose chains are well organized and interconnected by hydrogen bonding, i.e., from O(6) to O(2)H and from O(3)H to the ring O(5) (Figure 6b). Hydrogen bonding also exists between cellulose chains, such as from O(3) to O(6)H (Figure 6b). These internal hydrogen bonds provide cellulose with a stable structure and impart poor solubility in water as well as many common solvents. The degree of hydrogen bonding and the local conformation of the C(6)H_2OH group vary with the state of cellulose (Figure 6c). In wood, the natural state of cellulose, called cellulose I, is less strongly hydrogen bonded and may not be locally highly ordered. In contrast, regenerated cellulose (cellulose II) derived from chemical dissolution and redeposition or in a process called mercerization exhibits a modified hydrogen-bonding pattern and is usually more stable compared with cellulose I.[39,40] The proportion of ordered and disordered cellulose depends on the origin of the samples and the chemical processes used to prepare them. The

DOI: 10.1021/acs.chemrev.6b00225
Chem. Rev. XXXX, XXX, XXX−XXX

term, cellulose allomorph, refers to cellulose materials with different crystalline structures.

Although cellulose was discovered more than 175 years ago, the detailed cellulose supermolecular or ultramolecular structure is still a subject of debate. The penetration depth of water through the various structural levels of cellulose fibrils is still an open question without definitive answers. Different models describing cellulose organization within a microfibril have been proposed. Of the two commonly accepted models, one is a disordered (amorphous, or para-crystalline, or water accessible) region of cellulose that exists between two regions of highly ordered (crystalline or water inaccessible) cellulose[35,41] (Figure 7). The structural size of the region described in this model is on

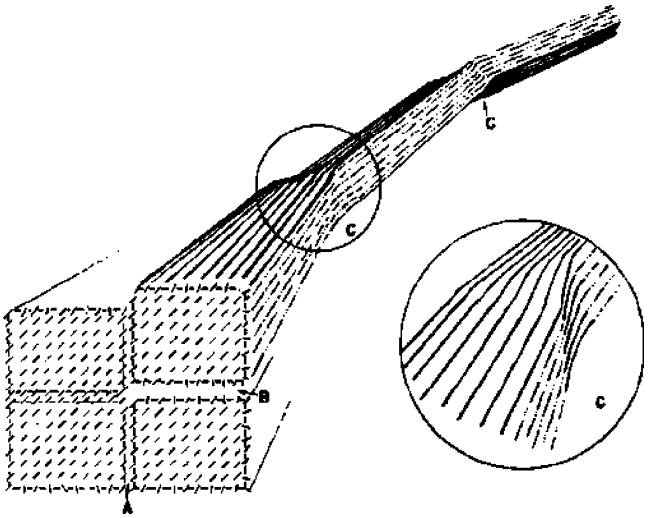

Figure 7. Schematic representation of cotton cellulose fibril structure according to Rowland and Roberts.[35] (a) Coalesced surfaces of high order. (b) Readily accessible slightly disordered surfaces. (c) Readily accessible surfaces of strain-distorted tilt and twist regions. Reproduced with permission from ref 35. Copyright 1972 WILEY-VCH.

the order of elementary fibrils, i.e., water is only accessible to the surface of elementary fibrils.[36] Using controlled acid hydrolysis, one can isolate crystallites from natural cellulose (or cellulose I) with dimensions speculated to be reflective of crystalline domains within elementary fibrils by selectively hydrolyzing the water-accessible crystal defects and disordered regions. However, the concept of isolating pre-existing crystallites in natural cellulose microfibrils was recently challenged by the hypothesis that water penetrates wood at the cellulose chain level,[42] and therefore, the elemental crystallite structure[35] may not exist in wood. This new model is supported by the observation that cellulose nanocrystals (CNCs) could not be isolated from untreated wood and of water accessibility in wood cellulose samples as measured by D_2O exchange detected by Raman scattering at 1380 cm^{-1}. The Raman band at 1380 cm^{-1} is due to $C(6)H_2OH$ bending modes. Furthermore, the crystallinities of CNC samples produced from bleached pulp fibers using strong acid hydrolysis were not substantially greater than that of the original fibers.[43] The observed increase in crystallinity measured by X-ray diffraction (XRD) may well be due to the cellulose enrichment in the CNC samples after hydrolyzing amorphous hemicelluloses in the fibers.

In spite of this debate, isolation or production of cellulose nanomaterials from plant biomass is important because cellulose is a very strong material. As shown in Table 1, crystalline cellulose

Table 1. Comparisons of Mechanical Properties of Cellulose with Those of Other Materials

material	modulus (GPa)	density (g/cm^3)	tensile (GPa)
cellulose	140[45]	1.5	7.5[46]
wood	16	0.6	0.008
aluminum	70	2.7	0.3
steel (AISI 4130)	207	7.8	1.1
glass fiber	85	2.5	4.8
carbon nanotube (CNT)[47]	270−950 (18−68)	1.5−1.7	11−63 (1.4−2.9)

tensile strength and modulus are 140 and 7.5 GPa, respectively, or approximately 10−100 times that of wood, respectively. Cellulose is stronger than steel when density difference is factored in and comparable to carbon nanotubes (CNT). However, the strength of wood is substantially reduced compared to cellulose, because its structure is a polymeric composite of cellulose, hemicelluloses, and lignin. In the following section, we will describe the production of two types of cellulose nanomaterials, CNCs and cellulose nanofibrils, which are useful as building blocks for a variety of applications using renewable plant biomass.

2.2.1.1. Cellulose Nanocrystals (CNCs). The term CNC generally refers to a type of cellulose nanomaterial with a typical length of 50−500 nm or a DP between 100 and 300[48−50] and a 3−10 nm diameter with a certain degree of crystallinity. CNC should be highly crystalline by definition. However, the term CNC is not scientifically defined; for example, the range of crystallinity of CNC has not been specified. In some literature, the rod-like cellulose nanomaterials produced by enzymatic hydrolysis[51] or oxidation[52−54] were termed crystalline cellulose. For example, the rod-like cellulose micromaterials (bioplus, American Process Inc., Atlanta, GA) produced by a dissolving pulping process were also called CNC. The limited accuracy in crystallinity measurements of CNC using the traditional XRD technique[55,56] added more ambiguity to the definition of CNC. Furthermore, all crystallinity measurement techniques, including XRD[55] and Raman,[57] are ensemble measurements taken from a small volume of cellulose sample and spatially averaged rather than resolved to the cellulose surface. If the crystallite model of natural cellulose (cellulose I) structure[35,36] is accurate then CNC represents isolated crystallites and have the diameter of elementary fibrils with the lengths of crystallites. It should be noted that almost all of the reported studies on CNC production used cellulosic materials that went through chemical processes, such as pulping, that consolidated or hornified fibers to certain degrees to be more ordered. Therefore, strictly speaking and as mentioned above, CNC should be described as a material that is produced rather than extracted and the terms “extracted” or “isolated” which are used in some key literature[2,58] are not accurate descriptions of these process. Only when crystalline cellulose occurs and is used in its natural form, such as in the case of cotton, can the term “isolated” or “isolation” be used.

Despite the published ambiguity in the definition of CNC, here we will use the term CNC to broadly represent crystalline rod-like cellulose nanomaterials. CNC is primarily produced from cellulosic fibers through acid hydrolysis. The production of CNC was first reported in the late 1940s and early 1950s[48,59−61] and remains the dominant process today.[29,62−69] Reported studies on CNC production are limited to the use of mineral acids. Hydrochloric acid was used with typical acid concentration between 2.5 and 6.0 N.[70,71] Phosphoric acid was also used for

DOI: 10.1021/acs.chemrev.6b00225
Chem. Rev. XXXX, XXX, XXX−XXX

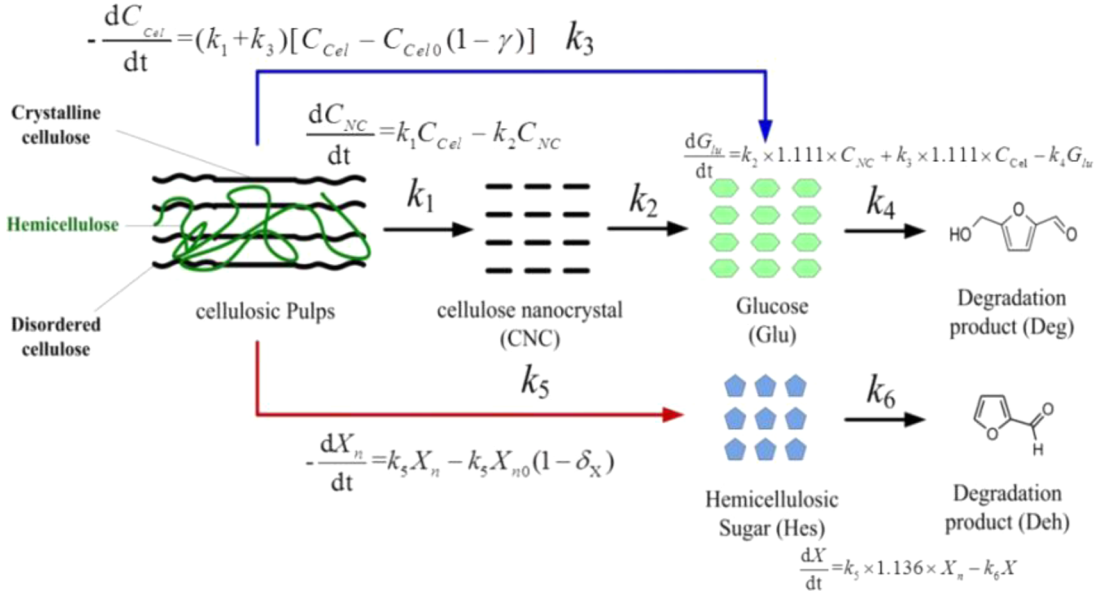

Figure 8. Reaction kinetic model for concentrated acid hydrolysis of bleached fibers only containing cellulose and hemicelluloses.[66] Reproduced with permission from ref 66. Copyright 2014 American Chemical Society.

CNC production.[72] However, high sulfuric acid concentrations (approximately 64 wt %) are commonly used, including at the first commercial facility and two pilot-scale operations in North America. This is due in part to the formation of sulfate groups (see Figure 6d) that impart electrostatic stability to CNC to facilitate aqueous processing. There have been several recent review papers[2,33,58,73,74] that provide a great deal of information about the production of CNC through strong acid hydrolysis and the potential of CNC for a variety of applications. Here, we focus on progress made in the last 5 years in this field, with emphasis on improving CNC yield and tailoring CNC properties, especially a recent study that used dicarboxylic acids to achieve integrated productions of thermal stable and carboxylated CNC with CNF with fully recovery of chemicals (acid).[75] Because sustainable and economic CNC production is one of the key factors dictating future commercial success in the utilization of cellulose nanomaterials, the importance of these recent advances cannot be overemphasized.

Low CNC yields (approximately 30 wt %) have been the main drawback as reported in the literature.[62,65,68] Optimization studies for CNC production using traditional statistical experimental designs have been carried out, but all resulted in low CNC yields of approximately 35%. These studies used large acid steps in experimental designs that were unable to resolve the rapid cellulose hydrolysis and degradation reactions. DP reduction, cellulosic solids sulfation, and the production of CNC occurred abruptly and simultaneously when acid hydrolysis parameters were varied,[68] which leads to the common belief that the coexistence of CNC and non-CNC cellulosic solids is not possible. As a result, simultaneous recoveries of CNC and any remaining cellulosic solids were not attempted in almost all reported studies on CNC production.

Battista[48] mentioned the potential to reduce CNC yield loses using a mild acid hydrolysis. However, the idea was never attempted. Recently, Wang et al.[29] used a slightly lower sulfuric acid concentration (58 wt %) with simultaneous recovery of CNC and partially hydrolyzed fibers, which they termed "fibrous cellulosic solids residues" (CSR). They achieved near zero loss of cellulose to sugars and created the possibility to substantially improve CNC yield. The authors later proposed a reaction kinetics model (Figure 8) and conducted an experimental kinetic study[66] which discovered the abrupt CNC production phenomenon at acid concentrations of between 56 and 58 wt % (Figure 9). This work demonstrated that acid concentration is

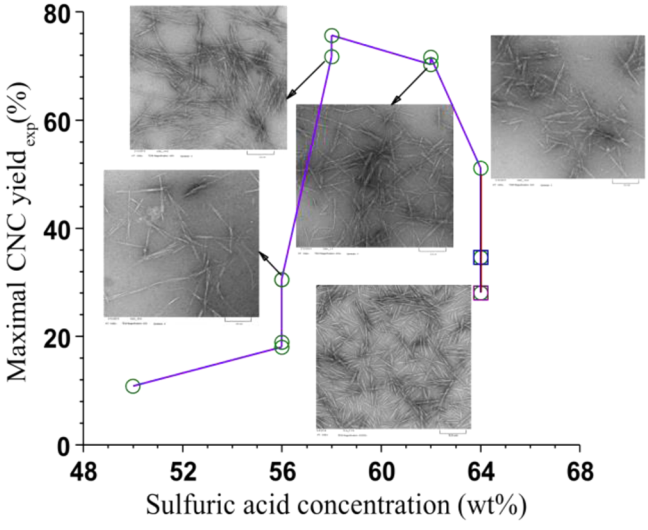

Figure 9. Effects of acid concentration on maximal CNC yield and morphology. Here maximal CNC yield represents the highest yield obtainable in ranges of reaction temperatures and durations at a given acid concentration.[43] All scales in TEM images are 200 nm. Reproduced with permission from ref 43. Copyright 2015 Springer.

the key parameter to control CNC production yield. Below 58 wt %, only a very small amount of CNC can be produced due to insufficient cellulose depolymerization, which was also reported previously,[62,68] whereas above 62 wt % the CNC were rapidly hydrolyzed to glucose, also resulting in low yield. Furthermore, hydrolysis temperature and reaction time in the range studied (35 °C ≤ T ≤ 80 °C; 15 min ≤ t ≤ 240 min) had no substantial effects on CNC yield. This finding provides a mechanism for controlling CNC yield by simply controlling acid concentration.

DOI: 10.1021/acs.chemrev.6b00225
Chem. Rev. XXXX, XXX, XXX−XXX

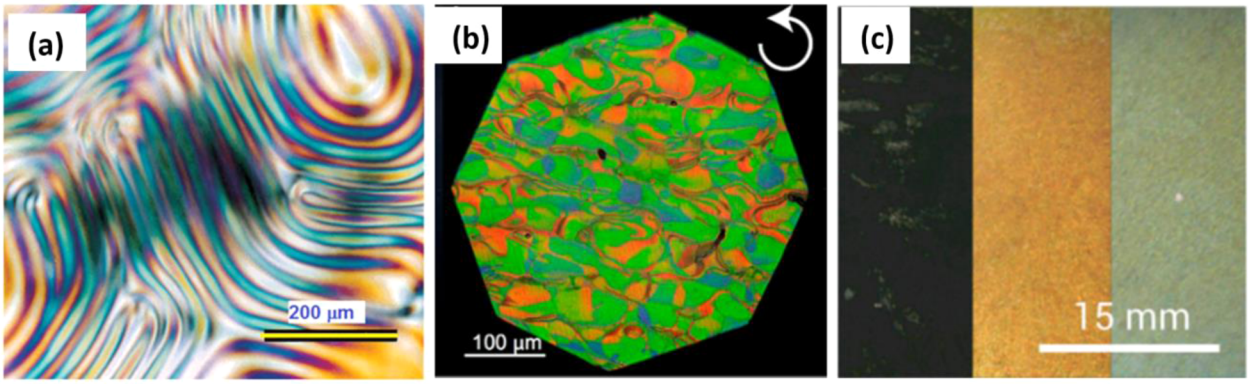

Figure 10. Chiral nematic properties of CNC-produced birefringent patterns from (a) fingerprint pattern in the chiral nematic phase of the directly sulfuric acid hydrolyzed CNC suspension of solid content 5.4%.[78] Reproduced with permission from ref 78. Copyright 2000 American Chemical Society. (b) Polarization optical micrographs at the center of a CNC film showing reflected left-handed circularly polarized light.[79] Reproduced with permission from ref 79. Copyright 2014 American Chemical Society. (c) Iridescent PAAm nanocomposite hydrogels (66 wt % CNC) and varying amounts of sodium chloride; increasing the ionic strength blue shifts the reflectance across the visible region.[84] Reproduced with permission from ref 84. Copyright 2013 WILEY-VCH.

Laboratory bench-scale experiments verified that CNC yield of over 70 wt % was achievable using a bleached kraft pulp with cellulose content of only approximately 80 wt %.[66] This study substantially improves the economics of CNC production for commercial applications.

CNC from mineral acid, especially sulfuric acid, have poor thermal stability due to the sulfate group which poses a significant barrier for thermal processing in composites. The thermal stability of the hydrogen form of CNC (H−CNC) can be improved by exchanging a hydrogen atom with sodium to obtain the sodium form (Na−CNC) through neutralization,[71,76,77] as shown in Figure 6d. Thermal stability as represented by the temperature of onset degradation can be improved to slightly below that of the pulp fibers used to produce the CNC.[71,77] Increasing the degree of sodium substitution to a 20-fold NaOH dosage can further improve thermal stability.[76]

CNC has interesting optical properties, such as forming a chiral nematic phase in suspension as revealed by many studies.[78−85] Different birefringent patterns were observed from CNC suspensions as well as CNC film and hydrogels as shown in Figure 10a−c. These optical properties are affected by the CNC characteristics, such as morphology. For example, the polydispersity of the size distribution of CNC was found to dictate the iridescent colors and the ordering of the nematic layers from a CNC film.[79] Therefore, tailoring the CNC chemical, optical, and morphological properties is of vital importance for a variety of applications. CNC with large aspect ratio may be more suitable as polymer reinforcement for composites, for example. An early study found that the properties of wood CNC were not much affected by varying other hydrolytic conditions, including temperature and reaction times, at the standard acid concentration of 64 wt %.[69] When microcrystalline cellulose was hydrolyzed using 6 N HCl under varied hydrolytic conditions, different crystal lengths of CNC were reported.[71] A recent study by Chen et al. revealed that proper control of sulfuric acid concentration can not only improve CNC yield[66] but also produce CNC with desired morphology[43]—as clearly shown in Figure 9. The average CNC length increased from approximately 100 to over 200 nm when acid concentration was decreased within the small range of 64−58 wt %. The effects of other reaction conditions (i.e., temperature and reaction time) were insignificant, in agreement with an early study.[69] CNC crystallinity and sulfate group content also can be tailored by properly controlled acid hydrolysis conditions.[43] Using acid concentration to control CNC yield while tailoring CNC morphology and surface properties is probably one of the most important discoveries in the last 70 years on the subject of CNC production. This new understanding provides an effective tool for application-specific optimization of CNC production.

One of the main drawbacks of using mineral acids for CNC production is difficulties in economic recovery of acids. Because of the large amount of acid that has to be used when conducting hydrolysis at high acid concentrations, e.g., approximately 9 kg of sulfuric acid per kg of CNC based on current pilot plant operating data, in addition to the requirement of disposal a large amount of sulfate, e.g., 13 kg per kg CNC, current CNC production practice is environmentally unsustainable, expensive, and economically out of reach for most product development. There is a strong need to develop green and low-cost CNC production technologies.

Recently, organic dicarboxylic acids were used for CNC production.[75] However, organic acids are weak acids, which resulted in low CNC yield due to insufficient cellulose depolymerization. Moreover, the partially hydrolyzed fibers, or CSR, can be easily recovered and used for producing CNF through subsequent mechanical fibrillation to achieve integrated production of CNC with CNF as will be discussed later. The key advantages of using dicarboxylic acids are (1) the resultant CNC and CNF are carboxylyzed, as polycarboxylic acids can react with cellulose to form semiester (carboxylation) that is not cross-linked,[86] (2) full chemical (catalyst) recovery can be easily realized through commercially proven crystallization technology when using solid carboxylic acid such as maleic or oxalic acids, (3) the resultant CNC and CNF are thermally stable, critically important for composite applications under elevated processing temperatures; and (4) the morphology and surface chemical properties of the resultant CNC and CNF can be controlled by control the acid hydrolysis conditions as discussed below Overall, concentrated dicarboxylic acid hydrolysis addressed all the problems associated with using mineral acids for CNC production. It is expected that this process will attract commercial and academic interests.

DOI: 10.1021/acs.chemrev.6b00225
Chem. Rev. XXXX, XXX, XXX−XXX

Maleic acid may be preferred more than oxalic acid due to equipment corrosion by oxalate with metals in woody materials. Typical hydrolysis conditions are at concentrations of 50−80 wt % and 100 °C for approximately 45−90 min. The resultant CNC typically have a longer length of around 300 nm with thicker diameters between 10 and 30 nm, especially at milder conditions than CNC produced using sulfuric acid. They also have a higher crystallinity than sulfuric CNC produced from the same feed fibers, which explains the improved thermal stability. Typical carboxyl groups contents were between 0.1 and 0.4 mmol/g CNC with a zeta potential of 40−45 mV that provides good dispersion for aqueous processing. Carboxylation can be improved by using acid catalyst or solvent processing.

CNC production by oxidation was also reported in several recent studies, even when using a lignin-containing feedstock. Ammonia persulfate as an oxidant has the advantage of low cost and low long-term toxicity. It can oxidize cellulose to CNC at 60 °C for 16 h with a chemical loading of 0.1 mol per gram cellulose and relatively good yield.[52] The produced CNC are carboxylated and can be easily separated through membrane filtration. However, reaction time of 16 h is very long which can create capacity problem. Oxidation using TEMPO was also carried out for CNC production.[54,87,88] However, TEMPO was not as effective as ammonia persulfate in cellulose oxidation; only a small portion of the cellulose was oxidized to CNC. The remaining partially oxidized cellulose has much larger dimensions, and its properties depend on the chemical loading. It was found that the CNC from TEMPO oxidation are highly carboxylated,[53,89] which provides the opportunity for functionalization.[90,91] Overall, oxidation reactions for CNC production were often conducted at low solids loading of 2%, which requires a substantial amount of water. Oxidants are consumed and cannot be recovered. The resultant CNC like classical CNC from mineral acid hydrolysis suffer from the problem of low thermal stability,[92] a major disadvantage for composite applications.

2.2.1.2. Cellulose Nanofibrils (CNF). The term CNF is loosely defined as cellulosic fibrils with a diameter on the order of 100 nm or less and length of 500 nm or longer. The only criterion to fit to the CNF definition is the physical dimensions. Indeed, CNF was first produced through mechanical fibrillation[93] and was termed as microfibrillated cellulose, because most of the fibrils had diameters in the submicrometer range. The separation of cellulose microfibrils and nanofibrils by mechanical fibrillation can be clearly seen from SEM (Figure 11a). However, the fibrillated cellulose are mostly entangled fibril networks as shown in the literature[94,95] and in Figure 11b. Depending on the scale level of observation and the degree of fibrillation, the morphology of the resultant fibrils varies significantly and can be very diverse. When bleached hardwood pulp was fibrillated[95] structures resembling trees with distinct kinks as well as soft looking structures were clearly observed (Figure 12a and 12b).

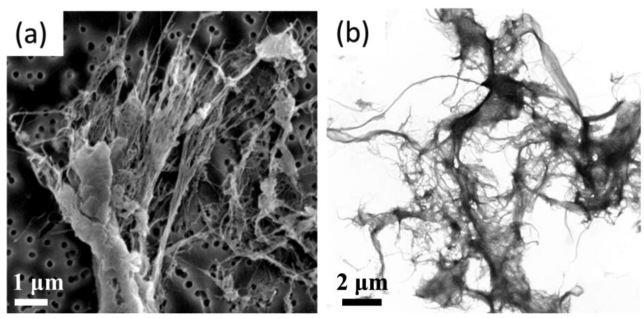

Figure 11. (a, b) TEM images show the fibril structure and breakdown of fibrils of a bleached wood pulp microfiber.[95] Reproduced with permission from ref 95. Copyright 2012 Springer.

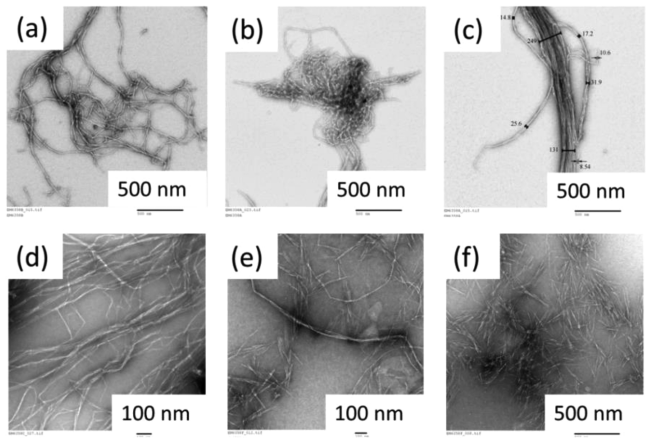

Figure 12. (a−f) TEM images show different CNF morphologies from pure mechanical fibrillation of a bleached eucalyptus pulp.[95] Reproduced with permission from ref 95. Copyright 2012 Springer.

Interconnected fibril bundles with diameter from 5 to 250 nm were also observed (see Figure 12c and 12d). A twisting of cellulose fibrils was clearly visible from the TEM images in Figure 12a−d. "Whiskerization" of the fibrils was also observed with extended fibrillation (Figure 12e). Individual whiskers of about 100 nm can be produced (Figure 12f).

Mechanical fibrillation for CNF production is very energy intensive. Although the entangled network structure of mechanical CNF can be advantageous for producing strong pure CNF films or composites through direct mixing,[96] it can cause difficulties for producing high-grade products through alignment or electrospinning.[97] Chemical pretreatment has been extensively used to reduce energy consumption in refining for producing chemical−thermomechanical pulps in the pulp and paper industry or for producing fine substrates to improve cell wall accessibility to cellulose for sugar production through enzymatic scarification.[98] Similarly, chemical treatment can be used to produce CNF with reduced energy input. TEMPO-mediated oxidation is one of the most studied chemical treatments for CNF production.[99−102] Mechanical energy consumption is minimal after TEMPO oxidation for producing uniform cellulose nanofibrils (Figure 13). Furthermore, large fibrils may be present when incomplete oxidation occurs, as shown in Figure 13. The CNF are long fibrils that facilitate the production of films with good mechanical properties. The very small CNF diameter of approximately 5−10 nm ensured excellent optical transparency (Figure 13). TEMPO/NaBr/NaClO treatment was very selective and efficient in converting the C6-primary hydroxyl group to C6-carboxyl group under aqueous alkaline conditions.[103,104,102] As a result, TEMPO-mediated oxidation produced highly carboxylated CNF (Figure 13). Also, as for CNC, the charged carboxyl group facilitated dispersion for aqueous processing and functionalization.[90,91] Because TEMPO is an expensive chemical, recovery of TEMPO is the key to commercial success of this technology.

Enzymatic treatment has also been employed to reduce energy consumption in mechanical fibrillation.[105−109] Both commercial and laboratory endoglucanase or purified exoglucanase were

DOI: 10.1021/acs.chemrev.6b00225
Chem. Rev. XXXX, XXX, XXX−XXX

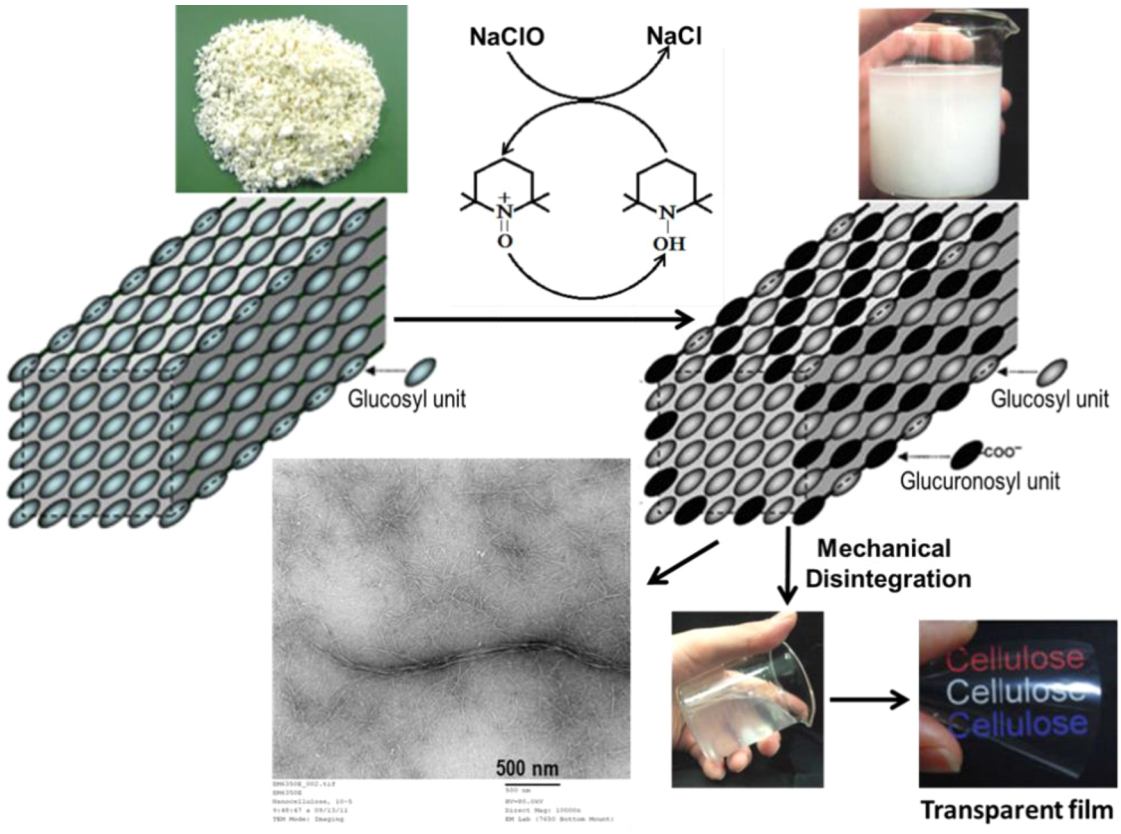

Figure 13. TEMPO-mediated oxidation of wood pulp into CNF after gentle mechanical disintegration showing carboxylation of surface cellulose.[104] Reproduced with permission from ref 104. Copyright 2013 Springer.

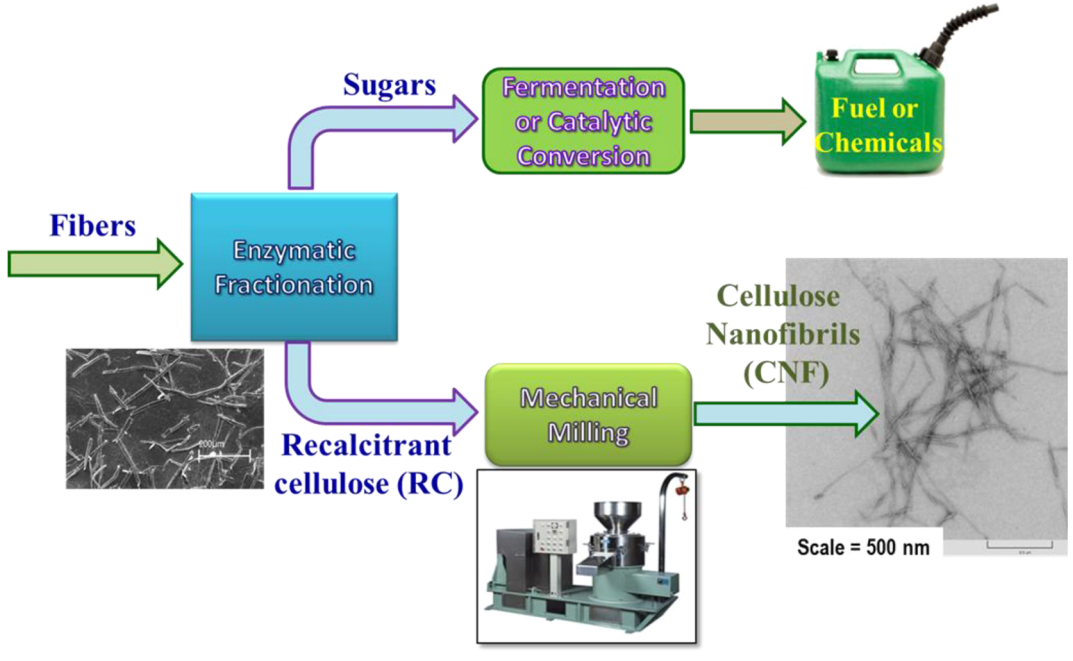

Figure 14. Enzymatic fractionation of wood fibers for the integrated production of sugars and CNF.[108] Reproduced from ref 108 with permission from The Royal Society of Chemistry. Copyright 2011.

used with very limited carbohydrate loss to sugars.[109] Commercial endoglucanase is very effective even at very low enzyme loadings.[109] Enzyme cost should be minimal as loading is substantially lower than the amount used for sugar production.[106,109,110] Xylanase treatment was also used to produce CNF with different water interaction properties from hardwood or nonwoody fibers that contain a significant amount xylan.[111] Some level of energy savings can be achieved based on the authors own laboratory study because xylan is one of the main polymers that connects cellulose microfibrils.[112] However, the

DOI: 10.1021/acs.chemrev.6b00225
Chem. Rev. XXXX, XXX, XXX−XXX

amount of energy savings are limited, because maximal xylan removal is only approximately 30% by most xylanase treatment.[113] This result is due, in part, to the chemical complexity of plant hemicelluloses, where breaking the β-(1−4) bond in xylan does not fully deconstruct cell wall hemicellulose.

A recent study for the first time demonstrated an interesting approach that integrated two major research areas in wood fiber utilization science, i.e., sugar and cellulose nanomaterials production. The study used a mixture of endoglucanase and exoglucanase to purposely fractionate an easy sugar stream and a recalcitrant cellulose fraction that can be used for CNF production through subsequent mechanical fibrillation (Figure 14). The sugar stream is very clean and can be used for producing high-value chemicals. The CNF produced are less aggregated than those from purely mechanical fibrillation (Figure 14).

2.2.1.3. Integrated Production of Thermal Stable and Carboxylated CNF with CNC. The production of CNF can be integrated with CNC using acid hydrolysis as demonstrated recently.[29,114] When using solid dicarboxylic acids, the resultant CNC and CNF are carboxylated as discussed previously. Only a portion of the cellulosic fibers can be hydrolyzed to CNC with the remaining partially hydrolyzed fibrous cellulosic solid residue (CSR). The CSR can be further mechanically fibrillated to carboxylated CNF with only a small amount of energy input as shown in Figure 15. Depending on the acid hydrolysis severity,

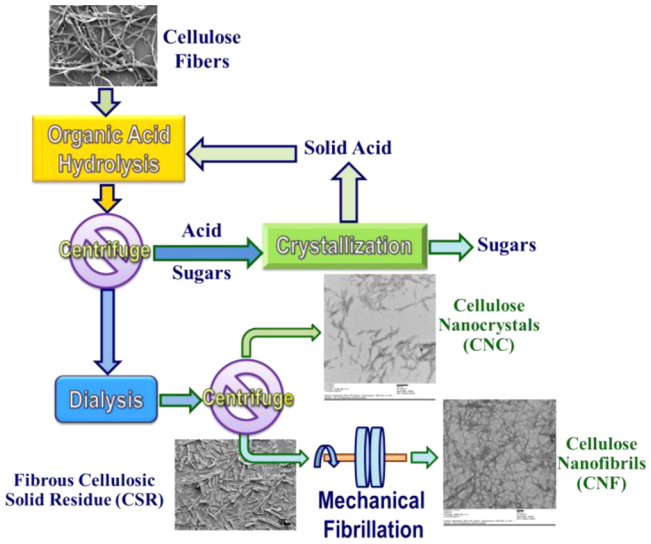

Figure 15. Integrating the production of CNC with CNF through acid hydrolysis. Reproduced from ref 75 with permission from The Royal Society of Chemistry. Copyright 2016.

the yield ratio between CNC and CNF can be tailored.[29,66,75] Furthermore, the morphology of the resultant CNF also varies with hydrolysis severity and the degree of mechanical fibrillation. Typical CNF were individual straight fibrils with a uniform diameter of approximately 10 nm and can form mechanically strong and highly transparent films.[114,75] This integrated production using dicarboxylic acids can achieve near zero cellulose loss to produce carboxylated CNC with full acid recovery simply through crystallization. It also provided the flexibility to meet market needs in cellulose nanomaterial production.

Most existing processes for CNC and CNF production are expensive. Many are not environmentally sustainable due to difficulties in economic recovery of chemicals such as concentrated mineral acid hydrolysis for producing CNC. Despite these difficulties, precommercial production was pursued by a few companies throughout the world using some of the processes described in this review. Using concentrated dicarboxylic acid hydrolysis to produce CNC and CNF appears very attractive in terms of ease chemical recovery, surface carboxylation, along with high thermal stability of the resultant CNC and CNF.[75] Furthermore, reactions can be conducted at ambient pressure, and weak acid allows less expensive metallurgy, both of which can reduce capital cost. The process however is new and yet needs to be further evaluated.

2.2.2. Hemiscellulose. It is rare that cellulose in nature is present without other types of polysaccharides, although seed hairs of cotton and "bacterial cellulose" produced by the bacteria *Acetobacter xylonium* and some other species are almost pure cellulose in natural form. Generally, cellulose as a component in plant cell walls occurs together with other polysaccharides. Interestingly, nonplant celluloses, as in the tunic of tunicates, in a corresponding way can occur together with proteins. The noncellulosic polymers are known as hemicelluloses and pectins—cell wall polymers that were historically distinguished from cellulose by order of purification and later by discrete structural and physical/chemical properties. Pectins are more easily extracted with chelating compounds and generally more rapidly degraded in hot alkali than hemicelluloses. Pectins also have molecular structures that differ from most hemicelluloses, such as a main chain that is connected by other types of bonds. In hemicellulose, the main chain in most cases is connected with β-(1,4) glycosidic bonds, whereas in pectin the main chain is connected with α-(1,4) or α-(1,2) glycosidic bonds. Furthermore, the side chains are often much longer and complex in pectin than in hemicelluloses. For details in pectin structure see the review by Yapo (2011).[115]

Whereas the molecular structure of cellulose is the same in all plants, the structure and monosaccharide composition of hemicelluloses varies highly between different phylogenic groups of plants. Still, the details of the hemicellulose structures are not well understood, especially for phylogenic groups with little commercial value, such as vascular cryptogams, etc. However, there are some common structural properties of hemicelluloses; one is as mentioned above, that the main chain consists of monosaccharide connected with β-(1,4) glycosidic bonds in similarity to cellulose, although some other bonds can occur in lower amounts.[116] However, there are also differences from cellulose: hemicelluloses have a relatively low degree of polymerization (DP $\approx$ 200 residues), which can be contrasted to cellulose (DP > 10 000); hemicelluloses are generally heteropolysaccharides, consisting of two or more types of hexoses and pentoses, whereas cellulose is a homopolysaccharide of glucose. A few exceptions, such as the mixed linkage glucan, exist in plants; however, hemicelluloses contain varied and modified backbone and branching residues, such as deoxy sugars, uronic acids, acetylations, and methylations. Cellulose in its natural form is unmodified. It is important to note that the glycosidic bonds in hemicellulose main chains are less stabilized by hydrogen bonds than are the glycosidic bonds in cellulose (Figure 16). Exceptions are the glycosidic bonds of the hemicellulose xyloglucan and some of the glycosidic bonds in glucomannan.

Due to all these differences, the physical properties of hemicelluloses are rather different from those of cellulose.[117] First, cellulose has a rigid and crystalline structure due to its molecular homogeneity, whereas hemicelluloses are more

DOI: 10.1021/acs.chemrev.6b00225
Chem. Rev. XXXX, XXX, XXX−XXX

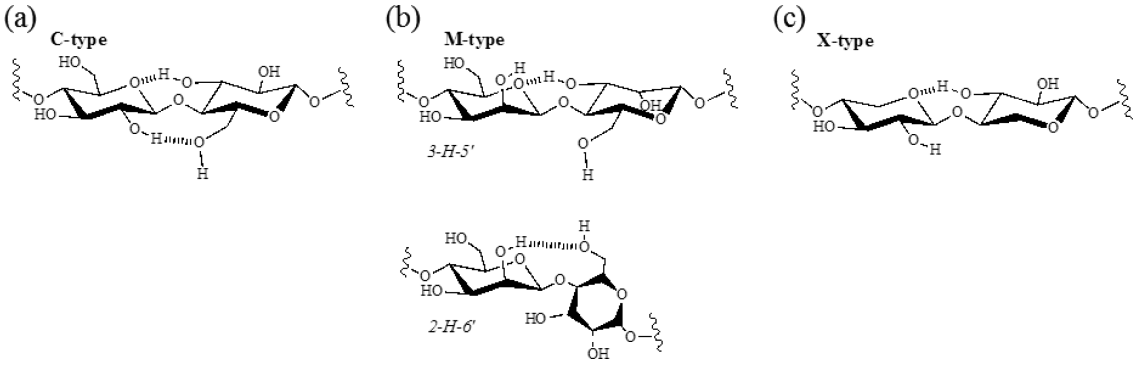

Figure 16. Comparison between the typical β-(1,4-glucosidic) bond in cellulose and the same bond in hemicelluloses. (a) C-type, the glycosidic bond in cellulose, xyloglucan, mixed structure glucan, and after glucose in glucomannan. The covalent bond is stabilized by two hydrogen bonds. (b) M-type, the glycosidic bond in glucomannan after mannose. This type is stabilized by two hydrogen bonds, but they cannot be fully active on the same time. Maybe it has two main conformations as indicated in the picture. (c) X-type, the glycosidic bond in arabinoxylans. This bond is stabilized only by one hydrogen bond.

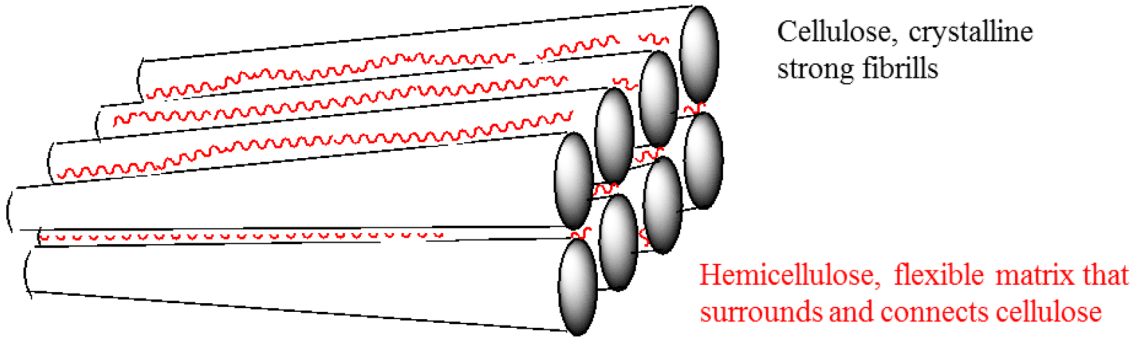

Figure 17. Depiction of the suggested role of hemicellulose in plant cell wall seen as a composite material.

flexible and amorphous; second, hemicelluloses generally are more soluble than cellulose, although it varies highly between different kinds of hemicelluloses; third, hemicellulose is generally more chemically reactive than cellulose, for example, more rapid degradation by alkali.

The differences between cellulose and hemicellulose have large technical significance. Whereas hemicellulose often can be extracted from biomass (wood, chemical pulp, etc.), cellulose remains insoluble. During chemical pulping, hemicelluloses are degraded to a much larger extent than cellulose; however, hemicelluloses deposited on the fiber surface most likely play an important role in the fiber−fiber interactions in paper.[118] Yet, what do the differences in properties between cellulose and hemicelluloses mean for biological function? There have been several suggestions for the biological role of hemicellulose, but perhaps the most interesting idea is that hemicelluloses directly play a role in the mechanical properties of plant cell walls. One possibility is that the plant cell wall can be seen as a composite material, where the crystalline cellulose fibrils act as enforcing fibers and the amorphous hemicelluloses (and lignins) establish a flexible matrix (Figure 17).[119] In other words, the role of hemicelluloses should be to connect the cellulose fibrils together and at the same time contribute with some flexibility to the overall material. The fact that rather large amounts of the plant cell wall (normally 20−35%) consists of hemicellulose fits well with this idea. There are also other possibilities for the function of hemicellulose, such as they might form covalent bonds to lignin and also influence the structure of lignin (discussed below). However, since hemicelluloses exist also among mosses (that do not synthesize lignin), it is doubtful that this was the original function of hemicellulose.[120]

Hemicelluloses can be divided into several classes, i.e., *arabinoxylans*, *glucomannans*, *noncellulose glucans*, and *galactans*. As mentioned above, the structure, occurrence, and properties of the most important hemicellulose varies much between different phylogenic groups, both in the hemicellulose type which dominates and in the number of different hemicelluloses present. For example, the most common hemicellulose in softwood (i.e., xylem of conifers) is glucomannans, whereas the dominant hemicellulose in hardwood (xylem of woody eudicotyedons) is arabinoxylan.[121]

Furthermore, the composition of hemicellulose/pectin often varies between the different cell wall layers in plant cell walls. For example, xyloglucan is present in larger amounts in the primary cell walls, whereas arabinoxylan often is a dominating hemicellulose in the secondary cell wall. Since secondary cell walls are much thicker than primary cell walls in wood, arabinoxylans often dominate composition. Table 2 summarizes the characteristics of the most common classes of hemicelluloses.

The fact that monosaccharide composition and properties of different hemicellulose varies has—not unexpectedly—both biological and technical significance. Biologically, xyloglucan, glucomannan, and arabinoxylan have been suggested to play somewhat different roles:

Xyloglucan, in spite of having a high solubility in water, has a strong affinity for cellulose; this is explained by the two conformations of xyloglucan, one helical with high solubility and one "plain" with a conformation of the main chain that is similar to the one cellulose chains. It is probably the latter

DOI: 10.1021/acs.chemrev.6b00225
Chem. Rev. XXXX, XXX, XXX−XXX

Table 2. Structural Properties of Common Types of Hemicellulose

name	main chain	side chain	modifications	occurrence (as hemicellulose)	comment
arabinoglucuronoxylan and glucuronoxylan	xylose residues connected with β-(1,4) glycosidic bond	methyl glucuronic acid and arabinose (the latter mostly in softwoods)	acetylations in hardwood	softwood, hardwood, and monocotyledons	unusually stable under alkaline conditions
galactoglucomannan and glucomannan	mannose and glucose residues connected with β-(1,4)-glycosidic bonds	galactonse in softwood and none in hardwoods	acetylations	softwood, hardwood, at least some vascular cryptogams	content of galactose can vary between two versions of softwood glucomannans, and the high-galactose version has much higher solubility than the low-galactose version, easily degraded during alkaline pulping
xyloglucan	glucose residues	xylose, connected with galactose and fucose residues	none	primary cell walls in most plants	very high affinity to cellulose

structure that has strong affinity for cellulose, possibly by cocrystallization on the cellulose structure. Thus, xyloglucan has been suggested to cross-link cellulose fibrils with alternating "plain" and "helical structures". Furthermore, in the primary cell wall, xyloglucan can interact with xyloglucan endotransglucosidase, which cleaves and relegates the xyloglucan chains, something that may have importance in the expansion of the primary cell wall.[116,122,123]

Glucomannan has, in a study by Sahlmén and co-workers, been suggested to have a closer interaction with cellulose than with xylans. This should be the case for both hardwoods and softwoods.[124] In many softwoods, the glucomannan appears to occur in two forms (Table 2) with high and low content of galactose side groups, where the former is more soluble.[121] Arabinoxylan has, according to the studies by Sahlmén and co-workers, a less tight interaction with cellulose than glucomannan (Figure 18).[124] Arabinoxylan also differs from other hemicelluloses in the aspect that it carries charges. Structural studies indicate that lignin bound to arabinoxylan is more linear and has less structure than glucomannan-bound lignin.[125]

Hemicelluloses in woody tissues also undergo an additional chemical modification. During lignification, covalent bonds to lignin are formed that can be ethers, esters, and phenyl glycoside bonds. By these covalent bonds, different hemicellulose molecules are cross-linked to lignin and entire networks are created. In this way, hybrid molecules that carry both lignin and hemicellulose functionality are created.[126] Also, bonds to pectin and cellulose can occur in these networks. Knowledge about the structure of these hybrid molecules is incomplete, but it appears that many of the covalent bonds between lignins and polysaccharides are located on hemicellulose side groups.[127]

We also note that there exist polysaccharides that are produced in seeds or intracellular in roots and other storage tissues that have very similar structure to those hemicelluloses described above. For example, there are mannans in the corm of konjac (Devils tongue) and in locust beans and xyloglucan in tamarind seed. However, these polysaccharides generally have a much higher degree of polymerization, and there might also be structural differences. They also carry out other biological functions, i.e., in most cases nutrition/energy storage, and should not be regarded as structural hemicelluloses.

2.2.3. Lignin. Figure 19 shows a suggested lignin structure from softwood. As can be seen, lignin is a very complex structure and in many ways an oddity among biopolymers, possessing unusual properties for being a biologically synthesized molecule.[128] Its monomers (*monolignols*) are connected with several types of covalent bonds, i.e., different ethers and carbon−carbon bonds. The lignin polymer is neither unbranched linear, linear with side chains, nor cross-linked but can probably rather be described as a "chemical web". It does not have a well-defined primary structure.

In contrast to most other biopolymers, lignin is not synthesized by a controlled condensation inside the active site of an enzyme or enzyme complex but by a radical polymerization process[129] that is widely considered to be uncatalyzed. Others have, however, suggested that special direction sites, or templates, in the cell wall could catalyze the coupling,[130] and there are also indications that the hemicellulose might affect the coupling pattern. The issue has been a matter of intensive debate. The monomers of lignin, monolignols, involved in this process that consist of phenyl propanoids, with a double bond conjugated with the aromatic rings, occur in three main forms with varying numbers of methoxy groups attached to the

DOI: 10.1021/acs.chemrev.6b00225
Chem. Rev. XXXX, XXX, XXX−XXX

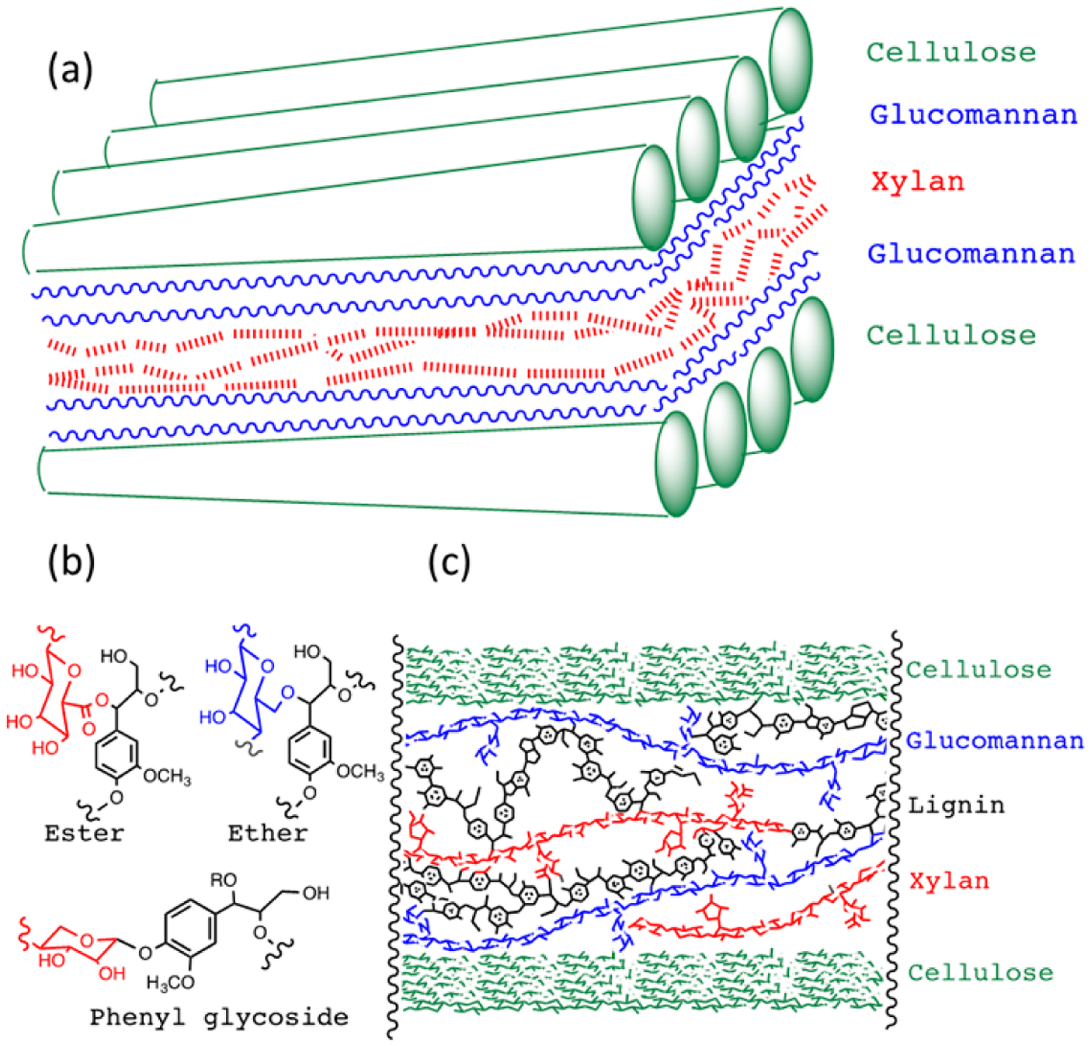

Figure 18. (a) Suggested structural organization of hemicelluloses and cellulose in hardwood and softwood by Sahlmén et al.[124] (b) Three different types of covalent bonds between lignin and polysaccharides. (c) Schematic presentation of how lignin cross-links hemicelluloses in wood.

aromatic ring (Table 3). The composition of monolignols in the lignin varies between different types of plants (Table 3).[131]

Lignin biopolymerization from the monolignols occurs entirely in the cell wall and takes place in several stages (Figure 20).[133] Monolignols are oxidized by laccase and peroxidases, possibly via electron shuttles to radicals that are very stable due to the conjugated structure, i.e., resonance stabilization. In a similar way, phenolic groups on lignin are oxidized to stable radicals. The lifetimes of such radicals can be very long under suitable conditions.

Covalent bonds can be formed by the combination of two radicals. Specifically, it appears that covalent bonds are formed by a monolignol radical and by a radical on a lignin phenol or by two lignin phenol radicals. Since the unpaired electron is located on 4-O-, 1-, 3-, 5-, and β-positions (Figure 19 for explanation of the nomenclature system), principally all combinations of these could be possible, i.e., ethers and carbon−carbon bonds. However, in the case of coupling of two 4-O-radicals, the coupling product will be a peroxide (4-O-O-4′) that most likely is instable and will decouple. Sterical hindrance of substituents on the aromatic ring will also influence the coupling pattern; coupling involving the 1-position rarely occurs in wood, whereas methoxy groups on 3- and 5-positions efficiently block formation of covalent bonds. Thus, lignin-derived sinnapyl alcohol has a low content of condensed bonds and a high content of β-O-4 ethers.

The intermediate coupling product will undergo rearrangement that leads to stable products, i.e., aromatics, and in the case of coupling involving the β-positions, a reactive quinomethide intermediate will be formed. This can be attacked by water giving a hydroxylation of the α-position. If alcohols or carboxylic acid functionalities of cell wall carbohydrates perform the attack, covalent bonds between lignin and polysaccharides will be created (Figure 18).

Since the polymerization reaction of the enzymatic-generated radicals is uncatalyzed, lignin will have a racemic structure and an unordered distribution of the different bond types.[133] This does not mean that the lignin structure is totally random; most likely the pH and polymerization rate will affect the frequency of the different bonds. Most studies indicate that the β-O-4 bond is the by far most common and that this bond type dominates in all lignins, although the content is lower in softwoods than in hardwoods. This outcome is most likely due to the fact that monolignol composition varies with wood type; for example, hardwoods contain a significant amount of sinapyl alcohol residues which contain two methoxy groups (Table 3), thereby blocking coupling in the 5-position. This background gives an explanation as to why hardwoods generally are delignified faster

DOI: 10.1021/acs.chemrev.6b00225
Chem. Rev. XXXX, XXX, XXX−XXX

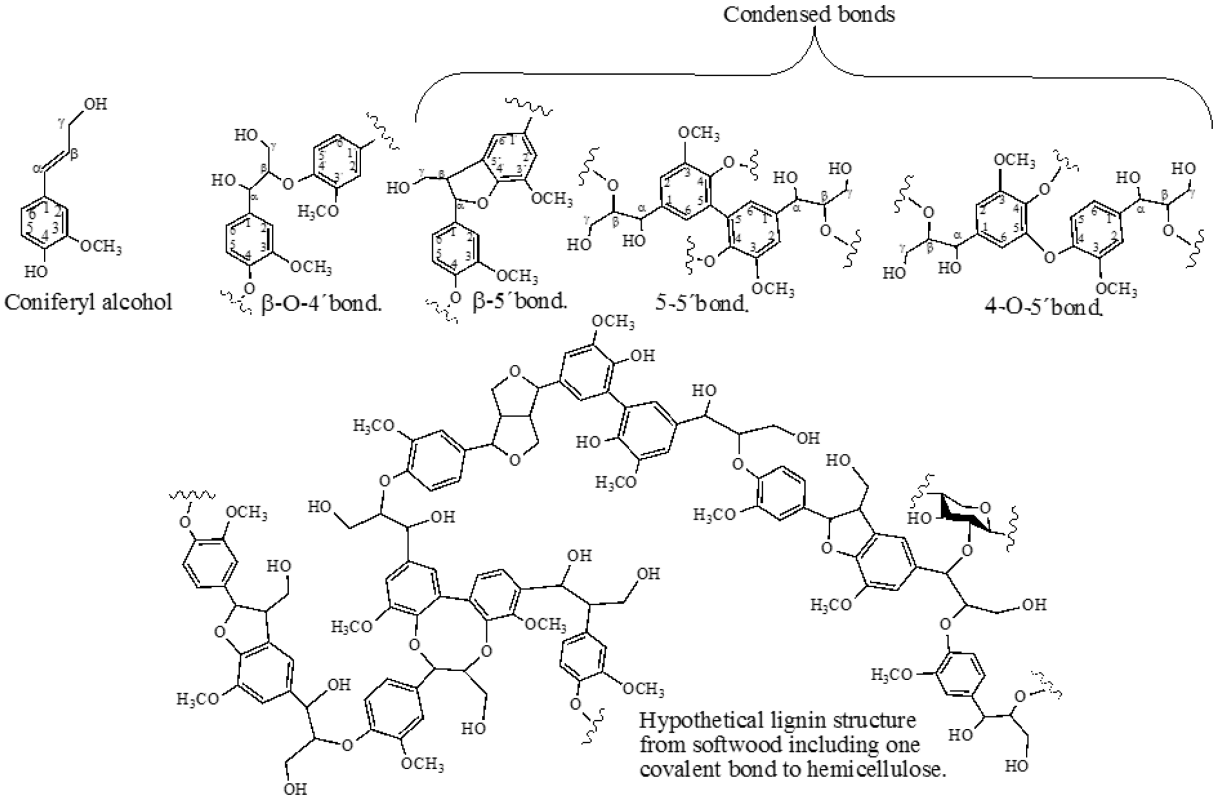

Figure 19. Suggested softwood lignin structure.[128] Reproduced with permission from ref 128. Copyright 2008 Elsevier. Structure of the monolignol (coniferyl alcohol) and the most important intermonolignol bonds are shown with the nomenclature system explained. "Condensed bonds" is a common notification for other bonds than the *β*-O-4′ether, and they are generally more stable in chemical pulping.

Table 3. Monolignol Composition in Different Types of Plants

Name	Structure	Occurrence in hardwood	Occurrence in softwood	Comment.
p-coumaryl alcohol	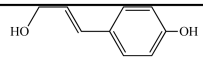	in most cases, low or insignificant	mostly in compression wood	give a lignin rich in condensed bonds
coniferyl alcohol	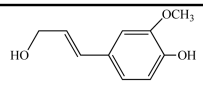	yes	yes, dominates	"standard lignin" for lignin chemists.
sinnapyl alcohol	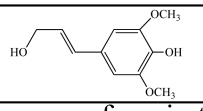	yes the most common	no	give a lignin rich in β-O-4 bonds
others	many for instance aldehyde or carboxylic acid on γ-carbon.	rare	γ-aldehydes occur on primary cell wall in low amounts	grasses can contain several modified monolignols including γ-carboxylic acids

than softwoods in kraft pulping.[118] The monolignol composition and frequency of different bonds are, however, not homogeneous over the different cell wall layers. Generally, the contents of condensed bonds are higher in the middle lamella and in the primary cell wall, where the content of *β*-O-4 bonds is higher—these differences are larger in hardwoods than in softwoods.[134] A consequence of this is that hardwoods need to be pulped to lower lignin content than softwoods to obtain fiber separation.

Also, between different types of cells there are differences in lignin structure. In hardwoods, vessel cells generally have a higher content of coniferyl alcohol and more condensed bonds than libriform fibers. In softwoods, the compression wood lignins contain considerable amounts of *p*-hydroxycoumaryl alcohol, are more condensed, and therefore are a more resistant structure. Both these inhomogeneities have consequences for chemical pulping, where vessel cells might be incompletely delignified and

DOI: 10.1021/acs.chemrev.6b00225
Chem. Rev. XXXX, XXX, XXX−XXX

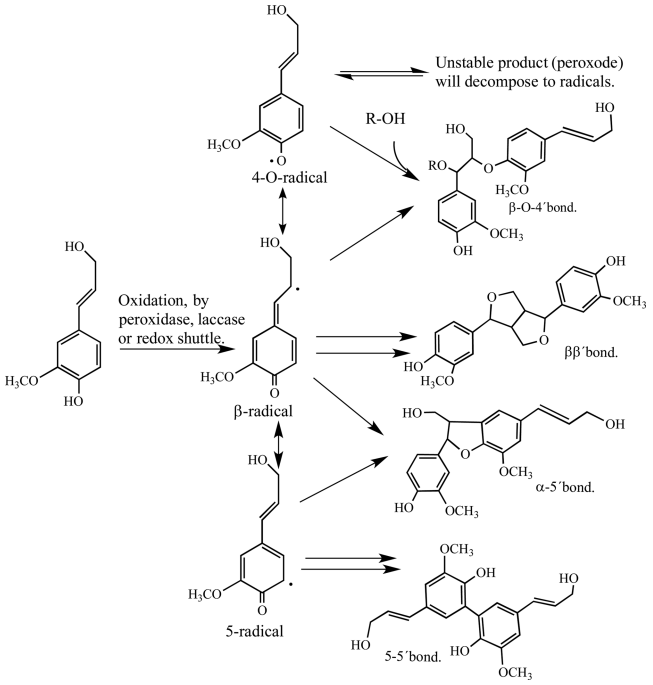

Figure 20. Depicted are the polymerization of monolignols into lignin and the most important bond types. R = H or polysaccharide (hemicellulose, etc.). Enzymatic oxidation can be either direct or mediated by a radical shuttle.[132] Similar reactions are also carried out on phenolic end groups on lignin polymer, which thereby can couple to monolignols.

compression wood—often found in branches—are incompletely defiberized.[135]

The molecular weights of lignin in Nature are still a matter of debate. Theoretically, lignin in wood can obtain very high molecular weights, but molecular weights determined from isolated lignin had indicated a low degree of polymerization and are thus better described as oligomers rather than polymers.[136] However, these molecular weights were obtained from lignin extracted from milled wood in far from quantitative yields. Thus, lignin in intact wood can still have a higher degree of polymerization. Furthermore, the covalent bonds between lignin and polysaccharides (LCC) discussed above allow the creation of "hybrid molecules" carrying both lignin and polysaccharide functionality[126] (Figure 18). Such bonds seem to exist in at least three forms: esters and ethers to the α-position in lignin and phenyl glycosides. The bonds to the α-carbon might be explained by the mechanisms described above, but the origin for the phenyl glycosides is more unclear; one possible explanation is that they are created by transglycosylation activities.[137] Under all circumstances it was demonstrated that lignin covalently cross-links different polysaccharide molecules and that one hemicellulose molecule can carry several lignin functionalities.[127] Thus, the formation of large covalent networks in wood seems likely, consisting of altering lignin and hemicellulose structures.

Back to the question asked in the beginning of the lignin section, why is lignin so different from other biopolymers? One explanation might be that lignin, by its random structure, becomes a physical and chemical obstacle for biological degradation.[138] It appears also that the monolignin structures are "designed" to stimulate the formation of covalent bonds to polysaccharides,[139] thereby suggesting a central role for the lignin−carbohydrate networks in the biological function of lignin.

2.3. Biopolymer Extraction

Extraction of biopolymers for technical purposes can be made for two main reasons: (i) To purify a valuable soluble product. One example here is the cold extraction of prehydrolysis dissolving kraft pulp, where mainly hemicellulose is removed for producing a relatively pure cellulose, that can be used for manufacturing cellulose derivative, etc. (ii) To obtain a valuable soluble product. One example here is the extraction of lignosulfonate from sulfite process liquors. Thus, for the development of more advanced biorefinery projects based on wood, extractions will likely be of elevated importance, since it allows the production of purer substances, either by selective extraction or by postextraction fractionation. Economic and environmental aspects are of course central for extractions at the industrial scale; this means that if chemicals or solvents other than water and cheap chemicals, such as sulfuric acid and sodium hydroxide, are to be used, efficient, and often costly, chemical recovery systems are likely to be needed. Thus, water is the first choice for extraction solvents. Cellulose is insoluble in water, except for conditions using high pH, low temperature, and zinc salts or urea.[140] However, although cellulose dissolution is interesting for making regenerated cellulose, extraction in biorefinery concepts mostly leaves the cellulose intact as valuable fibers. Thus, the discussion here will focus on extraction of lignin and hemicelluloses.

Lignin in its natural form is soluble in certain mixtures of water and organic solvents such as water/dioxin, whereas technical lignins, such as black liqueur lignin, that have been fragmented and chemically modified is soluble in water at high pH but generally not at low or neutral pH. Nonpolar organic solvents, such as hexane, are generally poor solvents for lignin, whereas "half-polar" solvents, such as those based on alcohols (methanol, ethanol, and propanol), and general solvents, such as furfural, dimethyl sulfoxide, tetrahydrofuran, and acetic acid, are best for lignins. This finding is in line with the structure of lignin itself (Figure 19) with altered hydrophilic and hydrophobic structures. Not unexpectedly, lignin with lower molecular weight typically has higher solubility.[141] The solubility of hemicellulose varies very much upon its chemical structure. Arabinoxylan that carries a large amount of charged groups at neutral and alkaline pH have rather good solubility in water, especially at higher pH. Also, galactoglucomannan with a high content of galactose side groups has good solubility in water as well, whereas glucomannan, with its low galactose content, has poor solubility properties in water, although it is soluble in alkali with barium salts present.

Except for pH, temperature is an important parameter for extraction. Both low and high temperature can provide increased extractions. At lower temperature, the entropy effects become weaker and it is therefore a way to lower σ-interaction (hydrophobic interaction).[142] Low temperatures can be used, for example, for extracting hemicellulose from dissolving pulps under alkaline conditions (as mentioned above). Higher temperatures are useful when the entropy favors dissolution and enthalpy disfavors it, but there are also other effects. At high temperatures (under overpressure) of 180 °C and above, the properties of water as a solvent are changed and it starts to behave like a less polar solvent and can, in this way, dissolve hemicelluloses at high yield from wood even at neutral pH. However, in such hot water extractions, wood polymers are partly degraded. This can be due to autohydrolysis, i.e., that acetic acid is created by deacetylation of hemicelluloses, and

DOI: 10.1021/acs.chemrev.6b00225
Chem. Rev. XXXX, XXX, XXX−XXX

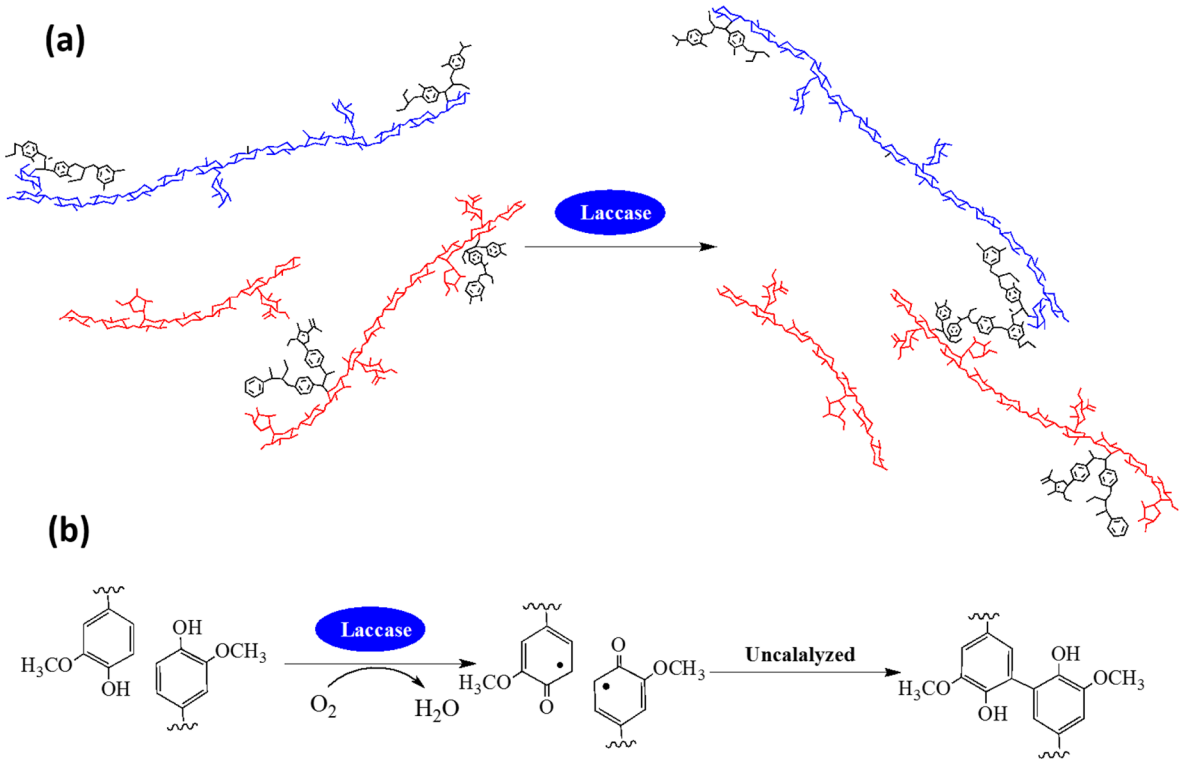

Figure 21. Increase of molecular weight of extracted hemicellulose by laccase treatment. (a) Hemicellulose molecules that carry covalently bound lignin functionality can be covalently cross-linked by treatment with the enzyme, laccase. (b) This is done when phenolic end groups of the lignin moiety of these molecules are oxidized to resonance-stabilized radicals that undergo uncatalyzed radical−radical couplings which covalently cross-link the molecules.

thereby lowers the pH. This effect can be compensated by addition of buffering substances, but degradation occurs to some extent nevertheless, which indicates that other mechanisms, such as hemolysis, might be involved.[143]

Also, mechanical treatment in water can lead to extraction of material from wood. Much interest has been focused on the materials obtained in water solution after mechanical pulping, which have been shown to be rich in glucomannans and also some lignins.[144] As described above, wood is a cross-linked structure, and direct extraction from wood without any pretreatment or breaking of covalent bonds is difficult. Furthermore, the morphology of wood itself is an obstacle, and extractions are easier from sawdust than from wood chips due to mass transport limitations. One way to enhance extraction of hemicellulose from wood is to degrade and solubilize at least part of the lignin. A problem here is that the most important chemical pulping process, kraft pulping, rapidly degrades glucomannans. One way to overcome this problem is to reduce or oxidize the end groups of polysaccharides. To further enhance extractability, the partially pulped wood can be treated with xylanase enzymes that selectively cleave bonds in the covalent networks. The concept has been tested, and both yield of extraction and molecular mass increased after enzymatic treatment.[145] If more selective enzymes can be available in large amounts, the results can probably be further improved. Hot water extraction as described above has the advantage that acetyl groups remain on the polysaccharides, which have positive effects on solubility. However, degradation also occurs here even if buffer systems are included.[143] In this case, the lower molecular mass of extracted hemicelluloses might be an obstacle for some applications.

However, a large fraction of extracted hemicelluloses carry covalently bonded lignin oligomers, a bit like the lignin carbohydrate complexes (LCC) networks in wood. If such material is treated with the laccase, phenols on the lignin functionalities will be oxidized to radicals that undergo radical couplings, i.e., hemicellulose molecules are cross-linked by the lignin functionalities and the molecular weight is increased (Figure 21). Such treatments have been shown to improve the properties of the hemicellulose in various applications,[146] and similar techniques can also increase the molecular mass of technical lignin.[147,148]

Technically, the solubility of lignin and hemicelluloses has been utilized in different ways; in chemical pulping, water can be partially exchanged with good solvents for lignin, such as ethanol, methanol, acetone, and organic acids. Subsequently, larger and more hydrophobic lignin molecules can be extracted than is possible during water-based pulping. This concept is important for different biorefinery concepts, partly due to the production of lignin with different properties, such as enhanced hydrophobicity because this property may open up new applications in composites. Organosolv pulping can be integrated with enzymatic hydrolysis of the cellulose and fermentation to ethanol, and separation of sugars, furfural, and other molecules from the solubilized lignin is possible.[149] An interesting version of integrated hydrolysis and extraction was presented by Luterbacher et al., which used a mixture of water, sulfuric acid, and γ-valerolactone, obtaining high-yield extraction and hydrolysis of both softwood and hardwood. Interestingly, the chemical used could be manufactured from the biomass.[150]

Carbon fiber is intensively used today in large-scale engineering, including aerospace, wind turbine blade, and automotive industries, comfort fabrics, special sport textiles, and various commercial membranes, as well as the emerging markets for wearable batteries, sensors, and electronics.[151−160] Continuous

DOI: 10.1021/acs.chemrev.6b00225
Chem. Rev. XXXX, XXX, XXX−XXX

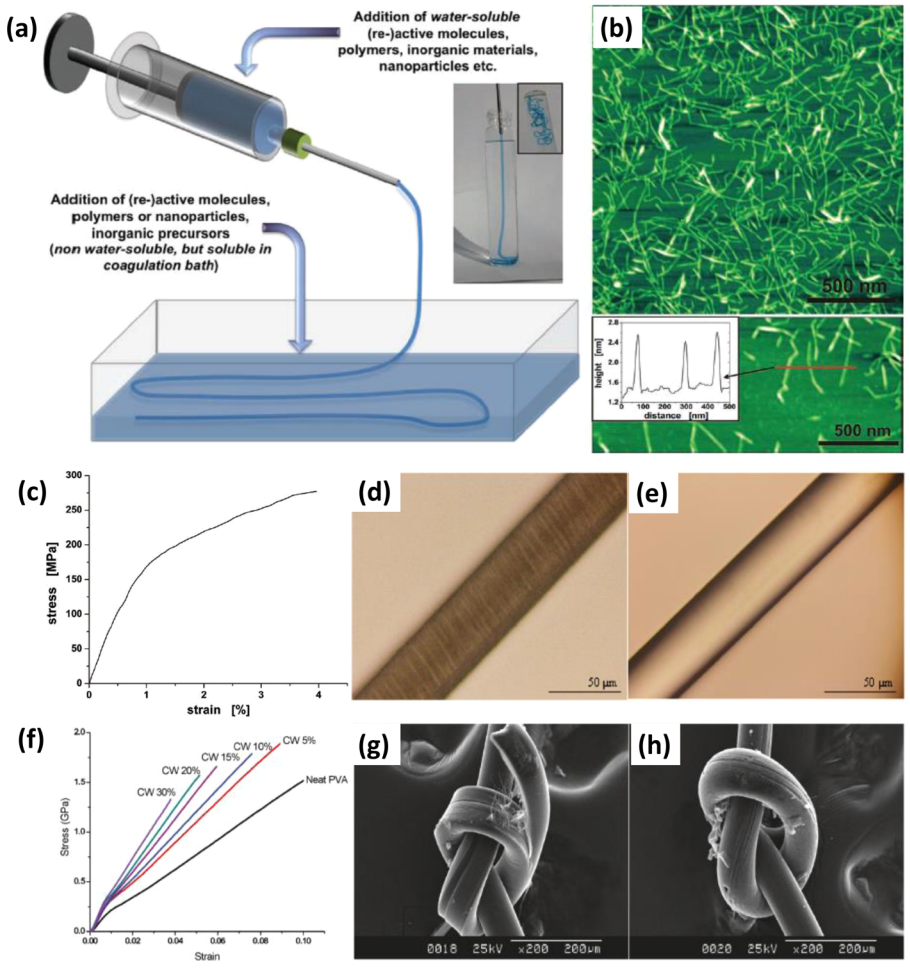

Figure 22. (a) Schematic of preparation NFC macrofibers by extrusion of NFC gel into a coagulation bath. (b) SPM image of NFC. (c) Representative stress−strain curve of a macrofiber of ca. 0.17 mm diameter.[171] Reproduced with permission from ref 171. Copyright 2011 WILEY-VCH. Optical microscopic images of the (d) neat PVA and (e) PVA-CNC 5% fibers. (f) Stress−strain curve of fibers made with different CNC loading. Structure of knotted (g) neat PVA and (h) PVA-CNC 5 wt % fibers.[170] Reproduced with permission from ref 170. Copyright 2011 American Chemical Society.

carbon fibers are conventionally produced from solutions of polyacrylonitrile (PAN) spun into a coagulation with a good mechanical strength and high yield. However, the PAN precursor is expensive. Fiber with cellulosic material as precursor is much less costly than PAN; also this resource is sustainable. Moreover, cellulosic precursor-derived fibers have unique optical properties as well as excellent biocompatibility and biodegradability.

3. ONE-, TWO-, AND THREE-DIMENSIONAL NANOSTRUCTURES FROM WOOD BIOMATERIALS: SYNTHESIS AND CHARACTERIZATION

3.1. Multifunctional Fibers

Fibers play an important role in several industries, including aerospace, textiles, membranes, wearable electronics, and reinforcing materials because of their lightweight, mechanical flexibility, versatility, high tensile strength, and other functionalized electrical, optical, and magnetic properties.[161−167] In Nature, there are a variety of organisms containing fibers, such as trees, animals (muscle tissue), lower eukaryotes, and bacteria. The development of a cost-efficient natural fiber with unique biocompatibility has been the subject of keen interest.[168,169] In this section, we will discuss multifunctional fibers based on materials derived from wood.

3.1.1. Mechanically Strong Fibers. The CNF and CNCs are well known for their excellent mechanical strength. Naturally derived nanocellulose is a remarkable emerging nanomaterial because of its extraordinary mechanical properties, combining a high stiffness of up to 140 GPa and expected tensile strength on the order of GPa with a low density of 1.5 g/cm^3. Fibers with only cellulose fibers or with nanocomposites containing poly(vinyl alcohol) (PVA), poly(ethylene oxide) (PEO), poly(methyl methacrylate) (PMMA), PAN, and alginate have been developed, which can be produced by wet spinning and electrospinning methods.[170−178]

Figure 22a outlines the preparation of microfibers by drying a CNF hydrogel strand extruded into a coagulation bath of ethanol, dioxane, or tetrahydrofuran. Figure 22b is a scanning probe microscope (SPM) image of the CNF with a height profile along the red line included in the inset. The fibers have a high aspect ratio and asymmetrical rectangular sections.[171] The obtained fibers have stiffness values of 0.4 GPa and an ultimate tensile strength of 275 ± 14.7 MPa (Figure 22c). Higher values are expected when the alignment of cellulose nanofibers in the axial direction is improved by post drawing.

Nanocomposite fibers containing nanocellulose crystals or nanofibers as reinforcing material components have also been demonstrated.[170,179,180] Figure 22d and 22e shows optical

DOI: 10.1021/acs.chemrev.6b00225
Chem. Rev. XXXX, XXX, XXX−XXX

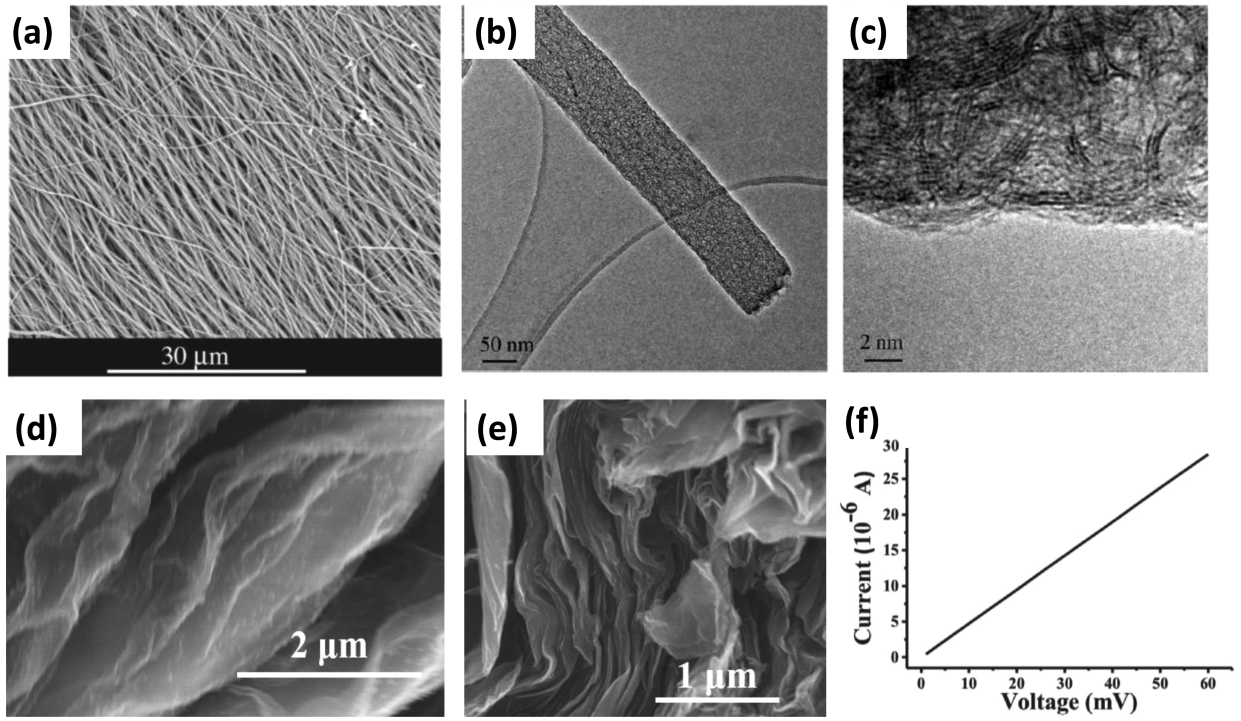

Figure 23. (a) SEM image of electrospun carbon nanofibers treated at 2200 °C. (b and c) TEM image of a carbon nanofiber treated at 2200 °C.[188] Reproduced with permission from ref 188. Copyright 2013 Elsevier. (d and e) SEM images of carbonized GO/NFC microfiber. (f) Typical $I-V$ curve of a carbonized GO/NFC microfiber with a fiber length of 35 mm and average diameter of 18 μm.[190] Reproduced with permission from ref 190. Copyright 2014 WILEY-VCH.

microscope images of a pure PVA fiber and a PVA fiber hybridized with 5% CNC. The existence of voids in the neat PVA fiber in Figure 22d decreases optical transparency and reduces the ductility of the fiber. With the introduction of only 5 wt % CNC, the optical transparency of fibers increases due to the suppression of void generation. Additionally, the tensile strength of the fiber increases to 1.89 GPa (Figure 22f). The Young's modulus continues to increase with CNC loading, but the elongation at break decreases. Extreme slippage and inhomogeneous shearing occur on highly localized fibrils separated by voids, which induces the deformation of neat PVA fiber. The dilapidated knot structure results in poor knot-pull strength. Conversely, the PVA/CNC 5% fiber maintains its original structure well when bent and has a high knot strength, which is attributed to the lack of voids and the interaction between PVA and CNC leading to a more homogeneous shear force and smoother chain slippage (Figure 22g and 22h). In summary, earth-abundant nanocellulose is a promising component toward super strong fibers, which can be produced via scalable wet drawing and gel-spinning processes.

3.1.2. Electrically Conductive Carbon Fibers. Electrically conductive fibers are essential for flexible electronics, particularly for wearable electronics. The low-cost, earth-abundant woody materials are attractive as precursors making high-performance fibers.[181−186] The cellulosic precursor fiber was first used by Thomas Edison in the 1880s as the basis for his revolutionary electric lamp filament.[187] Figure 23a is an SEM image of a carbon nanofiber electrospun from cellulose acetate and treated at 2200 °C.[188] The fiber maintains the same morphology and macroscopic alignment after carbonization. There is no skin-core structure observed in Figure 23b, in contrast to the structure of conventional polyacrylonitrile (PAN)- and cellulose-based carbon fibers.[189] The reason for this observation is that the nanoscale precursor overcomes the issues of incomplete oxidation of the core region during stabilization and the radial temperature gradient in the fiber during carbonization. Graphitic carbon is formed under 2200 °C (see Figure 23c). In addition to using pure cellulose as a precursor for carbon fiber, nanocellulose is also used in the hybrid nanocomposites to improve the electrical conductivity of carbon fiber. Microcarbon fibers are produced through the carbonization of well-aligned graphene oxide (GO)−nanocellulose hybrid fibers.[190] Without GO, the morphology of carbon derived from nanocellulose is microspherical; with the GO as template; however, the carbonized nanocellulose repairs defects in the reduced GO (rGO) and links the rGO together. Figure 23d shows the surface morphology of the microfiber, in which there are no microspheres observed. Figure 23e presents the cross section of the carbon fiber. The building blocks of the fiber after carbonization have excellent alignment. The GO-templated carbonization as well as the high alignment of building blocks along the fiber direction lead to a high electrical conductivity of 649 ± 60 S/cm (see Figure 23f). The conductive fiber was further evaluated for use as an anode in lithium-ion batteries. The conductive flexible fiber has great potential applications in wearable electronics and smart textiles. Replacing the expensive PAN precursor with abundant wood-derived biomaterials opens a broad avenue for low-cost conductive carbon fiber manufacturing.[191]

3.1.3. Other Functional Fibers. Optically transparent fibers have broad applications in optical transfer and biobased waveguides. The colloidal NFC gel can be used to fabricate fibers that are highly transparent; a property that is difficult to achieve in regular carbon fibers. Additionally, the mechanically robust macrofibers produced from nanocellulose precursors can be further functionalized by entrapping and immobilizing a multitude of functional molecules and fillers, polymers, or even

DOI: 10.1021/acs.chemrev.6b00225
Chem. Rev. XXXX, XXX, XXX−XXX

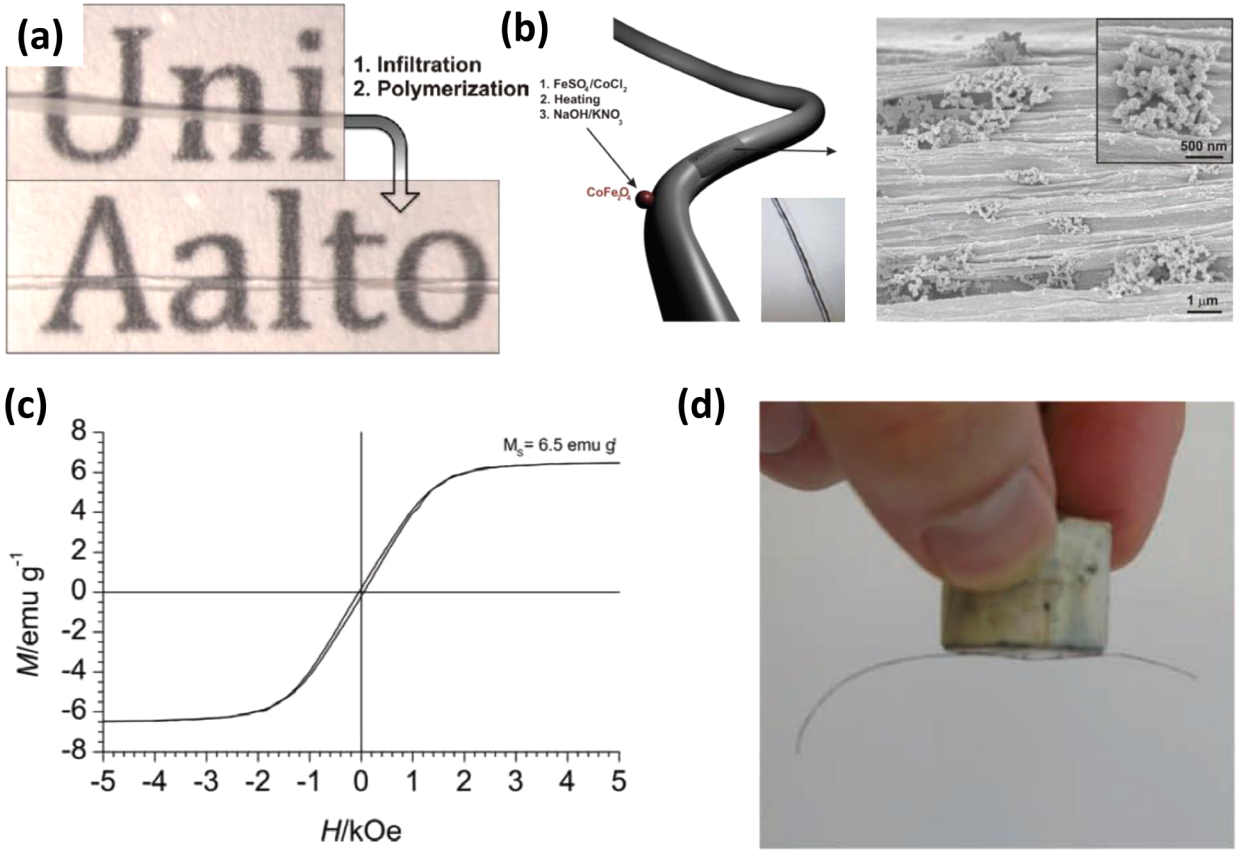

Figure 24. (a) Opaque macrofibers are made transparent by infiltration of a resin with a refraction index similar to the component nanocellulose. (b) Schematic of a magnetic hybrid fiber and SEM image of the fiber and magnetic particle morphology. (c) SQUID magnetization loop of the magnetic hybrid filaments. (d) External manipulation the magnetic filament with a small household magnet.[171] Reproduced with permission from ref 171. Copyright 2011 WILEY-VCH.

inorganic nanoparticles.[171] Figure 24a shows that the transparency of pure NFC microfibers increases with the infiltration with resin.[171] The refractive index of resin (1.53) is close to NFC (1.54−1.62), which effectively reduces the refraction index difference between the NFC and air within the cavities. As a result, light scattering at the air/cellulose interface is dramatically suppressed, leading to high fiber optical transmittance.

Methods to functionalize the microfiber generally include chemical modification and physical entrapment before or after fiber fabrication. Figure 24b shows a schematic of an inorganic/organic hybrid magnetic fiber obtained by attaching ferromagnetic cobalt ferrite nanoparticles to the fiber surface. The $CoFe_2O_4$ particles were synthesized by a simple aqueous coprecipitation reaction of $FeSO_4$ and $CoCl_2$ in the presence of an already prepared macrofiber. The addition of the $CoFe_2O_4$ particles causes the fiber to turn dark brown, as seen in the inset picture. SEM analysis reveals that the magnetic particles of average particle size 50−90 nm cluster on the fiber surface. The magnetization loop in Figure 24c shows that the modified fiber has a saturation moment of 6.5 emu/g. The magnetic fiber can be easily manipulated with a fingertip-sized magnet (see Figure 24d). The magnetic fiber is flexible and has great potential applications in intelligent textiles for magnetic shielding, magnetically actuated biocomposites, microwave technology, etc.

3.2. Multifunctional Membranes, Films, and Paper

3.2.1. Optically Transparent Paper and Its Modifications. Optically transparent paper exhibits better visual appearance, stronger mechanical strength, as well as higher barrier properties compared to common paper.[192,193] These unique properties enable the application of transparent paper in a variety of fields ranging from architecture and packaging to flexible electronics and energy-storage devices. Theoretically, paper made out of cellulose fibers should be optically transparent due to the colorless cellulose. In fact, most papers, such as graphic paper, art paper, rice paper, and copy paper, are apparently opaque. This phenomenon can be ascribed to the porous structure of paper that invokes light scattering at the fiber/air interface due to the mismatch refractive index between cellulose (1.5) and air (1.0).[194,195] To bring optical transmission to paper, the air existing in the porous configuration of paper must be removed as much as possible by mechanical or/and chemical approaches.

Cellulose fibers with various fiber dimensions are able to fabricate transparent papers by careful structure designs (Figure 52a).[58,196,197,17] Transparent paper can be developed by impregnating opaque paper into transparent materials (for example, oil, resin, wax), partially dissolving fiber surface, employing cellulose solution, or using intensively mechanically treated wood fibers followed by a process of supercalendering or impregnation to further improve the light transmission.[198−203] Here, we focus on three types of transparent papers: transparent paper with microsized wood fibers, transparent paper with nanoscale fibers, and transparent paper with dissolved cellulose.

Transparent paper fabricated by microsized wood fibers has been developed for over 150 years, and many manufacturing

DOI: 10.1021/acs.chemrev.6b00225
Chem. Rev. XXXX, XXX, XXX−XXX

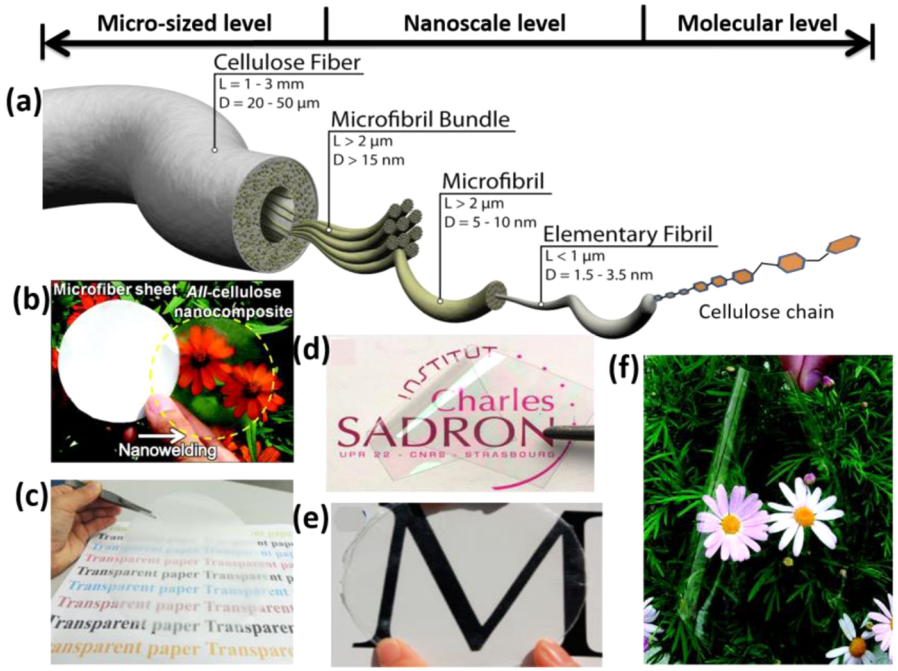

Figure 25. Various transparent papers made of cellulose materials with dimensions from the macro- to the molecular level. (a) Hierarchical configuration of wood fiber.[17] Reproduced with permission from ref 17. Copyright 2013 American Chemical Society. (b) Transparent paper prepared by using welding of wood microfibers.[201] Reproduced with permission from ref 201. Copyright 2011 American Chemical Society. (c) Transparent paper made of TEMPO-oxidized microscopic wood fibers by vacuum filtration.[204] Reproduced with permission from ref 204. Copyright 2014 American Chemical Society. (d) Transparent paper obtained by layer-by-layer assembly of NFC.[222] Reproduced with permission from ref 222. Copyright 2015 American Chemical Society. (e) Transparent paper made of NFC by a vacuum filtration.[219] Reproduced with permission from ref 219. Copyright 2013 American Chemical Society. (f) Transparent paper fabricated by casting cellulose solution on substrates.[220] Reproduced with permission from ref 220. Copyright 2011 American Chemical Society.

techniques were used on an industrial scale. Unfortunately, these transparent papers demonstrated a light transmission of <80%. Yousefi et al. proposed a welding method to prepare transparent paper made of cellulose microfibers. Filter paper with an optical transmittance of 0.3% at a wavelength of 800 nm was immersed into ionic liquid 1-butyl-3-methylimidazolium chloride (BMIM-Cl) at a temperature of 85 °C for diverse times spanning from 5 min to 8 h, followed by a step of extracting BMIMCl using methanol and then drying.[201] The obtained paper exhibited a maximum transparency of 76% at 800 nm (see Figure 25b). However, the optical transmittance is still unsatisfied for optoelectronic applications. Fang and colleagues illustrated a transparent paper with a total optical transmittance of >90% by using cellulose nanofibers to fill the voids of paper made of cellulose microfibers.[195] Through this method the paper achieved a desirable transparency. However, the fabrication process is time consuming. Hence, Fang et al. made a further step toward efficient manufacturing of transparent paper.[204] Wood pulp was first pretreated to modulate the fiber morphologies by TEMPO oxidation system in aqueous solution, and the TEMPO-oxidized wood fibers tend to display a higher fine content, shorter fiber length, yet easier collapse of fiber hollow structure than original wood fibers, thereby facilitating the follow-up sheet forming of dense fibrous network that suppresses backward light scattering. As a consequence, transparent paper with a light transmittance of >90% was prepared in less than 1 h (see Figure 25c).[204]

As the disintegration of cellulose nanofibers from wood fiber by mechanical treatments was achieved in the 1980s,[205,206] transparent paper made of CNFs has garnered particular attention over the past decade due to its excellent flexibility, superior surface smoothness, outstanding optical transparency, strong tensile strength, prominent gas barrier properties in dry conditions, and low coefficient of thermal expansion (CTE).[207−214] These unique properties enable nanopaper to be a promising substrate candidate for "green" optoelectronics. CNC and CNF are two types of cellulose nanofibers widely used to prepare nanopaper.[215,193] Nanopaper made of pure CNC is highly transparent but brittle due to the rod-like shape and high crystallinity; hence, plasticizing agents, such as glycerol, were added into CNC dispersion.[216] In comparison with CNC, CNF is much more suitable to prepare nanopaper with desirable properties because it has a higher aspect ratio, relatively lower crystallinity, and more flexibility.

Nogi et al. first reported the fabrication of nanopaper using CNF by vacuum filtration, which has a maximum transmittance of 71.6% at 600 nm.[208] A variety of literature reports regarding nanopaper have since been reported in the scientific community.[217−221] Figure 25d is an image of a free-standing CNF film built from a PVAm (cationic poly(vinyl amine)) solution at pH 10.5 by "layer-by-layer" assembly; this nanopaper has an optical transmittance of over 85% in the visible spectra and outstanding flexibility.[222] To enhance the optical transmittance, TEMPO-oxidized CNF was used to prepare nanopaper, demonstrating an excellent light transmittance up to 90% (see Figure 25e). This enhanced transparency can be contributed to the smaller fiber width and narrower fiber width distribution of TEMPO-oxidized CNF compared to other CNFs. Despite the unique properties of nanopaper, the low dewatering performance of CNF suspension restricts its industrial application. VTT in Finland and Oji Holding Corp. in Japan have separately set up a pilot line to produce nanopaper in large scale; although a small

DOI: 10.1021/acs.chemrev.6b00225
Chem. Rev. XXXX, XXX, XXX−XXX

roll of nanopaper was displayed in their presentation, no commercial nanopaper is currently on sale.

Regenerated cellulose was used to prepare transparent paper (regenerated cellulose film, RCF) at the beginning of 20th century.[223] Wood fiber was first dissolved in cellulose solvents, such as NaOH/CS_2,[224] ionic liquids,[225−229] *N*-methylmorpholine-*N*-oxide (NMMO),[223] and alkali/urea solution,[230−232] to free the cellulose chains from the cell wall. The obtained cellulose solution was then coated onto a substrate or extruded through a slit into the coagulation solution to prepare the RCF, followed by several steps of water washing to remove surplus solvents. Recently, great attention has been paid to the dissolution of wood using economical and environmentally benign cellulose solvents. To this end, Zhang's group has developed an alkali/urea low-temperature aqueous system to efficiently dissolve wood pulp. Figure 25f shows the clear and transparent appearance of RCF using cellulose solution produced by an alkali/urea solution. RCF presents a transmittance of ∼90% in the visible region that matches the appearance of plastics, but its mechanical strength and CTE are considerably lower than nanopaper and transparent paper with microfibers due to the destruction of the crystalline regions.[220]

Materials, such as alkyl ketene dimer (AKD),[211,221] resins,[202,233] nanoclay,[234,235] and graphene,[236] are employed to enhance the intrinsic properties of transparent paper. As we know, cellulose is inherently hygroscopic, which will deteriorate the performance of transparent paper when exposed to moisture. Yang et al. modified the hydrophobicity of RCF by immersing it into AKD solution widely used in papermaking industry. With a 0.1% AKD content of RCF, the water contact angle reaches 110°. In addition, Yano et al. attempted to improve the water resistance of transparent paper by dipping opaque paper into transparent resins (epoxy or acrylic resin) having a refractive index similar to cellulose.[237−239] The final paper was not only transparent but also exhibited excellent water-resistant performance. Platelets (such as nanoclay and graphene) were added into transparent paper to improve its barrier properties, tensile strength, conductivity, and heat resistance while maintaining prominent light transmission.

3.2.2. Mesoporous Membrane with Tailored Porosity. Although the fast advance of synthetic polymers is well known, cellulose and its derivatives still play an important role in the fabrication of various mesoporous membranes (pore size 2−50 nm) for separation and purification applications because they possess high hydrophilicity, good solubility in a wide variety of solvent systems, affinity for proteins, easy chemical modification, and low cost.[240] Cellulose can be dissolved in various solvents, such as MMNO monohydrate solution, to prepare cellulose membrane for gas separation. Cellulose acetate is also cheap, commercial, and environmentally benign material for preparing various membranes. In general, it was dissolved in acetate acid/water solution followed by a wet phase inversion approach to prepare the membranes. The pore size of these membranes can be tuned by altering the weight ratio of water to acetic acid.

Chu's group initially proposed a variety of filtration membranes for water purification using cellulose nanofibers over the past 5 years because of their unique properties, such as small diameter (5−10 nm), easy surface functionalization, good mechanical performance, and prominent chemical resistance. By developing different structures, consisting of asymmetric layers of nonwoven fibers with diverse diameters, mesoporous membranes with tailored pore sizes were presented for nanofiltration and microfiltration, respectively. Mesoporous membranes for microfiltration were fabricated by infusing cellulose nanofibers into the electrospun polyacrylonitrile (PAN) nanofibrous scaffold (Figure 26a), and the mesoporous

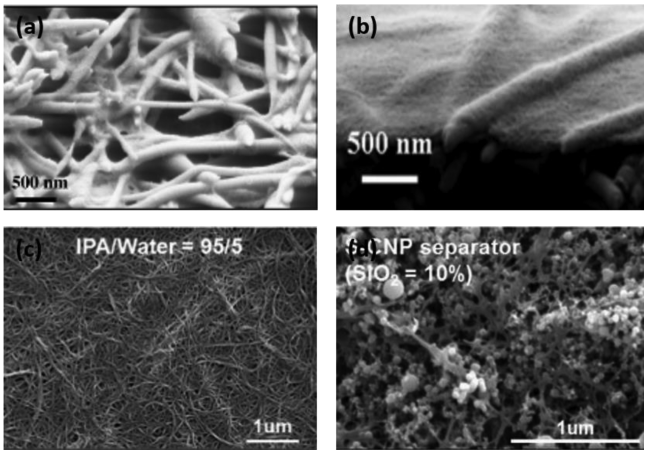

Figure 26. Various mesoporous membranes. (a) Cross-sectional SEM image of cellulose nanowhisker-infused PAN electrospun nanofibrous scaffold. (b) Top view SEM image of thin-film nanofibrous composite membrane with cellulose nanofiber barrier layer.[241] Reproduced with permission from ref 241. Copyright 2011 The Royal Society of Chemistry. (c) SEM photo of cellulose nanofiber paper-derived separator (IPA/water = 95/5).[243] Reproduced with permission from ref 243. Copyright 2012 The Royal Society of Chemistry. (d) SEM image of cellulose nanofiber paper-derived separator (SiO_2 = 10%).[245] Reproduced with permission from ref 245. Copyright 2013 Elsevier.

membranes for nanofiltration were prepared by coating a thin layer of cellulose nanofibers on the top of the electrospun PAN nanofibrous scaffold (Figure 26b).[241] These mesoporous membranes with cellulose nanofibers not only exhibited a high retention and permeation flux but are also energy saving, antifouling, and durable.[241] In spite of the prominent properties of these mesoporous membranes, their capacity and lifetime must be enhanced when they were used for virus removal.

In addition, mesoporous membranes prepared from cellulose or its derivatives demonstrate their potential application in lithium-ion battery separators in place of the currently, widely used petroleum-based polyolefin separators due to their unique properties, such as renewability, thermal stability, relatively lower cost, and good electrolyte wettability.[242−244] Kuribayashi first used fine fibrillated cellulosic fibers (diameter 0.5−5.0 μm) to produce mesoporous membranes with pore diameters in the range 10−200 nm for lithium-ion batteries.[242] Chun et al. proposed a mesoporous membrane made of CNF for lithium-ion battery separator by a papermaking process (Figure 26c).[243] Cellulose nanofibers were first dispersed into a mixture of isopropyl alcohol (IPA) and water to prepare CNF suspension that was then filtrated into paper in a vacuum condition. The porous structure of NFC film was fine tuned by altering the volume ratio of IPA to water in the CNF suspension. As the IPA content increased, the CNF mesoporous membrane tended to exhibit a higher porosity. Kim and colleagues made an additional step to control the porous structure of CNF film by incorporating colloidal SiO_2 nanoparticles into a CNF fibrous network as a disassembling agent. As we can see from Figure 26d, silicate was evenly distributed in the CNF matrix. The pore size of SiO_2/CNF mesoporous membrane is rationally tuned by varying the SiO_2 content in the CNF suspension.[245]

DOI: 10.1021/acs.chemrev.6b00225
Chem. Rev. XXXX, XXX, XXX−XXX

Utilizing electrospinning and dip-coating techniques to fabricate a novel cellulose-based composite nonwoven separator for lithium-ion batteries was demonstrated by Zhang et al.[246] Cellulose acetate was dissolved into 2:1 DMAc/acetone mixture with a volume ratio of 2:1 at a concentration of 15% by weight. The solution was then electrospun into a membrane and dried under vacuum at 70 °C for 8 h, followed by a dipping process of PVDF to reduce the pore size of membrane and increase the mechanical properties. Cellulose-based separators may be a good candidate for lithium-ion batteries; however, several issues should be resolved before they can enter into the commercial market, for example, relatively lower tensile strength and the hydrophilicity of cellulose.

Nanopaper fabricated from TEMPO-oxidized cellulose nanofibers was recently used to separate molecules or particles with a molecular weight of some hundreds to thousands of Daltons from an organic solvent. The results showed that the diameter of cellulose nanofibers primarily contributed to the permeability and pore dimension of the nanopaper and that tailored membrane performance can be achieved by modifying the nanofiber diameter.[247]

3.2.3. Photonic Film with CNC. CNC is a rigid and rod-like cellulose crystallite that behaves as a chiral nematic liquid crystal.[248,249] At dilute concentrations, CNC are randomly dispersed in an aqueous solution (isotropic phase) and appear as spheroids. As the CNC suspension reaches a critical concentration, the randomly oriented CNCs are inclined to self-assemble into chiral nematic ordered structures (anisotropic phase), presented by the appearance of a "fingerprint" pattern observed by polarized optical microscopy. This phenomenon widely exists in rod-like nanomaterials, such as DNA fragments,[74,250] tobacco mosaic viruses,[251] and crystallites obtained from polysaccharides,[252] and is ascribed to the favorably excluded volume interactions resulting in higher packing entropy compared to the homogeneous configuration.[74]

It was not until 1992 that the chiral nematic phase of CNC was discovered.[252] Since then Gray and co-workers showed an exciting finding that the chiral nematic ordering organization of CNC suspensions could be retained in solid film after full water evaporation displaying iridescent color under polarized light.[253] The chiral nematic configurations are 1D photonic crystals that can change refractive index periodically in one, two, or three dimensions, resulting in the selective diffraction of certain wavelengths of light.[254] For a chiral nematic structure, the wavelength of reflected light depends on the refractive index of the substance and the pitch of chiral nematic structure.[255] Figure 27a displays the schematic of the chiral nematic structure in CNC film, and P/2 represents the half-helical pitch.[256] As the half value of the pitch of the chiral nematic structure matches the wavelengths of visible light, the CNC film presents iridescence.

CNC film, indicative of a chiral nematic phase, exhibits unique and tunable photonic properties that are of interest for reflectors, security purposes, coloration, and sensors. Nevertheless, the chiral nematic structure of sulfated CNCs in iridescent film is not stable due to the easy redissolution of CNC in water, which restricts the utilization of iridescent CNC film with excellent photonic properties in various areas. Parameters, such as ionic strength, temperature, suspension concentration, and exposure to magnetic field, may influence the chiral nematic structure of CNC film. Several methods have been investigated to perpetuate the chiral nematic arrangement of CNC. Tatsumi and colleagues mixed the CNC suspension with poly(2-hydroxyethyl methacrylate) (PHEMA) in an aqueous 2-hydroxyethyl methacrylate

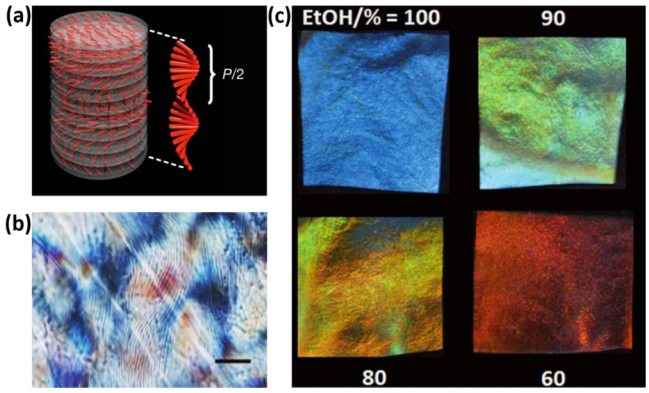

Figure 27. (a) Schematic of the chiral nematic ordering structure in CNC film, P/2 denotes the half-helical pitch.[256] Reproduced with permission from ref 256. Copyright 2010 Nature Publishing Group. (b) Polarized optical image of hot-pressed film of PHEMA-CNC_{aniso} (scale bar 50 μm).[257] Reproduced with permission from ref 257. Copyright 2012 American Chemical Society. (c) Sensing performance of mesoporous photonic cellulose soaked in EtOH/H_2O at different ratios.[258] Reproduced with permission from ref 258. Copyright 2014 WILEY-VCH.

(HEMA) monomer solution.[257] Through polymerizing HEMA in diverse phase situations of blending suspensions, three types of polymer composite films were obtained from the isotropic phase, anisotropic phase, and embryonic nonseparating mixture: PHEMA-CNCiso, PHEMA-CNCaniso, and PHEMA-CNCmix, respectively. As shown in Figure 27b, PHEMA-CNCaniso exhibits much more obvious fingerprint texture than that of PHEMA-CNCiso due to its longer pitch.[257]

Moreover, Micheal and colleagues developed a two-step synthesis to yield mesoporous photonic cellulose films (MPCFs) with a stable chiral nematic structure.[258] First, the mixture of urea formaldehyde precursor and CNC in aqueous solution was dried at ambient conditions to form chiral nematic composite films, followed by a heating curing processing. Second, the UF within CNC-UF composite materials was eliminated by alkaline treatment to achieve MPCFs with stable chiral nematic order. The prepared MPCFs have striking sensing performance to polar solvents. As the weight ratio of ethanol to water varies, the visible color of MPCF is changed from blue in pure alcohol to red in pure water due to the variation of helical pitch upon swelling (see Figure 27c). This change can be detected by UV−vis or circular dichroism (CD) spectroscopy, which may provide guidance for development of new sensors.

3.2.4. Other Multifunctional Papers. The intrinsic performance of cellulose and the hierarchical configuration of wood fibers are primarily due to various properties of the aforementioned paper, membranes, and films, for example, tailored optical properties, strong mechanical strength, and tunable porosity. With increasing demand in advanced materials for high-tech applications, these intrinsic properties of paper, however, cannot fulfill the requirements in these areas. Hence, to extend the utility of paper in high-tech fields, the original properties of paper should be enhanced or novel functionality should be introduced into paper. Plenty of organic and inorganic conducting, semiconducting, dielectric materials, as well as stimulus-responsive functional materials (magnetic nanoparticles,[259,260] carbon dots,[261] semiconductor nanocrystals,[262,263] metallic nanoparticles,[264] bioactive molecules,[265−267] polymer[268]) have emerged to meet the increasing demand from high-tech areas in the past several decades. Moreover, paper, well

DOI: 10.1021/acs.chemrev.6b00225
Chem. Rev. XXXX, XXX, XXX−XXX

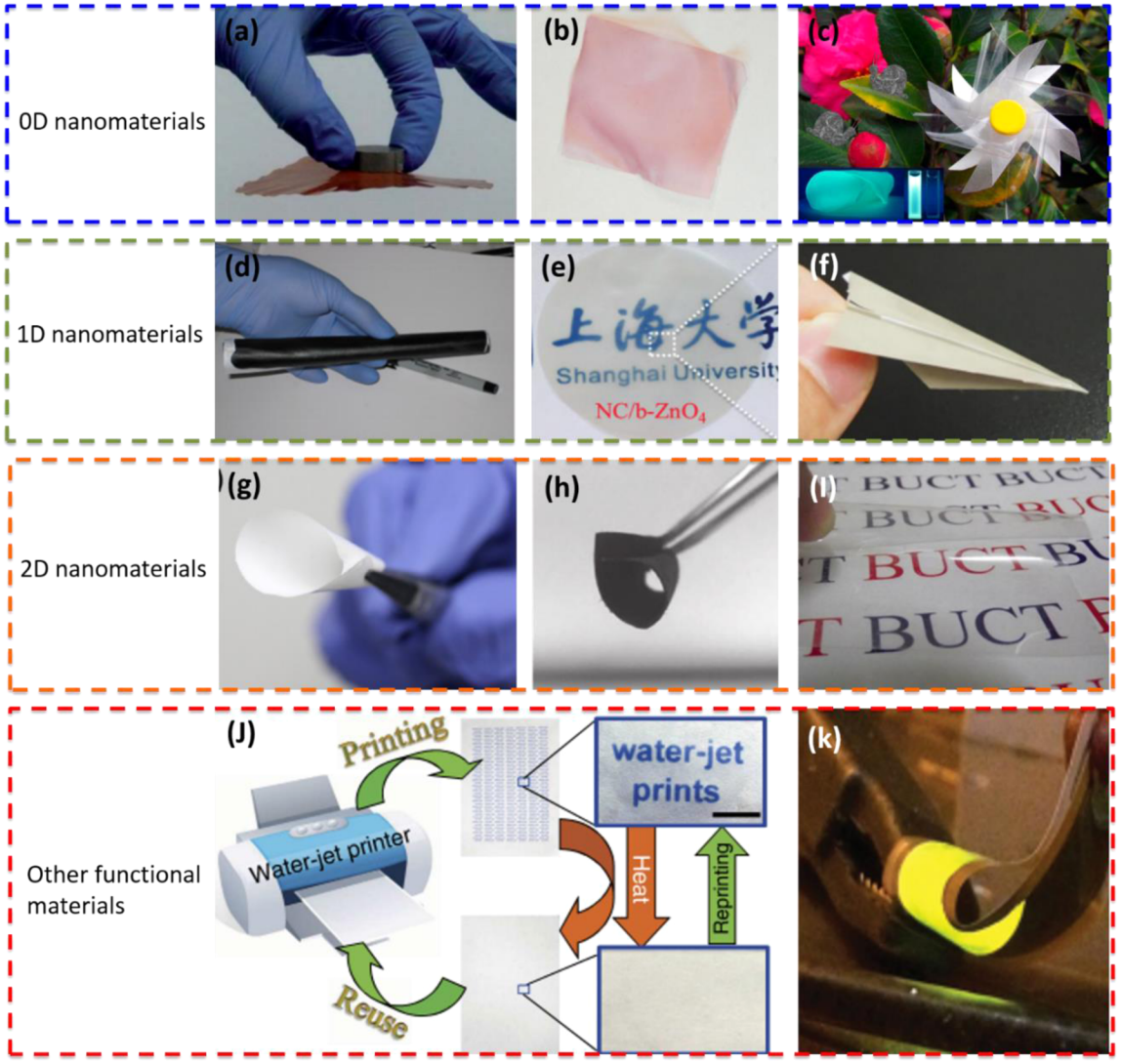

Figure 28. Multifunctional papers with 0D nanomaterials: (a) transparent and magnetic nanopaper with ferromagnetic nanoparticles.[281] Reproduced from ref 281 with permission from The Royal Society of Chemistry. Copyright 2013. (b) Antibacterial and fluorescent nanopaper with silver nanoclusters.[282] Reproduced with permission from ref 282. Copyright 2011 WILEY-VCH. (c) Luminescent nanopaper with ZnSe QD as a filler; multifunctional papers with 1D nanomaterials.[286] Reproduced with permission from ref 286. Copyright 2015 American Chemical Society. (d) CNTs-coated conductive paper.[273] Reproduced with permission from ref 273. Copyright 2009 National Academy of Sciences, U.S.A. (e) UV-blocking transparent nanopaper.[289] Reproduced from ref 289 with permission from The Royal Society of Chemistry. (f) Silver nanowire-embedded nanopaper. (g) Thermal conductive paper with boron nitride.[275] Reproduced with permission from ref 275. Copyright 2014 American Chemical Society. (h) Graphene−cellulose paper.[292] Reproduced with permission from ref 292. Copyright 2011 WILEY-VCH. (i) Layered double hydroxide/cellulose acetate hybrid paper.[278] Reproduced with permission from ref 278. Copyright 2014 WILEY-VCH. Other multifunctional papers: (j) rewritable paper.[297] Reproduced with permission from ref 297. Copyright 2014 Nature Publishing Group. (k) Light-emitting paper.[300] Reproduced with permission from ref 300. Copyright 2015 WILEY-VCH.

known as an inexpensive, flexible, biodegradable, light, earth-abundant, conveniently processable, and chemically active material, has been considered as an ideal platform for energy-storage devices,[269−273] electronic devices,[274−276] food packaging,[277,278] and security.[279,280] Through integrating these emerging functional materials with paper by coating, printing, dipping, blending, printing, or in-situ synthesis, and so on, the inherent properties of paper can be reinforced such as mechanical, optical, barrier, and dialectical properties. Even more important, novel functionality, such as electrical, magnetic, catalytic, anticounterfeiting, and chemical performance, is incorporated into paper. These enhanced or novel properties enable paper to novel uses in a variety of fields. Herein, four types of multifunctional papers and their latest advances are depicted in detail on the basis of the dimensional size of functional materials (zero-dimensional (0D) nanomaterials, one-dimensional (1D) nanomaterials, two-dimensional (2D) nanomaterials, and other functional materials.

Zero-dimensional nanomaterials refer to nanocluster materials and nanodispersions and are made of metals, semiconductors, and oxides. Magnetic nanoparticles, silver nanoclusters or nanoparticles, and diverse quantum dots (QD) are extensively explored to endow the paper with novel functionality, extremely expanding the application scope of paper. Magnetic nanomaterials have been extensively studied for data storage, purification/filtration, electronic device, and biomedical applications, etc. Generally, there are two ways to impart magnetic performance to paper. One involves embedding magnetic

DOI: 10.1021/acs.chemrev.6b00225
Chem. Rev. XXXX, XXX, XXX−XXX

nanoparticles into cellulose fibers network of paper; another is related to the in-situ synthesis of magnetic nanoparticles at the surface of cellulose fibers within the paper. Li et al. proposed a transparent, flexible, and strong magnetic nanopaper by immobilizing ferrimagnetic nanoparticles with a diameter of 20 nm into a NFC network in an aqueous medium (see in Figure 28a),[281] showing a desirable candidate for mageto-optical applications. Directly dispersing ferrimagnetic nanoparticles into cellulose fibers is an easy process to prepare paper with magnetic properties, this method, however, is limited by the heterogeneous dispersion and low loading content of magnetic ferrite nanoparticles within paper. Berglund's group developed a single-step approach to fabricate magnetic NFC by in-situ precipitation of ferrimagnetic nanoparticles onto cellulose nanofibrils; the ferromagnetic nanoparticle-decorated NFC was used to prepare magnetized membranes with 60% uniformly dispersed nanoparticles.[259,260]

Silver nanoparticles exhibit surface plasmon resonance and antibacterial properties; as their size reaches very few atoms (silver nanoclusters), they will present unusual properties compared to bulk silver or even silver nanoparticles, for example, fluorescence. Díez et al. demonstrated a fluorescent nanopaper with antibacterial activity by simply dipping nanopaper into a silver nanoclusters solution (Figure 28b).[282] Moreover, metallic nanoparticles, such as silver, gold, copper, and platinum nanoparticles, can also be precipitated along their length of cellulose nanofibers by using a cationic surfactant cetyltrimethylammonium bromide (CTAB), which can be used to prepare functionalized nanopaper.[90]

QD designates nanocrystals made of semiconductor materials that consist of few atoms.[283,284] By embedding QD into cellulose matrix or anchoring QD on the hydroxyl group of cellulose fibers via coordination effects,[285] remarkable electrical and optical properties of paper were achieved. Figure 28c is a photo of ZnSe QD-decorated nanopaper, which not only has excellent flexibility and optical transparency but also exhibits prominent photoluminescence.[286] Recently, luminescent carbon nanodots (CD) have emerged as fascinating carbon nanomaterials for bioimaging, sensors, optical electronics, and energy conversion/storage devices due to their prominent physical, chemical, and optical properties. CD were partially functionalized with alkyl chains (CD-Ps) that make them easy to self-assemble into supra-CD in toluene.[287] Paper was then immersed into supra-CD contained in toluene. The self-assembled supra-CD could decompose as the appearance of water in the paper due to the water-induced properties of supra-CD and the paper exhibited an enhanced luminescence. In combination with water-jet printing technique, ink-free printing luminescent paper can be prepared for information storage and anticounterfeiting applications.

One-dimensional nanomaterials include carbon nanotubes (CNT), metallic nanowires, oxides, etc. One primary application of 1D nanomaterial is to improve the conductivity of paper. Hu et al. proposed a simple method to make common paper conductive by coating aqueous CNT dispersion on the surface of paper using a rod coating method (see Figure 28d).[273] This conductive paper possessed a sheet resistance of about 10 Ω/sq, which is lower than previous reports due to the effective removal of surfactant by capillary force caused by the porous structure of paper. Silver nanowires can also be used to prepare conductive paper. Preston et al. fabricated a highly transparent and conductive electrode (TCE) that has the potential to apply in solar cells.[288] Silver nanowires dispersed in ethanol first formed a random thin silver nanowires network at the surface of filter membrane with an average pore size of 0.45 μm by vacuum filtration, followed by transferring the thin silver nanowire network onto transparent paper. Through this simple transfer method a silver nanowire transparent conducting paper-based electrode was fabricated, which demonstrated a figure of merit of 300—the highest value in the existing solution-based TCE.

In addition to endowing paper with excellent electrical performance using metallic nanowires or carbon nanotubes, other 1D nanomaterials can be added to impart novel functionality to paper. Belt-like zinc oxide was also added into CNF suspension to prepare transparent paper with excellent UV-blocking properties (see Figure 28e),[289] which can be applied to the UV-blocking fields. Furthermore, silver nanowires with high aspect ratios were combined with CNF to improve the dielectric constant (k value) of nanopaper.[290] Only 2.48 vol % of silver nanowires within the nanopaper can effectively increase the k value from 5.3 to 726.5; moreover, the silver nanowire contained nanopaper presented prominent flexibility (see Figure 28f).

Two-dimensional nanomaterials, such as graphene, graphene oxide, MoS_2, and boron nitride (BN), have triggered great interest in the scientific community recently. Paper has a very low thermal conductivity of 0.03 W/mk, which is much lower than that of plastic (0.23 W/mk). For some applications, paper with good thermal conductivity is desirable due to the requirement of quick removing surplus heat produced by devices. Zhu et al. first exfoliated hexagonal BN powder in isopropanol alcohol by bath sonication.[275] The obtained BN was then mixed with NFC to get homogeneous BN/CNF suspension followed by vacuum filtration to fabricate BN/CNF paper with excellent thermal conductivity. As the content of BN reached 50%, the obtained paper presented a little higher thermal conductivity (145.7 W/mK) than that of aluminum alloy (130 W/mK) while maintaining the flexibility of paper (see Figure 28g).[275]

Graphene possesses superior electrical and mechanical properties; however, the pure graphene film presented a limited stretchable capability (normally lower than 6%); therefore, to extend its stretchability, Yan et al. prepared a three-dimensional macroporous nanopaper including crumpled graphene and nanocellulose that was embedded in stretchable elastomer matrix.[291] This stretchable nanopaper showed a maximum stretchability of 100% that is suitable for sensor applications. A graphene−cellulose paper was proposed by Weng et al. using vacuum filtration (see Figure 28h).[292] Graphene nanosheet suspension penetrated throughout the regular filter paper and filled the internal voids during the filtration. As a consequence, graphene nanosheets distributed uniformly in the 3D interwoven structure of filter paper and were strongly anchored to the surface of cellulose fibers by electrostatic interaction. The achieved graphene−cellulose paper demonstrated a low resistivity of 6 Ω cm, excellent mechanical stability, and good specific capacitance and power performance, which is suitable for a supercapacity application, such as an electrode.

Nanoclay, for example, montmorillonite,[277,293] layered double hydroxide (LDH),[294] and silicate,[295,296] were also incorporated into paper to improve its barrier and mechanical properties and fire retardancy, which could be potentially used in flexible electronics and food and drug packaging. Several approaches, such as water evaporation, filtration, layer-by-layer assembly, and coating, were utilized to prepare paper with tailored barrier, mechanical, and optical properties and fire retardant performance by modulating the nanoplatlets content in aqueous cellulose-based system. Figure 28i is the photo of a transparent and flexible film with excellent oxygen barrier properties

DOI: 10.1021/acs.chemrev.6b00225
Chem. Rev. XXXX, XXX, XXX−XXX

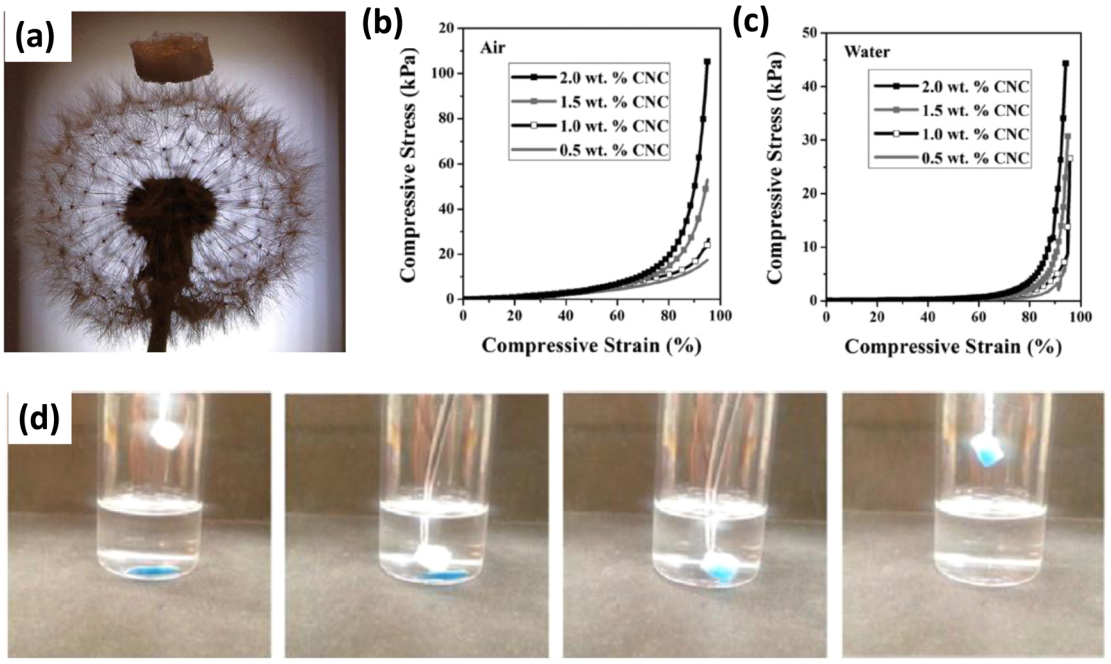

Figure 29. (a) Photograph of a piece of CNC aerogel standing on top of a dandelion flower. Compressive stress−strain curves of aerogels prepared from 0.5, 1.0, 1.5, and 2.0 wt % CNC suspensions from 0 to 95% strain in (b) air and (c) water. (d) Chronological images of an aerogel picking up water from a dodecane/water mixture. Water has been dyed with blue color for easier visualization.[311] Reproduced with permission from ref 311. Copyright 2014 American Chemical Society.

fabricated by a spin coating of cellulose acetate and layered double hydroxide alternatively, followed by a course of thermal annealing. Nacre-mimetic paper was prepared by mixing cellulose nanofibers and clay, followed by a paper-making procedure.[278] By modulating the content of clay, the nacre-mimetic paper exhibited tunable gas barrier, mechanical, optical, and fire-shielding properties. Synthetic silicate nanoplatelets were also blended with TEMPO-treated nanofibrillated cellulose to manufacture highly tough and transparent cellulose-based paper by a casting process. The paper had a maximum tensile strength of around 420 MPa, a Young's modulus of 14 GPa, and a strain-to-failure of 10%.[296]

Apart from 0D, 1D, and 2D nanomaterials, microscale functional materials were integrated with common paper to prepare functional paper with enhanced or novel characteristics. Recently, stimulus-responsive functional materials, such as dyes, transition metal complexes, and conjugated polymers, have been used to prepare multifunctional paper that can find its applications in rewritable paper, security paper, colorimetric sensing, and flexible electrothermochromic display. Recently, rewritable paper based on stimulus-responsive dyes or transition metal complexes has been garnered a great deal of attention, aiming to solve the environment and sustainability problem caused by large-scale production and usage of paper. Sheng et al. proposed a water-induced rewritable paper with dozens of write−erase cycles using hydrochromic dyes.[297] As shown in Figure 28j, the rewritable paper was printed by a commercial water-jet printer with a cartridge filled with sole water to produce words or images with good resolution, which is due to the color appearance of hydrochromic dyes induced by water, and the printed words and images were then erased by simple heating. In addition, a light-triggered rewritable paper consisting of hydroxyethyl cellulose (HEC), commercial redox dyes, and titanium oxide was demonstrated.[298] This rewritable paper has a rewritable time over 20 without significant loss of resolution, and its color changing mechanism is that redox dyes in paper become colorless when exposed to UV irradiation caused by the titanium oxide-assisted photocatalytic reactions and develop color when exposed to heat and oxygen. A rewritable paper based on the thermochromic mechanism of transition metal complexes was developed by Nagy et al. Through integrating thermochromic spin-crossover particles of $[Fe(NH_2trz)_3]Br_2$ or $[Fe(Htrz)_2(trz)]BF_4$ into paper by the conventional papermaking technique, heat-triggered paper with excellent rewritable performance was obtained.[299]

In addition to stimulus-responsive functional materials for rewritable paper, conjugated polymers, known as polydiacetylenes (PDAs), have been incorporated in paper for security purposes. PDAs exhibit many fantastic properties, such as facile synthesis, rich morphologies, as well as their stimulus-responsive color and fluorescence when exposed to environmental stimuli (heat, mechanical stress, chemical and biological interaction). A Korean research group attempted to prepare stimuli-responsive inks using four types of diacetylene monomers and four surfactants and then used these inks to print graphical art with sensing and display abilities on paper by a thermal inkjet office printer.[279] The PDAs printed paper exhibits a chromic transition stimulated by heat, UV irradiation, solvent, pH, and mechanical pressure, showing the potential application ranging from authentic identification systems for security printing to disposable chromogenic sensors. Lastly, light-emitting conjugated polymers can be deposited on paper by various solution-phase processing to prepare light-emitting paper. Edman et al. first demonstrated a flexible light-emitting paper using copy paper as a substrate (Figure 28k).[300] From the bottom to top, the light-emitting paper constitutes paper substrate, conducting anode layer, active layer, and cathode layer and displays a homogeneous light emission with a luminance of 200 cd/m^2 at a current conversion efficiency of 1.4 cd/A.

DOI: 10.1021/acs.chemrev.6b00225
Chem. Rev. XXXX, XXX, XXX−XXX

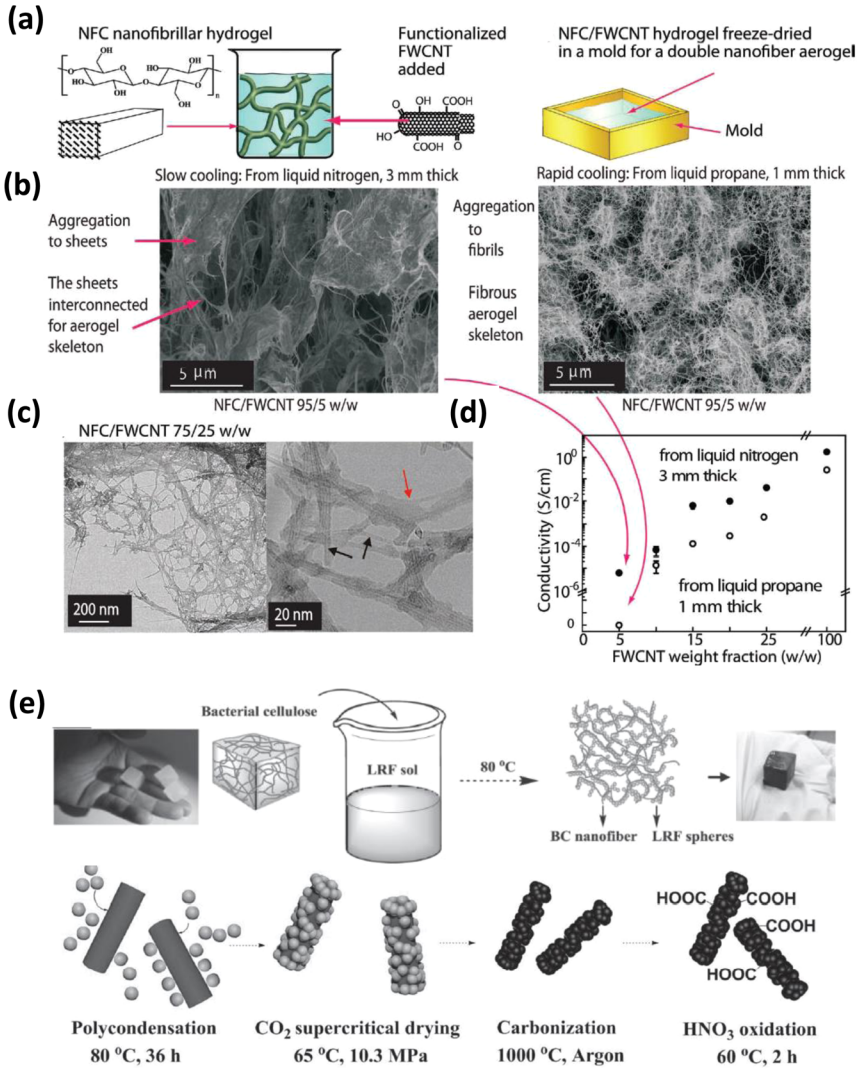

Figure 30. (a) Schematic to show the CNF/FWCNT aerogel preparation. (b) Freeze drying from liquid nitrogen leads to slow cooling and to sheet-like morphology due to aggregation of CNF and FWCNT, whereas freeze drying from liquid propane leads to quicker cooling and to fibrillary morphology. (c) TEM images of CNF/FWCNT 75/25 w/w aerogel; at high magnification the FWCNT (black arrow) can be distinguished from CNF (red arrow). (d) Conductivity vs different FWCNT weight fraction. Aerogel with sheet-like structure prepared by slow cooling has better electrical conductivity.[322] Reproduced with permission from ref 322. Copyright 2013 WILEY-VCH. (e) Process to prepare bacterial nanocelluose–lignin–resorcinol–formaldehyde (LRF) hydrogel and microstructure evolution of the carbon aerogel.[320] Reproduced with permission from ref 320. Copyright 2015 WILEY-VCH.

In the United States, the White House launched the Materials Genome Initiative (MGI) in 2011, aiming to help businesses discover, develop, and deploy new materials twice as fast in the United States; a variety of advanced materials would emerge resulting from MGI in the near future. Therefore, paper, well known as an earth-abundant, inexpensive, flexible, environmentally benign, and recyclable natural material with tunable properties, would be an ideal platform for incorporating with advanced materials to prepare multifunctional papers, extremely expanding their application scope from traditional areas to emerging fields.

3.3. Three-Dimensional Aerogels and Hydrogels

Aerogels are porous solid materials with extremely low density and low thermal conductivity derived from a gel through the replacement of solvent with air. The first aerogels were produced from silica gel, which are also most widely used today due to their high porosity, low density, and large surface area.[301] Aerogels made from inorganic materials are usually brittle, which limited their application when mechanical robustness is required. Aerogels made from natural polymer can overcome the fragility because of excellent flexibility, high Young's modulus (140 GPa), and good tensile strength (7.5 GPa). Shanyu et al. synthesized multiscale superinsulating silica-silylated nanocellulosic hybrid aerogel with robust mechanical properties promoted by adding nanocellulose as strengthening agent.[302] Meanwhile, the natural biopolymer, such as cellulose, is biocompatible, biodegradable, and easy to handle.[303−310]

3.3.1. Lightweight and Mechanically Robust Aerogel.

Both CNF and CNC aerogels are prepared from solvent-swollen gel networks by removing solvent, and the network structure is maintained through freeze drying and critical point drying.[302] Figure 29a shows a picture of aerogel prepared by a facial sol–gel method, consisting of mixing, freezing, solvent exchanging, and critical point drying the mixture of hydrazide-modified CNC ($NHNH_2$–CNC) and aldehyde-modified CNC (CHO–CNC).[311] The obtained aerogel has a density of 5.6 mg/cm^3

DOI: 10.1021/acs.chemrev.6b00225
Chem. Rev. XXXX, XXX, XXX−XXX

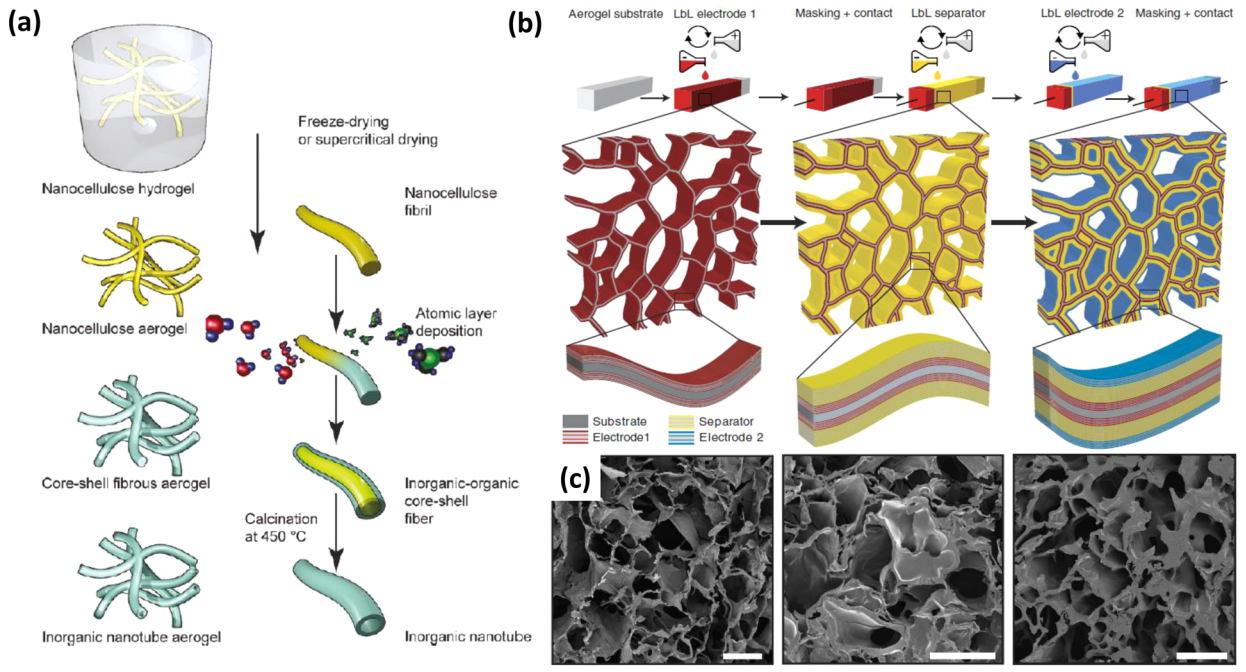

Figure 31. (a) Schematic to show the inorganic nanotube preparation procedure.[328] Reproduced with permission from ref 328. Copyright 2011 American Chemical Society. (b) Schematic of a 3-dimensional energy-storage device on cellulose aerogel. Electrode and separator are deposited with layer-by-layer methodology. (c) SEM cross-section image of the PEI/CNT electrode (left), PEI/CNT/separator (middle), and PEI/CNT/separator/copper hexacyanoferrate (right). Scale bars: 50 μm.[335] Reproduced with permission from ref 335. Copyright 2015 Nature Publishing Group.

and porosity of 99.6% with a bimodal pore distribution. The CNC aerogels are strong and compressible both in air and in water, Figure 29b and 29c. At 80% strain, the compressive stress of CNC aerogels prepared from 0.5, 1.0, 1.5, and 2.0 wt % CNC is 8.9, 11.6, 15.7, and 20.5 kPa, respectively. Aerogels prepared with higher initial concentrations exhibit higher compression stress than aerogels prepared with lower initial concentrations, and the aerogels exhibit lower compression stress in water than in air because the water acts as a plasticizer and softens the hydrogel by forming hydrogen bonds between water molecules and CNC and disrupts some CNC−CNC hydrogen bonding.[312] Furthermore, the aerogel has good shape recovery property and super absorption capacity. Figure 29d shows a series of images of an aerogel picking up water from a dodecane/water mixture. As an aerogel is immersed into the vial, it first absorbs dodecane; however, as it comes into contact with water, the dodecane is displaced less than 1 s. The ultralight and robust aerogel with excellent liquid adsorption properties with earth-abundant biopolymer derived from wood paves the way of functional nanomaterial for potential commercial applications.

3.3.2. Conductive Aerogel. Conductive carbon aerogels have broad applications in responsive electroactivity, pressure sensing, electromagnetic interference shielding, nerve regeneration, carbon capture, catalyst support, gas sensor, and so forth.[313−318] Generally, there are three ways to produce conductive nanocellulose aerogel: (1) chemical modification the surface of nanocelluose building block; (2) adding conductive filler into the aerogel skeleton, such as carbon nanofiber, carbon nanotube, graphene, polypyrrole, polyaniline, etc.;[316,319] (3) carbonization of the aerogel to flexible and highly conductive graphitized carbon.[320,321] Figure 30a is the schematic of conductive aerogel made from cellulose nanofiber hydrogel and functionalized few-walled carbon nanotubes, where cellulose hydrogel is the majority phase with ratios of CNF/FWCNT 100/0, 95/5, 90/10, 85/15, 80/20, 75/25 w/w. The high-speed mixer and ultrasonic treatment are applied for the preparation of well-dispersed homogeneous hybrid hydrogel.[322] The CNF/FWCNT hydrogels were freeze dried in a mold to a hydrogel. The cooling speed plays an important role of the aerogel morphology. Slow cooling in liquid nitrogen, boiling point of −196 °C, leads to sheet-like structures with micrometer lateral dimensions. A rapid cooling with less thickness leads to a dramatically different morphology, wherein the nanofibrillar network is mostly preserved upon freezing and sublimation of ice, see Figure 30b. Figure 30c displays the excellent interaction of FWCNT with CNF because of the attended hydroxyl group. The aerogel with sheet-like structure has higher electrical conductivity than the fiber-like structure because of the better percolation in both 2-dimensional aggregate sheets within the matrix and 3-dimensional aerogel overall volume (see Figure 30d). By incorporating the CNT and CNF into the aerogel the attractive features of both components are combined: good accessibility, excellent ductility, and high electrical conductivity, combining the best properties of both components even toward large-scale application.

Figure 30e shows a process to prepare flexible, highly graphitized carbon aerogels based on lignin/bacterial nanocellulose. Bacterial cellulose (BC) was impregnated with lignin−resorcinol−formaldehyde (LRF) solution, and the BC/LRF hydrogels are obtained through polycondensation of LRF. BC/LRF aerogel and carbon aerogel are subsequently obtained through supercritical drying and catalyst-free carbonization. The final carbon is highly graphitic and has core−shell structure, where the core is graphited BC and shell is graphited LRF. The carbon aerogel derived from BC/LRF has comparable mechanical deformation and recovery capability as CNT- or graphene-based carbon sponges, which are produced through a catalyst-assisted chemical vapor deposition method. These aerogels are usually produced in small scale, relatively expensive, and not environmentally friendly. Earth-abundant biomass-based

DOI: 10.1021/acs.chemrev.6b00225
Chem. Rev. XXXX, XXX, XXX−XXX

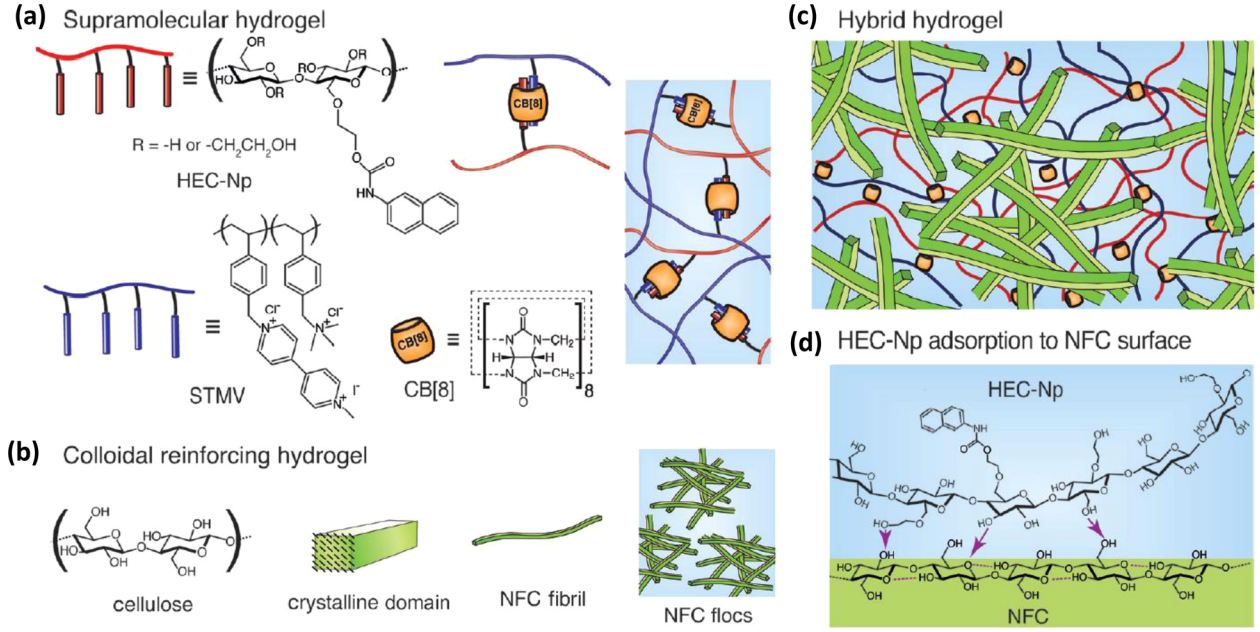

Figure 32. (a) Supermolecular hydrogel consisting of the first guest HEC-NP, the second guest STMV, and the host motif CB. (b) Colloidal reinforcing hydrogel made from NFC. (c) Hybrid hydrogel made from cross-linking the supermolecular and NFC. (d) HEC-Np adsorption to NFC surface via hydrobonding.[346] Reproduced from with permission ref 346. Copyright 2015 WILEY-VCH.

carbon aerogel features low cost, high scalability, and sustainability.

Aerogel made from native biopolymer fiber has superior flexibility and ductility. The scaffold of porous and vigorous aerogel made from native cellulose fiber opens new possibilities as host for organic and inorganic materials for various functionality. In addition to conductive aerogels, there are other functional aerogels, such as magnetic aerogels and thermally stable aerogels.[323−327] Magnetic nanomaterials have been investigated for biomedical, data storage, and devices applications.

3.3.3. Application of Aerogel. Aerogels have various applications in different areas. For example, aerogels are outstanding thermal and acoustic insulating materials in construction. A layer of transparent aerogel allows penetration of the sun's radiation to a building but prevents the generated heat from evaporating. Figure 31a is an example of an aerogel used to prepare inorganic nanotubes including zinc oxide, titanium oxide, and alumina oxide, which can be used in energy storage, sensors, absorbent, drug release, filtration, and so on.[328−334] Nanocellulose aerogel was used as a template for the deposition of inorganic materials via atomic layer deposition to form core−shell fibrous aerogel. The thickness of the shell can be controlled by the cycle numbers of the atomic layer deposition. An inorganic nanotube aerogel with excellent percolation is obtained by removing the cellulose template via calcination at 450 °C. A TiO_2 nanotube humidity sensor with relatively fast response times in the humidity region of 40−80% was demonstrated. Figure 31b shows a reversible, compressible, 3-dimensional supercapacitor with carbon nanotube electrode and a 3-dimensional hybrid battery with a copper hexacyanoferrate ion intercalating cathode and a carbon nanotube anode. The electrode and separator are deposited on the surface of an open cell aerogel with the layer-by-layer method.[335] The SEM images in Figure 31c show the gradual thickening of the pore walls when the first electrode, the separator, and the second electrode were added onto the aerogel. The high-porosity aerogel with an open structure guarantees a good accessibility for the deposition solution and makes it feasible to self-assemble a thin layer of functional material for the device. Furthermore, the whole device is bendable and compressible and can be made with arbitrary form factors. The design and concept presented here can be applied to other advanced functional materials and other diverse 3D devices.

3.3.4. Hydrogel Made from CNF and CNC. Cellulose-based superabsorbent hydrogels have a hydrophilic network with a high capacity for water uptake and are biodegradable, biocompatible, low cost, and renewable. There are different ways to prepare cellulose hydrogel. In general, there are two methods: (1) Chemical polymerization methods, mainly including aqueous solution polymerization, inverse phase suspension polymerization, and microwave irradiation polymerization; (2) Physical synthesis methods through hydrogen bonds, ionic bonds, or interaction between polymers and the emerging approach by rapid contact between the solid and the liquid interface.[336] A number of cellulose-based hydrogels have been either available commercially or in the process of development. Most of the applications are in the personal health care field, biomedical fields, water treatments, agricultural and horticulture, and the stimuli-response smart behavior applications.[337−345] Emma-rose et al. glue supramolecular (naphthyl-functionalized hydroxyethyl cellulose (HEC-Np), see Figure 32a) to the CNF colloidal nanoscale network (see Figure 32b) to bridge multiple length scales, see Figure 32c and 32d, and lead to significantly enhanced storage modulus values and improved maximum elastic yield values. This was promoted by the fast dissociation/association dynamics of the supramolecular-based cross-links in combination with the adsorption of hydroxyethyl cellulose component of the supramolecular hydrogel to the NFC nanofibers.[346] With the continuous research on cellulose-based hydrogel, the functionality will be modified and the application will be extended to various fields.

DOI: 10.1021/acs.chemrev.6b00225
Chem. Rev. XXXX, XXX, XXX−XXX

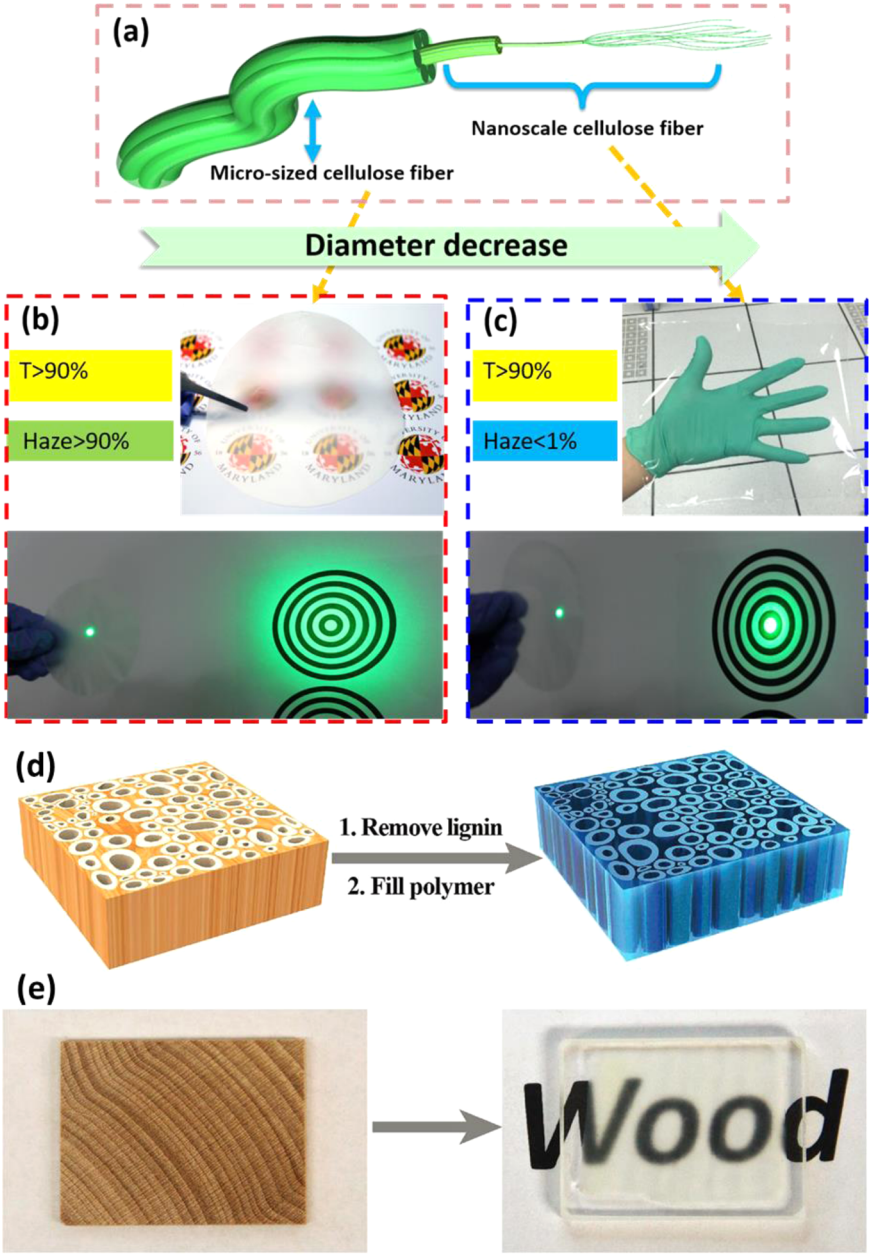

Figure 33. (a) Cellulose fiber with a diameter spanning from microsized to nanoscale. Reproduced from ref 348 with permission from The Royal Society of Chemistry. Copyright 2013. (b) Highly transparent paper with a high optical transmission haze: visual appearance (upper) and light-scattering behavior (bottom) of transparent and hazy paper. (c) Highly transparent paper with a low optical transmission haze: visual appearance (upper) and light-scattering behavior (bottom) of transparent clear paper. Reproduced from ref 349 with permission from The Royal Society of Chemistry. Copyright 2014. (d, e) Highly transparent wood composite. Reproduced with permission from ref 350. Copyright 2016 WILEY-VCH.

4. WOOD-DERIVED GREEN ELECTRONICS

4.1. Unique Properties of Cellulosic Biopolymers

4.1.1. Optical Properties. In general, optical properties of paper refer to brightness, color, fluorescent properties, gloss, formation uniformity, and so on, which are extremely dependent on its structure and chemical composition.[347] Numerous literature reports have focused on the aforementioned optical properties of paper over the past decades. However, reports regarding total light transparency and optical transmission haze in the visible spectra are still scarce and yet are of extreme significance for paper to partially replace traditional plastic films widely used as substrates for flexible and transparent electronics. Figure 33a is the schematic of the hierarchical structure of wood fiber; millions of cellulose macrofibrils/microfibrils are assembled into the main component of the cell wall of wood fibers.[348] According to the mechanism for making paper transparent, both macrosized wood fibers and cellulose microfibrils can be used to prepare paper with a high transparency of over 90% by specific methods, but for paper's optical haze, it is primarily relevant to fiber diameter and the structure, thickness, density, and surface roughness of paper. Zhu et al. investigated the factors that related to optical properties of paper made of cellulose nanofibers with a fiber diameter lower than 100 nm (nanopaper) and found out that fiber diameter and nanopaper's density have a significant influence on its total light transmission and optical haze.[348] These authors also simulated the electromagnetic scattering cross-section for fibers with diameters of 25

DOI: 10.1021/acs.chemrev.6b00225
Chem. Rev. XXXX, XXX, XXX−XXX

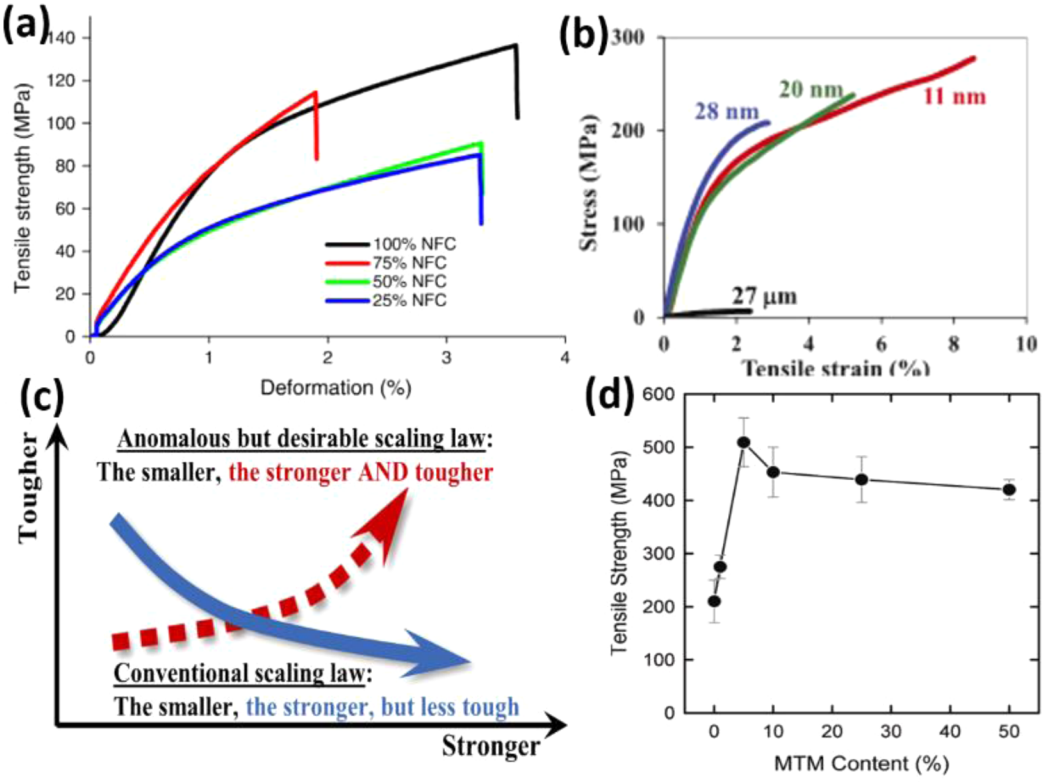

Figure 34. (a) Stress−strain curves of paper with different weight ratios of microfibers to NFC. Reproduced with permission from ref 353. Copyright 2014 Springer. (b) Stress−strain curves of nanopaper made of NFC with different fiber diameter and common paper. (c) Unconventional but desirable scaling law for the mechanical properties of nanopaper. Reproduced with permission from ref 355. Copyright 2015 National Academy of Sciences, U.S.A. (d) Tensile strength of transparent nanopaper with different MTM content. Reproduced with permission from ref 277. Copyright 2012 American Chemical Society.

and 50 nm, respectively, and the results showed that light-scattering behavior decreases dramatically as fiber diameter is decreased. Furthermore, reducing the surface roughness of nanopaper by polishing, lamination of transparent plastic, deposition of transparent resins, or inkjet printing of transparent resins could also increase its total optical transparency.[208]

As shown in Figure 33b, both the light transmittance and the optical transmission haze of obtained paper made of microsized wood fibers could be over 90% by rational structure design or using specific manufacturing methods. This paper exhibits an intensive light-scattering behavior (bottom photo in Figure 33a) that facilitates the enhancement of the light absorption of photovoltaic devices or the light extraction of OLED devices.[204] In contrast, paper comprised of cellulose nanofibers with a uniform and narrow fiber diameter distribution presents a transparency > 90% but an optical haze < 1%, which is similar to plastics (Figure 33c).[349] As we can see from the bottom image in Figure 33c, the nanopaper shows minimum light-scattering effects compared to the paper in Figure 33b. Cellophane made of cellulose or cellulose derivatives also shows an optical transmittance of ∼90% and a haze < 1%. The highly transparent paper with lowest light-scattering effect demonstrates its potential application in the field of displays. Moreover, the Bing group developed a strategy to fabricate highly transparent paper with tunable optical haze by simple blending cellulose nanofibers with TEMPO-oxidized microsized wood fibers.[349] Through this approach paper possesses a transmission haze ranging from 18% to 60% while maintaining a total transmittance of ∼90%. The thickness of paper has a significant influence on the optical transmission haze but no significant effect on light transmission when the density of paper is identical. Most recently, Hu's group successfully demonstrated a transparent wood composite. By removing colored lignin and filling the porous cellulose structure with refractive index matching polymer, the wood composite exhibits a high transmittance of up to 90%. It also displays enhanced mechanical property and excellent light-scattering ability. The readily achieved transparent wood composites can find many applications as structural materials where mechanical strength and optical appearance are both important (Figure 33d and 33e).[350]

4.1.2. Mechanical Properties. Mechanical properties of paper include tensile strength, elastic modulus, toughness, tearing strength, bursting strength, etc., and are of significance for its applications in various areas. In this review, we focus on the tensile strength, elastic modulus, and toughness of paper that are of great interest for green electronics and energy applications. Paper is a network of natural cellulose fibers held together by mechanical interlocking, electrostatic interactions, van der Waals forces, and hydrogen bonds.[351,352] Although the tensile strength and elastic modulus of a single wood fiber are 0.3−1.4 GPa and 14−27 GPa,[1] respectively, the actual mechanical strength of common paper is relatively low for high-tech use, because its strength is primarily dependent on the hydrogen-bonding strength of neighboring individual fibers.

To increase the hydrogen bonds within paper, mechanical treatments (refining, beating) of wood fibers or addition of strength additives (polyacrylamide, starch) into paper are used. Mechanical treatments are the widespread method to enhance the strength of common paper by improving the specific surface area of wood fibers that facilitates the formation of hydrogen

DOI: 10.1021/acs.chemrev.6b00225
Chem. Rev. XXXX, XXX, XXX−XXX

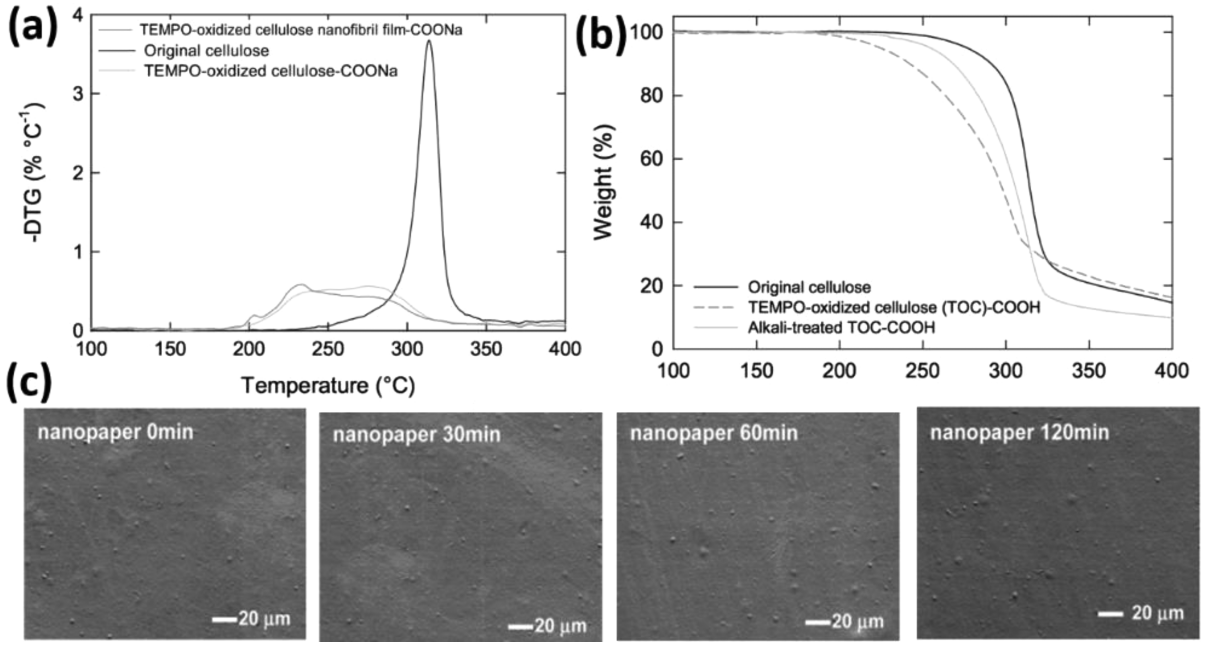

Figure 35. (a) Derivative thermogravimetric (DTG) curves of the original cellulose, TEMPO-oxidized cellulose (TOC) with sodium carboxylate groups, and TOC nanofibril film with sodium carboxylate groups. (b) TG curves of the original cellulose, TOC with free carboxyl groups of 1.68 mmol/g, and alkali-treated TOC with free carboxyl groups of 0.23 mmol/g. Reprinted with permission from ref 92. Copyright 2010 Elsevier. (c) Top view SEM images of nanopaper treated at a temperature of 150 °C for different times. Reproduced with permission from ref 210. Copyright 2013 AIP Publishing.

bonds between neighboring fibers. A research group tried to add CNF into regular paper as a paper additive to enhance its strength.[353] With the rise of CNF content in common paper, more hydrogen bonds were formed in the sheet that results in the sharp enhancement of the strength of paper (shown in Figure 34a). To completely improve the mechanical strength of paper, Schmied et al. utilized the nanometer-scale probing capabilities of the well-established AFM technique to explore the mechanical properties of individual fiber−fiber bonds on the nanometer scale and revealed that fibrils or fibril bundles play a pivotal role in fiber−fiber bonding, because they act as mechanical interlocks.[351]

Nanopaper made of cellulose nanofibers with 3.5−100 nm in width and hundreds of nanometers to several micrometers in length possess excellent mechanical properties, such as superior tensile strength, high elastic modulus, and excellent toughness, showing its potential as a strong and lightweight substrate for green electronics or as reinforcement materials for energy application. Sehaqui et al. studied the effects of the types of NFC and the porosity on the mechanical properties of nanopaper.[354] In comparison with nanopaper made of CNF, nanopaper with TEMPO-oxidized CNF has a higher tensile strength and higher toughness values for work-to-fracture, which is attributed to the smaller diameter of TEMPO-oxidized NFC compared to NFC.[102] Once in a while, higher porosity could reduce the modulus and tensile strength of nanopaper due to the reduced contact area for forming hydrogen bonds. Zhu et al. utilized wood fiber with a diameter of 27 μm, TEMPO-oxidized NFC with a width of 28, 20, and 11 nm, respectively, to prepare paper (Figure 34b).[355] The yield stress and the ductility increase as the fiber diameter decreases.[355] The toughness and strength of nanopaper increase simultaneously with the decrease of fiber diameter, which is an anomalous but desirable scaling law for engineering materials (Figure 34c). The surprising mechanical properties of nanopaper could be ascribed to reduced inherent defect domain and easy formation of strong interfibril hydrogen bonding.

Despite the high tensile strength and toughness achieved by nanopaper, its mechanical properties are still much lower than that of the cellulose fibers themselves that were used to prepare the paper. Nanocrystalline cellulose has a tensile strength of 7.5−7.77 GPa and an elastic modulus of 110−220 GPa.[1] However, the nanopaper exhibits a tensile strength of up to 300 MPa and a Young's modulus of up to 30 GPa,[356,357] which is much lower than that of nanocrystalline cellulose. Therefore, considerable effort has been made to enhance the mechanical properties of nanopaper. Wu et al. mixed TEMPO-oxidized cellulose nanofibrils in an aspect ratio of >200 with montmorillonite (MTM) nanoplatelets in an aqueous system.[277] With only 5% MTM content, the final nanopaper has a Young's modulus of 18 GPa and tensile strength of 509 MPa (see Figure 34d). Cold drawing was also applied to improve the mechanical performance of nanopaper by partially aligning the nanofibers within the nanopaper.[358] The obtained nanopaper exhibited maximum modulus and tensile strength of 33 GPa and 430 MPa, respectively. Tang et al. grafted poly(ethylene glycol) (PEG) on the surface of TEMPO-oxidized cellulose nanofibril to reduce friction while still retaining the adhesion between them.[359] The PEG-grafted cellulose nanofibrils were aligned through a stretching process followed by drying to produce a ribbon with oriented cellulose nanofibrils bearing PEG. This ribbon had a maximum tensile strength and modulus of 576 ± 54 MPa and 32.3 ± 5.7 GPa, respectively.

To summarize, downsizing the fiber diameter and aligning the fibers in the paper are two promising approaches to achieve paper with desirable mechanical properties. The technologies for efficiently disintegrating cellulose nanofibrils which are 3.5−5 nm in width from fiber walls are well reported, but we still lack effective methods to align the cellulose fibers within the paper,

DOI: 10.1021/acs.chemrev.6b00225
Chem. Rev. XXXX, XXX, XXX−XXX

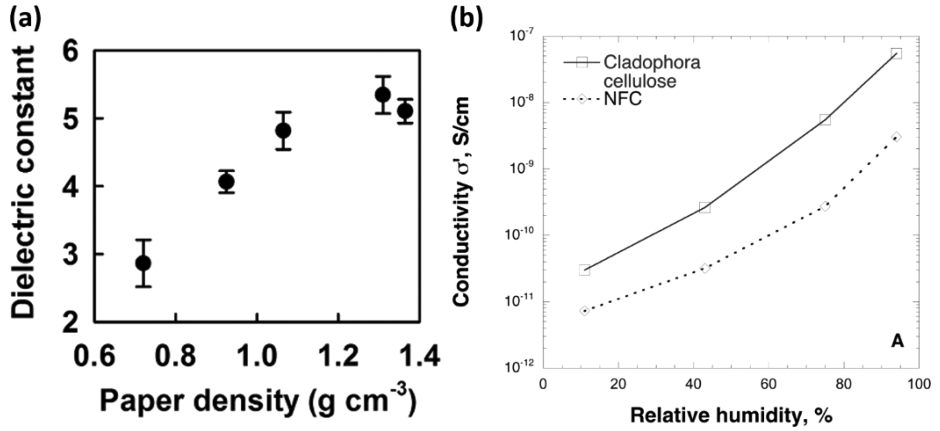

Figure 36. (a) Dielectric constant of nanopaper as a function of paper density (at 1.1 GHz). Reproduced with permission from ref 290. Copyright 2015 WILEY-VCH. (b) Conductivity versus relative humidity at <60 Hz for Cladophora cellulose and CNF using dielectric spectroscopy. Reproduced with permission from ref 367. Copyright 2015 American Chemical Society.

which limits further enhancement of the mechanical properties of paper.

4.1.3. Thermal Properties. Cellulose is a biopolymer that could decompose when exposed to high temperature. Hence, the thermal properties of paper should be considered when high-tech applications are considered. Here, we will discuss the thermal properties of paper in terms of thermal chemical degradation and CTE. Generally, native cellulose is quite thermally stable under a temperature of 300 °C. In some cases, especially for cellulose nanofibers, chemical modifications were inevitably used to treat wood pulp to achieve desirable properties, which could affect its thermal chemical degradation performance. Sulfuric acid hydrolysis and TEMPO oxidation are two effective approaches to prepare cellulose nanofibers with uniform and small diameter.[360] However, the introduction of carboxyl or sulfonic groups into cellulose chains would decrease the thermal decomposition temperature.[361] As shown in Figure 35a, the derivative thermogravimetric (DTG) peak temperature of TEMPO-oxidized cellulose is much lower than that of original cellulose.[92] Figure 35b demonstrated the increased onset of thermal decomposition temperature was observed for TEPMO-oxidized cellulose after alkali treatment.[92]

The crystalline cellulose has a CTE of ~0.1 ppm/k in the axial direction,[362,363] which is comparable to carbon fibers. Native cellulose nanofibers contain crystalline regions where the cellulose chains are arranged in a highly ordered structure and amorphous region that cellulose chains are disordered. Nanopaper with cellulose nanofibers shows a CTE of 8.5 ppm/k,[208] which is much higher than that of crystalline cellulose but lower than that of plastic (CTE, 20−100 ppm/k).[219] The low CTE of cellulose endows the paper with excellent thermal dimensional stability that is of significance for device fabrications (e.g., annealing procedures). Nanopaper with cellulose nanofibers obtained from alkali pretreatment and mechanical treatments retains the excellent dimensional stability of original cellulose. When the nanopaper was treated at a temperature of 150 °C, no obvious surface topography changes were observed with the increase of heating time (see Figure 35c).[210]

4.1.4. Refraction Index and Dielectric Constant. Pure cellulose has a reported dielectric constant (k) of 6−8.[364] In practice, dry common paper presents a typical k value of around 1.3−4 (at 1 MHz),[365] which is due to the porous structure of paper that contains an amount of air with a low k value of 1. The low k value of air would definitely result in a decrease of the dielectric constant of paper. Therefore, when paper was used as an insulating material for power transformers and cables, the voids in the paper should be filled with materials with a higher k value, such as oil, resin, water, and inorganic particles.[366] As shown in Figure 36a, the dielectric constant is almost linearly proportional to the density of the paper. Nanopaper made of cellulose nanofibers with a density of 1.3 g/cm^3 exhibits a k value of 5.3, which is higher than typical PET (k = 3.1), PEN (k = 3.4), and PI (k = 3.4) substrates.[290] Inorganic nanoparticles or metallic nanowires/nanoparticles were added into nanopaper to further improve the k value of final nanostructured paper. Inui et al. studied the addition of barium titanate ($BaTiO_3$) with a high k of 5000, silver nanoparticles, and silver nanowires into nanopaper, and results showed that the k value of these composites gradually increased with the increase of nanomaterials content.[290] The addition of silver nanowires may dramatically increase the k value of silver nanowires/cellulose nanofibers composite. The obtained nanopaper composite presents a k value of 726.5 when the content of silver nanowires in nanocomposite is only 2.48 vol %.[290] Bras et al. investigated the dielectric properties of CNF from wood and algae (Cladophora cellulose) and demonstrated that the solid-state properties of nanocellulose, such as the degree of crystallinity, porosity, the state of water, impurities, and water sorption properties, have a significant impact on the dielectric properties at varying frequencies. In comparison to CNF, Cladophora cellulose has a higher crystallinity and porosity but is less hygroscopic; however, as we can see from Figure 36b, the dielectric properties of CNF are higher than that of Cladophora cellulose because the free water is less tightly bound in Cladophora cellulose resulting in the higher mobility of ions in the sample.[367]

4.1.5. Barrier Properties. Water vapor transmission rate (WVTR) and oxygen transmission rate (OTR) were usually selected to evaluate the barrier properties of paper.[368] Common paper is a porous material that permits air and liquids to easily pass through. Nevertheless, superior barrier properties of paper are needed for its applications in packaging, flexible displays, and OLED. Hence, biopolymers (starch, protein, PVA, CMC, chitosan, sodium alginate, etc.) and synthetic polymers such as PE, PET, and polylactic acid (PLA) were generally coated on the surface of paper to improve its barrier properties. For some barrier coatings with hydrophilic performance, water-repellent agents must be added to reinforce their water resistance.

DOI: 10.1021/acs.chemrev.6b00225
Chem. Rev. XXXX, XXX, XXX−XXX

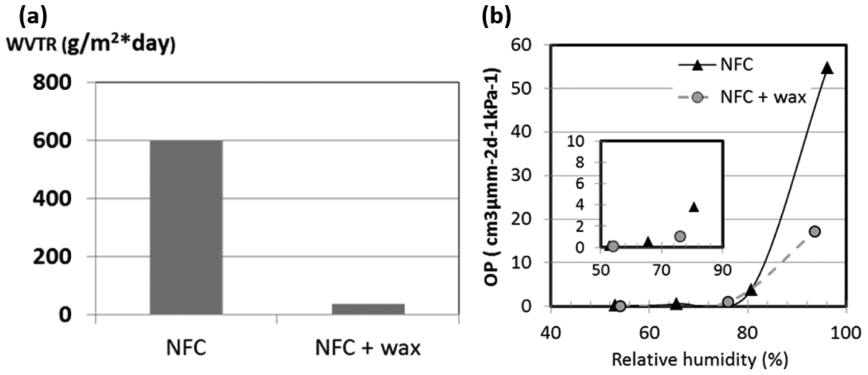

Figure 37. (a) Water vapor transmission rate. (b) Oxygen transmission rate of pure nanopaper and wax-treated nanopaper. Reproduced with permission from ref 370. Copyright 2013 American Chemical Society.

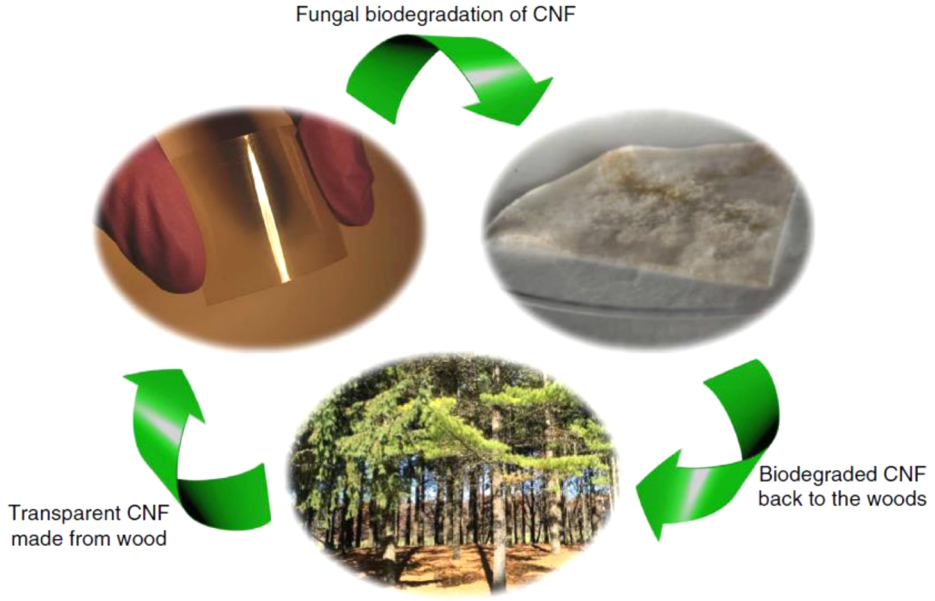

Figure 38. Illustration of the likely life cycle of transparent paper made from wood. Reproduced with permission from ref 376. Copyright 2015.

In recent years, the excellent barrier properties of nanopaper have attracted a great deal of attention in scientific and industrial communities.[211,356,357,369] Many factors, including the raw materials, disintegration methods, crystallinity, and morphologies of cellulose fibrils, fabrication processes, and density of nanopaper, may have a significant influence on the barrier properties of nanopaper, which have been reviewed recently by Lavoine et al.[368] Syverud and Stenius investigated the barrier properties of MFC film prepared by vacuum filtration, which showed a minimum OTR of 17 mL/m^2/d with a thickness of 21−30 μm resulting from the combination of the high crystallinity of cellulose nanofibrils and a highly dense cellulose nanofibril network.[356] Fukuzumi et al. pretreated the wood fibers using the TEMPO oxidation system prior to mechanical disintegration of CNF.[211] In comparison with CNF obtained by other pretreatments, the TEMPO-oxidized CNF has a much smaller diameter when they were then treated with identical mechanical processes and could form a much denser nanopaper with better barrier properties. The OTR of PLA reduced from 746 to 1 mL/m^2/d/Pa after coating a layer of TEMPO-oxidized CNF film with a thickness of 0.4 μm. Furthermore, sheet-like nanomaterials were also added to nanopaper to form brick-and-mortar structure with an extended diffusion path for permeating gas, which could improve the OTR of nanopaper.[277,293,289]

Unfortunately, one of the major challenges for the barrier properties of nanopaper is the inherent hydrophilicity of cellulose nanofibers. The barrier properties of nanopaper are quite sensitive to moisture content. Hence, chemical modifications of CNF or addition of hydrophobic materials in nanopaper were applied to improve the WVTR and OTR of nanopaper. Österberg et al. proposed a strategy to prepare nanopaper with excellent barrier properties under moisture environment.[370] The dry nanopaper was immersed into melted wax to make it less hydrophilic. Both WVTR and OTR of wax-treated nanopaper decreased considerably. As illustrated in Figure 37a, the WVTR of wax-treated nanopaper was only 40 g/m^2 per d, which is much lower than that of unmodified nanopaper with a WVTR of 600 g/m^2 per d. The oxygen permeability of wax-treated nanopaper was approximately 18 cm^3 μm m^{-2} d^{-1} kPa^{-1} at 96% RH (see Figure 37b), which is suitable for food packaging.

4.2. Cellulosic Biopolymer-Based Green Electronics

4.2.1. Overview of Green Electronics Using New Materials. Electronics play an important role in our everyday life. People use electronics, including laptops, cellphones, sensors, and other portable electronics, ubiquitously. Meanwhile,

DOI: 10.1021/acs.chemrev.6b00225
Chem. Rev. XXXX, XXX, XXX−XXX

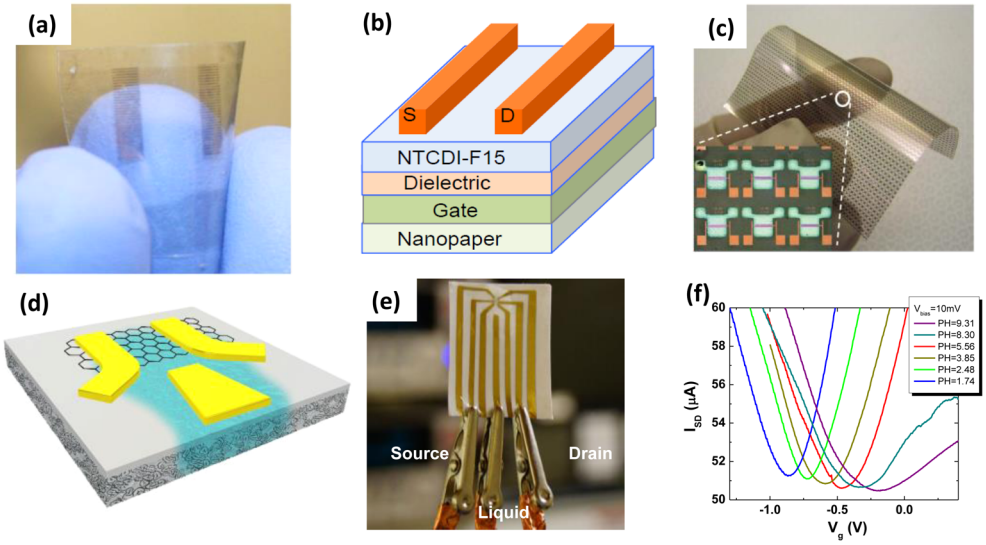

Figure 39. (a) Image of fabricated flexible and transparent transistor on nanopaper. (b) Schematic drawing of FET device with a top contact geometry in a. Reproduced with permission from ref 219. Copyright 2013 American Chemical Society. (c) Photograph and optical microscopy image of 20 μm thick transparent nanopaper-based OTFT array. Short-channel TFTs with a resolution of 70 × 70 were integrated in a 70 mm × 70 mm area. Reproduced with permission from ref 385. Copyright 2014 WILEY-VCH. (d) Schematic illustration of the configuration of the device. Two-dimensional materials (graphene, MoS2) exfoliated on a piece of bilayer mesoporous nanopaper, followed by contact electrodes fabrication (yellow). Liquid electrolyte can be absorbed by the porous side (blue). (e) Transistor measurement setup. Center electrode contact electrolyte adsorbed. (f) Source-drain current (I_{sd}) as a function of V_g at pH values of 1.74, 2.48, 3.85, 5.56, 8.30, and 9.31. Reproduced with permission from ref 274. Copyright 2014 American Chemical Society.

people change electronics frequently, which poses a growing ecological problem, because most of the electronics are nonbiodegradable and nonrecyclable. For example, the plastic containers required 450 years to decompose. On average, cellphones are used <18 months and laptops <3 years before being discarded.[371,372] The total electronic waste generated in the United States is around 3.2 M every year, and most of it is composed of nonbiodegradable materials, such as plastic and silicon.[373,374] People more and more realized the importance to build our society, economy, and manufacturing in a sustainable way. Biodegradable and abundant materials are desired to replace petroleum-derived nonbiodegradable material.[375]

High-performance, biodegradable electronics on biodegradable substrates have been intensively investigated with the motivation of minimizing the dependence on petroleum and reducing the pollution to the environment. Furthermore, the biodegradability and biocompatibility are critical for bioimplantable electronics and biofunctional electronics.[376,377,375] Cellulose is the largest biopolymer on earth, with the feature of excellent biodegradability, biocompatibility, sustainability, versatility, and accessibility, high mechanical strength, and unique optical properties. As illustrated in Figure 38, using the cellulose nanofibers disintegrated from wood we can make flexible, transparent, and strong substrate with small surface roughness and small thermal expansion coefficient. Paper can be degraded by fungi and fed back to the soil and tree growth with no footprint to the environment.[376] In addition to being environmentally friendly, the paper substrate, when compared to glass, possesses a smaller bending radius, lighter weight, and higher mechanical strength. When compared to plastic, the paper substrate is characterized with a smaller thermal expansion coefficient, which is more suitable for writing and large-scale roll-to-roll printing.[219] Furthermore, the TEMPO-oxidized cellulose has very good O_2 and H_2O barrier properties. Svagan et al. use NFC protective coating to improve the lifetime of triplet−triplet annihilation photon energy upconversion (TTA-UC) by blocking the O_2 in air.[378] Paper electronics featured with cost-efficient, environmentally friendly, and large-scale roll-to-roll processes attract intensive attention in academic research and commercial applications, because they enable a wide range of disposable and green electronics for consumer usage.

4.2.2. Flexible Transistors. The transistor, a semiconductor device used to amplify and switch electronic signal and power, is the essential building block of various electronics. For example, the transistor is ubiquitous in the display system. Flexible display has a huge market in flexible mobile devices, such as ebook, iPad, and so forth. Paper made from cellulose is flexible and lightweight. Paper has been used as either substrate or functional dielectric layer in transistors.[379−383] Huang et al. first demonstrated the field effect transistor (FET) on transparent nanopaper made from CNF.[219] Figure 39a shows an optical picture of this device, which demonstrated an outstanding transmittance and flexibility.

One of the unique and distinct characterizations of paper electronics is that they are flexible and printable. Traditionally, transparent conductive oxides (TCO), such as indium tin oxide (ITO), zinc oxide (ZnO), and cadmium oxide (CdO), inorganic semiconductors, such as silicon, and metal oxide dielectrics, such as alumina oxide have been widely used in nonflexible electronics. ITO generates cracks when the device is bent, and electrical conductivity will reduce dramatically; therefore, the device performance will decay severely. CNT, graphene, metal nanowires, and conductive polymers are intensively investigated for the application in transparent and flexible electronics.[384] In this work, as illustrated in Figure 39b, the authors use CNT as gate, PMMA as dielectric, and the n-type organic semiconductor, NTCDI-F15, a naphthalenetetracarboxylic diimide derivative which is highly transparent in visible light and has relatively good stability in air. The obtained device not only has good transmittance but also has excellent flexibility. The mobility is

DOI: 10.1021/acs.chemrev.6b00225
Chem. Rev. XXXX, XXX, XXX−XXX

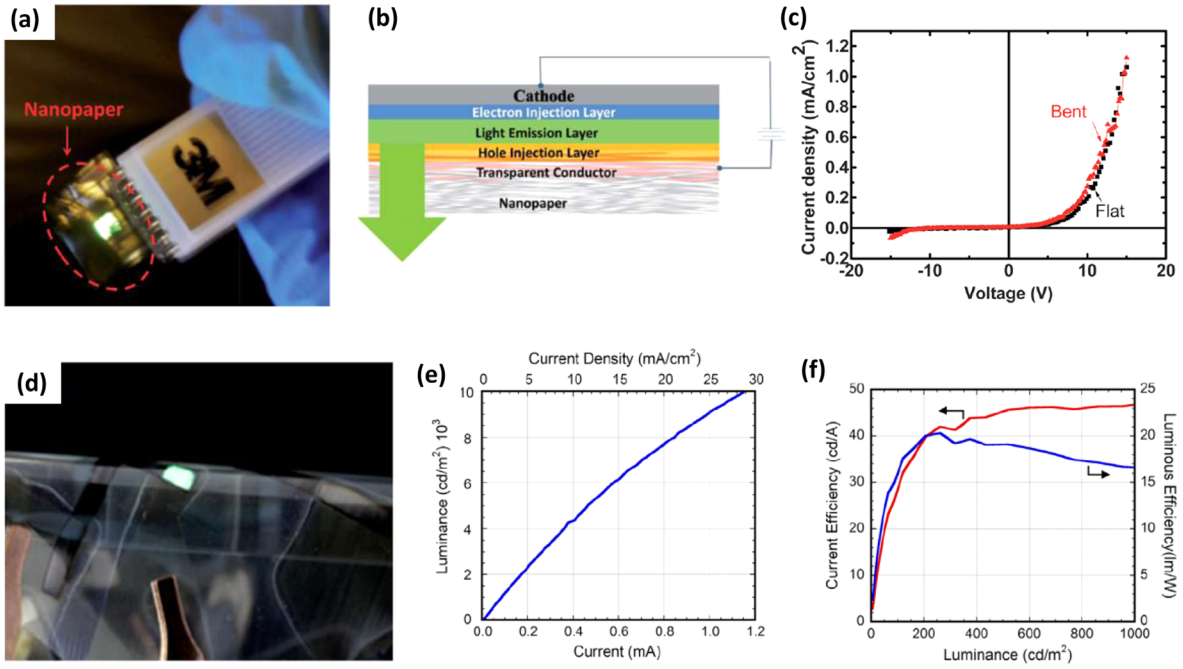

Figure 40. (a) Picture of the OLED fabricated on the pure wood−cellulose paper. (b) Schematic drawing of a nanopaper OLED device. (c) *J*−*V* curve of the flexible OLED in the flat and bent states, respectively. Bending radius is 1.5 mm. Reproduced from ref 218 with permission from The Royal Society of Chemistry. Copyright 2013. (d) Picture of OLEDs operating on cellulose substrates rolled into a cylindrical structure demonstrating good flexibility and transmittance. Emission characteristics of phosphorescent OLED on transparent cellulose: (e) luminance versus voltage, highest luminance ≈ 10 000 cd/m^2; (f) current efficiency and luminous efficiency versus luminance in the range of several hundred cd/m^2. Reproduced with permission from ref 387. Copyright 2014 IOP Publishing.

only reduced by around 10% at the bent stage. Note that the small surface roughness of nanopaper made from nanofiber plays a key role here to prevent the pinhole problem. Fujisaki et al. demonstrated the flexible organic transistor array on nanopaper, see Figure 39c.[385] The inset shows an optical microscope image of the device, where the source and drain (featured in purple line) and gate (featured in green) are well defined. The resulting thin film transistor exhibited high mobility of up to 1 cm^2 V^{-1} s^{-1}, almost hysteresis-free characteristics, and good operational and mechanical stability.

Even though the cellulose nanofiber and regular microfibril are composed of the same cellulosic material, the optics, mechanics, and structure of these two kinds of fibers are totally different. Therefore, the paper made from these two kinds of fibers also has totally different properties. Bao et al. designed a bilayer paper with a porous bottom layer made from regular wood fiber and a smooth top layer composed with cellulose nanofiber (see Figure 39d).[274] In the novel configuration, the semiconductor (MoS_2, graphene), source/drain, and gate are fabricated at the same smooth side with the dry shadow mask process, and the aqueous electrolyte was back gated attributed to the capillary capacity of the porous layer (see Figure 39e). The Dirac point shifted to the positive direction with the increase of pH value, which can be interpreted as the attachment of hydroxyl ions make graphene more p-doped (see Figure 39f).[386] The device can be potentially used as pH sensor and can be potentially used in other chemical and biological application. The combined technologies of low-cost and ecofriendly materials disintegrated from wood with solution-based organic transistors are promising for use in future flexible electronics.

4.2.3. Organic Light-Emitting Diode (OLED) for Lighting. The organic light-emitting diode (OLED) is a versatile platform for electronic displays, which people ubiquitously used. Flexible and even foldable displays attract worldwide attention. Traditionally, OLED is fabricated on rigid glass or flexible plastic substrates, such as polyethylene terephthalate (PET) and polyethylene naphthalate (PEN). One major barrier of plastic is its thermal stability. The coefficient of thermal expansion (CTE) of paper can reach 12−28.5 ppm/K. Most plastic has a large coefficient of thermal expansion (CTE), which cause the destruction of functional materials of the OLED layers during temperature fluctuation in the device assembly and mounting processes. The rigidity and density property of glass not only increase the cost in the manufacturing line but also bring the inconvenience for the device carriers. Furthermore, glass is not a promising substrate for roll-to-roll manufacturing. Paper as a substrate for flexible electronics is attractive for its excellent thermal stability, recyclability, sustainability, lightweight, flexibility, and the mature roll-to-roll large-scale manufacturing technology. However, the regular paper is opaque, which is the barrier to be used in the OLED device. Moreover, the large surface roughness is another serious drawback for using it as a diode substrate. Recently, transparent nanopaper has attracted broad interest for its high optical transmittance, low CTE, and excellent mechanical strength. Zhu et al. demonstrated an OLED manufactured on a pure cellulose nanofiber transparent paper (see Figure 40a).[218] From top to bottom, the device consists of a 20 nm calcium (Ca) electron injection layer, a light-emitting layer of green polyfluorene, a 10 nm molybdenum oxide (MoO_3), and 30 nm PEDOT:PSS (poly(3,4-ethylenedioxythiophene):poly(styrenesulfonate)) hole injection layer sandwiched between the two conductive electrodes (see Figure 40b). Figure 40c shows the *J*−*V* curve at flat and bending states, respectively. There is little difference between the curves before and after bending.

DOI: 10.1021/acs.chemrev.6b00225
Chem. Rev. XXXX, XXX, XXX−XXX

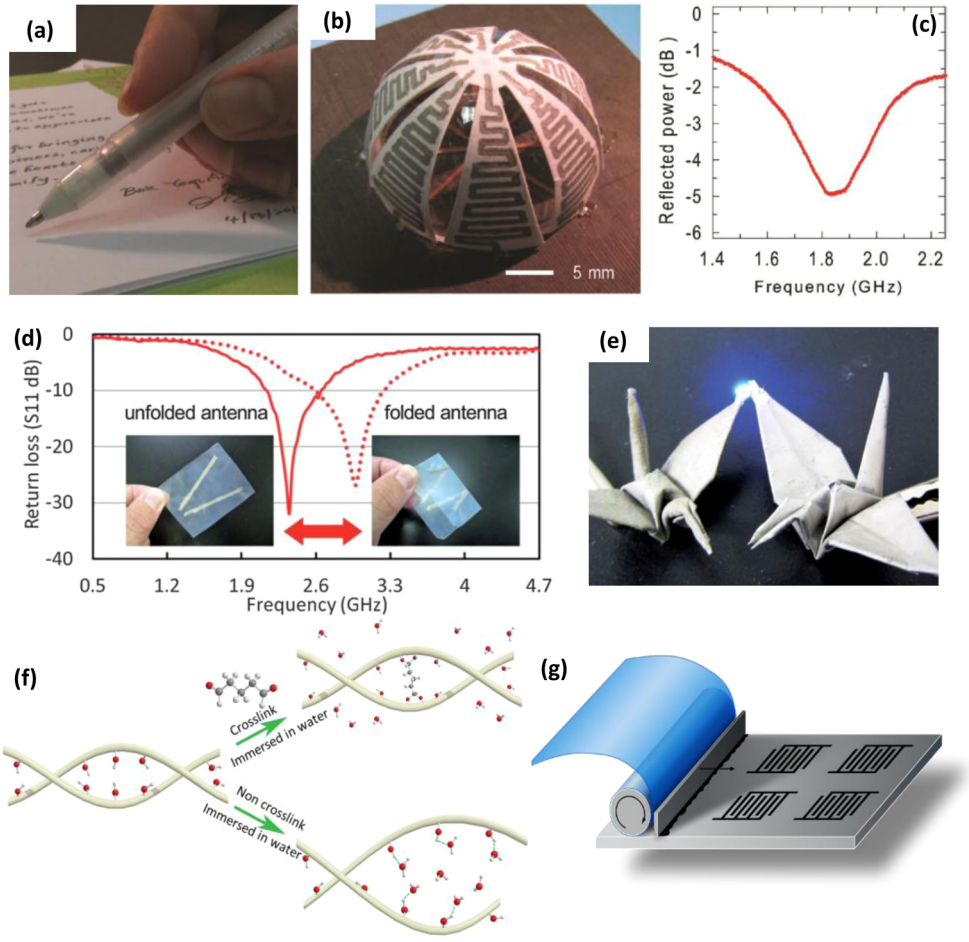

Figure 41. (a) Optical image of a rollerball pen loaded with a conductive silver ink. (b) Optical image of a 3D antenna fabricated by drawing conductive silver tracks onto paper. (c) Reflected power of the 3D antenna as a function of frequency. Reproduced with permission from ref 389. Copyright 2011 WILEY-VCH. (d) Return loss of pristine and folded nanopaper antennas. (e) LED illuminated via folded silver nanowire printed paper. Reproduced with permission from ref 390. Copyright 2013 The Royal Society of Chemistry. (f) Schematic illustrating the mechanism of nanopaper shape stability improvement by glutaraldehyde treatment. (g) Schematic of the laboratory gravure press used to print antennae onto modified robust nanopaper. Reproduced from ref 276 with permission from The Royal Society of Chemistry. Copyright 2014.

Following the above-mentioned work, Sumit et al. demonstrated high-brightness phosphorescent OLED on transparent and flexible cellulose films (see Figure 40d).[387] Here, the regenerated cellulose is used for nanopaper fabrication instead of cellulose nanofiber with a transmittance of 85%. The OLEDs achieved a maximum brightness of 10 000 cd/m^2 and current and luminous emission efficiencies as high as 47 cd/A and 20 lm/W, respectively (Figure 40e and f). The transparent nanopaper is a promising substrate for transparent and flexible OLED device.

4.2.4. Printed Antenna and Radiofrequency Identification (RFID) Devices. Paper substrates offer many advantages for printing electronics, which are not only biodegradable, ubiquitous, and cheap but also able to be written on, printed on, and folded into a 3D structure. Antennae convert electric power into radiowaves and vice versa and are widely used in various communication technologies, including televisions, mobile phones, GPS, and radios.[388] Russo et al. used conductive silver ink to write a 3D antenna operating at 1.9 GHz directly on a piece of paper (see Figure 41a and 41b).[389] The measured center frequency is 1.87 GHz with an efficiency of 20−30% (see Figure 41c), which is significantly lower than that recently achieved by conformally printing conductive features directly onto glass hemispheres. However, the portable conductive ink pen writes smoothly on paper, a trait not possible on glass or plastic.

The aforementioned paper antenna is ideal for small, portable electronics due to the excellent foldability, but device sensitivity is low due to the high surface roughness of the paper substrate. Compared to regular paper, nanopaper is foldable and possesses a smooth surface. Nogi et al. used silver nanowire ink to mask-print a "V" shape onto a nanopaper substrate. In the return loss versus frequency plot shown in Figure 41d, we see the resonance peaks shift between 2.3 and 3 GHz when the substrate is pristine and folded, respectively. The nanopaper antenna maintains good sensitivity even after folding with a return loss less than −26 dB. The excellent foldability of nanopaper substrates is illustrated in Figure 41e, which depicts an LED illuminated via two folded cranes printed with silver nanowire ink.[390] However, nanopaper has poor shape stability in water, which hinders solution-based large-scale printing processes, including gravure printing, screen printing, and inkjet printing. Zhu et al. uses glutaraldehyde with hydrochloric (HCl) acid as a catalyst to cross-link hydroxyl groups within and between cellulose chains, improving the shape stability of the nanopaper in solution (Figure 41f and 41g).[277] With the robust nanopaper as a substrate, an antenna is fabricated via the gravure printing method. Insertion losses of −37.9 and −38.85 dB for the 100 and 120 lpi antennas, respectively, were demonstrated at a maximum gain of 683.75 MHz. These studies pave the way for the development of low-cost, disposable devices

DOI: 10.1021/acs.chemrev.6b00225
Chem. Rev. XXXX, XXX, XXX−XXX

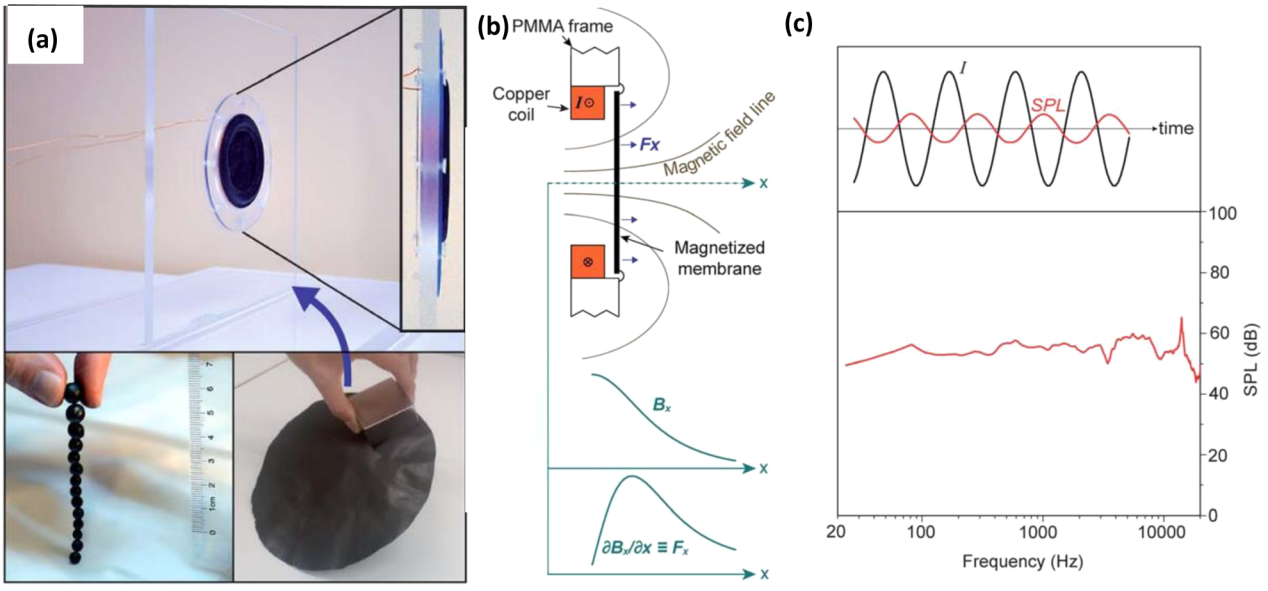

Figure 42. (a) Ferrimagnetic balls (bottom left image) and membrane (bottom right image) and constructed loudspeaker (top image). (b) Illustration of the working principle of the loudspeaker. Membrane is 50 μm thick with a 60 wt % $CoFe_2O_4$ nanoparticle mass loading. Poly(methyl-methacrylate) (PMMA) is used as a baffle plate. (c) Frequency response of the loudspeaker. Reproduced from ref 259 with permission from The Royal Society of Chemistry. Copyright 2013.

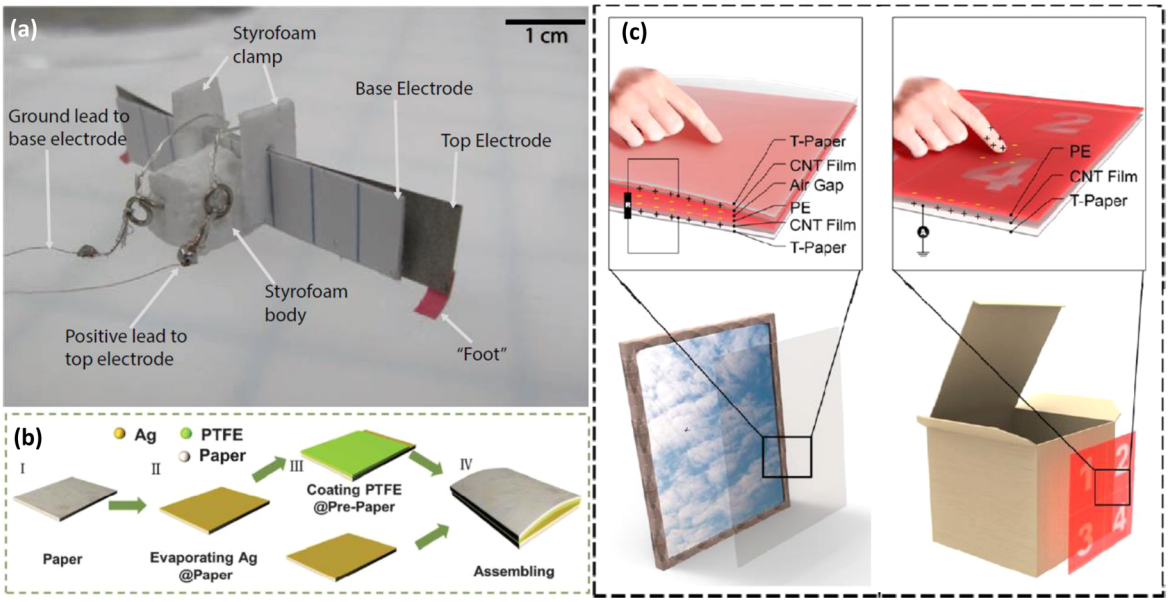

Figure 43. (a) Picture of 6 cm × 1 cm × 1 cm, 550 mg paper robot. (b) Schematic diagram illustrating the process of fabricating the paper-based nanogenerator. Reproduced with permission from ref 394. Copyright 2013 The Royal Society of Chemistry. (c) Schematic illustrating the self-powered, interactive transparent nanopaper actuator for antitheft and smart mapping applications. Reproduced with permission from ref 395. Copyright 2015 American Chemical Society.

via large-scalable writing and printing processes, maximizing one of the advantages of paper as a printable substrate.

4.2.5. High-Performance Loudspeaker. Loudspeakers convert electrical audio signals into their corresponding sounds. The diaphragm is the most important component in loudspeakers. Ultrathin, mechanically robust nanomaterials with low mass are investigated as diaphragm materials. For example, CNT and graphene are used as thermoacoustic and electrostatic diaphragms, respectively.[391,392] The low mass ensures good high-frequency response, while high strength allows for the relatively large free-standing diaphragms necessary for effective low-frequency response. Cellulose nanofiber disintegrated from wood is lightweight and strong, and can be fabricated into thin films with facile vacuum filtration processes.

Galland et al. decorated nanocellulose with magnetic nanoparticles to produce a magnetized, high-toughness membrane for a prototype loudspeaker.[259] Ferrimagnetic balls or membranes are fabricated from NFC uniformly decorated in situ with magnetic ferrite particles. The authors use the thin, magnetized, and mechanically strong membrane as a diaphragm in the loudspeaker seen in Figure 42a. Figure 42b illustrates the working mechanism for the loudspeaker. The copper coil

DOI: 10.1021/acs.chemrev.6b00225
Chem. Rev. XXXX, XXX, XXX−XXX

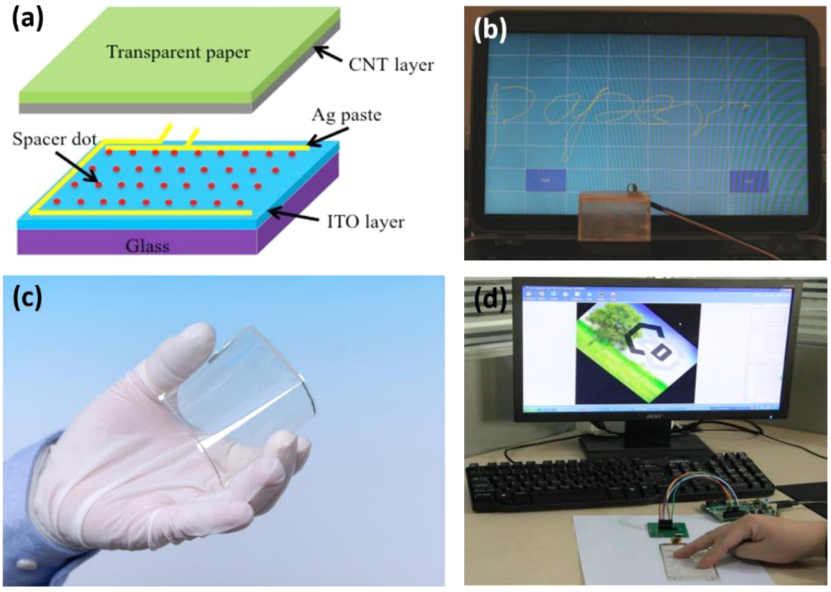

Figure 44. (a) Schematic structure of transparent paper-based touchscreen. (b) Assembled paper touchscreen was used to simulate typical "paper". Reproduced from ref 195 with permission from The Royal Society of Chemistry. Copyright 2013. (c) Photo of a highly flexible paper touchscreen. (d) Demonstration of rotating the image on a computer by the paper touchscreen. Reproduced with permission from ref 396. Copyright 2016 American Chemical Society.

generates a magnetic field gradient exerting a force on the magnetized membrane, and the electric signal is reproduced as an acoustic vibration of the membrane, i.e., audible sound. Figure 42c shows the frequency response of the loudspeaker recorded for 1 W active input power; the top plot qualitatively illustrates the nondeformed acoustic signal (red) recorded for a monofrequency input current (black). The sound output has good quality as characterized by the flat frequency response at frequencies ranging from 20 Hz to 15 kHz (see Figure 42c). The wide variety of functional materials on the market provides several potential uses for functionalizing membranes, including portable loudspeakers and hearing aids. Furthermore, scaling up to commercial manufacturing is made easier with the use of inexpensive materials and facile fabrication methods.

4.2.6. Lightweight Paper Actuators. Paper-based power generators that are lightweight, portable, flexible, and adhere to a wide range of objects are very attractive for use in energy harvesting.[393−395] For example, people can attach a paper actuator to a book to collect energy while turning pages. Figure 43a shows a paper-based electrostatic zipper actuator made from CNF for printable robots. A mylar or parylene dielectric layer is sandwiched between two conductive paper electrodes coated with CNT. A 5 cm × 1 cm actuator demonstrates a maximum static deflection of 1.8 cm and a bandwidth of approximately 12 Hz. Static power dissipation was under 1 μW. Two of these paper actuators are combined to demonstrate simple motion in a 6 cm × 1 cm × 1 cm robot. Taking advantage of asymmetric friction with the ground, the robot achieves speeds up to 33 mm/min. The demonstrated device can be applied to paper robots used in smart detection in places inaccessible to humans.

Figure 43b illustrates a process of fabricating a self-powered paper actuator. Silver (Ag), ~100 nm, is deposited on two sheets of paper to form electrodes. Polytetrafluoroethylene (PTFE) was added to one sheet of the Ag−paper by spin coating. The PTFE−Ag−paper is pressed together with the Ag−paper, and an air gap is maintained between the two sheets. The device is prepolarized via the corona method to create a generator that operates via electrostatic induction. Pressing the device narrows the air gap, bringing the PTFE-coated electrode closer to the other electrode and increasing the positive charge on that electrode. This change in charge balance between the Ag electrodes results in a flow of current through the device. Releasing the pressure causes electrons to flow back, so repeated cycling creates a continuous current.[394] The whole device is sensitive to pressure. On the basis of the same electrostatic mechanism, Zhong et al. used transparent nanopaper made from nanocellulose to fabricate a self-powered and interactive transparent nanopaper actuator. In order to maintain transparency, CNT is used instead of Ag. Furthermore, environmentally PE is used as medium layer instead of PTFE. This device has good transparency and is sensitive to pressure changes, and as such, it is promising for antitheft applications in museums (see Figure 43c left column) or in smart mapping of important documents, such as a will or birth certificate. These actuators are adaptable for massive production and eventually environmentally friendly disposal.

4.2.7. Touchscreens by Writing. Fabricating electronics on the flexible substrate to replace rigid substrate has garnered tremendous attention since they are ductile, lightweight, and portable. Fang et al. developed a highly transparent and dimensionally stable paper with bilayer structure: a thin layer of pure NFC film to provide nanoscale surface roughness, and a hybrid layer made of regular wood fibers and NFC acted as supporting layer.[195] A thin CNT layer was then deposited on the smooth surface of this transparent paper by rod coating to prepare transparent paper electrode for resistive touchscreen. The schematic of a paper-based touchscreen is shown in Figure 44a. A letter "paper" was written on the assembled paper touchscreen by a stylus pen and successfully displayed on the computer (see Figure 44b), showing the potential of this transparent paper in the field of touchscreen. Furthermore, Zhu et al. prepared a super clear nanopaper with a total light transmittance of >90% and a transmission haze < 1%. To make it conductive, a single-layer graphene was transferred onto the surface of super clear and smooth paper via the thermal transfer

DOI: 10.1021/acs.chemrev.6b00225
Chem. Rev. XXXX, XXX, XXX−XXX

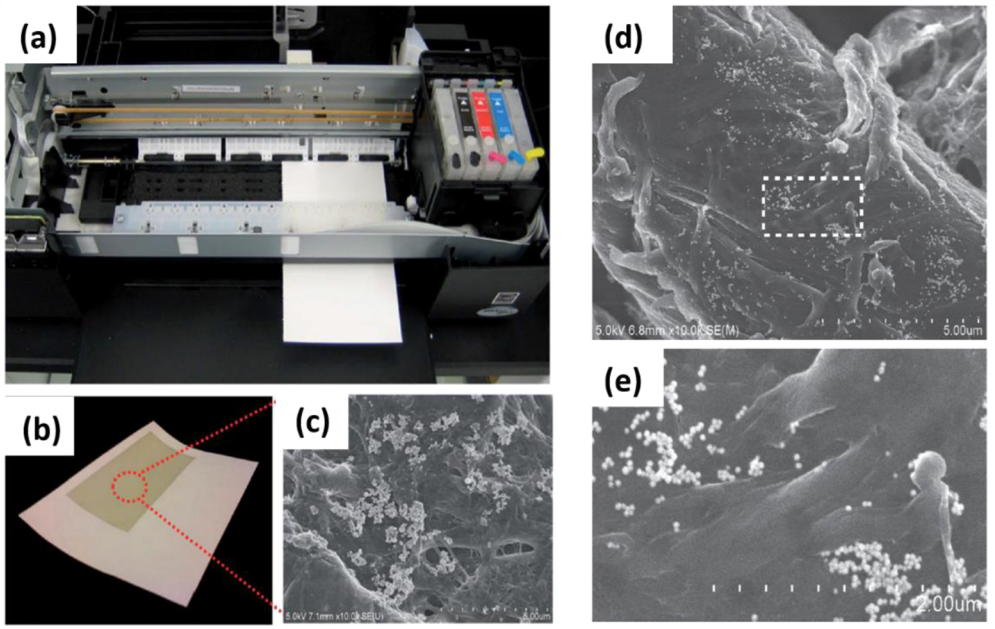

Figure 45. (a) Picture of inkjet printing of silver nanoparticles onto cellulose paper. (b) Inkjet-printed SERS substrate, and corresponding (c) SEM image of the indicated region in b. Reproduced from ref 399 with permission from The Royal Society of Chemistry. Copyright 2013. (d) SEM image of a gold nanoparticle-printed region on cellulose paper. (e) Clustered gold nanoparticles on the cellulose fiber (from box in d). Reprinted with permission from ref 400. Copyright 2013 Elsevier.

method. This transparent and conductive clear paper was then used to assemble a high-performance capacitive multitouch paper touchscreen (Figure 44c).[396] The electrode pattern was generated with a laser cutter. As shown in Figure 44d by the super clear paper touchscreen, we can rotate the image on a computer with sensing performance comparable to a commercial touchscreen.

5. WOOD-DERIVED BIOLOGICAL APPLICATIONS

Cellulose has high potential in biological applications due to its biodegradability, biocompatibility, and fluid transfer properties. There are two major cellulose fiber types to consider: natural microfiber and disintegrated nanofiber. Natural fiber has good mechanical flexibility and excellent capillary properties. CNF with high hydrophilicity, good mechanical properties, and high chemical modification capacity have gained increased interest during the past decade. Moreover, these two fibers have different biological applications.

5.1. Surface-Enhanced Raman Spectroscopy (SERS)

Surface-enhanced Raman spectroscopy (SERS) is a powerful technology for biomolecular and chemical detection. Due to the signal enhancement from noble metal nanoparticles, single-molecular identification has been detected with SERS.[397,398] However, in most cases, SERS requires expensive microfabrication or nanofabrication to produce a surface with metal nanostructures. Paper-based microfluidics and biosensors present a low-cost methodology and device for molecular detection. White et al. used inkjet printing to print silver nanoparticles onto hydrophobic paper for SERS (see Figure 45a).[399] Figure 45b is an inkjet-printed SERS substrate, SEM analysis of which reveals clusters of silver nanoparticles on the paper fiber (see Figure 45c). These silver nanoparticles are responsible for the SERS enhancement. In addition to silver nanoparticles, gold nanoparticles can also be used to enhance Raman spectroscopy. Figure 45d shows an SEM image of printed gold nanoparticles on paper. Figure 45e is a higher magnification image of the clusters of gold nanoparticles in the outlined region in Figure 45d.[400] SERS on paper is a highly sensitive technique. The Thiram Raman peak at 1384 cm^{-1} is detectable with only 10 ng of fungicide present on the paper substrate. Paper-based SERS devices can be easily used to trace chemical residues at an extremely low cost.

5.2. Bioplasmonic Sensor on Paper

Bioplasmonics is a technology that integrates nano-optics and plasmonic devices to study the biophysical and chemical properties of the receptors by Raman, fluorescence, and UV–vis spectroscopies. This approach can be translated to many different cells and tissues with applications in biomedicine as well as biosensor development and drug targeting. Compared to glass and silicon, paper has many advantages as a bioplasmonic device substrate including excellent wicking properties, high specific surface area, mechanical flexibility, printability, disposability, and low cost. The use of a paper substrate allows for inexpensive plasmonic biochips for point-of-care diagnostics.[401] Limei Tian et al. demonstrated a common laboratory filter paper with uniformly adsorbed biofunctionalized plasmonic nanostructures that enables rapid urine analysis for the detection of kidney cancer biomarkers in artificial urine down to a concentration of 10 ng/mL.[402] Figure 46a shows a highly uniform distribution of Au nanorod (NR)–immunoglobulin G(InG) conjugates on the paper surface with no aggregation. Localized surface plasmon resonance (LSPR) was used for characterization. Figure 46b shows the extinction spectra of the AuNR paper substrate (black) and AuNR-IgG conjugates on the paper substrate before (red) and after binding of anti-IgG (blue). The LSPR wavelength exhibited a ~17 nm red shift with partial replacement of the cetyltrimethylammonium bromide (CTAB) layer with AuNR-IgG conjugates and a further red shift of ~23 nm upon specific binding of anti-IgG to IgG. Ying Hui Ngo et al. investigated the effects of gold nanoparticle (AuNP) additions to paper substrates

DOI: 10.1021/acs.chemrev.6b00225
Chem. Rev. XXXX, XXX, XXX–XXX

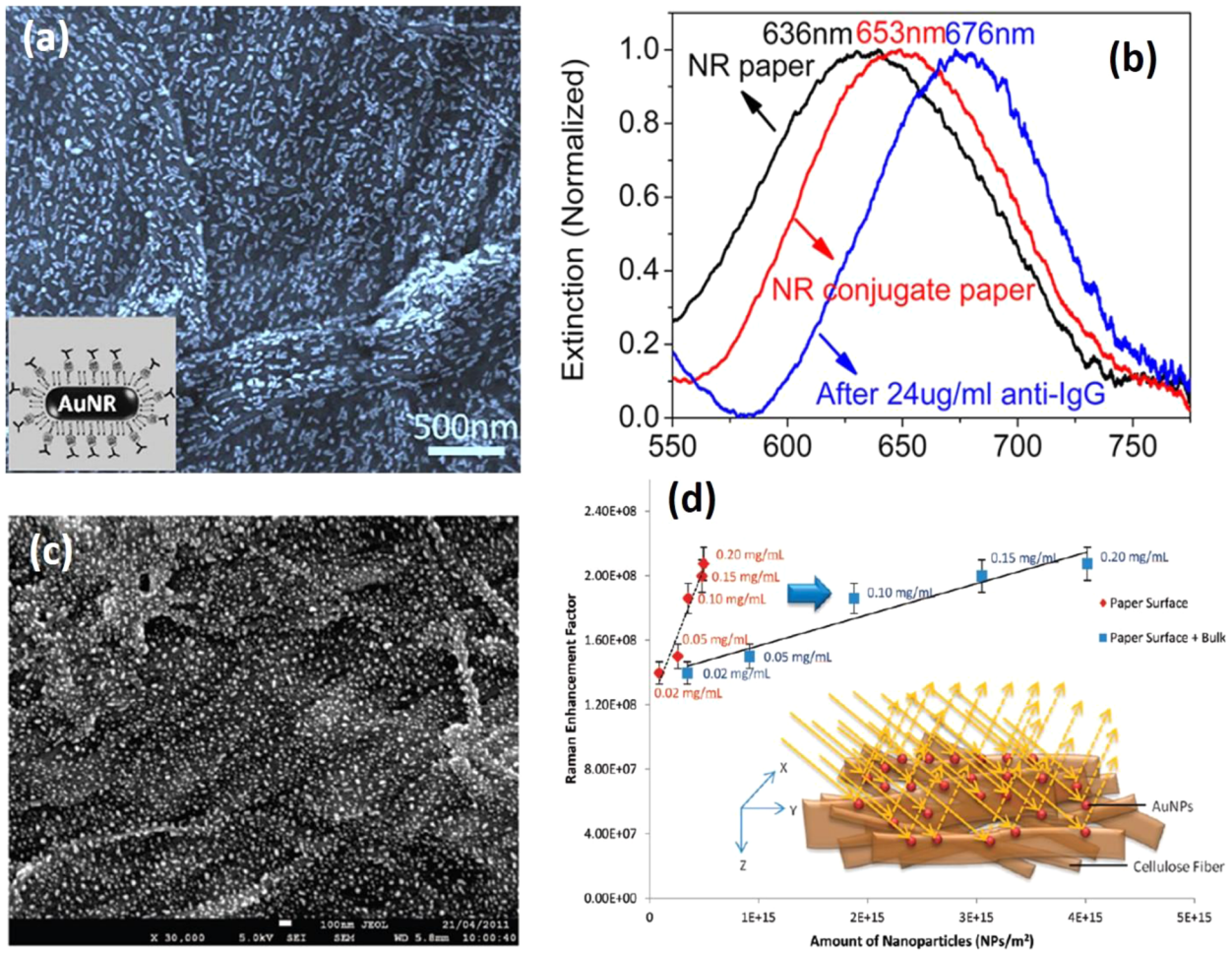

Figure 46. (a) SEM images of paper with adsorbed Au nanorod (NR)−immunoglobulin G(InG) conjugates. (b) Extinction spectra of AuNR paper substrate (black) and AuNR-IgG conjugates on the paper substrate before (red) and after binding of anti-IgG (blue). Reproduced with permission from ref 402. Copyright 2012 American Chemical Society. (c) FESEM images of filter paper dipped into 0.20 mg/mL of Au nanoparticle (NP) solution. (d) Relationship between the amount of AuNPs and the EF of 4-ATP for filter paper and silicon. Reproduced with permission from ref 403. Copyright 2012 American Chemical Society.

and examined the ability of these composite materials to amplify the SERS signal (see Figure 46c and 46d).[403] The AuNP is uniformly distributed at the paper surface (see Figure 46c). Paper as an inert and robust substrate maintains a controlled adsorption state of AuNPs. Compared to AuNP-treated silicon, the Raman enhancement factor from paper is higher due to a more uniform and greater degree of adsorption of AuNPs. As shown in Figure 46d, the SERS intensity scales linearly with the density of AuNPs on paper. The z distribution of AuNPs within the bulk of the paper produces a 3D multilayer structure to allow inter- and intralayer plasmon coupling, amplifying the SERS signal as illuminated in the inset schematic in Figure 46d. The SERS performance of nanoparticle-functionalized paper can thus be optimized by controlling the 3D distribution of the metallic nanoparticles. Recently, Nahid et al. published work presenting in-situ-synthesized silver nanoparticles embedded in bacterial cellulose nanopaper as a bionanocomposite plasmonic sensor.[404]

Paper SERS substrates are highly sensitive, robust, and amiable to several different environments and target analytes. They are also cost efficient and have high sample collection efficiency and do not require complex fabrication methodologies. There are two modes to test the signal intensity: reflection and transmission. The testing sensitivity from transmission is higher than reflection due to more efficient signal collection. Nanopaper is an emerging transparent substrate that is ideal for bioplasmonic nanoparticles. The nanopaper substrate is a novel platform for integrating SERS with already existing analytical techniques such as chromatography and microfluidics, imparting chemical specificity to these techniques. We expect the study and application of nanopaper biosensors to gain popularity in academics and industry.

5.3. Microfluidic Devices for Diagnostics

Microfluidic paper-based analytical devices (μPADs) appeared as an attractive platform for disposable, portable, high-efficiency devices for use not only in health diagnostics but also in environmental monitoring and food quality testing. The advantages of using paper in microfluidic devices include (1) compatibility with many biochemical/medical applications, (2) the cellulose fiber is printable, allowing for large-scale production of μPADs, (3) the paper transports fluids via capillary force with no assistance of external forces, and (4) the paper is ubiquitously used and extremely inexpensive.[405,406]

Whitesides and co-workers first demonstrated microfluidic paper-based analytical devices in 2007;[407] since then, research with μPADs has flourished with both functionalization of microfluidic components to increase μPAD performance and

DOI: 10.1021/acs.chemrev.6b00225
Chem. Rev. XXXX, XXX, XXX−XXX

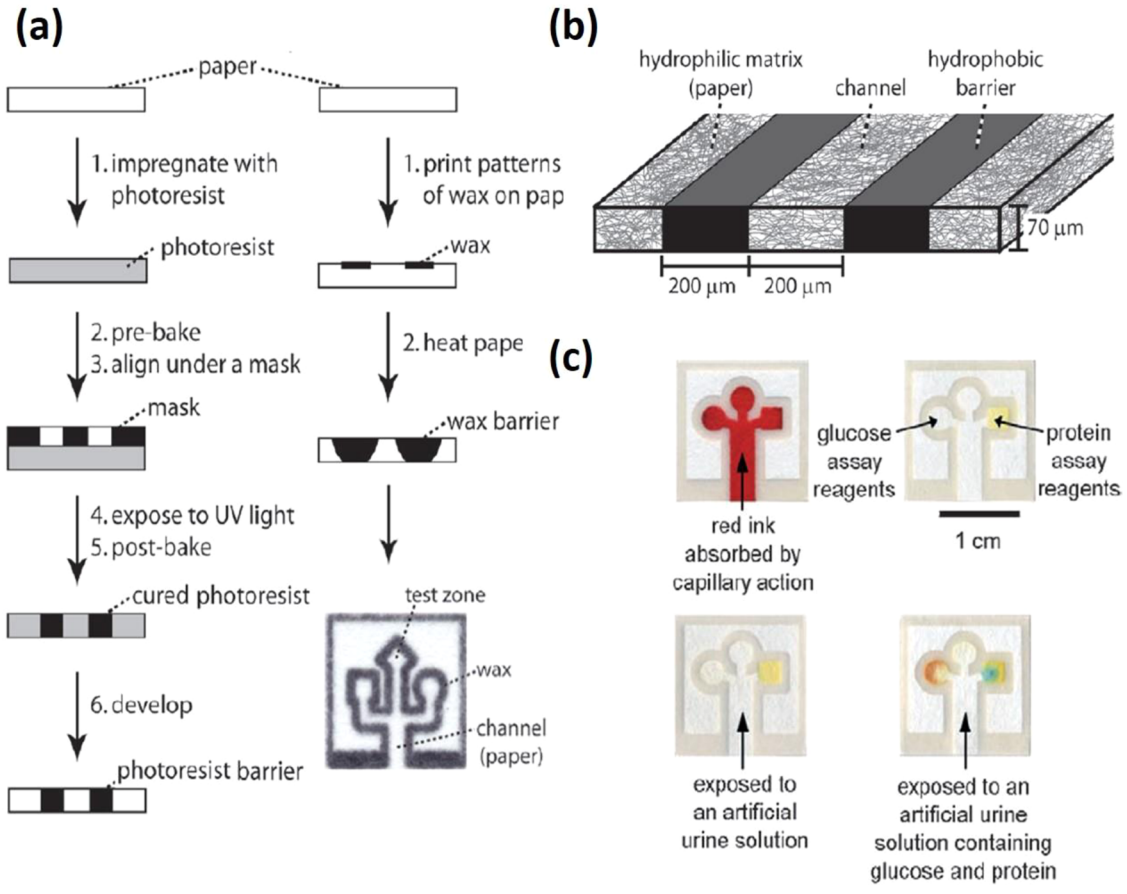

Figure 47. (a) Procedure of photolithography and wax printing on paper. (b) Schematic of a paper-based microfluidic channel. Reproduced with permission from ref 412. Copyright 2010 American Chemical Society. (c) Examples of a device fabricated by photolithography which contains a central channel that wicks fluids into three independent test zones. Reproduced with permission from ref 407. Copyright 2007 Wiley-VCH.

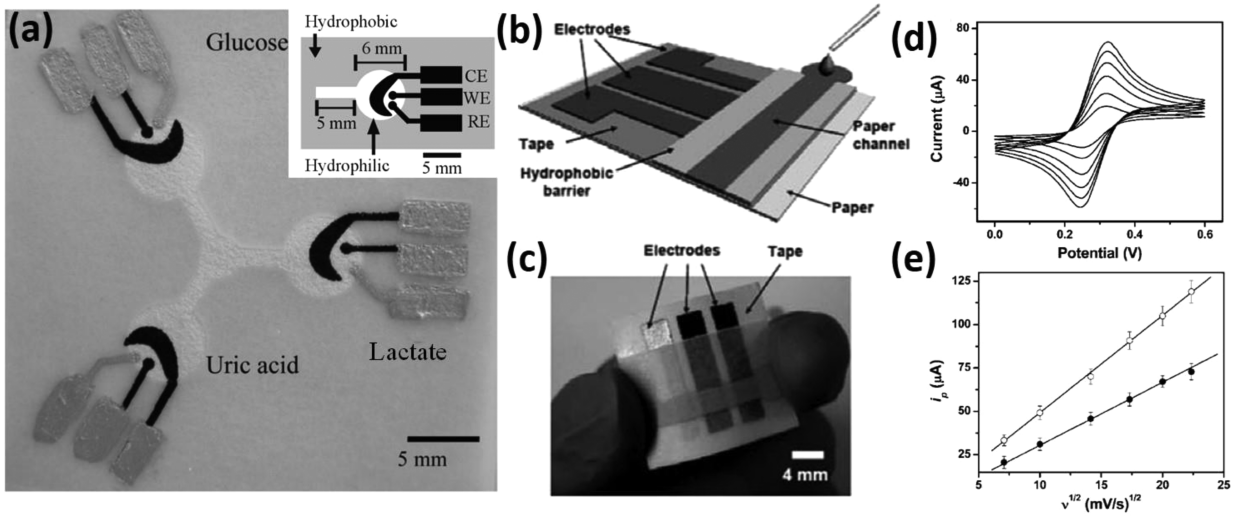

Figure 48. (a) Picture of three-electrode paper-based microfluidic devices. Reproduced with permission from ref 415. Copyright 2009 American Chemical Society. (b) Schematic of a paper-based electrochemical device. (c) Photograph of a paper-based electrochemical sensing device for the analysis of glucose. (d) Cyclic voltammograms of 2.0 mM ferrocene carboxylic acid in 0.5 M KCl aqueous solution at various scan rates. (e) Plot of anodic peak current vs square root of the scan rate ($n^{1/2}$) for CV experiments conducted on a paper device (solid circle) and in a bulk solution (blank circle). Reproduced from ref 413 with permission from The Royal Society of Chemistry. Copyright 2010.

with the introduction of exciting fabrication and detection techniques to the paper platforms.[405] There are different methods to print the patterns, including inkjet etching,[408] plasma treatment,[409] wax printing, screen printing, etc.[410,411] Figure 47a details the procedure for printing the microfluidics on the paper in a manner that produces well-defined hydrophobic barriers that extend through the depth of the paper.[412] The height of the channel is defined by the thickness of the paper.

AQ

DOI: 10.1021/acs.chemrev.6b00225
Chem. Rev. XXXX, XXX, XXX−XXX

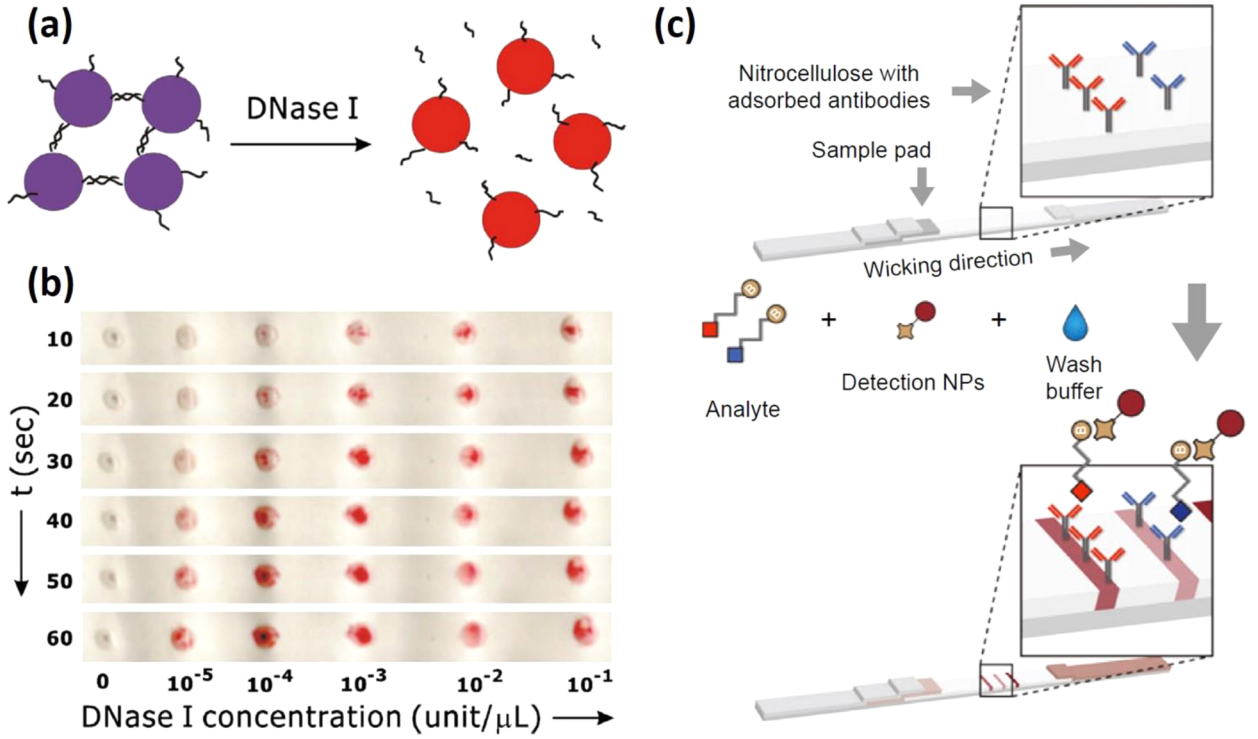

Figure 49. (a) Paper-supported sensor measuring the presence of DNase. Decomposition of the DNA chains on the nanoparticles induces a better dispersion, giving a color change. (b) DNase sensing assay on hydrophobic paper as a function of assay time and target analyst DNase I concentration. Reproduced with permission from ref 419. Copyright 2008 American Chemical Society. (c) Paper assay development and detection of protease activity. Reproduced with permission from ref 421. Copyright 2014 National Academy of Sciences, U.S.A.

Wax printing requires two steps and produces hydrophobic barriers of wax that extend through the thickness of the paper. When the paper is heated, the wax melts and spreads both vertically and laterally into the paper. The vertical spreading creates the hydrophobic barrier. The lateral spreading lowers the resolution of the method and produces barriers that are much larger than the initially printed pattern. Figure 47b shows the mechanism of the μPAD. The channel is comprised of a porous matrix of hydrophilic cellulose fibers that wick fluids along the path defined by the channel. The sides of the channel are bounded by hydrophobic barriers, and the top and bottom of the channel are open to air environment. Figure 47c shows the excellent capillary action of the paper and the diagnostic capability via detection of protein and glucose. The color changes depend on the concentration of reagents. Paper-based microfluidics are promising point-of-care diagnostic devices.[413] Chen et al. describes enzyme-linked immunosorbent assays (ELISA) performed in a 96-microzone plate fabricated in paper (paper-based ELISA, or P-ELISA) and proved that the combination of ELISA and patterned paper will provide a useful new platform for performing immunoassays.[414]

5.4. Biosensor on Paper

Electrochemical paper biosensors demonstrate the successful integration of paper-based microfluidics and electrochemical detection as an easy-to-use, inexpensive, highly sensitive, and portable alternative for point of care monitoring. This type of detection has four advantages: (1) it is lightweight, portable, single use, and disposable; (2) the sensors are flexible and foldable; (3) it has excellent reproducibility with high sensitivity and accuracy; and (4) it does not require professional medical personnel or complicated instruments.[413] Dr. Henry's group first demonstrated electrochemical detection with paper-based electrochemical devices.[415] Figure 48a shows three-electrode paper-based microfluidic devices. The hydrophilic area at the center of the device wicks sample into three separate test zones, where independent enzyme reactions occur with glucose, uric acid, or lactate. The silver electrodes and contact pads are made from Ag/AgCl paste, and the black electrode portions are Prussian blue-modified carbon electrodes. The inset image shows the basic design of the paper-based electrochemical detection, with WE being the working electrode, CE the counter electrode, and RE the reference electrode. Nie et al. describes the fabrication and performance of similar paper-based electrochemical biosensor devices. Figure 48b is a schematic of a paper-based electrochemical device. The sensor is comprised of three electrodes printed on a piece of paper substrate. Figure 48c shows a hydrophobic paper-based device for the detection of heavy metal. The continuous wicking of the sample solution across the paper dramatically enhances the efficiency of metal deposition during anodic stripping voltammetry, resulting in improved sensitivity and reliability. Figure 48d and 48e plots the electrochemical characterization of the device. Reversible cyclic voltammograms in Figure 48d indicate that no side reactions take place and that, as expected, the kinetics of electron transfer are sufficiently rapid to maintain the surface concentrations of redox-active species at the values required by the Nernst equation (Figure 48e). Low-cost, paper-based diagnostic and analytical devices are attractive for use in developing countries, in the field, or in home health-care settings.

5.5. Bioactive Paper

Bioactive paper is a paper-based device that uses the inherent hydrophilic and capillary properties of paper to perform analytical functions such as pathogen detection. Due to its low cost, portability, and disposability, bioactive paper has attracted

DOI: 10.1021/acs.chemrev.6b00225
Chem. Rev. XXXX, XXX, XXX−XXX

Table 4. Timeline of Paper Solar Cell

year	type of paper	PCE (%)	transmittance (%)	function
2005[422]	newspaper	~0.3	NA	substrate
2010[423]	starch coated paper	~0.13	NA	substrate
2011[425]	tracing paper	<1.5	~84	substrate
2011[426]	glossy paper	~1.31	NA	substrate
2012[424]	polyethylene-coated carton	~0.4	NA	substrate
2013[428]	nanopaper	~0.21	~90	substrate
2013[216]	cellulose nanocrystal film	~2.7	~75	substrate
2014[204]	highly transparent and hazy paper	~5.9	96	light management layer
2014[429]	highly transparent and hazy paper	~23.8 (increment of PCE)	96	light management layer
2015[427]	coated paper	~3.4	NA	substrate

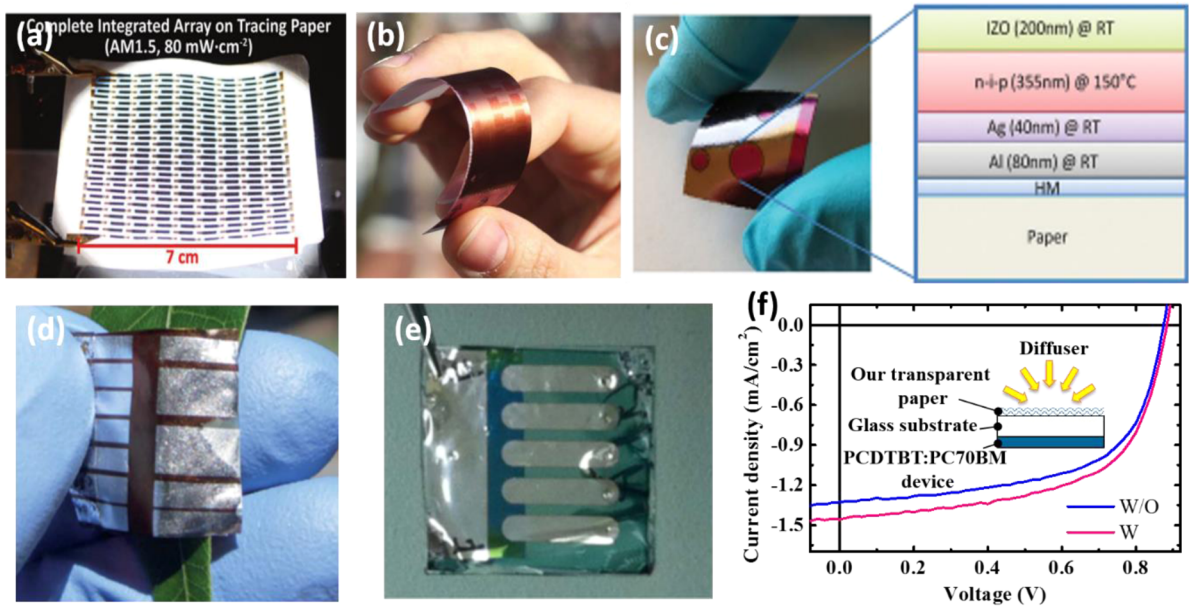

Figure 50. (a) Photovoltaic arrays on tracing paper. Reproduced with permission from ref 425. Copyright 2011 Wiley-VCH. (b) Printed paper photovoltaic cell. Reproduced with permission from ref 426. Copyright 2011 Wiley-VCH. (c) a-Si:H PV cells on the paper (left), and schematic of a-Si:H PV cells (right). Reproduced with permission from ref 427. Copyright 2015 Wiley-VCH. (d) Solar cells on nanopaper made of TEMPO-oxidized NFC. Reproduced from ref 428 with permission from The Royal Society of Chemistry. Copyright 2013. (e) Organic solar cells on nanopaper fabricated by CNCs. Reproduced with permission from ref 216. Copyright 2013 Nature Publishing Group. (f) *I*−*V* curves of the organic photovoltaic device with/without transparent paper made of microfibers. Reproduced with permission from ref 204. Copyright 2014 American Chemical Society.

much attention.[416−418] Figure 49a shows a paper-supported sensor which measures the presence of DNase. Au nanoparticles are cross-linked via DNA hydridization to form a blue-colored aggregation.[419] The addition of DNase I cleaves the DNA cross-linkers to break the aggregate into well-dispersed Au nanoparticles, which appear red. Figure 49b plots the DNase I sensor assay on hydrophobic paper at various times and DNase I concentrations. The red color intensity increases with both higher DNase I concentration and longer assay time. Paper substrates show excellent properties for use in cost-effective, easy-to-use colorimetric bioassays with Au nanoparticles as the signal transducer. Figure 49c shows a paper assay developed for the detection of protease activity.[420] Captured antibodies are adsorbed in spatially multiplexed lines on paper. The lateral flow assays are developed by application of analyte, wash buffer, and streptavidin−gold detection NPs that wick past the captured antibodies and develop lines. Lateral flow assays may be scanned, and the reporter concentration is proportional to band intensity. This work designed nanoscale agents that are capable of revealing the presence of diseased tissues by interacting with a biomarker in the urine that can be detected using paper strips. This platform does not require expensive instruments, invasive procedures, or trained medical personnel and may allow low-cost diagnosis of diseases at the point of care in resource-limited settings in developing countries.

The stability of antibodies on bioactive paper will directly affect the printing or other roll-to-roll manufacturing procedures. Dr. Pelton's group investigated the stability of paper-immobilized antibodies over a range of temperature (40−140 °C) and relative humidity (RH 30−90%) using both unmodified filter paper and the same paper impregnated with polyamide−epichlorohydrin as support.[421] Between 40 and 60 °C, there is a slow decline of up to 20% loss in activity, which did not depend on relative humidity. Temperatures higher than 100 °C cause complete deactivation. Moreover, hydration of the antibody promotes the deactivation. The shelf life of bioactive paper is critical for commercial applications. Future work should include finding an antibody stable with respect to long-term storage and use.

DOI: 10.1021/acs.chemrev.6b00225
Chem. Rev. XXXX, XXX, XXX−XXX

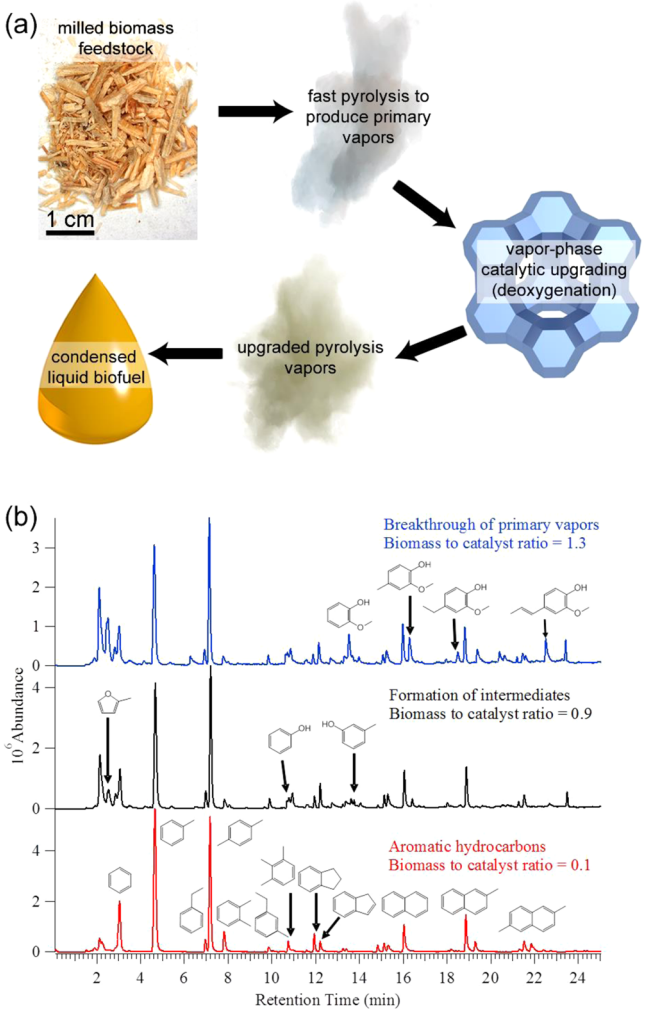

Figure 51. (a) Simplified conceptual depiction of a catalytic fast pyrolysis process. Solids are fed into a 2 in. fluidized bed reactor (FBR). Effluent from the reactor is sent through a cyclone to remove solid char particles and then through a hot gas filter prior to condensation. (b) Gas chromatograms illustrating chemical products of catalytic fast pyrolysis as a function of catalyst activity. Fully active catalyst results in nearly complete deoxygenation of pyrolysis vapors (red spectrum); however, as catalysts they exhibit a loss of activity with continued exposure to pyrolysis vapors (black and blue spectra) and must be regenerated periodically to maintain optimal performance.[462] Reproduced with permission from ref 462. Copyright 2007 American Chemical Society.

6. WOOD-DERIVED SUSTAINABLE ENERGY

Recently, widespread attention has been paid to wood and its derived materials in energy-related researches. For example, cellulose-based substrates have exhibited great promise for solar cells considering the lightweight, abundance, flexibility, and biodegradability of cellulose compared to plastic. Furthermore, wood-based materials are widely used for producing biofuels, which can significantly help to lower the dependence on the ever-depleting fossil fuels and reduce the environmental pollution from the emission of greenhouse gases. Today, electrochemical energy conversion and storage technologies have intensively employed wood-based materials as carbon precursors, binders, separators, etc. In this section, we will review the work in energy-related research using wood and its derived materials.

6.1. High-Performance Solar Cells Enabled by Printing and Advanced Light Management

Both the high production cost and the high material cost hinder the widespread popularization of solar cells for energy harvesting in our society. Paper, as a lightweight and inexpensive substrate, is potentially an efficient solution to the current challenges of solar cells. However, the microsized surface roughness and porous structure of paper make it challenging to fabricate photovoltaics with good performance on such substrate.[364] Recently, extensive research has focused on overcoming the shortcomings of paper to make it an attractive substrate for solar cells. Detailed information for paper solar cells is listed in Table 4. Hu et al. demonstrated extreme light management in mesoporous paper in which the light scattering can be dramatically modulated.[396] For example, we recently demonstrated transparent paper with a high forward transmittance and high optical haze, which leads to effective light trapping in solar cells and moves us toward a high energy conversion efficiency.

In 2005, the first paper-based organic photodiodes were fabricated on newspaper by depositing a thin layer of Parylene C on the newspaper surface. These paper-based organic photodiodes presented a power conversion efficiency (PCE) of <0.3%.[422] Polymers, such as starch and polyethylene, were utilized to smooth the paper surface while enhancing its barrier properties prior to fabrication with solar cells.[423,424] Researchers developed an all-dry fabrication and monolithic integration strategy to produce solar cell arrays on tracing paper by combining oxidative chemical vapor deposition with in-situ shadow masking, followed by capsulation (see Figure 50a). These photovoltaic arrays presented a lifetime of over 500 h despite the observation that their PCE was less than 1.5%.[425] Hübler et al. demonstrated photovoltaic cells on glossy paper with a PCE of 1.31% by employing three printing methods (e. g., gravure, transfer, flexography) commonly used in conventional printing processes (see Figure 50b).[426] To attain good-performing photovoltaic cells, a printing paper with a cast-coated layer of a hydrophilic mesoporous material, demonstrating an RMS roughness of 9.42 nm, was used to successfully fabricate a-Si:H cells with 3.4% cell efficiency. The optical image of obtained solar cells and its structure are illustrated in Figure 50c.[427]

The above solar cells were fabricated on commercial paper made from microsized wood fibers. Nanopaper made of cellulose nanofibers has recently garnered tremendous attention due to its mechanical ductility, high transparency, and ultrasmoothness. Hu et al. demonstrated solar cells on highly transparent nanopaper substrate made of NFC (~90% at 550 nm). The obtained nanopaper solar cells presented a PCE of ~0.21% (see Figure 50d).[428] To further enhance the PCE of nanopaper solar cells, Kippelen et al. displayed solar cells on nanopaper substrate fabricated from CNC. The solar cells not only exhibited 2.7% cell efficiency but also presented the potential recyclability of nanopaper solar cells (see Figure 50e).[216]

Various paper-based solar cells were demonstrated by a variety of fabrication approaches in the past decade; however, the paper in these paper solar cells only acts as a flexible and affordable substrate for depositing conductive, semiconductive, and dielectric materials rather than as a functional component. Fang et al. developed a highly transparent paper with highly optical haze by using TEMPO-oxidized wood pulp. In comparison to glass and plastic films widely used in photonic devices, this paper has a similar optical transmittance (>90% at 550 nm) while possessing a high transmission haze (~60% at 550

DOI: 10.1021/acs.chemrev.6b00225
Chem. Rev. XXXX, XXX, XXX−XXX

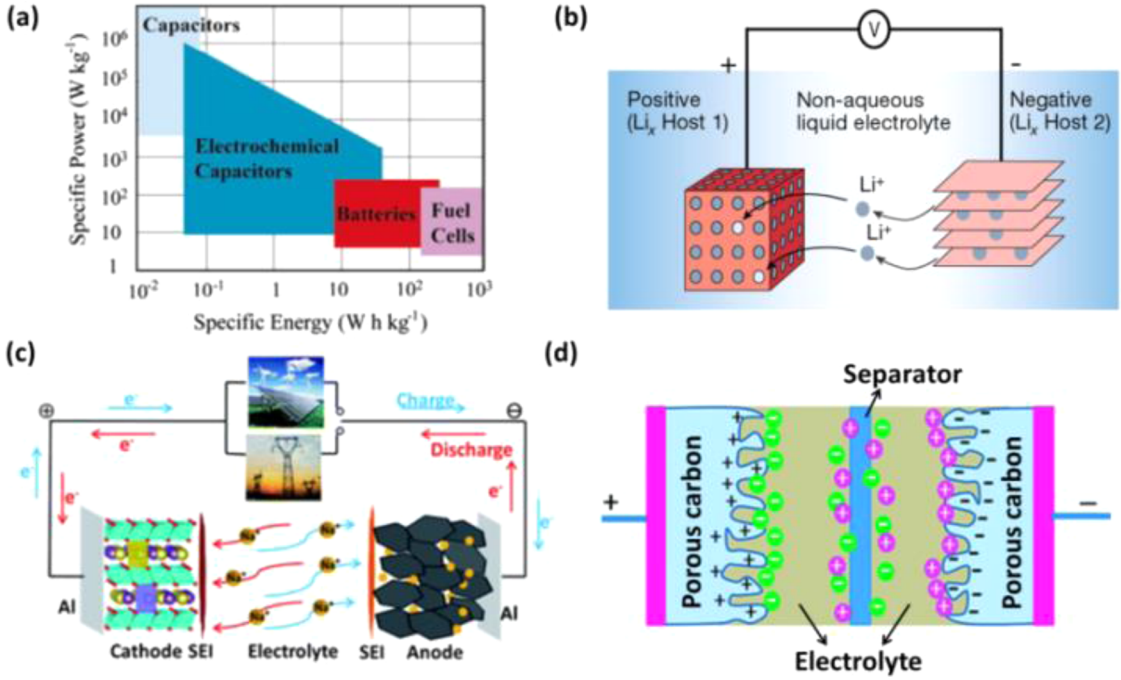

Figure 52. (a) Ragone plot of specific power versus specific energy for the various EES technologies.[473] Reprinted with permission from ref 473. Copyright 2013 Elsevier. (b) Working mechanism of Li-ion batteries.[474] Reproduced with permission from ref 474. Copyright 2001 Nature Publishing Group. (c) Working mechanism of Na-ion batteries.[475] Reproduced with permission from ref 475. Copyright 2013 The Royal Society of Chemistry. (d) Working mechanism of double-layer electrochemical capacitors.[476] Reproduced with permission from ref 476. Copyright 2014 The Royal Society of Chemistry.

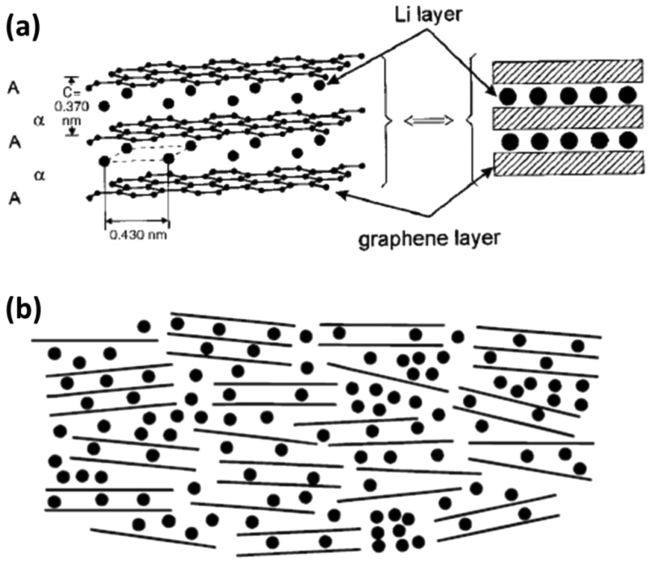

Figure 53. (a) Li-ion storage in graphite.[488] Reproduced with permission from ref 488. Copyright 1998 Wiley-VCH. (b) "House of cards" model for Na/Li ions filled in hard carbon.[497] Reproduced with permission from ref 497. Copyright 2000 The Electrochemical Society.

nm). High transmission haze enables the enhancement of the light traveling length within the active layer of solar cells that increases the light-trapping capability. Through simply laminating this paper into the surface of organic photovoltaic (OPV) as a light management layer, the PCE of OPV increased by 10% compared to the OPV without this transparent paper layer (see Figure 50f), showing the excellent light management of highly transparent paper with high optical haze. In addition, this transparent paper was applied to GaAs solar cells as an antireflection layer. A piece of this paper was laminated into GaAs solar cells by a transparent binder; an improved PCE of 23.8% was observed by simple lamination.[429]

6.2. Biofuels from Woody Feedstocks and Other Biomass

The biopolymers that constitute cell wall tissue are rich in chemical energy and thus hold great potential for direct conversion to liquid biofuels. Methods employed to convert woody biomass are largely similar to those used to convert other lignocellulosic feedstocks; therefore, the content of this section will be generalized to lignocellulose conversion. Strategies for conversion of lignocellulosic biomass into liquid biofuels can be typically classified into biochemical routes and thermochemical routes. Each of these encompass vast, well-established, and active areas of research which will not be extensively reviewed here; however, the importance of biofuels to the utilization of wood and other lignocellulosic resources warrants an overview in the present work.

6.2.1. Biochemical Conversion Processes. The modern biofuels industry had its roots in the turmoil of World War I when Germany developed processes to convert biomass sugars to ethanol.[430] This process was based on dilute acid pretreatment of woody biomass and was suitable only for wartime economics. In World War II, the United States revisited lignocellulosic ethanol for butadiene production to make synthetic rubber.[431,432] The U.S. DOE began funding research in biofuels production vigorously in the early 1980s, with the advent of the Biofuels Program managed by the Office of Energy Efficiency and Renewable Energy (EERE).[433] In the later part of the 20th century, the primary focus of EERE-sponsored biofuels research was optimization of the conversion of corn stover by dilute sulfuric acid pretreatment followed by enzymatic saccharification of the neutralized biomass slurry.[434] This conversion step is called simultaneous saccharification and fermentation, or SSF,

DOI: 10.1021/acs.chemrev.6b00225
Chem. Rev. XXXX, XXX, XXX−XXX

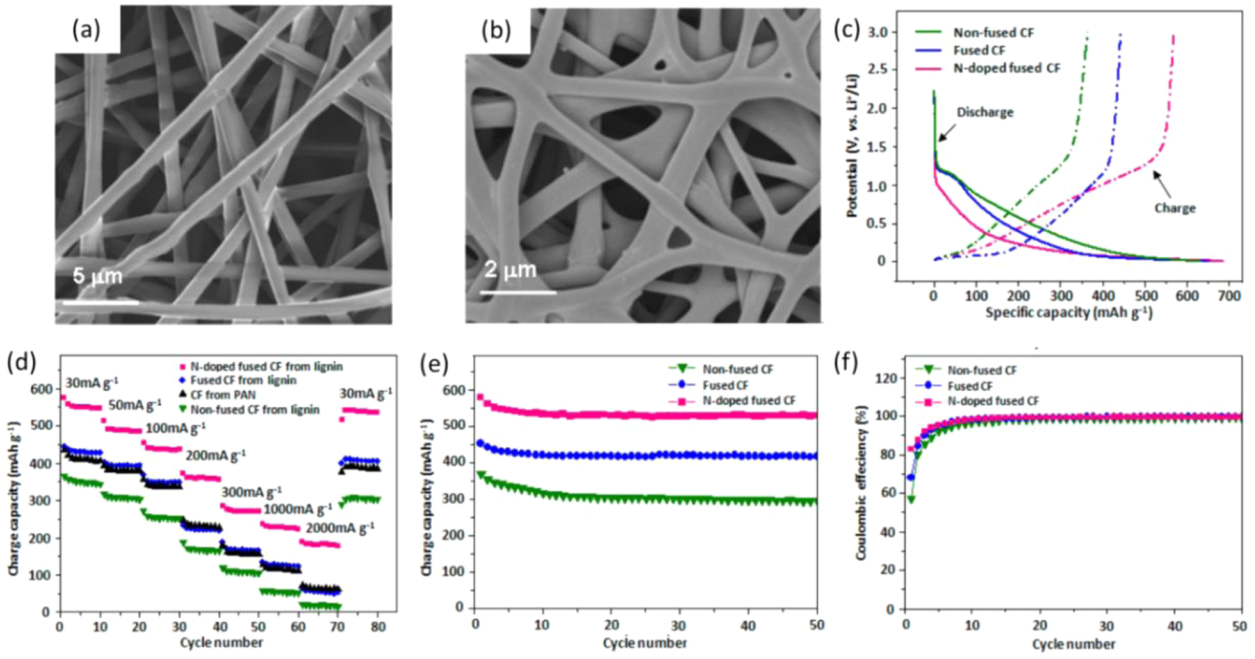

Figure 54. SEM images of electrospun lignin-PEO fibers before (a) and after (b) thermal carbonization. (c) First potential profiles of lignin-based carbon anodes at 30 mA/g. (d) Specific capacities of lignin-based carbon anodes at different current densities. (e) Cycling performance and (f) corresponding Coulombic efficiency of lignin-based carbon anodes at 30 mA/g.[184] Reproduced with permission from ref 184. Copyright 2013 American Chemical Society.

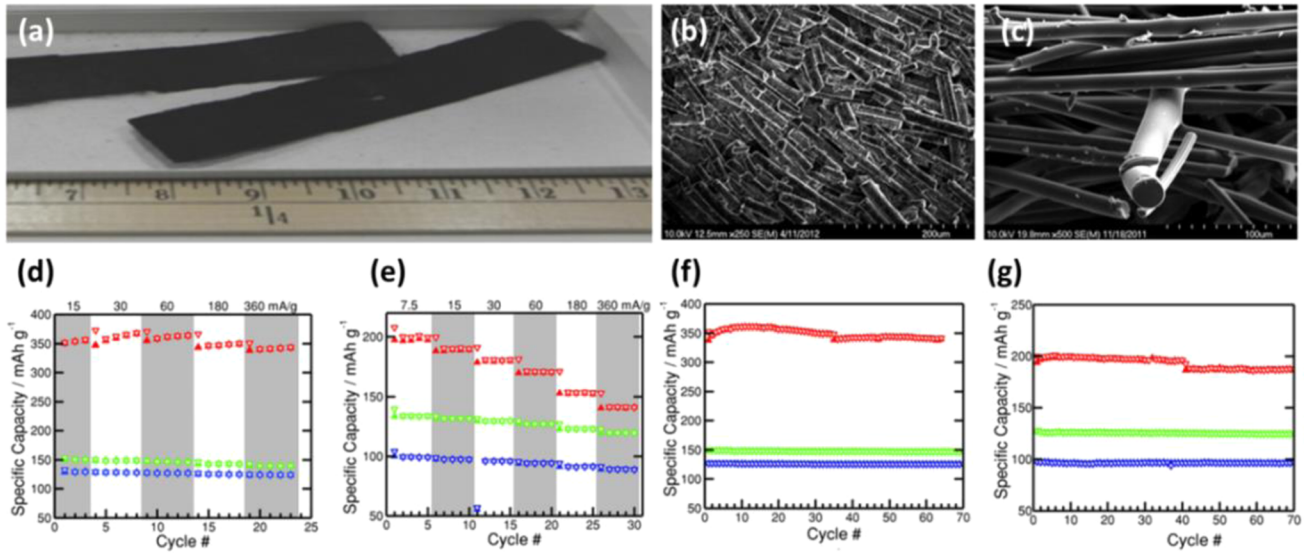

Figure 55. (a) Digital image of lignin-based carbon fibers (LCFs) fused mat. (b, d, f) LCFs electrode on copper via slurry coating method and its corresponding rate/cycling performance. (c, e, g) LCFs-fused mats electrode and its corresponding rate/cycling performance. Different color represents different carbonization temperature: 1000 (red), 1500 (green), and 2000 °C (blue).[185] Reproduced with permission from ref 185. Copyright 2014 Wiley-VCH.

because the cellulase preparation is added to the slurry during the fermentation process. SSF application required that the cellulase cocktail and fermentative microorganism function at compatible pH and temperature. Thus, the options for exploring more effective enzymes and organisms were limited. Of particular note is the progress made during the first decade of the millennia toward improving the performance, and thus reducing the cost, of the cellulase enzymes. For example, round robin testing established the estimated cost of enzyme needed to produce a gallon of ethanol from corn stover at about $5 in 2004.[431] After several rounds of DOE funding provided competitively to the enzyme companies, this value was reported to be closer to 1/10th this cost (i.e., $0.68/gallon ethanol) in 2012.[435] Also during this time, the pretreatment and lignin removal steps were optimized to reduce cost. It was found that a value known as the pretreatment severity factor (based on acidity, time, and temperature) could be optimized using state of the art auger-powered pretreatment reactors which were scalable.[436,437] Conditions were found which reduced the production of inhibitors (furfural and hydroxymethyl furfural) and enhanced the subsequent enzymatic saccharification step. Fermentative microorganisms, yeast (*Saccharomyces cerevisiae*), and bacteria

DOI: 10.1021/acs.chemrev.6b00225
Chem. Rev. XXXX, XXX, XXX−XXX

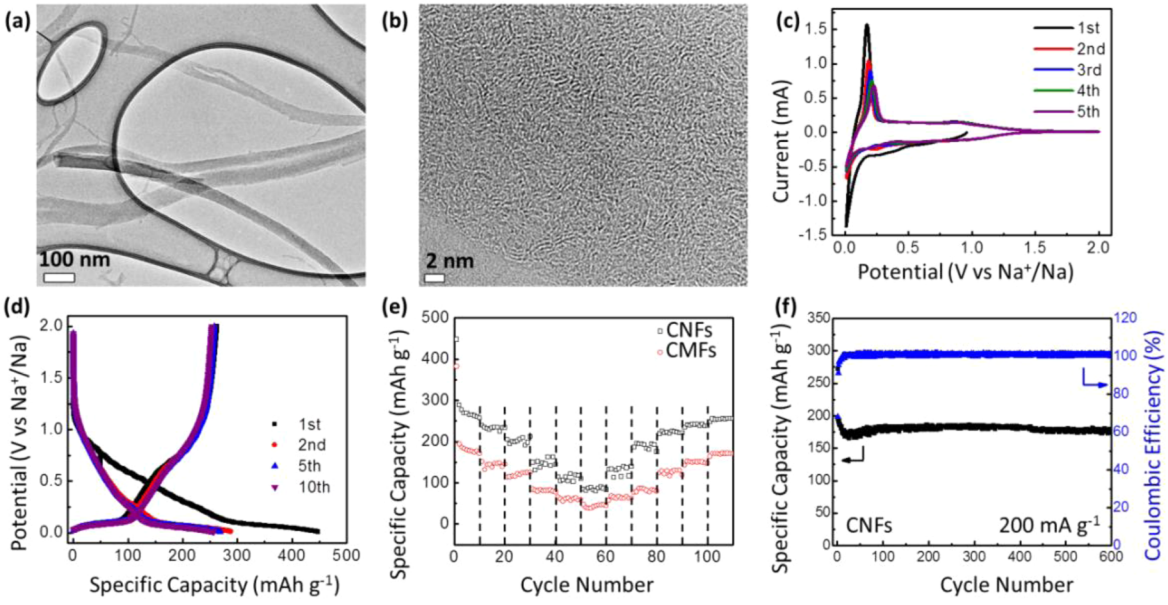

Figure 56. Cellulose nanofibers-derived CNF as anode for NIBs: (a, b) TEM images of CNF, (c) CV curves, (d) potential profiles at 40 mA/g, (e) rate performances, and (f) cycling performance of the CNF electrode.[186] Reproduced from ref 186 with permission from The Royal Society of Chemistry. Copyright 2013.

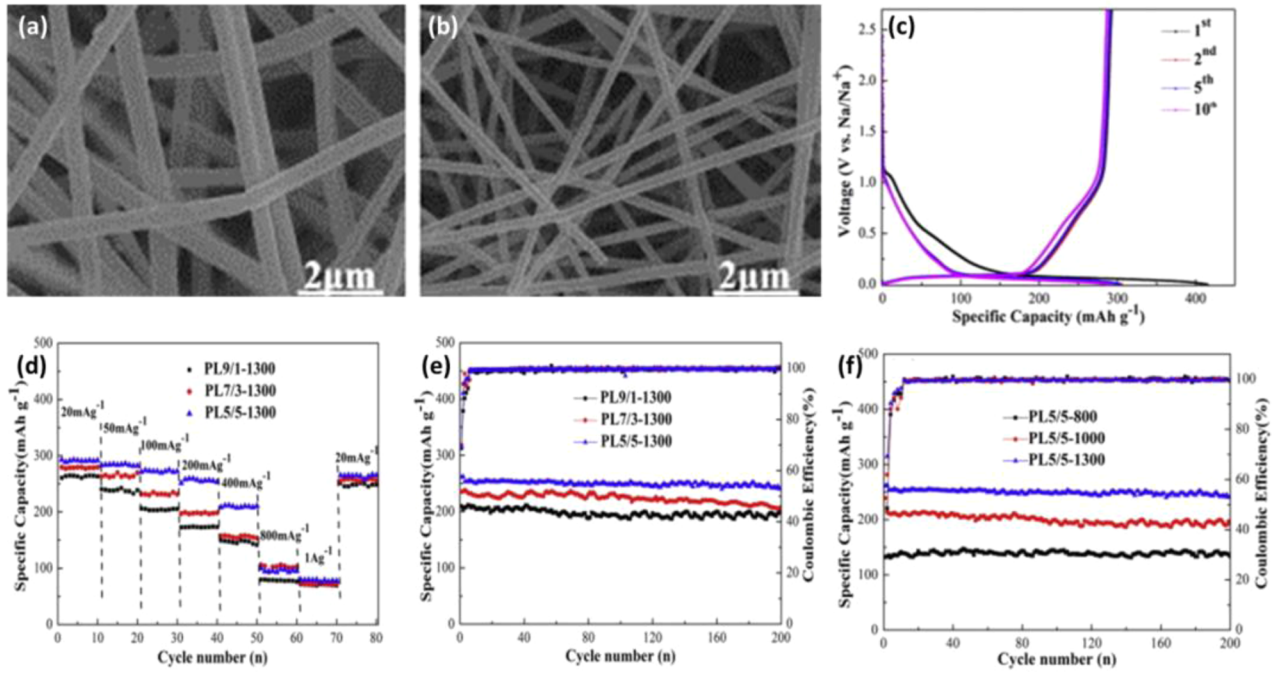

Figure 57. Lignin-based carbon nanofibers as anode for NIBs: (a, b) SEM images, (c) potential profiles, (d–f) rate and cycling performances.[501] Reprinted with permission from ref 501. Copyright 2014 Elsevier.

(*Zymomonas moblis*) were also improved by genetic engineering to ferment both C5 as well as C6 sugars without diauxic effects (the preferential fermentation of glucose displayed by most organisms).[438,439] A final report was issued by NREL at the close of 2011 which outlined the State of Technology process for bioethanol production from corn stover at about $2.15 per gallon in 2007 dollars.[440]

A more complex and effective biochemical conversion process is envisioned today. For example, essentially all aspects of the traditional biomass to ethanol process, including feedstocks, pretreatment, saccharification, and biofuel production, are being revisited. DOE now supports work to explore the suitability of other biofuels feedstocks, which include switch grass, poplars, soft woods, municipal solid waste, and construction waste. A new emphasis has emerged in the last half decade on the use of genetic engineering to enhance these feedstocks, with special focus on reducing biomass recalcitrance by modifying the lignin synthetic pathways. Recent work by several groups has shown that enzyme loadings and/or pretreatment severity can be reduced by altering the lignins produced in plants, for example, the caffeic acid *O*-methyltransferase (COMT) pathway mutants in switchgrass,[441,442] the *med5a/5b ref8 Arabidopsis* mutants which

DOI: 10.1021/acs.chemrev.6b00225
Chem. Rev. XXXX, XXX, XXX−XXX

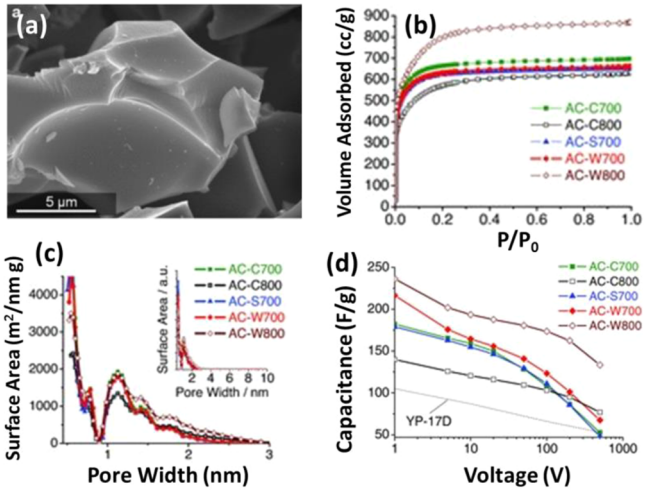

Figure 58. (a) SEM image of microporous carbon. (b) N_2 adsorption/desorption isotherms and (c) pore size distribution for hydrothermally synthesized carbons after activation. (d) Specific capacitance of carbon samples at different CV scan rates.[507] Reproduced with permission from ref 507. Copyright 2011 WILEY-VCH.

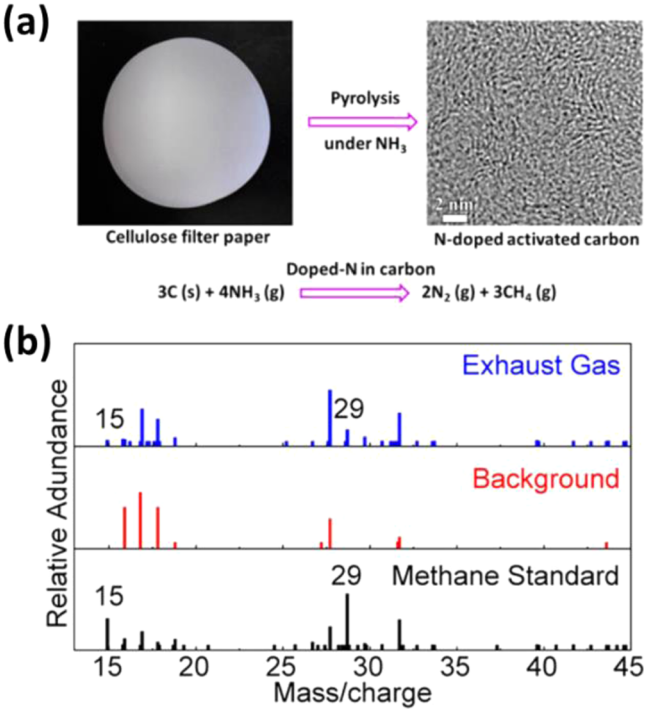

Figure 59. Fabricating N-doped porous carbon by a one-step annealing of cellulose filter paper under NH_3: (a) Schematic shows the activation mechanism. (b) MS study on exhaust gases from the activation reaction.[508] Reproduced with permission from ref 508. Copyright 2014 American Chemical Society.

contain almost exclusively of *p*-hydroxyphenyl lignin,[443] and the expression of glycoside hydrolases,[444] as well as iron binding proteins, in *Arabidopsis* cell walls.[445,446] The genetic engineering of biofuels feedstocks is a rich and promising endeavor which should be followed closely.

It is likely that all biochemical biomass conversion processes using enzymes for saccharification will require some form of pretreatment, although the severity and energy input of these steps will surely be reduced by improvements in plants and enzymes.[447] The dilute acid pretreatments of the past decade have not given way to new concepts based on the use of alkali. Alkaline pretreatments offer some distinct advantages for acidic processes, including operability in stainless steel reactors with no corrosion-related costs. For example, treatment of grassy biomass at pH 9−10 and <100 °C deacetylates the cell walls, a process step which removes one of the most toxic components to fermentative microorganisms, acetic acid. Deacetylation can be followed by dilute acid treatments, more concentrated alkaline steps, or mechanical refining. Treatment of biomass at pH 10−12 and >100 °C removes most of the lignin and hemicellulose fractions in biomass, leaving behind some protected hemicellulose and cellulose. This alkaline process stream is rich in soluble lignins and intact hemicellulose, both of which can be converted to high value by products via fermentative or catalytic routes. The effect of mechanical disruption has been identified as an important characteristic of successful pretreatment technologies in both acidic and alkali pretreatment process. Processes that result in nanofibrillation of the cellulose fibrils within the cell wall matrix greatly enhance the accessibility of these carbohydrates to enzymes and result in dramatically enhanced conversion.[448] A new pretreatment approach reported in 2013 is based on the use of combined low-severity alkaline treatment followed by mechanical milling. In the DDR (deacetylation disk refining) process, the biomass is subjected to pH 10 mixing and then various shear levels in disk refiners (mills) without neutralization.[449] The resulting biomass is considerably more digestible by traditional cellulose preparations than that from the dilute acid pretreatment process. Similar biofuel production processes developed by the USDA Forest Products Lab have been shown to be effective for both softwood[450] and hardwood feedstocks.[451] Such processes, which have been reviewed extensively elsewhere,[452] employ largely similar mechanical comminution methods, pretreatments such as dilute acid, steam explosion, alkaline, or Organosolv variations, as well as commercial cellulase cocktails that are identical to those used for saccharification of other forms of lignocellulosic biomass. As we go forward, new combinations of biomass pretreatment will be developed as the feedstocks and process conditions evolve.

Cellulase cost remains a key obstacle to the commercialization of biofuels.[435] The traditional biomass conversion scheme has been based on the addition of extraneous cellulase/hemicellulase preparations grown and refined off site, i.e., delivery in tanker cars. The most recent biofuels plant designs show on-site enzyme production, and it is assumed that the enzyme companies will operate such facilities in this way to take advantage of the power and heat abundance offered by the much larger biofuels plant.[440] Additionally, the addition of stabilizers should not be required in this scenario. As stated above, the recent improvement in the cost of cellulases is primarily due to reduced cost of production. Also, although performance improvements in enzyme formulations have been reported, mainly by the addition of lacking and essential enzymes, modern commercial enzyme products harbor few if any enzymes engineered to have higher specific activity. This then is an arena for future growth, as the accounts of cellulases improved to achieve higher activity (not thermal tolerance) by engineering are few.[12,453,454] Another approach holding promise is the continued mining of glycoside hydrolases produced by naturally occurring lignocellulose degraders. For example, the CelA multidomain cellulase, produced by *Caldicellulosiruptor bescii*, was shown recently to be the highest performing single-gene product cellulase reported.[455] Obviously, efforts to discover new cellulase/hemicellulase structural

DOI: 10.1021/acs.chemrev.6b00225
Chem. Rev. XXXX, XXX, XXX−XXX

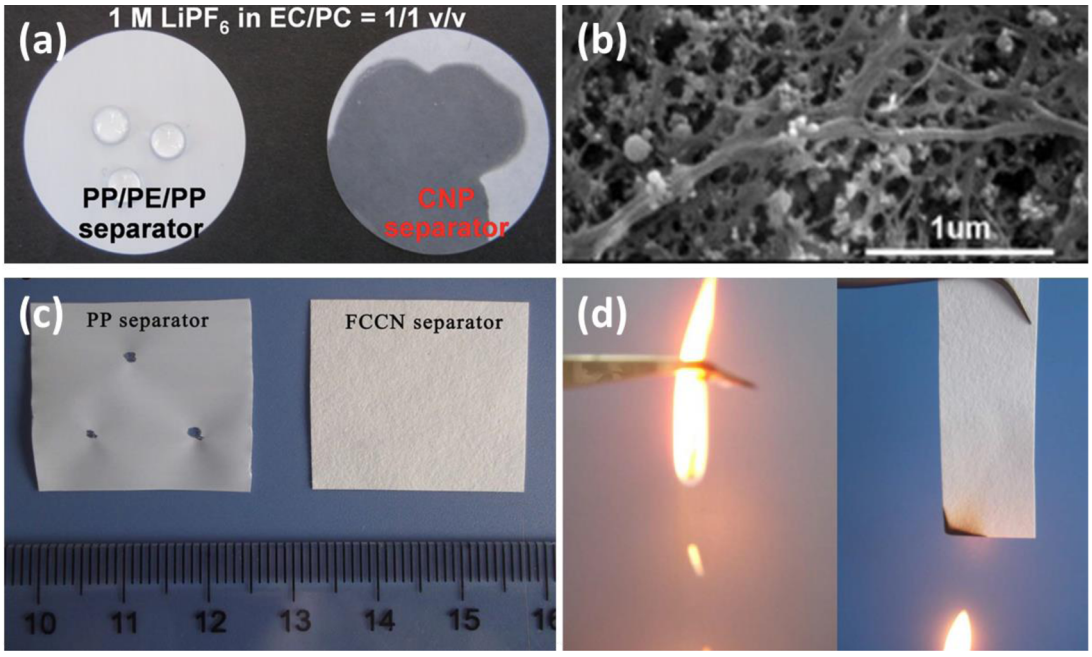

Figure 60. (a) Photographs depicting wettability of PP/PE/PP and cellulose nanofiber paper separators.[243] Reproduced with permission from ref 243. Copyright 2012 The Royal Society of Chemistry. (b) SEM image of SiO_2-incorporated cellulose nanofiber paper separator.[245] Reprinted with permission from ref 245. Copyright 2013 Elsevier. (c) Contact test between hot electric iron tip and separators. (d) Combustion behavior of PP and FCCN separators.[513] Reproduced with permission from ref 513

paradigms will play into ongoing enzyme engineering work to continuously improve the performance of these key enzymes. The traditional bioethanol process was based on SSF (stated above); however, new process options have been raised recently to take advantage of thermal tolerant enzymes and the desirability to generate by product streams from the biofuels plant. Thermal tolerant cellulases and hemicellulases permit the addition of enzymes to the neutralized but still hot effluent coming from pretreatment[456] in a process option called separate hydrolysis and fermentation, or SHF. Other process designs are driven by the need for new process streams, especially for the new advanced biofuels production schemes.

In early 2014, the notion of turning the attention of the U.S. DOE from the long-standing bioethanol production technology to the so-called advanced biofuels or specifically "high-performance biofuels and bioproducts" was introduced.[457] Advanced biofuels are defined as any liquid transportation biofuel derived from lignocellulosic sugars, sometimes referred to as Generation 2 biofuels processes. Note that Generation 1 biofuels are currently in production, i.e., ethanol from starch. Thus, production of advanced biofuels includes primarily mid- and long-chain alkanes (jet and diesel fuels) as well as lipids (free fatty acids and fatty acid methyl esters which are fuels precursors) from lignocellulose. Compared to the bioethanol production research and development, advanced biofuels production technologies are just beginning. For example, some progress has been reported for the anaerobic production of farnesene (C-15) from glucose by pathway engineering;[458] however, initially the titers are low (<400 mg/L). More recent work has improved production to a more commercially interesting level (~1.1 g/L).[459] A common problem shared by the hydrocarbons and fatty acids producing strains is the requirement to extract the products into an immiscible phase, such as dodecane. In the case of solvent extractions of biomass fermentation broth, the costs of operating this critical step at ultralarge scale are uncertain. The production of lipids from biomass sugars utilizing so-called oleaginous yeast is more promising and probably more achievable in the near term. Strains of *Yarrowia lipolytica* and *Lipomyces starkeyi* have been shown to produce fatty acids as high as 70% total cellular dry weight.[460,461] However, of concern for the application of lipogenic yeast for advanced biofuels production is the challenge afforded by the requirement for aerobic culture of these organisms at ultralarge scale (>10 000 gallons). Thus, both the aerobic and the anaerobic production routes to advanced biofuels present challenges for demonstration and scale up, which supports the vigorous research and development agenda set forth by the U.S. DOE today.

6.2.2. Thermochemical Conversion Processes. Thermochemical conversion pathways encompass technologies such as fast pyrolysis, gasification, and hydrothermal liquefaction that employ elevated temperatures to deconstruct the biopolymers in wood and other biomass into lower molecular weight hydrocarbons and carbohydrate derivatives.

Fast pyrolysis is a process that involves the rapid heating of biomass in an inert environment to temperatures typically ranging from 400 to 600 °C. This process results in the formation of light, noncondensable gases including, CO, CO_2, and C1−C5 hydrocarbons, higher molecular weight condensable vapors, including aromatics and heavier carbohydrate derivatives, and residual solids termed, char. Condensation of the high molecular weight vapors yields a viscous liquid mixture of compounds collectively termed "pyrolysis oil" or simply "bio-oil." Fast pyrolysis employs high heating rates on the order of ~1000 °C/s, small particle sizes on the order of a few millimeters, and short residence times on the order of several seconds to tens of seconds to minimize char production and increase the carbon yield in the bio-oil. Raw bio-oil typically has a high oxygen content which necessitates subsequent hydrotreating before it becomes a suitable transportation fuel or may be integrated with product streams in conventional petroleum refineries.[462] Catalytic fast

DOI: 10.1021/acs.chemrev.6b00225
Chem. Rev. XXXX, XXX, XXX−XXX

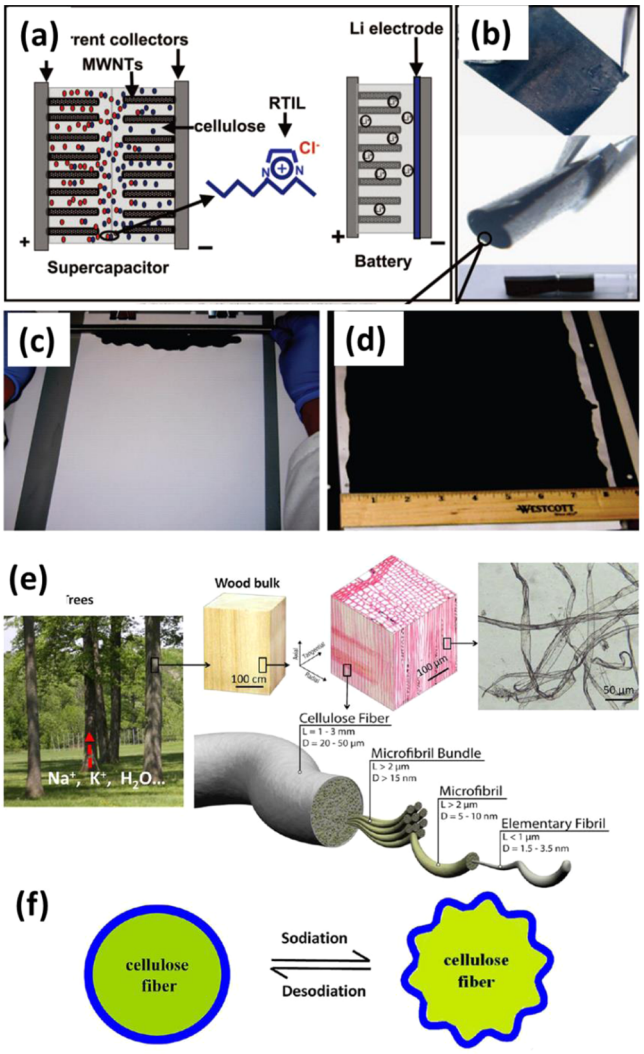

Figure 61. (a) Schematic of batteries or ECs assembled by using CNT/cellulose/ionic liquid nanocomposite. (b) Photographs of the nanocomposite, demonstrating the mechanical flexibility.[514] Reproduced with permission from ref 514. Copyright 2007 National Academy of Sciences, U.S.A. (c) Meyer rod coating of CNT ink on commercial Xerox paper. (d) Conductive Xerox paper after CNT coating.[273] Reproduced with permission from ref 273. Copyright 2009 National Academy of Sciences, U.S.A. (e) Hierarchical structure of wood fiber. (f) Soft wood fiber substrates effectively address the stresses during electrochemical reactions by structural wrinkling.[17] Reproduced with permission from ref 17. Copyright 2013 American Chemical Society.

pyrolysis (CFP) is one strategy being considered to overcome this problem and involves exposing pyrolysis vapors to deoxygenation catalysts prior to condensation. A simplified conceptual depiction of a CFP process is shown in Figure 51a. Various zeolite catalysts have been found to be effective for this purpose, although coke formation on the catalysts leads to deactivation over time[463] as demonstrated in Figure 51a and 51b, which will likely require their continuous regeneration to maintain sufficient catalytic activity. Another strategy to chemically reduce the products formed during pyrolysis is fast hydropyrolysis. In this process, biomass is pyrolyzed in the presence of H_2 gas, which promotes the loss of oxygen in the form of H_2O and increases the overall energy content of the oil.[464] Advantages of fast hydropyrolysis include its modest hydrogen consumption relative to other hydrotreating processes and the opportunity to altogether eliminate the downstream hydrotreating unit operation.[465]

Gasification is a thermochemical conversion process that produces syngas (i.e., a mixture H_2, CO, and CO_2) or other combustible gas from carbonaceous feedstocks including coal, biomass, and natural gas. The product gas can be used subsequently for production of electricity as well as other chemicals. The process is carried out using temperatures in the range of ~700−1000 °C and controlled quantities of oxygen and/or steam. Many such plants have been operational for several decades, and most are located in the United States and Europe.[466] Pyrolysis is the first step of a gasification process, which is required to vaporize the feedstock, followed by high-temperature gas-phase reactions that decompose the higher molecular weight pyrolysis products to light gas products.[467] Alkali metals, which are naturally present in coal and biomass, are well known to have a catalytic effect during gasification.[468] Gasification of biomass has received a resurgence of attention in recent years due to the migration toward renewable and sustainable fuels, and recent assessment of this technology projects it to make a viable contribution to the renewable systems for heat and power generation of the future.[469]

Hydrothermal liquefaction (HTL) is a thermochemical conversion process which is also called hydrous pyrolysis because it employs moderately high temperatures (~300−400 °C) and very high pressures in the presence of liquid water, which reacts with and catalyzes the depolymerization of biomass.[470] This technology provides the advantage that the biomass need not be dried prior to entering the reactor, which can reduce the overall energy input of the conversion process. Furthermore, the ability of this process to accept wet feedstocks makes it an attractive conversion route for biomass derived from aquatic species, such as algae.[471] Recently, a direct comparison of fast pyrolysis and hydrothermal liquefaction of the same biomass feedstock was conducted. The results demonstrated that the oils produced by the two processes differed in chemical composition and that fast pyrolysis provided a higher oil yield than that obtained from HTL, which was largely attributed to water content.[472]

The various biomass-to-fuel and biomass-to-energy conversion processes described here should be considered complementary to one another rather than competitive. Each of these technologies can be used to produce a different suite of fuel and chemical products. The vastly different process conditions and conversion pathways represented by these conversion technologies enables the utilization of a wide variety of renewable feedstocks. However, the fate of wood and other biomass, whether converted into fuel or utilized in the other renewable materials applications described here, should be weighed carefully to ensure that both materials and energy demands are met efficiently, economically, and sustainably.

6.3. Batteries and Electrochemical Capacitors

Electrical energy-storage (EES) technologies play a critical role in our modern society to meet the ever-increasing demands of energy and reduce the dependence on imminent depletion of fossil fuels. Among various EES technologies, electrochemical energy-storage devices, such as batteries and electrochemical capacitors (see Figure 52a), have been used in various applications. Due to the abundance and renewability, wood and its derived materials have exhibited great potential in battery- and capacitor-related studies. For example, wood and its components are attractive candidates for the preparation of

DOI: 10.1021/acs.chemrev.6b00225
Chem. Rev. XXXX, XXX, XXX−XXX

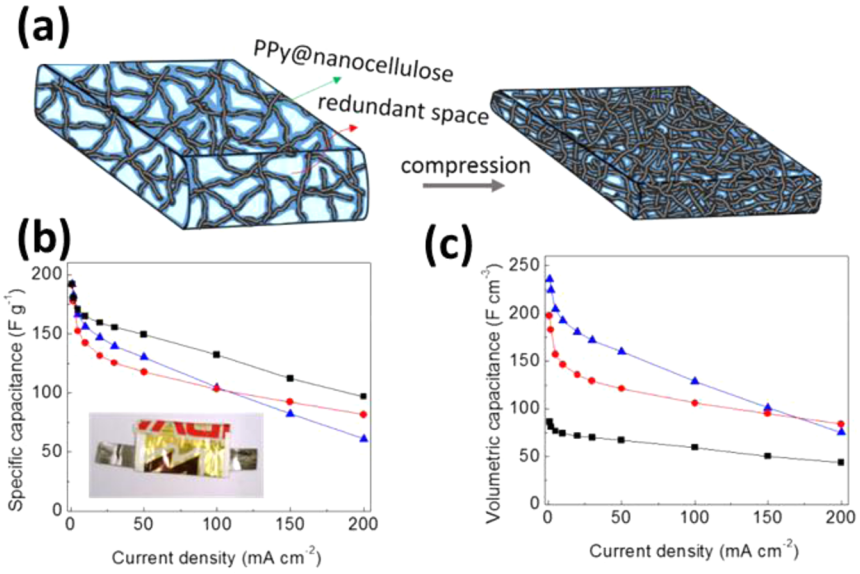

Figure 62. (a) Schematic illustrations of the PPy@nanocellulose fiber electrodes. Gravimetric (b) and volumetric (c) capacitances for paper electrodes.[517] Reproduced with permission from ref 517. Copyright 2014 The Royal Society of Chemistry.

carbon materials, which can be promising electrodes for both batteries and electrochemical capacitors. Cellulose-based separators, scaffolds, and binders are also intensively investigated in these fields.

6.3.1. Carbon Electrodes Derived from Wood and Wood Components. Since the commercialization of Li-ion batteries (LIBs) by Sony in the 1990s, graphite anodes have been widely used because Li ions can be reversibly inserted into carbon materials at low potential with a high capacity.[477] Most recently, Na-ion batteries (NIBs) have become a research focus considering their potential for low-cost, large-scale energy storage.[478,479] Unlike LIBs, only a small amount of Na ions can be intercalated into graphite; thus, wood-derived amorphous carbons have attracted great attention considering their high capacities.[480,481] Furthermore, electrochemical capacitors also use activated carbon as the electrodes; thus, wood-derived porous carbon is very promising.[482−484]

6.3.1.1. Li-Ion Batteries. In the past several decades, considerable attention has been paid to LIBs because of their high energy density and long life. Typically, LIBs are composed of a layer-structured cathode (e.g., $LiCoO_2$), graphite anode, Li salt dissolved in nonaqueous solvent electrolyte, and a porous separator (see Figure 52b).[474] The working mechanism is based on the intercalation/deintercalation concept, where Li ions are released from $LiCoO_2$ and intercalated into graphite during charging. Conversely, Li ions are deintercalated from graphite and returned into $LiCoO_2$ during discharging. Such a shuttling of Li ions enables the conversion and storage of electrical energy within LIBs.[485,486]

Currently, LIBs have dominated the market for powering portable electronics, such as mobile phones and laptops. Electrical vehicles (EVs), like TESLA, have also considered LIBs as their most promising power sources. To date, the range of EVs is still less than conventional cars due to the limited capacity of LIBs; thus, high-energy-density LIBs are intensively pursued. In order to increase the energy density, developing high-capacity electrode materials is the key.[487] Graphite, the commercial anode, exhibits a low capacity based on the intercalation mechanism (the theoretical capacity of graphite is only 372 mAh/g) (see Figure 53a).[488] Therefore, considerable effort has been devoted to the study of high-energy anodes, such as the Li metal anode and the Si anode. Although the Li metal anode[489−491] and Si anode[492−494] are very attractive, the well-known problems of dendritic Li associated with this anode as well as the volume expansion problem observed for the Si anode have significantly hampered their practical application. Thus, researchers still paid considerable attention on carbon-based anodes considering their advantages for safety, low cost, and cycle life.[477,495,496] In contrast to crystalline graphite, hard carbon is an amorphous carbon, which comprises small turbostratic graphitic nanodomains and a large number of nanopores in between these domains.[477] Besides intercalating into the small graphitic nanodomains, Li ions can also fill the nanopores between these nanodomains in a process analogous to adsorption (see Figure 53b).[497] Combining the intercalation and adsorption, hard carbon anodes can deliver a maximum capacity of 740 mAh/g, corresponding to the formation of Li_2C_6. Interestingly, as demonstrated above, wood and its components-derived carbon are normally hard carbon, which exhibits high capacity in LIBs.

Early studies have demonstrated thermosetting resins from biomass sources, such as coconut shell, can be promising precursors for high-performance hard carbon anode. Researchers also discovered that wood and its components-derived carbon can be used to produce promising anodes for LIBs. To fabricate conventional LIB electrodes, slurry-coating technologies are employed where active materials are mixed with conductive carbon additives and polymer binders using organic solvents, such as *N*-methyl-2-pyrrolidone (NMP), to produce a slurry which is then coated onto a current collector (e.g., copper for anode and aluminum for cathode). Unfortunately, the additives and current collectors do not contribute energy during battery operation, which leads to a lower specific energy density. Therefore, considerable attention has been paid to synthesize free-standing electrodes where all electrodes are active materials. In 2013, Wang et al. reported that free-standing carbon anodes can be prepared by electrospinning lignin−poly(ethylene oxide) (mass ratio of lignin/PEO is 9:1) followed by thermal carbonization (see Figure 54a and 54b).[184] The as-prepared binder-free/current collector-free carbon anode showed a high

DOI: 10.1021/acs.chemrev.6b00225
Chem. Rev. XXXX, XXX, XXX−XXX

specific capacity of 445 mAh/g and good cyclic stability (see Figure 54c). Interestingly, nitrogen doping can be further obtained by annealing the lignin-based carbon with urea. The N-doped lignin-based carbon anode delivered a higher capacity of 576 mAh/g and a great rate capability of 200 mAh/g at 2 A/g as well as stable cycling performance (see Figure 54d–f). This research demonstrated that lignin can be an inexpensive precursor for producing high-performance carbon anode. However, it is still difficult to produce this kind of carbon material in large scale by electrospinning such that a new method is highly required.

Most recently, Tenhaeff et al. at Oak Ridge National Laboratory developed a novel anode synthesis method using fibrous hardwood-derived lignin as precursor.[185] Typically, fabricating carbon material from pure lignin consists of two separate steps: oxidative stabilization and carbonization, where the stabilization plays a very critical role in maintaining the 1D fiber structure and enhancing the tolerance at high carbonization temperature. To fuse the lignin fiber mat but yet avoid its melting fully, the lignin fiber mat is first stabilized at 250 °C in a convection furnace with a sufficiently fast heating rate. As shown in Figure 55a, self-standing carbon electrodes at pilot scale have been produced with the controlled oxidative stabilization and a conventional carbonization process. The SEM images show that carbonized lignin keeps the 1D fibrous structures even after grinding for slurry coating (see Figure 55b and 55c). When evaluated as a binder-free/current collector-free electrode in LIBs, the lignin-based carbon anode demonstrated a specific capacity of ∼200 mAh/g and a Coulombic efficiency (CE) of ∼99.9% over 70 cycles, characteristics that are comparable to commercialized graphite-based anodes in LIBs (see Figure 55d–g). Moreover, the lignin-based carbon anode can also deliver a high specific capacity of >350 mAh/g and stable cycling performance if the slurry-coating technology is employed (see Figure 55d and 55f). This new methodology for fabricating carbon electrodes from wood-derived lignin can effectively eliminate the use of extra inactive materials used in conventional methods, which will lower the cost of LIBs.

6.3.1.2. Na-Ion Batteries. As discussed above, LIBs have been widely used in portable electronics and are considered as the most promising power source for EVs. However, concerns about the price of LIBs are growing due to the rarity and uneven distribution of Li resources. In particular, LIBs are not competitive for perspective applications in large-scale grid energy storage that require a high cost efficiency. Recently, developing alternative battery technologies beyond LIBs has attracted great attention, such as Na-ion batteries (NIBs). As the next alkali metal element adjacent to Li, NIBs show very similar electrochemical properties to LIBs. More importantly, Na is one of the most abundant elements (sixth) and is widely available in earth, enabling NIBs an ideal alternative to LIBs for large-scale energy storage. As shown in Figure 52c, the working mechanism of NIBs is very similar to LIBs, where Na ions are shuttling between cathode and anode instead of Li ions. To achieve the success of NIBs, developing high-performance electrode materials is critical. Among various candidates for NIB anodes, hard carbon has demonstrated promising performance with low operating potentials and relatively high specific capacities. According to "card-house" model, Na ions can intercalate into graphitic nanodomains and insert into nanopores between these nanodomains of hard carbon anodes, respectively (see Figure 53b). Recently, some groups disproved the original model and proposed new mechanisms. Cao and co-workers believed that the potential plateau at low potentials is related to Na-ion intercalation into turbostratic nanodomains rather than nanopores.[498] Mitlin and co-workers proposed that defects such as divacancies and Stone Wales played an important role for storing Na ions at high voltages.[499] Although there may be a variation in the mechanism due to the structural or chemical differences, hard carbon is still the most promising anode in this stage.

Previous studies have shown that hard carbons derived from simple sugars, such as sucrose and glucose, can deliver a capacity of ∼250 mAh/g at a small current density. Besides sugars, wood and its components have also shown great promise as hard carbon precursors. For example, 1D carbon nanofibers (CNF) with diameters ranging from 50 to 100 nm can be prepared from cellulose nanofibers via a simple thermal carbonization process (see Figure 56a).[186] The high-resolution transmission electron microscopy (HRTEM) image revealed that these CNF consist of many short-range graphitic domains (see Figure 56b). When CNF was evaluated as an anode for NIBs, the cyclic voltammograms (CVs) and potential profiles presented typical electrochemical properties of hard carbon (see Figure 56c and 56d). Taking the potential profiles as an example, the slopes in discharge/charge curves correspond to the intercalation/deintercalation process and the plateaus below 0.2 V are due to the adsorption of Na ions into the nanopores of hard carbon (see Figure 56d). The CNF delivered a relatively high capacity of 255 mAh/g at 40 mA/g and a great rate capability of 85 mAh/g at 2000 mA/g (see Figure 56e). More importantly, the CNF exhibited an excellent cycling stability, in that a high capacity of ∼180 mAh/g can still be obtained over 600 cycles (see Figure 56f). Such a finding on cellulose-derived carbon anode for high-performance NIBs indicates that wood-based carbon materials are very attractive for NIBs.

Recently, Shen et al. observed that direct thermal carbonization of wood fiber could result in a porous carbon with a high specific surface area of 586 m^2/g. The high surface area wood fiber-derived carbon led to a low first cycle CE (25%) as an anode for NIBs. To further improve the first cycle CE, wood fiber was pretreated with 2,2,6,6-tetramethylpiperidine-1-oxyl (TEMPO), which effectively decreases the surface area of its carbon product to 126 m^2/g. Accordingly, when evaluating the low-surface-area carbon as anode, it shows a much higher first cycle CE of 72%. This anode also gives a stable cycling performance, because a capacity of 196 mAh/g can be delivered for 200 cycles, which suggests great promise for low-cost SIBs.[500]

To apply lignin-based carbon anodes for NIBs, Shi and Wang fabricated carbon nanofibers from electrospun polyacrylonitrile (PAN)/lignin nanofibers, as shown in Figure 57.[501] By investigating the effects of PAN/lignin mass ratios and carbonization temperatures, they found that carbon nanofiber derived from PAN/lignin nanofiber with a mass ration of 1/1 at 1300 °C showed a highest specific desodiation capacity of 292.6 mAh/g at 20 mA/g, with a first cycle CE of 70.5% (Figure 57a–c). The optimized carbon nanofiber also presented a good rate performance (80 mAh/g at 1000 mA/g) and great cycle stability of 90.2% capacity retention over 200 cycles, which suggested that the lignin-based carbon anode is promising (Figure 57d–f). Indeed, some other cellulose- or lignin-contained biomass-derived carbons also showed great performance as NIB anodes. For example, Miltin and co-workers reported that carbon anodes made from peat moss[502] and banana peels[503] can deliver a high reversible capacity of ∼300 mAh/g at 100 mA/g. Pomelo peels-derived carbon anode reported by Huang et al. also demonstrated a great rate capability (71 mAh/g at 5000 mA/

DOI: 10.1021/acs.chemrev.6b00225
Chem. Rev. XXXX, XXX, XXX−XXX

g) after an activation process using H_3PO_4.[504] Most recently, Hu's group demonstrated that directly carbonized wood can also be a promising anode for NIBs.[505] The authors discovered that carbonized wood has a low-tortuosity, mesoporous structure and straight channels, which can deliver a high areal capacity when a thick wood carbon was adopted (850 μm). Considering the simple process, low cost, and unique structure, carbonized wood opens a range of other energy and environmental-related applications.

6.3.1.3. Electrochemical Capacitors. Although batteries have considerable advantages in various applications, they failed to power some electrical devices which require fast power delivery and uptake. The power density of batteries is limited by the slow intercalation/deintercalation process of ions and transportation of electrons in bulk electrode materials. On the other hand, electrochemical capacitors (ECs) electrostatically adsorb ions onto the surface of electrode materials and store the energy in the electric field between the charges and the ions, which allows fast power delivery and uptake (see Figure 52d). Furthermore, ECs have a long life up to millions of cycles, whereas batteries can only survive around 1000 cycles.

At present, activated carbon (AC) is the first choice for ECs due to its high surface area, good conductivity, high chemical stability, low cost, and scalability. The most common precursors are petroleum pitch, coke, and coal. However, with the decreasing availability of fossil fuels, seeking new but sustainable precursors for AC production is important. As a consequence, the use of wood and its components as precursors is motivated by their abundance and attractive low cost. Typically, there are two steps for producing AC from its precursor: carbonization and activation. The activation agencies are normally oxidants, e.g., carbon dioxide, steam, KOH, and $ZnCl_2$. Among them, KOH is the most common chemical activation agency where well-known ACs, like Maxsorb and PX-21, are produced from petroleum cokes with this method. For wood-based precursor, KOH is also very useful. For example, annealing carbonized cellulose fibers/KOH mixture can give porous carbon fibers with a specific surface area of up to 1978 m^2/g.[506] In a three-electrode cell, this porous carbon fiber can deliver a high capacity of 340 F/g using a H_2SO_4 electrolyte. Interestingly, direct reaction of cellulose fibers with KOH cannot generate porous carbon fibers so that carbonization is necessary prior to activation. Recently, Mokaya and Yushin reported that hydrothermal carbonization can be another promising route prior to activation to form porous carbon from natural precursors (see Figure 58).[507] In their study, hydrochar materials were first prepared by hydrothermal carbonization of cellulose, potato starch, or wood sawdust in an autoclave at 230−250 °C for 2 h. After that activation of hydrochar materials with KOH at 700−800 °C for 1 h generated porous carbon with specific surface area from 2125 to 2967 m^2/g (Figure 58a and 58b). Moreover, these porous carbons exhibited very narrow pore size distributions of about 90% surface area and pore volume arise from micropores (Figure 58c). Among these microporous carbons, AC-W800 (activating wood-derived hydrochar at 800 °C) exhibited the highest capacitance (236 F/g at 1 mV/s) and the best rate capability in a two-electrode cell using an organic electrolyte of tetraethylammonium tetrafluoroborate ($TEABF_4$)/acetonitrile (AN), which is much higher than commercial devices with conventionally produced activated carbons (Figure 58d).

However, activation agency is normally oxidant agency, while reductant-based activation agency has been rarely reported. Most recently, Ji's group reported that NH_3 can be an effective chemical activation agency for generating nanopores in carbon materials (Figure 59a).[508] By simply annealing cellulose paper under NH_3 flow that nitrogen-doped (N-doped) nanoporous carbon membrane is formed. They found that nitrogen doping (up to 10.3%) takes place during pyrolysis of cellulose at temperatures as low as 550 °C. When increasing the pyrolysis temperature, activation started at 700 °C and above that porous carbon with high specific surface area (up to 1973.3 m^2/g) can be obtained. Interestingly, when annealing nondoped carbon at high temperature under NH_3, very little activation can be observed. Combining with mass spectrometry, they discovered that the doped nitrogen on carbon further reacts with NH_3, leading to carbon gasification and forming porous structure (see Figure 59b). Due to its high surface area and nitrogen doping, the as-prepared N-doped nanoporous carbon (1326.5 m^2/g) exhibits more than double the unit area capacitance (90 vs 41 mF/m^2) compared to conventional activated carbon (1533.6 m^2/g). However, activation agencies are expensive and corrosive or toxic, like KOH and NH_3 gas. Most recently, Bommier et al. fabricated porous carbon from cellulose by a one-step self-activation reaction.[509] They found that the specific surface area of the resulting carbon product can reach 2600 m^2/g when controlling the flow rate of inert gas at 10 cm^3/min (CCM). In contrast, when the flow rate was tuned to 200 CCM, the carbon product only exhibited 98 m^2/g. Through a series of control experiments, they identified that the releasing gases, e.g., H_2O, activated the resulting carbon during pyrolysis of cellulose at high temperatures when the flow rate is slow. The as-synthesized porous carbon delivered a capacitance of 130 F/g at 1 A/g, which is better than that of conventional ACs.

6.3.2. Separators. The separator is a key component in batteries and capacitors and used to electrically separate the cathode and anode. Failure of the separator may lead to short-circuit problems and potential danger. Among numerous separator candidate materials, cellulose has gained considerable attention due to its various advantages, including abundance, renewability, environmental friendless, chemical stability, and most importantly thermal stability. For example, separators made from alkaline-resistant cellulose pulp have been widely employed in commercial alkaline batteries (e.g., Zn/MnO_2 batteries, Ni/Cd batteries, and Zn−air batteries).[510] However, polyolefin (e.g., polyethylene (PE) or polypropylene (PP))-based microporous separators still dominated the LIB separator market due to their electrochemical stability, high ionic conductivity, and large-scale production. Unfortunately, the poor mechanical properties and thermal stability of polyolefin microporous separators have significantly limited their safe use. Therefore, considerable attention has moved toward developing cellulose-based separators for LIBs.

In 1996, Kuribayashi fabricated a cellulose-based separator by embedding fine fibrilliform cellulose fibers into microporous cellulose film, which showed comparable electrochemical performance to PE separators in $LiCoO_2$/petroleum coke battery systems.[242] Considering its reduced risk of meltdown under relatively high temperatures, the cellulose-based separator is very attractive. Nevertheless, the pure cellulosic separator encountered several problems, such as high moisture content, limited porous configuration, and flammability. To address these issues, one approach was to use cellulose nanofibers, which have strong mechanical properties and a suitable porous configuration (see Figure 60a).[243] When evaluating cellulose nanofiber-based separators in a $LiCoO_2$/graphite battery, they exhibited much enhanced wettability of electrolyte and better capacity retention

DOI: 10.1021/acs.chemrev.6b00225
Chem. Rev. XXXX, XXX, XXX−XXX

compared to commercial polyolefin-based separators. To further improve the porous structure, colloidal SiO_2 was introduced into the cellulose nanofiber separator. By varying the content of SiO_2, the ionic conductivity and electrolyte wettability can be much enhanced, resulting in improved electrochemical performance (see Figure 60b).[245]

Besides inorganic materials, some polymer materials have been also incorporated into cellulose nanofiber separators for improving their performance. In 2013, Cui's group synthesized a cellulose/poly(vinylidene fluoride-*co*-hexafluoropropylene) (PVDF-HPF) separator by an electrospinning strategy combined with subsequent dip-coating process.[246] Compared to the PP separator, the cellulose/PVDF-HPF separator exhibited higher porous structure, better electrolyte wettability, higher electrolyte uptake, and better thermal stability. More importantly, the higher ionic conductivity of the cellulose/PVDF-HPF separator resulted in a better rate capability in $LiCoO_2$/graphite batteries. Recently, the same group further incorporated polymeric lithium tartaric acid borate salt (PLTB) into the cellulose/PVDF-HPF separator, which exhibited enhanced flame-retardant performance without sacrificing electrochemical performance.[511] They also prepared a cellulose/polysulfonamide separator and a cellulose/polydopamine separator via a well-developed papermaking technology, which can greatly lower the cost of separator production.[512] Moreover, such cellulose/polymer composite separators showed excellent safety and promising electrochemical performance. Furthermore, a flame-proof separator, designated the FCCN separator, has been fabricated, where sodium alginate, flame retardant, and silica were deposited onto cellulose separators using vacuum filtration and hot pressing (see Figure 60c and 60d).[513] The FCCN separator exhibited excellent thermal stability up to 300 °C and superior inflame-retarding properties. Most importantly, when the FCCN separator was evaluated in $LiCoO_2$/graphite or $LiFePO_4$/Li batteries, it delivered better rate and cycling performance compared to the PP separator.

6.3.3. Scaffolds. Wood-derived materials, especially cellulose, have also been applied as substrates or scaffolds for batteries and ECs due to their high mechanical performance, flexibility, and tailorable surface functionalities.[514,515] In 2007, Ajayan et al. designed and fabricated a CNT/cellulose/ionic liquid nanocomposite sheet to form a flexible building block, which can be utilized in LIBs and ECs (see Figure 61a and 61b).[514] Hu et al. made a highly conductive paper by conformal coating CNT onto commercial paper, which demonstrated great promise as current collectors for energy-storage devices (see Figure 61c and 61d).[273] For example, such a CNT-coated paper delivered a specific capacitance of 200 F/g and a stable cycling life over 40 000 cycles when evaluated as supercapacitor electrodes. Moreover, LIBs using these CNT-coated paper as current collectors can also show stable cycling performance, which suggests that paper-based lightweight current collector can be great low-cost solution for electrochemical energy-storage devices.

Most recently, Zhu et al. developed a tin-based anode on a hierarchical wood fiber substrate, where the flexible substrate significantly addressed the challenges associated with Sn anodes.[17] They proposed that the soft nature of wood fibers can release the mechanical stresses encountered during electrochemical reactions. Moreover, the mesoporous structure of wood fiber can serve as an electrolyte reservoir, which allows for fast ion transportation (see Figure 61e and 61f). Such a design may open up a new direction which applies soft substrates for addressing the issues related to volume change during electrochemical reactions in batteries or ECs.

Furthermore, paper electrodes composed of conductive polymers and cellulose combine high conductivities and tunable mechanical properties, which can be used to obtain lightweight and self-standing electrodes for high-performance batteries and ECs.[516] For example, PPy@nanocellulose paper-based supercapacitors exhibit a typical gravimetric capacitance of 180 F/g, whereas the volumetric capacitance is found to differ depending on different electrode preparation processes.[517−519] By straightforward compression of the PPy@nanocellulose composites, compact supercapacitors with improved spatial utilization are obtained without significantly compromising the electrochemical performance of the devices (Figure 62a).[517] The most compressed sample remained higher than that of the pristine sample even at a current density of 200 mA/cm^2, which corresponds to a charge time of less than 4 s (see Figure 62b and 62c). Robust and compact nanocellulose-coupled PPy@GO paper electrodes can also be straightforwardly prepared via in-situ polymerization for use in high-performance paper-based supercapacitors, exhibiting stable cycling over 16 000 cycles at 5 A/g;,as well as large specific volumetric capacitance (198 F/cm^3).[519]

6.3.4. Lignin as Battery Electrodes. More recently, researchers have introduced the new concept that renewable and cheap wood derivatives can be used directly as low-cost battery electrodes. In 2012, Milczarek and Inganäs reported that the quinone group in lignin can function as an cathode, which demonstrated a significantly green and low-cost electrochemical energy-storage solution.[520] Brown liquor, a byproduct of paper processing, was adopted as the starting material in their study, where quinone groups were formed via oxidation. To improve the conductivity of lignin-based cathodes, polypyrrole was further added using an electrochemical polymerization process. The as-obtained product was referred to as Ppy(Lig), which exhibited clear redox peaks in 0.1 M aqueous $HClO_4$ electrolyte using cyclic voltammetry (CV) measurements. The capacitance values calculated from charge/discharge experiments spanned from 350 to 1000 F/g, which depends on the thickness of the electrode and charge/discharge rate.

From that point onward, fabricating lignin derivative electrodes with conductive polymers or other conductive materials has attracted wide attention.[521−526] For example, Zhu et al. made a Ppy-doped lignosulfonate electrode, which delivered a specific capacitance of 304 F/g at 0.1 A/g in a NaCl aqueous electrolyte.[527] Moreover, they used cotton fabrics as substrate, demonstrating great flexible advantage for wearable electronics. On the basis of a similar concept, Xu et al. reported a polyaniline (PANI)-doped lignosulfonate electrode for supercapacitors, which gives a high rate performance of 377 F/g at 10 A/g.[528] Furthermore, such a PANI-doped lignosulfonate showed a stable cycling life where the capacity retention rate is 74% after 10 000 cycles. To further increase the specific capacitance, phosphomolybdic acid (HMA) was introduced into the conductive polymer−lignin composite by Admassie et al.[529] They found that the addition of inorganic metal acid can increase the specific capacitance from 477 to 682 F/g, which suggests an effective route to improve the energy density of lignin-based electrodes.

7. CONCLUSIONS AND PERSPECTIVES

Biomaterials from wood are emerging as attractive solutions to a range of technological challenges. These materials, particularly cellulose, hemicellulose, and lignin, not only are biocompatible

DOI: 10.1021/acs.chemrev.6b00225
Chem. Rev. XXXX, XXX, XXX−XXX

and earth abundant but also have Nature-provided intrinsic structures for potentially transformative device performance. While many emerging devices and applications have been demonstrated, there are still grand challenges in fundamental research and understanding to accelerate woody biomaterials toward commercial reality, especially for emerging applications, such as green electronics, biological devices, and energy applications. These challenges include (1) high performance in devices with acceptable durability and lifetime, (2) low cost that includes extraction of biomaterials from wood, fabrications of components, and fabrications of devices, and (3) system level integrations with multiple device components. With worldwide effort, new developments using wood-derived materials elaborated in this review, especially nanofibrillated celluloses, will provide emerging technologies impacting our everyday life.

AUTHOR INFORMATION

Corresponding Authors

*E-mail: h.zhu@neu.edu.
*E-mail: binghu@umd.edu.

Author Contributions

§H.Z. and W.L. contributed equally to this paper.

Notes

The authors declare no competing financial interest.

Biographies

Hongli Zhu is currently an Assistant Professor in Northeastern University. Her group focuses on the research of energy storage, advanced manufacturing, and multifunctional materials. From 2012 to 2015, she worked at the University of Maryland as a postdoctoral fellow, focusing on the research of nanopaper electronics and battery. From 2009 to 2011, she conducted research on materials science and processing of biodegradable and renewable biomaterials from natural wood in the KTH Royal Institute of Technology in Sweden. She received her Ph.D. degree in Wood Chemistry from the South China University of Technology−Western Michigan University Alliance in 2009.

Wei Luo received his B.E. and M.E. degrees from Northwestern Polytechnical University (with Prof. Shibin Liu) and then obtained his Ph.D. degree in Materials Science from the Huazhong University of Science and Technology in 2012 under the supervision of Prof. Xianluo Hu and Prof. Yunhui Huang. After finishing 2 years' postdoctoral research with Prof. Xiulei Ji (2012−2014) at Oregon State University, he worked with Prof. Liangbing Hu and Prof. Bao Yang at the University of Maryland as a postdoctoral researcher until being promoted to Assistant Research Professor in 2016. His research focuses on sustainable and renewable biomass materials, energy storage, and conversion devices.

Peter Ciesielski received his B.S. degree in Chemical and Biological Engineering from Colorado State University in 2006 and then accepted an NSF Integrative Graduate Education and Research Traineeship from Vanderbilt University where he received his Ph.D. degree in Interdisciplinary Materials Science in 2010. He began studying at the Biosciences Center of the National Renewable Energy Lab in 2010, where his postdoctoral work focused on coupling advanced microscopy to modeling and simulation of biomaterials. Currently, he is a Research Scientist at NREL, where his multidisciplinary research aims to improve ways by which biomass can be used as a sustainable and renewable source of fuels, chemicals, and materials.

Zhiqiang Fang received his B.S. degree from Shaanxi University of Science and Technology majoring in Light Chemical Engineering in 2006. He received his Ph.D. degree in pulp and papermaking engineering at South China University of Technology in 2014. As a visiting scholar at the University of Maryland from 2012 to 2013 he worked on transparent paper for flexible electronics. Currently, he is a postdoctoral fellow at South China University of Technology. His research interests include nanomaterials and biodegradable materials for specialty paper and transparent paper for flexible electronics.

J. Y. Zhu received his Ph.D. degree in Engineering from the University of California—Irvine in 1991. After a brief appointment in Silicon Valley, he joined the Institute of Paper Science and Technology, Atlanta, GA, as Assistant Professor and later was promoted to Associate Professor. In 2003, he joined the U.S. Forest Service, Forest Products Lab, Madison, WI, as a research unit leader. Currently, he is leading several research programs in wood and fiber utilization. His research ranges from laboratory studies to commercial mill demonstrations. He research interests included a broad areas of wood utilization for production of fibers, cellulose nanomaterials, and sugar/biofuel through chemical and mechanical fractionation and enzymatic catalysis.

Gunnar Henriksson received his B.Sc. degree in Microbiology and Ph.D. degree in Biochemistry from the University of Uppsala (Sweden) in 1989 and 1995, respectively. He then worked as a postdoctoral fellow at the University of Georgia, and since 1997 has been at the Royal Institute of Technology (Stockholm, Sweden), where he presently is Professor in Wood Chemistry. Presently, he is also guest Professor in Pulp Technology at the University of Karlstad (Sweden). His research interests lie in the chemical structure of wood and in industrial processes based on wood and other lignocellulose. He is also interested in microbial degradation of wood polymers.

Michael E. Himmel received his B.Sc. and Ph.D. degrees in Chemistry and Biochemistry from the University of Northern Colorado and Colorado State University, respectively. He then worked at the Solar Energy Research Institute as a postdoctoral researcher and research scientist. He currently holds the position of Fellow and Principal Group Manager at the National Renewable Energy Laboratory in Golden, CO. His research interests lie in conducting, supervising, and planning research in protein biochemistry, recombinant technology, enzyme engineering, new microorganism discovery, and the physicochemistry of macromolecules.

Liangbing Hu received his B.S. degree in Physics from the University of Science and Technology of China (USTC) in 2002, where he worked with Prof. Yuheng Zhang on colossal magnetoresistance (CMR) materials for 3 years. He did his Ph.D. studies in at UCLA (with George Gruner), focusing on carbon nanotube-based nanoelectronics (2002−2007). In 2006, he joined Unidym Inc. (www.unidym.com) as a cofounding scientist. At Unidym, his role was the development of roll-to-roll printed carbon nanotube transparent electrodes and device integrations into touchscreens, LCDs, flexible OLEDs, and solar cells. He worked at Stanford University (with Yi Cui) from 2009 to 2011, where he work on various energy devices based on nanomaterials and nanostructures. Currently, he is an Associate Professor at the University of Maryland College Park. His research interests include nanomaterials and nanostructures, roll-to-roll nanomanufacturing, energy storage focusing on solid-state batteries and Na-ion batteries, and printed electronics.

ACKNOWLEDGMENTS

L.H. acknowledges support from the DOD (Air Force of Scientific Research) Young Investigator Program (FA95501310143) and 3M Non-Tenured Faculty and NSF-CBET Grant 1335979. This work also was supported as part of the Nanostructures for Electrical Energy Storage (NEES), an

DOI: 10.1021/acs.chemrev.6b00225
Chem. Rev. XXXX, XXX, XXX−XXX

Energy Frontier Research Center funded by the U.S. Department of Energy, Office of Science, Basic Energy Sciences under Award DESC0001160. Sections 2.1 and 6.2 were written with support from the National Renewable Energy Laboratory's Laboratory Directed Research and Development (LDRD) Program (MEH and PNC). H.Z. acknowledges the startup support from Northeastern University. We also acknowledge Mr. Jiaqi Dai from the University of Maryland for the help on figures.

REFERENCES

(1) Moon, R. J.; Martini, A.; Nairn, J.; Simonsen, J.; Youngblood, J. Cellulose Nanomaterials Review: Structure, Properties and Nanocomposites. *Chem. Soc. Rev.* **2011**, *40*, 3941−3994.
(2) Habibi, Y.; Lucia, L. A.; Rojas, O. J. Cellulose Nanocrystals: Chemistry, Self-assembly, and Applications. *Chem. Rev.* **2010**, *110*, 3479−3500.
(3) Zakzeski, J.; Bruijnincx, P. C. A.; Jongerius, A. L.; Weckhuysen, B. M. The Catalytic Valorization of Lignin for the Production of Renewable Chemicals. *Chem. Rev.* **2010**, *110*, 3552−3599.
(4) Xu, C.; Arancon, R. A. D.; Labidi, J.; Luque, R. Lignin Depolymerisation Strategies: Towards Valuable Chemicals and Fuels. *Chem. Soc. Rev.* **2014**, *43*, 7485−7500.
(5) Zhou, C.-H.; Xia, X.; Lin, C.-X.; Tong, D.-S.; Beltramini, J. Catalytic Conversion of Lignocellulosic Biomass to Fine Chemicals and Fuels. *Chem. Soc. Rev.* **2011**, *40*, 5588−5617.
(6) *Density, Fiber Length, and Yields of Pulp for Various Species of Wood*; 191; Forest Products Laboratory: Madison, WI, 1953.
(7) *Wood Handbook-Wood as an Engineering Material*; Forest Products Laboratory: Madison, WI, 2010.
(8) Stamm, A. J. Calculations of the Void Volume in Wood. *Ind. Eng. Chem.* **1938**, *30*, 1280−1281.
(9) Carpita, N. C.; Gibeaut, D. M. Structural Models of Primary Cell Walls in Flowering Plants: Consistency of Molecular Structure With the Physical Properties of the Walls During Growth. *Plant J.* **1993**, *3*, 1−30.
(10) Somerville, C.; Bauer, S.; Brininstool, G.; Facette, M.; Hamann, T.; Milne, J.; Osborne, E.; Paredez, A.; Persson, S.; Raab, T.; Vorwerk, S.; Youngs, H. Toward a Systems Approach to Understanding Plant Cell Walls. *Science* **2004**, *306*, 2206−2211.
(11) Booker, R. E.; Sell, J. The Nanostructure of the Cell Wall of Softwoods and its Functions in a Living Tree. *Holz Roh Werkst.* **1998**, *56*, 1−8.
(12) Himmel, M. E.; Ding, S.-Y.; Johnson, D. K.; Adney, W. S.; Nimlos, M. R.; Brady, J. W.; Foust, T. D. Biomass Recalcitrance: Engineering Plants and Enzymes for Biofuels Production. *Science* **2007**, *315*, 804−807.
(13) Xu, P.; Donaldson, L. A.; Gergely, Z. R.; Staehelin, L. A. Dual-axis Electron Tomography: a New Approach for Investigating the Spatial Organization of Wood Cellulose Microfibrils. *Wood Sci. Technol.* **2007**, *41*, 101−116.
(14) Fernandes, A. N.; Thomas, L. H.; Altaner, C. M.; Callow, P.; Forsyth, V. T.; Apperley, D. C.; Kennedy, C. J.; Jarvis, M. C. Nanostructure of Cellulose Microfibrils in Spruce Wood. *Proc. Natl. Acad. Sci. U. S. A.* **2011**, *108*, E1195−E1203.
(15) Ding, S. Y.; Liu, Y. S.; Zeng, Y. N.; Himmel, M. E.; Baker, J. O.; Bayer, E. A. How Does Plant Cell Wall Nanoscale Architecture Correlate with Enzymatic Digestibility? *Science* **2012**, *338*, 1055−1060.
(16) Ciesielski, P. N.; Matthews, J. F.; Tucker, M. P.; Beckham, G. T.; Crowley, M. F.; Himmel, M. E.; Donohoe, B. S. 3D Electron Tomography of Pretreated Biomass Informs Atomic Modeling of Cellulose Microfibrils. *ACS Nano* **2013**, *7*, 8011−8019.
(17) Zhu, H.; Jia, Z.; Chen, Y.; Weadock, N.; Wan, J.; Vaaland, O.; Han, X.; Li, T.; Hu, L. Tin Anode for Sodium-Ion Batteries Using Natural Wood Fiber as a Mechanical Buffer and Electrolyte Reservoir. *Nano Lett.* **2013**, *13*, 3093−3100.
(18) Donohoe, B. S.; Selig, M. J.; Viamajala, S.; Vinzant, T. B.; Adney, W. S.; Himmel, M. E. Detecting Cellulase Penetration Into Corn Stover Cell Walls by Immuno-Electron Microscopy. *Biotechnol. Bioeng.* **2009**, *103*, 480−489.
(19) Carpita, N.; Sabularse, D.; Montezinos, D.; Delmer, D. P. Determination of the Pore Size of Cell Walls of Living Plant Cells. *Science* **1979**, *205*, 1144−1147.
(20) Ishizawa, C. I.; Davis, M. F.; Schell, D. F.; Johnson, D. K. Porosity and its Effect on the Digestibility of Dilute Sulfuric Acid Pretreated Corn Stover. *J. Agric. Food Chem.* **2007**, *55*, 2575−2581.
(21) Esteghlalian, A. R.; Bilodeau, M.; Mansfield, S. D.; Saddler, J. N. Do Enzymatic Hydrolyzability and Simons' Stain Reflect the Changes in the Accessibility of Lignocellulosic Substrates to Cellulase Enzymes? *Biotechnol. Prog.* **2001**, *17*, 1049−1054.
(22) Chundawat, S. P. S.; Donohoe, B. S.; Sousa, L. D.; Elder, T.; Agarwal, U. P.; Lu, F. C.; Ralph, J.; Himmel, M. E.; Balan, V.; Dale, B. E. Multi-scale Visualization and Characterization of Lignocellulosic Plant Cell Wall Deconstruction During Thermochemical Pretreatment. *Energy Environ. Sci.* **2011**, *4*, 973−984.
(23) Zauer, M.; Hempel, S.; Pfriem, A.; Mechtcherine, V.; Wagenfuhr, A. Investigations of the Pore-size Distribution of Wood in the Dry and Wet State by Means of Mercury Intrusion Porosimetry. *Wood Sci. Technol.* **2014**, *48*, 1229−1240.
(24) Jakes, J. E.; Plaza, N.; Stone, D. S.; Hunt, C. G.; Glass, S. V.; Zelinka, S. L. Mechanism of Transport Through Wood Cell Wall Polymers. *J. For. Prod. Ind.* **2013**, *2*, 10−13.
(25) Zelinka, S. L.; Gleber, S. C.; Vogt, S.; Lopez, G. M. R.; Jakes, J. E. Threshold for Ion Movements in Wood Cell Walls Below Fiber Saturation Observed by X-ray Fluorescence Microscopy (XFM). *Holzforschung* **2015**, *69*, 441−448.
(26) Gierer, J. Chemical Aspects of Kraft Pulping. *Wood Sci. Technol.* **1980**, *14*, 241−266.
(27) Herrick, F. W.; Casebier, R. L.; Hamilton, J. K.; Sandberg, K. R. In Microfibrillated cellulose: morphology and accessibility. *Journal of Applied Polymer Science: Applied Polymer Symposium*; ITT Rayonier Inc.: Shelton, WA, 1983.
(28) Zimmermann, T.; Bordeanu, N.; Strub, E. Properties of Nanofibrillated Cellulose from Different Raw Materials and its Reinforcement Potential. *Carbohydr. Polym.* **2010**, *79*, 1086−1093.
(29) Wang, Q.; Zhu, J.; Reiner, R.; Verrill, S.; Baxa, U.; McNeil, S. Approaching Zero Cellulose Loss in Cellulose Nanocrystal (CNC) Production: Recovery and Characterization of Cellulosic Solid Residues (CSR) and CNC. *Cellulose* **2012**, *19*, 2033−2047.
(30) Zhu, J. Y.; Zhuang, X. S. Conceptual Net Energy Output for Biofuel Production from Lignocellulosic Biomass through Biorefining. *Prog. Energy Combust. Sci.* **2012**, *38*, 583−598.
(31) Pettersen, R. C. The Chemical Composition of Wood. In *The Chemistry of Solid Wood. Advances in Chemistry Series 207*; Rowell, R. M., Ed.; American Chemical Society: Washington D.C., 1984; pp 115−116.
(32) French, A. D.; Bertoniere, N. R.; Brown, R. M.; Chanzy, H.; Gray, D.; Hattori, K.; Glasser, W. Cellulose. In *Kirk-Othmer Encyclopedia of Chemical Technology*, 5th ed.; Seidel, A., Ed.; John Wiley & Sons, Inc.: New York, 2004; Vol. *5*.
(33) de Souza Lima, M. M.; Borsali, R. Rodlike Cellulose Microcrystals: Structure, Properties, and Applications. *Macromol. Rapid Commun.* **2004**, *25*, 771−787.
(34) Payen, A. Memoire sur la Composition du Tissu Propre des Plantes et du Ligneux. *Comptes Rendus* **1938**, *7*, 1052−1056.
(35) Rowland, S. P.; Roberts, E. J. Nature of Accessible Surfaces in the Microstructure of Cotton Cellulose. *J. Polym. Sci., Part A-1: Polym. Chem.* **1972**, *10*, 2447−2461.
(36) Frey-Wyssling, A. The Fine Structure of Cellulose Microfibrils. *Science* **1954**, *119*, 80−82.
(37) Ding, S. Y.; Himmel, M. E. The Maize Primary Cell Wall Microfibril: A New Model Derived from Direct Visualization. *J. Agric. Food Chem.* **2006**, *54*, 597−606.
(38) Sjostrom, E. *Wood Chemistry: Fundamentals and Application*, 2nd ed.; Academic Press, Inc.: San Diego, 1992; p 230.
(39) Kolpak, F. J.; Blackwell, J. Determination of the Structure of Cellulose II. *Macromolecules* **1976**, *9*, 273−278.
(40) Pizzi, A.; Eaton, N. J. The Structure of Cellulose by Conformational Analysis. Part 4. Crystalline Cellulose II. *J. Macromol. Sci., Part A: Pure Appl.Chem.* **1987**, *24*, 901−918.

DOI: 10.1021/acs.chemrev.6b00225
Chem. Rev. XXXX, XXX, XXX−XXX

(41) Nishiyama, Y. Structure and Properties of the Cellulose Microfibril. *J. Wood Sci.* **2009**, *55*, 241−249.
(42) Agarwal, U.; Ralph, S.; Reiner, R.; Baez, C. Probing Crystallinity of Never-Dried Wood Cellulose with Raman Spectroscopy. *Cellulose* **2016**, *23*, 125−144.
(43) Chen, L.; Wang, Q.; Hirth, K.; Baez, C.; Agarwal, U. P.; Zhu, J. Y. Tailoring the Yield and Characteristics of Wood Cellulose Nanocrystals (CNC) Using Concentrated Acid Hydrolysis. *Cellulose* **2015**, *22*, 1753−1762.
(44) Gardner, K. H.; Blackwell, J. The Hydrogen Bonding in Native Cellulose. *Biochim. Biophys. Acta, Gen. Subj.* **1974**, *343*, 232−237.
(45) Šturcová, A.; Davies, G. R.; Eichhorn, S. J. Elastic Modulus and Stress-Transfer Properties of Tunicate Cellulose Whiskers. *Biomacromolecules* **2005**, *6*, 1055−1061.
(46) Mark, R. E. *Cell wall mechanics of tracheids*; Yale University Press, 1967
(47) Yu, M.-F.; Lourie, O.; Dyer, M. J.; Moloni, K.; Kelly, T. F.; Ruoff, R. S. Strength and Breaking Mechanism of Multiwalled Carbon Nanotubes Under Tensile Load. *Science* **2000**, *287*, 637−640.
(48) Battista, O. A. Hydrolysis and Crystallization of Cellulose. *Ind. Eng. Chem.* **1950**, *42*, 502−507.
(49) Battista, O. A.; Coppick, S.; Howsmon, J. A.; Morehead, F. F.; Sisson, W. A. Level-off Degree of Polymerization: Relation to Polyphase Structure of Cellulose Fibers. *Ind. Eng. Chem.* **1956**, *48*, 333−335.
(50) Nishiyama, Y.; Kim, U. J.; Kim, D. Y.; Katsumata, K. S.; May, R. P.; Langan, P. Periodic Disorder Along Ramie Cellulose Microfibrils. *Biomacromolecules* **2003**, *4*, 1013−1017.
(51) Anderson, S. R.; Esposito, D.; William, G.; Zhu, J. Y.; Ulrich, B.; McNeil, S. E. Enzymatic Preparation of Nanocrystalline and Microcrystalline Cellulose. *TAPPI J.* **2014**, *13*, 35−41.
(52) Leung, A. C. W.; Hrapovic, S.; Lam, E.; Liu, Y.; Male, K. B.; Mahmoud, K. A.; Luong, J. H. T. Characteristics and Properties of Carboxylated Cellulose Nanocrystals Prepared from a Novel One-step Procedure. *Small* **2011**, *7*, 302−305.
(53) Hirota, M.; Furihata, K.; Saito, T.; Kawada, T.; Isogai, A. Glucose/Glucuronic Acid Alternating Co-polysaccharides Prepared from TEMPO-Oxidized Native Celluloses by Surface Peeling. *Angew. Chem., Int. Ed.* **2010**, *49*, 7670−7672.
(54) Montanari, S.; Roumani, M.; Heux, L.; Vignon, M. R. Topochemistry of Carboxylated Cellulose Nanocrystals Resulting From TEMPO-Mediated Oxidation. *Macromolecules* **2005**, *38*, 1665−1671.
(55) Segal, L.; Creely, J. J.; Martin, A. E.; Conrad, C. M. An Empirical Method for Estimating the Degree of Crystallinity of Native Cellulose Using the X-ray Diffractometer. *Text. Res. J.* **1959**, *29*, 786−794.
(56) Park, S.; Baker, J. O.; Himmel, M. E.; Parilla, P. A.; Johnson, D. K. Cellulose Crystallinity Index: Measurement Techniques and Their Impact on Interpreting Cellulase Performance. *Biotechnol. Biofuels* **2010**, *3*, 1−10.
(57) Agarwal, U. P.; Reiner, R. S.; Ralph, S. A. Celulose I Crystallinity Determination Using FT-Raman Spectroscopy: Univariate and Multivariate Methods. *Cellulose* **2010**, *17*, 721−733.
(58) Moon, R. J.; Martini, A.; Nairn, J.; Simonsen, J.; Youngblood, J. Cellulose Nanomaterials Review: Structure, Properties and Nanocomposites. *Chem. Soc. Rev.* **2011**, *40*, 3941−3994.
(59) Nickerson, R. F.; Habrle, J. A. Cellulose Intercrystalline Structure. *Ind. Eng. Chem.* **1947**, *39*, 1507−1512.
(60) Rånby, B. G. The Colloidal Properties of Cellulose Micelles. *Discuss. Faraday Soc.* **1951**, *11*, 158−164.
(61) Mukherjee, S. M.; Woods, H. J. X-Ray and Electron Microscope Studies of the Degradation of Cellulose by Sulphuric Acid. *Biochim. Biophys. Acta* **1953**, *10*, 499−511.
(62) Bondeson, D.; Matthew, A.; Oksman, K. Optimization of the Isolation of Nanocrystals from Microcrystalline Cellulose by Acid Hydrolysis. *Cellulose* **2006**, *13*, 171−180.
(63) Chen, Y.; Liu, C.; Chang, P. R.; Cao, X.; Anderson, D. P. Bionanocomposites Based on Pea Starch and Cellulose Nanowhiskers Hydrolyzed from Pea Hull Fibre: Effect of Hydrolysis Time. *Carbohydr. Polym.* **2009**, *76*, 607−615.
(64) Moran, J. L.; Alvarez, V. A.; Cyras, V. P.; Vazquez, A. Extraction of Cellulose and Preparation of Nanocellulose from Sisal Fibers. *Cellulose* **2008**, *15*, 149−159.
(65) Dong, S.; Bortner, M. J.; Roman, M. Analysis of the Sulfuric Acid Hydrolysis of Wood Pulp for cellulose Nanocrystal Production: A Central Composite Design Study. *Ind. Crops Prod.* **2016**, DOI: 10.1016/j.indcrop.2016.01.048.
(66) Wang, Q.; Zhao, X.; Zhu, J. Y. Kinetics of Strong Acid Hydrolysis of a Bleached Kraft Pulp for Producing Cellulose Nanocrystals (CNCs). *Ind. Eng. Chem. Res.* **2014**, *53*, 11007−11014.
(67) Revol, J.-F.; Bradford, H.; Giasson, J.; Marchessault, R. H.; Gray, D. G. Helicoidal Self-Ordering of Cellulose Microfibrils in Aqueous Suspension. *Int. J. Biol. Macromol.* **1992**, *14*, 170−172.
(68) Hamad, W. Y.; Hu, T. Q. Structure−Process−Yield Interrelations in Nanocrystalline Cellulose Extraction. *Can. J. Chem. Eng.* **2010**, *88*, 392−402.
(69) Beck-Candanedo, S.; Roman, M.; Gray, D. G. Effect of Reaction Conditions on the Properties and Behavior of Wood Cellulose Nanocrystal Suspensions. *Biomacromolecules* **2005**, *6*, 1048−1054.
(70) Araki, J.; Wada, M.; Kuga, S.; Okano, T. Flow Properties of Microcrystalline Cellulose Suspension Prepared by Acid Treatment of Native Cellulose. *Colloids Surf., A* **1998**, *142*, 75−82.
(71) Yu, H.; Qin, Z.; Liang, B.; Liu, N.; Zhou, Z.; Chen, L. Facile Extraction of Thermally Stable Cellulose Nanocrystals with a High Yield of 93% through Hydrochloric Acid Hydrolysis under Hydrothermal Conditions. *J. Mater. Chem. A* **2013**, *1*, 3938−3944.
(72) Camarero Espinosa, S.; Kuhnt, T.; Foster, E. J.; Weder, C. Isolation of Thermally Stable Cellulose Nanocrystals by Phosphoric Acid Hydrolysis. *Biomacromolecules* **2013**, *14*, 1223−1230.
(73) Klemm, D.; Kramer, F.; Moritz, S.; Lindstrom, T.; Ankerfors, M.; Gray, D.; Dorris, A. Nanocelluloses: A New Family of Nature-Based Materials. *Angew. Chem., Int. Ed.* **2011**, *50*, 5438−5466.
(74) Giese, M.; Blusch, L. K.; Khan, M. K.; MacLachlan, M. J. Functional Materials from Cellulose-Derived Liquid-Crystal Templates. *Angew. Chem., Int. Ed.* **2015**, *54*, 2888−2910.
(75) Chen, L.; Zhu, J. Y.; Baez, C.; Kitin, P.; Elder, T. Highly Thermal-Stable and Functional Cellulose Nanocrystals and Nanofibrils Produced Using Fully Recyclable Organic Acids. *Green Chem.* **2016**, *18*, 3835−3843.
(76) Wang, N.; Ding, E.; Cheng, R. Thermal Degradation Behaviors of Spherical Cellulose Nanocrystals with Sulfate Groups. *Polymer* **2007**, *48*, 3486−3493.
(77) Kargarzadeh, H.; Ahmad, I.; Abdullah, I.; Dufresne, A.; Zainudin, S. Y.; Sheltami, R. M. Effects of Hydrolysis Conditions on the Morphology, Crystallinity, and Thermal Stability of Cellulose Nanocrystals Extracted from Kenaf Bast Fibers. *Cellulose* **2012**, *19*, 855−866.
(78) Araki, J.; Wada, M.; Kuga, S.; Okano, T. Biréfringent Glassy Phase of a Cellulose Microcrystal Suspension. *Langmuir* **2000**, *16*, 2413−2415.
(79) Dumanli, A. G.; Van Der Kooij, H. M.; Kamita, G.; Reisner, E.; Baumberg, J. J.; Steiner, U.; Vignolini, S. Digital Color in Cellulose Nanocrystal Films. *ACS Appl. Mater. Interfaces* **2014**, *6*, 12302−12306.
(80) Beck-Candanedo, S.; Viet, D.; Gray, D. G. Triphase Equilibria in Cellulose Nanocrystal Suspensions Containing Neutral and Charged Macromolecules. *Macromolecules* **2007**, *40*, 3429−3436.
(81) Dong, X. M.; Gray, D. G. Induced Circular Dichroism of Isotropic and Magnetically-Oriented Chiral Nematic Suspensions of Cellulose Crystallites. *Langmuir* **1997**, *13*, 3029−3034.
(82) Revol, J.-F.; Godbout, L.; Dong, X.-M.; Gray, D. G.; Chanzy, H.; Maret, G. Chiral Nematic Suspensions of Cellulose Crystallites; Phase Separation and Magnetic Field Orientation. *Liq. Cryst.* **1994**, *16*, 127−134.
(83) Roman, M.; Gray, D. G. Parabolic Focal Conics in Self-Assembled Solid Films of Cellulose Nanocrystals. *Langmuir* **2005**, *21*, 5555−5561.
(84) Kelly, J. A.; Shukaliak, A. M.; Cheung, C. C. Y.; Shopsowitz, K. E.; Hamad, W. Y.; MacLachlan, M. J. Responsive Photonic Hydrogels Based on Nanocrystalline Cellulose. *Angew. Chem., Int. Ed.* **2013**, *52*, 8912−8916.
(85) Kelly, J. A.; Shopsowitz, K. E.; Ahn, J. M.; Hamad, W. Y.; MacLachlan, M. J. Chiral nematic stained glass: Controlling the Optical

DOI: 10.1021/acs.chemrev.6b00225
Chem. Rev. XXXX, XXX, XXX−XXX

Properties of Nanocrystalline Cellulose-Templated Materials. *Langmuir* **2012**, *28*, 17256−17262.
(86) Allen, T. C.; Cuculo, J. A. Cellulose Derivatives Containing Carboxylic Acid Groups. *Macromol. Rev.* **1973**, *7*, 189−262.
(87) Hirota, M.; Tamura, N.; Saito, T.; Isogai, A. Water Dispersion of Cellulose II Nanocrystals Prepared by TEMPO-Mediated Oxidation of Mercerized Cellulose at pH 4.8. *Cellulose* **2010**, *17*, 279−288.
(88) Peyre, J.; Pääkkönen, T.; Reza, M.; Kontturi, E. Simultaneous Preparation of Cellulose Nanocrystals and Micron-sized Porous Colloidal Particles of Cellulose by TEMPO-Mediated Oxidation. *Green Chem.* **2015**, *17*, 808−811.
(89) Okita, Y.; Saito, T.; Isogai, A. Entire Surface Oxidation of Various Cellulose Microfibrils by TEMPO-Mediated Oxidation. *Biomacromolecules* **2010**, *11*, 1696−1700.
(90) Ifuku, S.; Tsuji, M.; Morimoto, M.; Saimoto, H.; Yano, H. Synthesis of Silver Nanoparticles Templated by TEMPO-Mediated Oxidized Bacterial Cellulose Nanofibers. *Biomacromolecules* **2009**, *10*, 2714−2717.
(91) Mangalam, A. P.; Simonsen, J.; Benight, A. S. Cellulose/DNA Hybrid Nanomaterials. *Biomacromolecules* **2009**, *10*, 497−504.
(92) Fukuzumi, H.; Saito, T.; Okita, Y.; Isogai, A. Thermal Stabilization of TEMPO-Oxidized Cellulose. *Polym. Degrad. Stab.* **2010**, *95*, 1502−1508.
(93) Turbak, A. F.; Snyder, F. W.; Sandberg, K. R. Microfibrillated Cellulose, a New Cellulose Product: Properties, Uses, and Commercial Potential. *J. Appl. Polymer Sci., Appl. Polym. Symp.* **1983**, *37*, 815−827.
(94) Iwamoto, S.; Nakagaito, A. N.; Yano, H. Nano-Fibrillation of Pulp Fibers for the Processing of Transparent Nanocomposites. *Appl. Phys. A: Mater. Sci. Process.* **2007**, *89*, 461−466.
(95) Wang, Q.; Zhu, J.; Gleisner, R.; Kuster, T.; Baxa, U.; McNeil, S. Morphological Development of Cellulose Fibrils of a Bleached Eucalyptus Pulp by Mechanical Fibrillation. *Cellulose* **2012**, *19*, 1631−1643.
(96) Xu, X.; Liu, F.; Jiang, L.; Zhu, J. Y.; Haagenson, D.; Wiesenborn, D. P. Cellulose Nanocrystals vs. Cellulose Nanofibrils: A Comparative Study on Their Microstructures and Effects as Polymer Reinforcing Agents. *ACS Appl. Mater. Interfaces* **2013**, *5*, 2999−3009.
(97) Xu, X.; Wang, H.; Jiang, L.; Wang, X.; Payne, S. A.; Zhu, J. Y.; Li, R. Comparison between Cellulose Nanocrystal and Cellulose Nanofibril Reinforced Poly(ethylene oxide) Nanofibers and Their Novel Shish-Kebab-Like Crystalline Structures. *Macromolecules* **2014**, *47*, 3409−3416.
(98) Zhu, W.; Zhu, J. Y.; Gleisner, R.; Pan, X. J. On Energy Consumption for Size-Reduction and Yield from Subsequent Enzymatic Sacchrification of Pretreated Lodgepole Pine. *Bioresour. Technol.* **2010**, *101*, 2782−2792.
(99) Saito, T.; Isogai, A. TEMPO-Mediated Oxidation of Native Cellulose. The Effect of Oxidation Conditions on Chemical and Crystal Structures of the Water-Insoluble Fractions. *Biomacromolecules* **2004**, *5*, 1983−1989.
(100) Saito, T.; Nishiyama, Y.; Putaux, J.-L.; Vignon, M.; Isogai, A. Homogeneous Suspensions of Individualized Microfibrils from TEMPO-Catalyzed Oxidation of Native Cellulose. *Biomacromolecules* **2006**, *7*, 1687−1691.
(101) Okita, Y.; Saito, T.; Isogai, A. TEMPO-Mediated Oxidation of Softwood Thermomechanical Pulp. *Holzforschung* **2009**, *63*, 529−535.
(102) Isogai, A.; Saito, T.; Fukuzumi, H. TEMPO-Oxidized Cellulose Nanofibers. *Nanoscale* **2011**, *3*, 71−85.
(103) De Nooy, A. E.; Besemer, A. C.; van Bekkum, H. Highly Selective Nitroxyl Radical-Mediated Oxidation of Primary Alcohol Groups in Water-Soluble Glucans. *Carbohydr. Res.* **1995**, *269*, 89−98.
(104) Isogai, A. Wood Nanocelluloses: Fundamentals and Applications as New Bio-Based Nanomaterials. *J. Wood Sci.* **2013**, *59*, 449−459.
(105) Hayashi, N.; Kondo, T.; Ishihara, M. Enzymatically Produced Nano-Ordered Short Elements Containing Cellulose Iβ Crystalline Domains. *Carbohydr. Polym.* **2005**, *61*, 191−197.
(106) Henriksson, M.; Henriksson, G.; Berglund, L.; Lindström, T. An Environmentally Friendly Method for Enzyme-Assisted Preparation of Microfibrillated Cellulose (MFC) Nanofibers. *Eur. Polym. J.* **2007**, *43*, 3434−3441.
(107) Pääkkö, M.; Ankerfors, M.; Kosonen, H.; Nykänen, A.; Ahola, S.; Österberg, M.; Ruokolainen, J.; Laine, J.; Larsson, P. T.; Ikkala, O. Enzymatic Hydrolysis Combined with Mechanical Shearing and High-Pressure Homogenization for Nanoscale Cellulose Fibrils and Strong Gels. *Biomacromolecules* **2007**, *8*, 1934−1941.
(108) Zhu, J.; Sabo, R.; Luo, X. Integrated Production of Nano-Fibrillated Cellulose and Cellulosic Biofuel (ethanol) by Enzymatic Fractionation of Wood Fibers. *Green Chem.* **2011**, *13*, 1339−1344.
(109) Wang, W.; Mozuch, M. D.; Sabo, R. C.; Kersten, P.; Zhu, J.; Jin, Y. Production of Cellulose Nanofibrils from Bleached Eucalyptus Fibers by Hyperthermostable Endoglucanase Treatment and Subsequent Microfluidization. *Cellulose* **2015**, *22*, 351−361.
(110) Wang, W.; Sabo, R.; Mozuch, M.; Kersten, P.; Zhu, J. Y.; Jin, Y. Physical and Mechanical Properties of Cellulose Nanofibril Films from Bleached Eucalyptus Pulp by Endoglucanase Treatment and Microfluidization. *J. Polym. Environ.* **2015**, *23*, 551−558.
(111) Tenhunen, T.-M.; Peresin, M. S.; Penttilä, P. A.; Pere, J.; Serimaa, R.; Tammelin, T. Significance of Xylan on the Stability and Water Interactions of Cellulosic Nanofibrils. *React. Funct. Polym.* **2014**, *85*, 157−166.
(112) Busse-Wicher, M.; Gomes, T. C.; Tryfona, T.; Nikolovski, N.; Stott, K.; Grantham, N. J.; Bolam, D. N.; Skaf, M. S.; Dupree, P. The Pattern of Xylan Acetylation Suggests Xylan May Interact with Cellulose Microfibrils as a Twofold Helical Screw in the Secondary Plant Cell Wall of Arabidopsis Thaliana. *Plant J.* **2014**, *79*, 492−506.
(113) Zhang, C.; Zhuang, X.; Wang, Z. J.; Matt, F.; John, F. S.; Zhu, J. Xylanase Supplementation on Enzymatic Saccharification of Dilute Acid Pretreated Poplars at Different Severities. *Cellulose* **2013**, *20*, 1937−1946.
(114) Wang, Q. Q.; Zhu, J. Y.; Considine, J. M. Strong and Optically Transparent Films Prepared Using Cellulosic Solid Residue (CSR) Recovered from Cellulose Nanocrystals (CNC) Production Waste Stream. *ACS Appl. Mater. Interfaces* **2013**, *5*, 2527−2534.
(115) Yapo, B. M. Pectic substances: From Simple Pectic Polysaccharides to Complex Pectins—A New Hypothetical Model. *Carbohydr. Polym.* **2011**, *86*, 373−385.
(116) Pauly, M.; Gille, S.; Liu, L.; Mansoori, N.; de Souza, A.; Schultink, A.; Xiong, G. Hemicellulose Biosynthesis. *Planta* **2013**, *238*, 627−642.
(117) Yi, H.; Puri, V. M. Contributions of the Mechanical Properties of Major Structural Polysaccharides to the Stiffness of a Cell Wall Network Model. *Am. J. Bot.* **2014**, *101*, 244−254.
(118) Ek, M. *Pulping Chemistry and Technology*; Walter de Gruyter: 2009; Vol. *2*.
(119) Montero, C.; Clair, B.; Alméras, T.; Lee, A. v. d.; Gril, J. Relationship between Wood Elastic Strain under Bending and Cellulose Crystal Strain. *Compos. Sci. Technol.* **2012**, *72*, 175−181.
(120) Geddes, D. S.; Wilkie, K. C. B. Hemicelluloses from the Stem Tissues of the Aquatic Moss Fontinalis Antipyretica. *Carbohydr. Res.* **1971**, *18*, 333−335.
(121) Ek, M. *Wood chemistry and wood biotechnology*; Walter de Gruyter: 2009; Vol. *1*.
(122) Zabotina, O. A. Xyloglucan and its biosynthesis. *Front. Plant Sci.* **2012**, *3*.10.3389/fpls.2012.00134
(123) Hayashi, T.; Kaida, R. Functions of Xyloglucan in Plant Cells. *Mol. Plant* **2011**, *4*, 17−24.
(124) Åkerholm, M.; Salmén, L. Interactions between Wood Polymers Studied by Dynamic FT-IR Spectroscopy. *Polymer* **2001**, *42*, 963−969.
(125) Lawoko, M.; Henriksson, G.; Gellerstedt, G. Structural Differences between the Lignin−Carbohydrate Complexes Present in Wood and in Chemical Pulps. *Biomacromolecules* **2005**, *6*, 3467−3473.
(126) Lawoko, M.; Henriksson, G.; Gellerstedt, G. Characterisation of Lignin-Carbohydrate Complexes (LCCs) of Spruce Wood (Picea abies L.) Isolated with Two Methods. *Holzforschung* **2006**, *60*, 156−161.
(127) Oinonen, P.; Zhang, L.; Lawoko, M.; Henriksson, G. On the Formation of Lignin Polysaccharide Networks in Norway Spruce. *Phytochemistry* **2015**, *111*, 177−184.

DOI: 10.1021/acs.chemrev.6b00225
Chem. Rev. XXXX, XXX, XXX−XXX

(128) Vanholme, R.; Morreel, K.; Ralph, J.; Boerjan, W. Lignin Engineering. *Curr. Opin. Plant Biol.* **2008**, *11*, 278−285.
(129) Wang, Y.; Chantreau, M.; Sibout, R.; Hawkins, S. Plant Cell Wall Lignification and Monolignol Metabolism. *Front. Plant Sci.* **2013**, *4*, 220.
(130) Chen, Y.-r.; Sarkanen, S. Macromolecular Replication during Lignin Biosynthesis. *Phytochemistry* **2010**, *71*, 453−42.
(131) Boerjan, W.; Ralph, J.; Baucher, M. Lignin Biosynthesis. *Annu. Rev. Plant Biol.* **2003**, *54*, 519−546.
(132) Önnerud, H.; Zhang, L.; Gellerstedt, G.; Henriksson, G. Polymerization of Monolignols by Redox Shuttle−Mediated Enzymatic Oxidation A New Model in Lignin Biosynthesis I. *Plant Cell* **2002**, *14*, 1953−1962.
(133) Ralph, J.; Brunow, G.; Harris, P. J.; Dixon, R. A.; Schatz, P. F.; Boerjan, W. Lignification: Are Lignins Biosynthesized via Simple Combinatorial Chemistry or via Proteinaceous Control and Template Replication. *Rec. Adv. Polyphen. Res.* **2008**, *1*, 36−66.
(134) Christiernin, M.; Notley, S.; Zhang, L.; Nilsson, T.; Henriksson, G. Comparison between 10,000-Year Old and Contemporary Spruce Lignin. *Wood Sci. Technol.* **2009**, *43*, 23−41.
(135) Terashima, N. Diversification of Lignin Supramolecular Structure during the Evolution of Plants. *Mokuzai Gakkaishi* **2013**, *59*, 65−80.
(136) Crestini, C.; Melone, F.; Sette, M.; Saladino, R. Milled Wood Lignin: A Linear Oligomer. *Biomacromolecules* **2011**, *12*, 3928−3935.
(137) Trincone, A.; Pagnotta, E.; Tramice, A. Enzymatic Routes for the Production of Mono- and Di-Glucosylated Derivatives of Hydroxytyrosol. *Bioresour. Technol.* **2012**, *115*, 79−83.
(138) ten Have, R.; Teunissen, P. J. Oxidative Mechanisms Involved in Lignin Degradation by White-Rot Fungi. *Chem. Rev.* **2001**, *101*, 3397−3414.
(139) Holmgren, A.; Norgren, M.; Zhang, L.; Henriksson, G. On the Role of the Monolignol γ-Carbon Functionality in Lignin Biopolymerization. *Phytochemistry* **2009**, *70*, 147−155.
(140) Medronho, B.; Lindman, B. Competing Forces during Cellulose Dissolution: from Solvents to Mechanisms. *Curr. Opin. Colloid Interface Sci.* **2014**, *19*, 32−40.
(141) Giummarella, N.; Lindgren, C.; Lindström, M. E.; Henriksson, G. Lignin Prepared by Ultrafiltration of Black Liquor: Investigation of Solubility, Viscosity, and Ash Content. *BioResources* **2016**, *11*, 3494−3510.
(142) Arnoul-Jarriault, B.; Lachenal, D.; Chirat, C.; Heux, L. Upgrading Softwood Bleached Kraft Pulp to Dissolving Pulp by Cold Caustic Treatment and Acid-Hot Caustic Treatment. *Ind. Crops Prod.* **2015**, *65*, 565−571.
(143) Kilpeläinen, P.; Kitunen, V.; Hemming, J.; Pranovich, A.; Ilvesniemi, H.; Willför, S. Pressurized Hot Water Flow-Through Extraction of Birch Sawdust-Effects of Sawdust Density and Sawdust Size. *Nord. Pulp Pap. Res. J.* **2014**, *29*, 547−556.
(144) Ferrari, E.; Ranucci, E.; Edlund, U.; Albertsson, A. C. Design of Renewable Poly (amidoamine)/Hemicellulose Hydrogels for Heavy Metal Adsorption. *J. Appl. Polym. Sci.* **2015**, *132*, 41695.
(145) Wang, Y.; Azhar, S.; Lindström, M. E.; Henriksson, G. Stabilization of Polysaccharides During Alkaline Pre-Treatment of Wood Combined with Enzyme-Supported Extractions in a Biorefinery. *J. Wood Chem. Technol.* **2015**, *35*, 91−101.
(146) Oinonen, P.; Areskogh, D.; Henriksson, G. Enzyme Catalyzed Cross-Linking of Spruce Galactoglucomannan Improves its Applicability in Barrier Films. *Carbohydr. Polym.* **2013**, *95*, 690−696.
(147) Areskogh, D.; Li, J.; Gellerstedt, G. r.; Henriksson, G. Investigation of the Molecular Weight Increase of Commercial Lignosulfonates by Laccase Catalysis. *Biomacromolecules* **2010**, *11*, 904−910.
(148) Zhu, H.; Areskogh, D.; Helander, M.; Henriksson, G. Investigation on Enzymatic Oxidative Polymerization of Technical Soda Lignin. *Curr. Org. Chem.* **2012**, *16*, 1850−1854.
(149) Zhao, X.; Cheng, K.; Liu, D. Organosolv Pretreatment of Lignocellulosic Biomass for Enzymatic Hydrolysis. *Appl. Microbiol. Biotechnol.* **2009**, *82*, 815−827.
(150) Luterbacher, J. S.; Rand, J. M.; Alonso, D. M.; Han, J.; Youngquist, J. T.; Maravelias, C. T.; Pfleger, B. F.; Dumesic, J. A. Nonenzymatic Sugar Production from Biomass Using Biomass-Derived γ-Valerolactone. *Science* **2014**, *343*, 277−280.
(151) Morgan, P. *Carbon fibers and their composites*; CRC Press: Boca Raton, FL, 2005.
(152) Qin, X.; Lu, Y.; Xiao, H.; Hao, Y.; Pan, D. Improving Preferred Orientation and Mechanical Properties of PAN-based Carbon Fibers by Pretreating Precursor Fibers in Nitrogen. *Carbon* **2011**, *49*, 4598−4600.
(153) Hunt, M. A.; Saito, T.; Brown, R. H.; Kumbhar, A. S.; Naskar, A. K. Patterned Functional Carbon Fibers from Polyethylene. *Adv. Mater.* **2012**, *24*, 2386−2389.
(154) Liu, Y.; Kumar, S. Recent Progress in Fabrication, Structure, and Properties of Carbon Fibers. *Polym. Rev.* **2012**, *52*, 234−258.
(155) Lee, J. S.; Kwon, O. S.; Park, S. J.; Park, E. Y.; You, S. A.; Yoon, H.; Jang, J. Fabrication of Ultrafine Metal-Oxide-Decorated Carbon Nanofibers for DMMP Sensor Application. *ACS Nano* **2011**, *5*, 7992−8001.
(156) Lee, J. A.; Shin, M. K.; Kim, S. H.; Cho, H. U.; Spinks, G. M.; Wallace, G. G.; Lima, M. D.; Lepró, X.; Kozlov, M. E.; Baughman, R. H. Ultrafast Charge and Discharge Biscrolled Yarn Supercapacitors for Textiles and Microdevices. *Nat. Commun.* **2013**, *4*, 1970.
(157) Lee, M.; Chen, C. Y.; Wang, S.; Cha, S. N.; Park, Y. J.; Kim, J. M.; Chou, L. J.; Wang, Z. L. A Hybrid Piezoelectric Structure for Wearable Nanogenerators. *Adv. Mater.* **2012**, *24*, 1759−1764.
(158) Gumennik, A.; Stolyarov, A. M.; Schell, B. R.; Hou, C.; Lestoquoy, G.; Sorin, F.; McDaniel, W.; Rose, A.; Joannopoulos, J. D.; Fink, Y. All-in-Fiber Chemical Sensing. *Adv. Mater.* **2012**, *24*, 6005−6009.
(159) Wang, H.; Xu, Z.; Kohandehghan, A.; Li, Z.; Cui, K.; Tan, X.; Stephenson, T. J.; King'ondu, C. K.; Holt, C. M.; Olsen, B. C. Interconnected Carbon Nanosheets Derived from Hemp for Ultrafast Supercapacitors with High Energy. *ACS Nano* **2013**, *7*, 5131−5141.
(160) Fu, Y.; Cai, X.; Wu, H.; Lv, Z.; Hou, S.; Peng, M.; Yu, X.; Zou, D. Fiber Supercapacitors Utilizing Pen Ink for Flexible/Wearable Energy Storage. *Adv. Mater.* **2012**, *24*, 5713−5718.
(161) Lee, B. Review of the Present Status of Optical Fiber Sensors. *Opt. Fiber Technol.* **2003**, *9*, 57−79.
(162) Thostenson, E.; Li, W.; Wang, D.; Ren, Z.; Chou, T. Carbon Nanotube/Carbon Fiber Hybrid Multiscale Composites. *J. Appl. Phys.* **2002**, *91*, 6034−6037.
(163) Hill, K.; Fujii, Y.; Johnson, D. C.; Kawasaki, B. Photosensitivity in Optical Fiber Waveguides: Application to Reflection Filter Fabrication. *Appl. Phys. Lett.* **1978**, *32*, 647−649.
(164) Bhatia, V.; Vengsarkar, A. M. Optical Fiber Long-Period Grating Sensors. *Opt. Lett.* **1996**, *21*, 692−694.
(165) Hu, L. B.; Pasta, M.; La Mantia, F.; Cui, L. F.; Jeong, S.; Deshazer, H. D.; Choi, J. W.; Han, S. M.; Cui, Y. Stretchable, Porous, and Conductive Energy Textiles. *Nano Lett.* **2010**, *10*, 708−714.
(166) Xie, X.; Ye, M.; Hu, L.; Liu, N.; McDonough, J. R.; Chen, W.; Alshareef, H. N.; Criddle, C. S.; Cui, Y. Carbon Nanotube-Coated Macroporous Sponge for Microbial Fuel Cell Electrodes. *Energy Environ. Sci.* **2012**, *5*, 5265−5270.
(167) Sun, C.-F.; Zhu, H.; Baker Iii, E. B.; Okada, M.; Wan, J.; Ghemes, A.; Inoue, Y.; Hu, L.; Wang, Y. Weavable High-Capacity Electrodes. *Nano Energy* **2013**, *2*, 987−994.
(168) Saheb, D. N.; Jog, J. Natural Fiber Polymer Composites: A Review. *Adv. Polym. Technol.* **1999**, *18*, 351−363.
(169) Kadla, J.; Kubo, S.; Venditti, R.; Gilbert, R.; Compere, A.; Griffith, W. Lignin-Based Carbon Fibers for Composite Fiber Applications. *Carbon* **2002**, *40*, 2913−2920.
(170) Jalal Uddin, A.; Araki, J.; Gotoh, Y. Toward "Strong" Green Nanocomposites: Polyvinyl Alcohol Reinforced with Extremely Oriented Cellulose Whiskers. *Biomacromolecules* **2011**, *12*, 617−624.
(171) Walther, A.; Timonen, J. V.; Díez, I.; Laukkanen, A.; Ikkala, O. Multifunctional High-Performance Biofibers Based on Wet-Extrusion of Renewable Native Cellulose Nanofibrils. *Adv. Mater.* **2011**, *23*, 2924−2928.

DOI: 10.1021/acs.chemrev.6b00225
Chem. Rev. XXXX, XXX, XXX−XXX

(172) Vehviläinen, M.; Kamppuri, T.; Rom, M.; Janicki, J.; Ciechańska, D.; Grönqvist, S.; Siika-Aho, M.; Christoffersson, K. E.; Nousiainen, P. Effect of Wet Spinning Parameters on the Properties of Novel Cellulosic Fibres. *Cellulose* **2008**, *15*, 671−680.
(173) Zhou, C.; Chu, R.; Wu, R.; Wu, Q. Electrospun Polyethylene Oxide/Cellulose Nanocrystal Composite Nanofibrous Mats with Homogeneous and Heterogeneous Microstructures. *Biomacromolecules* **2011**, *12*, 2617−2625.
(174) Iwamoto, S.; Isogai, A.; Iwata, T. Structure and Mechanical Properties of Wet-Spun Fibers Made from Natural Cellulose Nanofibers. *Biomacromolecules* **2011**, *12*, 831−836.
(175) Lagerwall, J. P.; Schütz, C.; Salajkova, M.; Noh, J.; Park, J. H.; Scalia, G.; Bergström, L. Cellulose Nanocrystal-Based Materials: from Liquid Crystal Self-assembly and Glass Formation to Multifunctional Thin Films. *NPG Asia Mater.* **2014**, *6*, e80.
(176) Li, Y.; Zhu, H.; Zhu, S.; Wan, J.; Liu, Z.; Vaaland, O.; Lacey, S.; Fang, Z.; Dai, H.; Li, T. Hybridizing Wood Cellulose and Graphene Oxide Toward High-Performance Fibers. *NPG Asia Mater.* **2015**, *7*, e150.
(177) Chang, H.; Chien, A.-T.; Liu, H. C.; Wang, P.-H.; Newcomb, B. A.; Kumar, S. Gel Spinning of Polyacrylonitrile/Cellulose Nanocrystal Composite Fibers. *ACS Biomater. Sci. Eng.* **2015**, *1*, 610−616.
(178) Urena-Benavides, E. E.; Brown, P. J.; Kitchens, C. L. Effect of Jet Stretch and Particle Load on Cellulose Nanocrystal− Alginate Nanocomposite Fibers. *Langmuir* **2010**, *26*, 14263−14270.
(179) Chen, S.; Schueneman, G.; Pipes, R. B.; Youngblood, J.; Moon, R. J. Effects of Crystal Orientation on Cellulose Nanocrystals−Cellulose Acetate Nanocomposite Fibers Prepared by Dry Spinning. *Biomacromolecules* **2014**, *15*, 3827−3835.
(180) Peresin, M. S.; Habibi, Y.; Zoppe, J. O.; Pawlak, J. J.; Rojas, O. J. Nanofiber Composites of Polyvinyl Alcohol and Cellulose Nanocrystals: Manufacture and Characterization. *Biomacromolecules* **2010**, *11*, 674−681.
(181) Rhim, Y.-R.; Zhang, D.; Rooney, M.; Nagle, D. C.; Fairbrother, D. H.; Herman, C.; Drewry, D. G. Changes in the Thermophysical Properties of Microcrystalline Cellulose as Function of Carbonization Temperature. *Carbon* **2010**, *48*, 31−40.
(182) Hu, B.; Wang, K.; Wu, L.; Yu, S. H.; Antonietti, M.; Titirici, M. M. Engineering Carbon Materials from the Hydrothermal Carbonization Process of Biomass. *Adv. Mater.* **2010**, *22*, 813−828.
(183) Lv, Y.; Gan, L.; Liu, M.; Xiong, W.; Xu, Z.; Zhu, D.; Wright, D. S. A Self-Template Synthesis of Hierarchical Porous Carbon Foams Based on Banana Peel for Supercapacitor Electrodes. *J. Power Sources* **2012**, *209*, 152−157.
(184) Wang, S.-X.; Yang, L.; Stubbs, L. P.; Li, X.; He, C. Lignin-Derived Fused Electrospun Carbon Fibrous Mats as High Performance Anode Materials for Lithium Ion Batteries. *ACS Appl. Mater. Interfaces* **2013**, *5*, 12275−12282.
(185) Tenhaeff, W. E.; Rios, O.; More, K.; McGuire, M. A. Highly Robust Lithium Ion Battery Anodes from Lignin: An Abundant, Renewable, and Low-Cost Material. *Adv. Funct. Mater.* **2014**, *24*, 86−94.
(186) Luo, W.; Schardt, J.; Bommier, C.; Wang, B.; Razink, J.; Simonsen, J.; Ji, X. Carbon Nanofibers Derived from Cellulose Nanofibers as a Long-Life Anode Material for Rechargeable Sodium-Ion Batteries. *J. Mater. Chem. A* **2013**, *1*, 10662−10666.
(187) Edison, T. A. Manufacture of Filaments for Incandescent Electric Lamps. *Google Patents*, 1892.
(188) Deng, L.; Young, R. J.; Kinloch, I. A.; Zhu, Y.; Eichhorn, S. J. Carbon Nanofibres Produced from Electrospun Cellulose Nanofibres. *Carbon* **2013**, *58*, 66−75.
(189) Kong, K.; Deng, L. B.; Kinloch, I. A.; Young, R. J.; Eichhorn, S. J. Production of Carbon Fibres from a Pyrolysed and Graphitised Liquid Crystalline Cellulose Fibre Precursor. *J. Mater. Sci.* **2012**, *47*, 5402−5410.
(190) Li, Y.; Zhu, H.; Shen, F.; Wan, J.; Han, X.; Dai, J.; Dai, H.; Hu, L. Highly Conductive Microfiber of Graphene Oxide Templated Carbonization of Nanofibrillated Cellulose. *Adv. Funct. Mater.* **2014**, *24*, 7366−7372.
(191) Sudo, K.; Shimizu, K. A New Carbon Fiber from Lignin. *J. Appl. Polym. Sci.* **1992**, *44*, 127−134.
(192) Zhu, H.; Fang, Z.; Preston, C.; Li, Y.; Hu, L. Transparent Paper: Fabrications, Properties, and Device Applications. *Energy Environ. Sci.* **2014**, *7*, 269−287.
(193) Fang, Z.; Zhu, H.; Preston, C.; Hu, L. Development, Application and Commercialization of Transparent Paper. *Transl. Mater. Res.* **2014**, *1*, 015004.
(194) Hubbe, M. A.; Pawlak, J. J.; Koukoulas, A. A. Paper's appearance: A Review. *BioResources* **2008**, *3*, 627−665.
(195) Fang, Z.; Zhu, H.; Preston, C.; Han, X.; Li, Y.; Lee, S.; Chai, X.; Chen, G.; Hu, L. Highly Transparent and Writable Wood All-Cellulose Hybrid Nanostructured Paper. *J. Mater. Chem. C* **2013**, *1*, 6191−6197.
(196) Heyn, A. N. The Elementary Fibril and Supermolecular Structure of Cellulose in Soft Wood Fiber. *J. Ultrastruct. Res.* **1969**, *26*, 52−68.
(197) Eichhorn, S.; Dufresne, A.; Aranguren, M.; Marcovich, N.; Capadona, J.; Rowan, S.; Weder, C.; Thielemans, W.; Roman, M.; Renneckar, S. Review: Current International Research into Cellulose Nanofibres and Nanocomposites. *J. Mater. Sci.* **2010**, *45*, 1−33.
(198) Bachmann, K. The Treatment of Transparent Papers: A review; *The Book and Paper Annual*; The American Institute for Conservation, 1983; Vol. 2, pp 3−13.
(199) Koike, T.; Amano, M., Transparent Cellulosic Paper and Method for Making the Same. *Google Patents*, 1979.
(200) Yousefi, H.; Faezipour, M.; Nishino, T.; Shakeri, A.; Ebrahimi, G. All-Cellulose Composite and Nanocomposite Made from Partially Dissolved Micro-and Nanofibers of Canola Straw. *Polym. J.* **2011**, *43*, 559−564.
(201) Yousefi, H.; Nishino, T.; Faezipour, M.; Ebrahimi, G.; Shakeri, A. Direct Fabrication of all-Cellulose Nanocomposite from Cellulose Microfibers Using Ionic Liquid-Based Nanowelding. *Biomacromolecules* **2011**, *12*, 4080−4085.
(202) Nogi, M.; Yano, H. Optically Transparent Nanofiber Sheets by Deposition of Transparent Materials: A Concept for a Roll-to-Roll Processing. *Appl. Phys. Lett.* **2009**, *94*, 233117.
(203) Yano, H.; Sasaki, S.; Shams, M. I.; Abe, K.; Date, T. Wood Pulp-Based Optically Transparent Film: A Paradigm from Nanofibers to Nanostructured Fibers. *Adv. Opt. Mater.* **2014**, *2*, 231−234.
(204) Fang, Z.; Zhu, H.; Yuan, Y.; Ha, D.; Zhu, S.; Preston, C.; Chen, Q.; Li, Y.; Han, X.; Lee, S.; Chen, G.; Li, T.; Munday, J.; Huang, J.; Hu, L. Novel Nanostructured Paper with Ultrahigh Transparency and Ultrahigh Haze for Solar Cells. *Nano Lett.* **2014**, *14*, 765−773.
(205) Herrick, F. W.; Casebier, R. L.; Hamilton, J. K.; Sandberg, K. R. In *Microfibrillated cellulose: morphology and accessibility*; ITT Rayonier Inc.: Shelton, WA, 1983.
(206) Turbak, A. F.; Snyder, F. W.; Sandberg, K. R., Microfibrillated Cellulose. *Google Patents*, 1983.
(207) Eichhorn, S. J.; Dufresne, A.; Aranguren, M.; Marcovich, N. E.; Capadona, J. R.; Rowan, S. J.; Weder, C.; Thielemans, W.; Roman, M.; Renneckar, S.; Gindl, W.; Veigel, S.; Keckes, J.; Yano, H.; Abe, K.; Nogi, M.; Nakagaito, A. N.; Mangalam, A.; Simonsen, J.; Benight, A. S.; Bismarck, A.; Berglund, L. A.; Peijs, T. Review: Current International Research into Cellulose Nanofibres and Nanocomposites. *J. Mater. Sci.* **2010**, *45*, 1−33.
(208) Nogi, M.; Iwamoto, S.; Nakagaito, A. N.; Yano, H. Optically Transparent Nanofiber Paper. *Adv. Mater.* **2009**, *21*, 1595−1598.
(209) Nogi, M.; Iwamoto, S.; Nakagaito, A. N.; Yano, H., Optically Transparent Paper from Cellulose Nanofibers. *Abstr. Pap., Am. Chem. Soc.* **2009**, *237*.
(210) Nogi, M.; Kim, C.; Sugahara, T.; Inui, T.; Takahashi, T.; Suganuma, K. High Thermal Stability of Optical Transparency in Cellulose Nanofiber Paper. *Appl. Phys. Lett.* **2013**, *102*, 181911.
(211) Fukuzumi, H.; Saito, T.; Iwata, T.; Kumamoto, Y.; Isogai, A. Transparent and High Gas Barrier Films of Cellulose Nanofibers Prepared by TEMPO-Mediated Oxidation. *Biomacromolecules* **2009**, *10*, 162−165.

DOI: 10.1021/acs.chemrev.6b00225
Chem. Rev. XXXX, XXX, XXX−XXX

(212) Henriksson, M.; Berglund, L. A.; Isaksson, P.; Lindström, T.; Nishino, T. Cellulose Nanopaper Structures of High Toughness. *Biomacromolecules* **2008**, *9*, 1579−1585.
(213) Sehaqui, H.; Liu, A. D.; Zhou, Q.; Berglund, L. A. Fast Preparation Procedure for Large, Flat Cellulose and Cellulose/Inorganic Nanopaper Structures. *Biomacromolecules* **2010**, *11*, 2195−2198.
(214) Zheng, G.; Cui, Y.; Karabulut, E.; Wagberg, L.; Zhu, H.; Hu, L. Nanostructured Paper for Flexible Energy and Electronic Devices. *MRS Bull.* **2013**, *38*, 320−325.
(215) Postek, M. T.; Vladár, A.; Dagata, J.; Farkas, N.; Ming, B.; Wagner, R.; Raman, A.; Moon, R. J.; Sabo, R.; Wegner, T. H. Development of the Metrology and Imaging of Cellulose Nanocrystals. *Meas. Sci. Technol.* **2011**, *22*, 024005.
(216) Zhou, Y.; Fuentes-Hernandez, C.; Khan, T. M.; Liu, J.-C.; Hsu, J.; Shim, J. W.; Dindar, A.; Youngblood, J. P.; Moon, R. J.; Kippelen, B. Recyclable Organic Solar Cells on Cellulose Nanocrystal Substrates. *Sci. Rep.* **2013**, *3*, 1536.
(217) Nakagaito, A. N.; Nogi, M.; Yano, H. Displays from Transparent Films of Natural Nanofibers. *MRS Bull.* **2010**, *35*, 214−218.
(218) Zhu, H.; Xiao, Z.; Liu, D.; Li, Y.; Weadock, N. J.; Fang, Z.; Huang, J.; Hu, L. Biodegradable Transparent Substrates for Flexible Organic-Light-Emitting Diodes. *Energy Environ. Sci.* **2013**, *6*, 2105−2111.
(219) Huang, J.; Zhu, H.; Chen, Y.; Preston, C.; Rohrbach, K.; Cumings, J.; Hu, L. Highly Transparent and Flexible Nanopaper Transistors. *ACS Nano* **2013**, *7*, 2106−2113.
(220) Yang, Q.; Fukuzumi, H.; Saito, T.; Isogai, A.; Zhang, L. Transparent Cellulose Films with High Gas Barrier Properties Fabricated from Aqueous Alkali/Urea Solutions. *Biomacromolecules* **2011**, *12*, 2766−2771.
(221) Yang, Q.; Saito, T.; Isogai, A. Facile Fabrication of Transparent Cellulose Films with High Water Repellency and Gas Barrier Properties. *Cellulose* **2012**, *19*, 1913−1921.
(222) Merindol, R.; Diabang, S.; Felix, O.; Roland, T.; Gauthier, C.; Decher, G. Bio-Inspired Multiproperty Materials: Strong, Self-Healing, and Transparent Artificial Wood Nanostructures. *ACS Nano* **2015**, *9*, 1127−1136.
(223) Hyden, W. L. Manufacture and Properties of Regenerated Cellulose Films. *Ind. Eng. Chem.* **1929**, *21*, 405−410.
(224) Cross, C. F.; Bevan, E. T.; Beadle, C. Thiokohlensäureester der Cellulose. *Ber. Dtsch. Chem. Ges.* **1893**, *26*, 1090−1097.
(225) Zhang, H.; Wu, J.; Zhang, J.; He, J. 1-Allyl-3-methylimidazolium Chloride Room Temperature Ionic Liquid: A New and Powerful Nonderivatizing Solvent for Cellulose. *Macromolecules* **2005**, *38*, 8272−8277.
(226) Wang, H.; Gurau, G.; Rogers, R. D. Ionic Liquid Processing of Cellulose. *Chem. Soc. Rev.* **2012**, *41*, 1519−1537.
(227) Swatloski, R. P.; Spear, S. K.; Holbrey, J. D.; Rogers, R. D. Dissolution of Cellose with Ionic Liquids. *J. Am. Chem. Soc.* **2002**, *124*, 4974−4975.
(228) Pinkert, A.; Marsh, K. N.; Pang, S.; Staiger, M. P. Ionic Liquids and Their Interaction with Cellulose. *Chem. Rev.* **2009**, *109*, 6712−6728.
(229) Turner, M. B.; Spear, S. K.; Holbrey, J. D.; Rogers, R. D. Production of Bioactive Cellulose Films Reconstituted from Ionic Liquids. *Biomacromolecules* **2004**, *5*, 1379−1384.
(230) Cai, J.; Zhang, L. Rapid Dissolution of Cellulose in LiOH/urea and NaOH/urea Aqueous Solutions. *Macromol. Biosci.* **2005**, *5*, 539−548.
(231) Zhang, L.; Mao, Y.; Zhou, J.; Cai, J. Effects of Coagulation Conditions on the Properties of Regenerated Cellulose Films Prepared in NaOH/urea Aqueous Solution. *Ind. Eng. Chem. Res.* **2005**, *44*, 522−529.
(232) Zhang, L.; Ruan, D.; Zhou, J. Structure and Properties of Regenerated Cellulose Films Prepared from Cotton Linters in NaOH/urea Aqueous Solution. *Ind. Eng. Chem. Res.* **2001**, *40*, 5923−5928.
(233) Nogi, M.; Yano, H. Transparent Nanocomposites Based on Cellulose Produced by Bacteria Offer Potential Innovation in the Electronics Device Industry. *Adv. Mater.* **2008**, *20*, 1849−1852.
(234) Aulin, C.; Salazar-Alvarez, G.; Lindström, T. High Strength, Flexible and Transparent Nanofibrillated Cellulose−Nanoclay Biohybrid Films with Tunable Oxygen and Water Vapor Permeability. *Nanoscale* **2012**, *4*, 6622−6628.
(235) Nypelo, T.; Pynnonen, H.; Osterberg, M.; Paltakari, J.; Laine, J. Interactions between Inorganic Nanoparticles and Cellulose Nanofibrils. *Cellulose* **2012**, *19*, 779−792.
(236) Valentini, L.; Bon, S. B.; Fortunati, E.; Kenny, J. M. Preparation of Transparent and Conductive Cellulose Nanocrystals/Graphene Nanoplatelets Films. *J. Mater. Sci.* **2014**, *49*, 1009−1013.
(237) Yano, H.; Sasaki, S.; Shams, M.; Abe, K. Wood Pulp-Based Optically Transparent Film: A Paradigm from Nanofibers to Nanostructured Fibers. *Adv. Opt. Mater.* **2014**, *2*, 231−234.
(238) Okahisa, Y.; Yoshida, A.; Miyaguchi, S.; Yano, H. Optically Transparent Wood−Cellulose Nanocomposite as a Base Substrate for Flexible Organic Light-Emitting Diode Displays. *Compos. Sci. Technol.* **2009**, *69*, 1958−1961.
(239) Nogi, M.; Handa, K.; Nakagaito, A. N.; Yano, H. Optically Transparent Bionanofiber Composites with Low Sensitivity to Refractive Index of the Polymer Matrix. *Appl. Phys. Lett.* **2005**, *87*, 243110.
(240) Wu, J.; Yuan, Q. Gas Permeability of a Novel Cellulose Membrane. *J. Membr. Sci.* **2002**, *204*, 185−194.
(241) Ma, H.; Burger, C.; Hsiao, B. S.; Chu, B. Ultra-Fine Cellulose Nanofibers: New Nano-Scale Materials for Water Purification. *J. Mater. Chem.* **2011**, *21*, 7507−7510.
(242) Kuribayashi, I. Characterization of Composite Cellulosic Separators for Rechargeable Lithium-Ion Batteries. *J. Power Sources* **1996**, *63*, 87−91.
(243) Chun, S.-J.; Choi, E.-S.; Lee, E.-H.; Kim, J. H.; Lee, S.-Y.; Lee, S.-Y. Eco-friendly Cellulose Nanofiber Paper-Derived Separator Membranes Featuring Tunable Nanoporous Network Channels for Lithium-Ion Batteries. *J. Mater. Chem.* **2012**, *22*, 16618−16626.
(244) Zhang, L.; Sun, X.; Hu, Z.; Yuan, C.; Chen, C. Rice Paper as a Separator Membrane in Lithium-Ion Batteries. *J. Power Sources* **2012**, *204*, 149−154.
(245) Kim, J.-H.; Kim, J.-H.; Choi, E.-S.; Yu, H. K.; Kim, J. H.; Wu, Q.; Chun, S.-J.; Lee, S.-Y.; Lee, S.-Y. Colloidal Silica Nanoparticle-Assisted Structural Control of Cellulose Nanofiber Paper Separators for Lithium-Ion Batteries. *J. Power Sources* **2013**, *242*, 533−540.
(246) Zhang, J.; Liu, Z.; Kong, Q.; Zhang, C.; Pang, S.; Yue, L.; Wang, X.; Yao, J.; Cui, G. Renewable and Superior Thermal-Resistant Cellulose-Based Composite Nonwoven as Lithium-Ion Battery Separator. *ACS Appl. Mater. Interfaces* **2013**, *5*, 128−134.
(247) Mautner, A.; Lee, K. Y.; Lahtinen, P.; Hakalahti, M.; Tammelin, T.; Li, K.; Bismarck, A. Nanopapers for Organic Solvent Nanofiltration. *Chem. Commun.* **2014**, *50*, 5778−5781.
(248) Revol, J.-F.; Godbout, L.; Gray, D. Solid Self-assembled Films of Cellulose with Chiral Nematic Order and Optically Variable Properties. *J. Pulp Pap. Sci.* **1998**, *24*, 146−149.
(249) Tingaut, P.; Zimmermann, T.; Sèbe, G. Cellulose Nanocrystals and Microfibrillated Cellulose as Building Blocks for the Design of Hierarchical Functional Materials. *J. Mater. Chem.* **2012**, *22*, 20105−20111.
(250) Rizvi, T. Z. Liquid Crystalline Biopolymers: A New Arena for Liquid Crystal Research. *J. Mol. Liq.* **2003**, *106*, 43−53.
(251) Fraden, S.; Maret, G.; Caspar, D. L. D.; Meyer, R. B. Isotropic-Nematic Phase Transition and Angular Correlations in Isotropic Suspensions of Tobacco Mosaic Virus. *Phys. Rev. Lett.* **1989**, *63*, 2068.
(252) Revol, J. F.; Bradford, H.; Giasson, J.; Marchessault, R. H.; Gray, D. G. Helicoidal Self-ordering of Cellulose Microfibrils in Aqueous Suspension. *Int. J. Biol. Macromol.* **1992**, *14*, 170−172.
(253) Revol, J. F.; Godbout, L.; Gray, D. G. Solid Self-assembled Films of Cellulose with Chiral Nematic Order and Optically Variable Properties. *J. Pulp Pap. Sci.* **1998**, *24*, 146−149.
(254) von Freymann, G.; Kitaev, V.; Lotsch, B. V.; Ozin, G. A. Bottom-up Assembly of Photonic Crystals. *Chem. Soc. Rev.* **2013**, *42*, 2528−2554.

DOI: 10.1021/acs.chemrev.6b00225
Chem. Rev. XXXX, XXX, XXX−XXX

(255) de Vries, H. Rotatory Power and Other Optical Properties of Certain Liq Cryst. *Acta Crystallogr.* **1951**, *4*, 219−226.
(256) Shopsowitz, K. E.; Qi, H.; Hamad, W. Y.; MacLachlan, M. J. Free-Standing Mesoporous Silica Films with Tunable Chiral Nematic Structures. *Nature* **2010**, *468*, 422−425.
(257) Tatsumi, M.; Teramoto, Y.; Nishio, Y. Polymer Composites Reinforced by Locking-In a Liquid-Crystalline Assembly of Cellulose Nanocrystallites. *Biomacromolecules* **2012**, *13*, 1584−1591.
(258) Giese, M.; Blusch, L. K.; Khan, M. K.; Hamad, W. Y.; MacLachlan, M. J. Responsive Mesoporous Photonic Cellulose Films by Supramolecular Cotemplating. *Angew. Chem., Int. Ed.* **2014**, *53*, 8880−8884.
(259) Galland, S.; Andersson, R. L.; Salajkova, M.; Strom, V.; Olsson, R. T.; Berglund, L. A. Cellulose Nanofibers Decorated with Magnetic Nanoparticles - Synthesis, Structure and Use in Magnetized High Toughness Membranes for a Prototype Loudspeaker. *J. Mater. Chem. C* **2013**, *1*, 7963−7972.
(260) Olsson, R. T.; Azizi Samir, M. A. S.; Salazar Alvarez, G.; BelovaL; Strom, V.; Berglund, L. A.; Ikkala, O.; Nogues, J.; Gedde, U. W. Making Flexible Magnetic Aerogels and Stiff Magnetic Nanopaper Using Cellulose Nanofibrils as Templates. *Nat. Nanotechnol.* **2010**, *5*, 584−588.
(261) Junka, K.; Guo, J.; Filpponen, I.; Laine, J.; Rojas, O. J. Modification of Cellulose Nanofibrils with Luminescent Carbon Dots. *Biomacromolecules* **2014**, *15*, 876−881.
(262) Zhao, J.; Wei, Z.; Feng, X.; Miao, M.; Sun, L.; Cao, S.; Shi, L.; Fang, J. Luminescent and Transparent Nanopaper Based on Rare-Earth Up-Converting Nanoparticles Grafted Nanofibrillated Cellulose Derived from Garlic Skin. *ACS Appl. Mater. Interfaces* **2014**, *6*, 14945−14951.
(263) Niu, T.; Gu, Y.; Huang, J. Luminescent Cellulose Sheet Fabricated by Facile Self-assembly of Cadmium Selenide Nanoparticles on Cellulose Nanofibres. *J. Mater. Chem.* **2011**, *21*, 651−656.
(264) Padalkar, S.; Capadona, J. R.; Rowan, S. J.; Weder, C.; Won, Y.-H.; Stanciu, L. A.; Moon, R. J. Natural Biopolymers: Novel Templates for the Synthesis of Nanostructures. *Langmuir* **2010**, *26*, 8497−8502.
(265) Zhang, Y.; Carbonell, R. G.; Rojas, O. J. Bioactive Cellulose Nanofibrils for Specific Human IgG Binding. *Biomacromolecules* **2013**, *14*, 4161−4168.
(266) Uth, C.; Zielonka, S.; Hörner, S.; Rasche, N.; Plog, A.; Orelma, H.; Avrutina, O.; Zhang, K.; Kolmar, H. A Chemoenzymatic Approach to Protein Immobilization onto Crystalline Cellulose Nanoscaffolds. *Angew. Chem., Int. Ed.* **2014**, *53*, 12618−12623.
(267) Arola, S.; Tammelin, T.; Setälä, H.; Tullila, A.; Linder, M. B. Immobilization−Stabilization of Proteins on Nanofibrillated Cellulose Derivatives and Their Bioactive Film Formation. *Biomacromolecules* **2012**, *13*, 594−603.
(268) Dong, S.; Roman, M. Fluorescently Labeled Cellulose Nanocrystals for Bioimaging Applications. *J. Am. Chem. Soc.* **2007**, *129*, 13810−13811.
(269) Ha, D.; Murray, J.; Fang, Z.; Hu, L.; Munday, J. N. Advanced Broadband Antireflection Coatings Based on Cellulose Microfiber Paper. *IEEE J. Photovoltaics* **2015**, *5*, 577−583.
(270) Ha, D.; Fang, Z.; Hu, L.; Munday, J. N. Paper-Based Anti-Reflection Coatings for Photovoltaics. *Adv. Energy Mater.* **2014**, *4*, 1301804.
(271) Hu, L.; Cui, Y. Energy and Environmental Nanotechnology in Conductive Paper and Textiles. *Energy Environ. Sci.* **2012**, *5*, 6423−6435.
(272) Hu, L.; Wu, H.; La Mantia, F.; Yang, Y.; Cui, Y. Thin, Flexible Secondary Li-Ion Paper Batteries. *ACS Nano* **2010**, *4*, 5843−5848.
(273) Hu, L.; Choi, J. W.; Yang, Y.; Jeong, S.; La Mantia, F.; Cui, L.-F.; Cui, Y. Highly Conductive Paper for Energy-Storage Devices. *Proc. Natl. Acad. Sci. U. S. A.* **2009**, *106*, 21490−21494.
(274) Bao, W.; Fang, Z.; Wan, J.; Dai, J.; Zhu, H.; Han, X.; Yang, X.; Preston, C.; Hu, L. Aqueous Gating of Van der waals Materials on Bilayer Nanopaper. *ACS Nano* **2014**, *8*, 10606−10612.
(275) Zhu, H.; Li, Y.; Fang, Z.; Xu, J.; Cao, F.; Wan, J.; Preston, C.; Yang, B.; Hu, L. Highly Thermally Conductive Papers with Percolative Layered Boron Nitride Nanosheets. *ACS Nano* **2014**, *8*, 3606−3613.
(276) Zhu, H.; Narakathu, B. B.; Fang, Z.; Aijazi, A. T.; Joyce, M.; Atashbar, M.; Hu, L. A Gravure Printed Antenna on Shape-Stable Transparent Nanopaper. *Nanoscale* **2014**, *6*, 9110−9115.
(277) Wu, C.-N.; Saito, T.; Fujisawa, S.; Fukuzumi, H.; Isogai, A. Ultrastrong and High Gas-Barrier Nanocellulose/Clay-Layered Composites. *Biomacromolecules* **2012**, *13*, 1927−1932.
(278) Dou, Y.; Xu, S.; Liu, X.; Han, J.; Yan, H.; Wei, M.; Evans, D. G.; Duan, X. Transparent, Flexible Films Based on Layered Double Hydroxide/Cellulose Acetate with Excellent Oxygen Barrier Property. *Adv. Funct. Mater.* **2014**, *24*, 514−521.
(279) Yoon, B.; Ham, D. Y.; Yarimaga, O.; An, H.; Lee, C. W.; Kim, J. M. Inkjet Printing of Conjugated Polymer Precursors on Paper Substrates for Colorimetric Sensing and Flexible Electrothermochromic Display. *Adv. Mater.* **2011**, *23*, 5492−5497.
(280) Zhang, Y. P.; Chodavarapu, V. P.; Kirk, A. G.; Andrews, M. P. Nanocrystalline Cellulose for Covert Optical Encryption. *J. Nanophotonics* **2012**, *6*, 063516.
(281) Li, Y.; Zhu, H.; Gu, H.; Dai, H.; Fang, Z.; Weadock, N. J.; Guo, Z.; Hu, L. Strong Transparent Magnetic Nanopaper Prepared by Immobilization of Fe_3O_4 Nanoparticles in a Nanofibrillated Cellulose Network. *J. Mater. Chem. A* **2013**, *1*, 15278−15283.
(282) Díez, I.; Eronen, P.; Österberg, M.; Linder, M. B.; Ikkala, O.; Ras, R. H. A. Functionalization of Nanofibrillated Cellulose with Silver Nanoclusters: Fluorescence and Antibacterial Activity. *Macromol. Biosci.* **2011**, *11*, 1185−1191.
(283) Peng, Z. A.; Peng, X. Formation of high-quality CdTe, CdSe, and CdS Nanocrystals Using CdO as Precursor. *J. Am. Chem. Soc.* **2001**, *123*, 183−184.
(284) Peng, X.; Manna, L.; Yang, W.; Wickham, J.; Scher, E.; Kadavanich, A.; Alivisatos, A. P. Shape Control of CdSe Nanocrystals. *Nature* **2000**, *404*, 59−61.
(285) Yang, J.; Yu, J.; Fan, J.; Sun, D.; Tang, W.; Yang, X. Biotemplated Preparation of CdS Nanoparticles/Bacterial Cellulose Hybrid Nanofibers for Photocatalysis Application. *J. Hazard. Mater.* **2011**, *189*, 377−383.
(286) Xue, J.; Song, F.; Yin, X.-w.; Wang, X.-l.; Wang, Y.-z. Let It Shine: A Transparent and Photoluminescent Foldable Nanocellulose/Quantum Dot Paper. *ACS Appl. Mater. Interfaces* **2015**, *7*, 10076−10079.
(287) Lou, Q.; Qu, S.; Jing, P.; Ji, W.; Li, D.; Cao, J.; Zhang, H.; Liu, L.; Zhao, J.; Shen, D. Water-Triggered Luminescent "Nano-bombs" Based on Supra-(Carbon Nanodots). *Adv. Mater.* **2015**, *27*, 1389−1394.
(288) Preston, C.; Fang, Z.; Murray, J.; Zhu, H.; Dai, J.; Munday, J. N.; Hu, L. Silver Nanowire Transparent Conducting Paper-based Electrode with High Optical Haze. *J. Mater. Chem. C* **2014**, *2*, 1248−1254.
(289) Jiang, Y.; Song, Y.; Miao, M.; Cao, S.; Feng, X.; Fang, J.; Shi, L. Transparent Nanocellulose Hybrid Films Functionalized with ZnO Nanostructures for UV-blocking. *J. Mater. Chem. C* **2015**, *3*, 6717−6724.
(290) Inui, T.; Koga, H.; Nogi, M.; Komoda, N.; Suganuma, K. A Miniaturized Flexible Antenna Printed on a High Dielectric Constant Nanopaper Composite. *Adv. Mater.* **2015**, *27*, 1112−1116.
(291) Yan, C.; Wang, J.; Kang, W.; Cui, M.; Wang, X.; Foo, C. Y.; Chee, K. J.; Lee, P. S. Highly Stretchable Piezoresistive Graphene−Nanocellulose Nanopaper for Strain Sensors. *Adv. Mater.* **2014**, *26*, 2022−2027.
(292) Weng, Z.; Su, Y.; Wang, D.-W.; Li, F.; Du, J.; Cheng, H.-M. Graphene−Cellulose Paper Flexible Supercapacitors. *Adv. Energy Mater.* **2011**, *1*, 917−922.
(293) Liu, A.; Walther, A.; Ikkala, O.; Belova, L.; Berglund, L. A. Clay Nanopaper with Tough Cellulose Nanofiber Matrix for Fire Retardancy and Gas Barrier Functions. *Biomacromolecules* **2011**, *12*, 633−641.
(294) Dou, Y.; Zhou, A.; Pan, T.; Han, J.; Wei, M.; Evans, D. G.; Duan, X. Humidity-Triggered Self-healing Films with Excellent Oxygen Barrier Performance. *Chem. Commun.* **2014**, *50*, 7136−7138.
(295) Ho, T. T.; Zimmermann, T.; Ohr, S.; Caseri, W. R. Composites of Cationic Nanofibrillated Cellulose and Layered Silicates: Water Vapor Barrier and Mechanical Properties. *ACS Appl. Mater. Interfaces* **2012**, *4*, 4832−4840.

DOI: 10.1021/acs.chemrev.6b00225
Chem. Rev. XXXX, XXX, XXX−XXX

(296) Wu, C.-N.; Yang, Q.; Takeuchi, M.; Saito, T.; Isogai, A. Highly Tough and Transparent Layered Composites of Nanocellulose and Synthetic Silicate. *Nanoscale* **2014**, *6*, 392−399.
(297) Sheng, L.; Li, M.; Zhu, S.; Li, H.; Xi, G.; Li, Y.-G.; Wang, Y.; Li, Q.; Liang, S.; Zhong, K.; Zhang, S. X.-A. Hydrochromic Molecular Switches for Water-jet Rewritable Paper. *Nat. Commun.* **2014**, *5*, 3044.
(298) Wang, W.; Xie, N.; He, L.; Yin, Y. Photocatalytic Colour Switching of Redox Dyes for Ink-free Light-printable Rewritable Paper. *Nat. Commun.* **2014**, *5*, 5459.
(299) Salmon, L.; Bousseksou, A.; Nagy, V.; Csóka, L.; Molnár, G.; Suleimanov, I. Cellulose-spin Crossover Particle Composite Papers with Reverse Printing Performance: A Proof of Concept. *J. Mater. Chem. C* **2015**, *3*, 7897−7905.
(300) Asadpoordarvish, A.; Sandström, A.; Larsen, C.; Bollström, R.; Toivakka, M.; Österbacka, R.; Edman, L. Light-Emitting Paper. *Adv. Funct. Mater.* **2015**, *25*, 3238−3245.
(301) Hüsing, N.; Schubert, U. Aerogels—Airy Materials: Chemistry, Structure, and Properties. *Angew. Chem., Int. Ed.* **1998**, *37*, 22−45.
(302) Zhao, S. Y.; Zhang, Z.; Sebe, G.; Wu, R.; Virtudazo, R. V. R.; Tingaut, P.; Koebel, M. M. Multiscale Assembly of Superinsulating Silica Aerogels Within Silylated Nanocellulosic Scaffolds: Improved Mechanical Properties Promoted by Nanoscale Chemical Compatibilization. *Adv. Funct. Mater.* **2015**, *25*, 2326−2334.
(303) Aulin, C.; Netrval, J.; Wagberg, L.; Lindstrom, T. Aerogels from Nanofibrillated Cellulose with Tunable Oleophobicity. *Soft Matter* **2010**, *6*, 3298−3305.
(304) Bendahou, D.; Bendahou, A.; Seantier, B.; Grohens, Y.; Kaddami, H. Nano-fibrillated Cellulose-zeolites Based New Hybrid Composites Aerogels with Super Thermal Insulating Properties. *Ind. Crops Prod.* **2015**, *65*, 374−382.
(305) Bi, H. C.; Huang, X.; Wu, X.; Cao, X. H.; Tan, C. L.; Yin, Z. Y.; Lu, X. H.; Sun, L. T.; Zhang, H. Carbon Microbelt Aerogel Prepared by Waste Paper: An Efficient and Recyclable Sorbent for Oils and Organic Solvents. *Small* **2014**, *10*, 3544−3550.
(306) Carlsson, D. O.; Nystrom, G.; Zhou, Q.; Berglund, L. A.; Nyholm, L.; Stromme, M. Electroactive Nanofibrillated Cellulose Aerogel Composites with Tunable Structural and Electrochemical Properties. *J. Mater. Chem.* **2012**, *22*, 19014−19024.
(307) Demilecamps, A.; Beauger, C.; Hildenbrand, C.; Rigacci, A.; Budtova, T. Cellulose-Silica Aerogels. *Carbohydr. Polym.* **2015**, *122*, 293−300.
(308) Feng, J. D.; Nguyen, S. T.; Fan, Z.; Duong, H. M. Advanced Fabrication and Oil Absorption Properties of Super-hydrophobic Recycled Cellulose Aerogels. *Chem. Eng. J.* **2015**, *270*, 168−175.
(309) Fumagalli, M.; Sanchez, F.; Molina-Boisseau, S.; Heux, L. Surface-restricted Modification of Nanocellulose Aerogels in Gas-phase Esterification by Di-functional Fatty Acid Reagents. *Cellulose* **2015**, *22*, 1451−1457.
(310) Kobayashi, Y.; Saito, T.; Isogai, A. Aerogels with 3D Ordered Nanofiber Skeletons of Liquid-Crystalline Nanocellulose Derivatives as Tough and Transparent Insulators. *Angew. Chem., Int. Ed.* **2014**, *53*, 10394−10397.
(311) Yang, X.; Cranston, E. D. Chemically Cross-Linked Cellulose Nanocrystal Aerogels with Shape Recovery and Superabsorbent Properties. *Chem. Mater.* **2014**, *26*, 6016−6025.
(312) Cranston, E. D.; Eita, M.; Johansson, E.; Netrval, J.; Salajková, M.; Arwin, H.; Wågberg, L. Determination of Young's Modulus for Nanofibrillated Cellulose Multilayer Thin Films Using Buckling Mechanics. *Biomacromolecules* **2011**, *12*, 961−969.
(313) Huang, H. D.; Liu, C. Y.; Zhou, D.; Jiang, X.; Zhong, G. J.; Yan, D. X.; Li, Z. M. Cellulose Composite Aerogel for Highly Efficient Electromagnetic Interference Shielding. *J. Mater. Chem. A* **2015**, *3*, 4983−4991.
(314) Xu, X. Z.; Zhou, J.; Nagaraju, D. H.; Jiang, L.; Marinov, V. R.; Lubineau, G.; Alshareef, H. N.; Oh, M. Flexible, Highly Graphitized Carbon Aerogels Based on Bacterial Cellulose/Lignin: Catalyst-Free Synthesis and its Application in Energy Storage Devices. *Adv. Funct. Mater.* **2015**, *25*, 3193−3202.
(315) Wu, X.; Chabot, V. L.; Kim, B. K.; Yu, A.; Berry, R. M.; Tam, K. C. Cost-effective and Scalable Chemical Synthesis of Conductive Cellulose Nanocrystals for High-performance Supercapacitors. *Electrochim. Acta* **2014**, *138*, 139−147.
(316) Shi, Z.; Gao, H.; Feng, J.; Ding, B.; Cao, X.; Kuga, S.; Wang, Y.; Zhang, L.; Cai, J. In Situ Synthesis of Robust Conductive Cellulose/Polypyrrole Composite Aerogels and their Potential Application in Nerve Regeneration. *Angew. Chem., Int. Ed.* **2014**, *53*, 5380−5384.
(317) Carlsson, D. O.; Nyström, G.; Zhou, Q.; Berglund, L. A.; Nyholm, L.; Stromme, M. Electroactive Nanofibrillated Cellulose Aerogel Composites with Tunable Structural and Electrochemical Properties. *J. Mater. Chem.* **2012**, *22*, 19014−19024.
(318) Yavari, F.; Chen, Z.; Thomas, A. V.; Ren, W.; Cheng, H.-M.; Koratkar, N. High Sensitivity Gas Detection Using a Macroscopic Three-Dimensional Graphene Foam Network. *Sci. Rep.* **2011**, *1*, 166.
(319) Qi, H.; Mäder, E.; Liu, J. Electrically Conductive Aerogels Composed of Cellulose and Carbon Nanotubes. *J. Mater. Chem. A* **2013**, *1*, 9714−9720.
(320) Xu, X.; Zhou, J.; Nagaraju, D. H.; Jiang, L.; Marinov, V. R.; Lubineau, G.; Alshareef, H. N.; Oh, M. Flexible, Highly Graphitized Carbon Aerogels Based on Bacterial Cellulose/Lignin: Catalyst-Free Synthesis and its Application in Energy Storage Devices. *Adv. Funct. Mater.* **2015**, *25*, 3193−3202.
(321) Huang, Y.; Zheng, M.; Lin, Z.; Zhao, B.; Zhang, S.; Yang, J.; Zhu, C.; Zhang, H.; Sun, D.; Shi, Y. Flexible Cathodes and Multifunctional Interlayers Based on Carbonized Bacterial Cellulose for High-performance Lithium-sulfur Batteries. *J. Mater. Chem. A* **2015**, *3*, 10910−10918.
(322) Wang, M.; Anoshkin, I. V.; Nasibulin, A. G.; Korhonen, J. T.; Seitsonen, J.; Pere, J.; Kauppinen, E. I.; Ras, R. H. A.; Ikkala, O. Modifying Native Nanocellulose Aerogels with Carbon Nanotubes for Mechanoresponsive Conductivity and Pressure Sensing. *Adv. Mater.* **2013**, *25*, 2428−2432.
(323) Olsson, R. T.; Samir, M. A. S. A.; Salazar-Alvarez, G.; Belova, L.; Strom, V.; Berglund, L. A.; Ikkala, O.; Nogues, J.; Gedde, U. W. Making Flexible Magnetic Aerogels and Stiff Magnetic Nanopaper Using Cellulose Nanofibrils as Templates. *Nat. Nanotechnol.* **2010**, *5*, 584−588.
(324) Liu, D.; Wu, Q.; Andersson, R. L.; Hedenqvist, M. S.; Farris, S.; Olsson, R. T. Cellulose Nanofibril Core-shell Silica Coatings and Their Conversion into Thermally Stable Nanotube Aerogels. *J. Mater. Chem. A* **2015**, *3*, 15745−15754.
(325) Chin, S. F.; Binti Romainor, A. N.; Pang, S. C. Fabrication of Hydrophobic and Magnetic Cellulose Aerogel with High Oil Absorption Capacity. *Mater. Lett.* **2014**, *115*, 241−243.
(326) Li, W.; Zhao, X.; Liu, S. Preparation of Entangled Nanocellulose Fibers from APMP and its Magnetic Functional Property as Matrix. *Carbohydr. Polym.* **2013**, *94*, 278−285.
(327) Liu, S.; Yan, Q.; Tao, D.; Yu, T.; Liu, X. Highly Flexible Magnetic Composite Aerogels Prepared by Using Cellulose Nanofibril Networks as Templates. *Carbohydr. Polym.* **2012**, *89*, 551−557.
(328) Korhonen, J. T.; Hiekkataipale, P.; Malm, J.; Karppinen, M.; Ikkala, O.; Ras, R. H. A. Inorganic Hollow Nanotube Aerogels by Atomic Layer Deposition onto Native Nanocellulose Templates. *ACS Nano* **2011**, *5*, 1967−1974.
(329) Hao, P.; Zhao, Z.; Leng, Y.; Tian, J.; Sang, Y.; Boughton, R. I.; Wong, C. P.; Liu, H.; Yang, B. Graphene-based Nitrogen Self-doped Hierarchical Porous Carbon Aerogels Derived from Chitosan for High Performance Supercapacitors. *Nano Energy* **2015**, *15*, 9−23.
(330) Fan, Y.; Ma, W.; Han, D.; Gan, S.; Dong, X.; Niu, L. Convenient Recycling of 3D AgX/Graphene Aerogels (X = Br, Cl) for Efficient Photocatalytic Degradation of Water Pollutants. *Adv. Mater.* **2015**, *27*, 3767−3773.
(331) Van Aken, K. L.; Pérez, C. R.; Oh, Y.; Beidaghi, M.; Joo Jeong, Y.; Islam, M. F.; Gogotsi, Y. High Rate Capacitive Performance of Single-walled Carbon Nanotube Aerogels. *Nano Energy* **2015**, *15*, 662−669.
(332) Aliev, A. E.; Mayo, N. K.; Jung De Andrade, M.; Robles, R. O.; Fang, S.; Baughman, R. H.; Zhang, M.; Chen, Y.; Lee, J. A.; Kim, S. J.

DOI: 10.1021/acs.chemrev.6b00225
Chem. Rev. XXXX, XXX, XXX−XXX

Alternative Nanostructures for Thermophones. *ACS Nano* **2015**, *9*, 4743−4756.
(333) Xu, X.; Li, H.; Zhang, Q.; Hu, H.; Zhao, Z.; Li, J.; Qiao, Y.; Gogotsi, Y. Self-sensing, Ultralight, and Conductive 3D Graphene/Iron Oxide Aerogel Elastomer Deformable in a Magnetic Field. *ACS Nano* **2015**, *9*, 3969−3977.
(334) Zhu, C.; Han, T. Y. J.; Duoss, E. B.; Golobic, A. M.; Kuntz, J. D.; Spadaccini, C. M.; Worsley, M. A. Highly Compressible 3D Periodic Graphene Aerogel Microlattices. *Nat. Commun.* **2015**, *6*, 6962.
(335) Nystrom, G.; Marais, A.; Karabulut, E.; Wagberg, L.; Cui, Y.; Hamedi, M. M. Self-assembled Three-dimensional and Compressible Interdigitated Thin-film Supercapacitors and Batteries. *Nat. Commun.* **2015**, *6*, 7259.
(336) Ma, J.; Li, X.; Bao, Y. Advances in Cellulose-based Superabsorbent Hydrogels. *RSC Adv.* **2015**, *5*, 59745−59757.
(337) Rohrbach, K.; Li, Y.; Zhu, H.; Liu, Z.; Dai, J.; Andreasen, J.; Hu, L. A Cellulose Based Hydrophilic, Oleophobic Hydrated Filter for Water/Oil Separation. *Chem. Commun.* **2014**, *50*, 13296−13299.
(338) Abe, K.; Yano, H. Cellulose Nanofiber-based Hydrogels with High Mechanical Strength. *Cellulose* **2012**, *19*, 1907−1912.
(339) Rimdusit, S.; Somsaeng, K.; Kewsuwan, P.; Jubsilp, C.; Tiptipakorn, S. *Comparison of Gamma Radiation Crosslinking and Chemical Crosslinking on Properties of Methylcellulose Hydrogel. Engineering Journal* **2012**, *16* (4), 15−28.
(340) Li, N.; Bai, R. B. Copper Adsorption on Chitosan-cellulose Hydrogel Beads: Behaviors and Mechanisms. *Sep. Purif. Technol.* **2005**, *42*, 237−247.
(341) Abe, K.; Yano, H. Formation of Hydrogels from Cellulose Nanofibers. *Carbohydr. Polym.* **2011**, *85*, 733−737.
(342) Nakayama, A.; Kakugo, A.; Gong, J. P.; Osada, Y.; Takai, M.; Erata, T.; Kawano, S. High Mechanical Strength Double-network Hydrogel with Bacterial Cellulose. *Adv. Funct. Mater.* **2004**, *14*, 1124−1128.
(343) Fei, B.; Wach, R. A.; Mitomo, H.; Yoshii, F.; Kume, T. Hydrogel of Biodegradable Cellulose Derivatives. I. Radiation-Induced Crosslinking of CMC. *J. Appl. Polym. Sci.* **2000**, *78*, 278−283.
(344) Park, M.; Lee, D.; Hyun, J. Nanocellulose-Alginate Hydrogel for Cell Encapsulation. *Carbohydr. Polym.* **2015**, *116*, 223−228.
(345) Distantina, S.; Fahrurrozi, M. Preparation of Hydrogel Based on Glutaraldehyde-Crosslinked Carrageenan. *2012 3rd International Conference on Chemistry and Chemical Engineering*; IACSIT Press: Singapore, 2012; Vol. *38*, p 150.
(346) Janeček, E.-R.; McKee, J. R.; Tan, C. S. Y.; Nykänen, A.; Kettunen, M.; Laine, J.; Ikkala, O.; Scherman, O. A. Hybrid Supramolecular and Colloidal Hydrogels that Bridge Multiple Length Scales. *Angew. Chem., Int. Ed.* **2015**, *54*, 5383−5388.
(347) Hubbe, M. A.; Pawlak, J.; Koukoulas, A. A. Paper's Appearance: A Review. *BioResources* **2008**, *2*, 627−665.
(348) Zhu, H.; Parvinian, S.; Preston, C.; Vaaland, O.; Ruan, Z.; Hu, L. Transparent Nanopaper with Tailored Optical Properties. *Nanoscale* **2013**, *5*, 3787−3792.
(349) Fang, Z.; Zhu, H.; Bao, W.; Preston, C.; Liu, Z.; Dai, J.; Li, Y.; Hu, L. Highly Transparent Paper with Tunable Haze for Green Electronics. *Energy Environ. Sci.* **2014**, *7*, 3313−3319.
(350) Zhu, M.; Song, J.; Li, T.; Gong, A.; Wang, Y.; Dai, J.; Yao, Y.; Luo, W.; Henderson, D.; Hu, L. Highly Anisotropic, Highly Transparent Wood Composites. *Adv. Mater.* **2016**, *28*, 5181.
(351) Schmied, F. J.; Teichert, C.; Kappel, L.; Hirn, U.; Bauer, W.; Schennach, R. What Holds Paper Together: Nanometre Scale Exploration of Bonding between Paper Fibres. *Sci. Rep.* **2013**, *3*, 2432.
(352) Vainio, A.; Paulapuro, H. Interfiber Bonding and Fiber Segment Activation in Paper. *BioResources* **2007**, *2*, 442−458.
(353) González, I.; Alcalà, M.; Chinga-Carrasco, G.; Vilaseca, F.; Boufi, S.; Mutjé, P. From Paper to Nanopaper: Evolution of Mechanical and Physical Properties. *Cellulose* **2014**, *21*, 2599−2609.
(354) Sehaqui, H.; Zhou, Q.; Ikkala, O.; Berglund, L. A. Strong and Tough Cellulose Nanopaper with High Specific Surface Area and Porosity. *Biomacromolecules* **2011**, *12*, 3638−3644.
(355) Zhu, H.; Zhu, S.; Jia, Z.; Parvinian, S.; Li, Y.; Vaaland, O.; Hu, L.; Li, T. Anomalous Scaling Law of Strength and Toughness of Cellulose Nanopaper. *Proc. Natl. Acad. Sci. U. S. A.* **2015**, *112*, 8971−8976.
(356) Syverud, K.; Stenius, P. Strength and Barrier Properties of MFC Films. *Cellulose* **2009**, *16*, 75−85.
(357) Aulin, C.; Gällstedt, M.; Lindström, T. Oxygen and Oil Barrier Properties of Microfibrillated Cellulose Films and Coatings. *Cellulose* **2010**, *17*, 559−574.
(358) Sehaqui, H.; Ezekiel Mushi, N.; Morimune, S.; Salajkova, M.; Nishino, T.; Berglund, L. A. Cellulose Nanofiber Orientation in Nanopaper and Nanocomposites by Cold Drawing. *ACS Appl. Mater. Interfaces* **2012**, *4*, 1043−1049.
(359) Tang, H.; Butchosa, N.; Zhou, Q. A Transparent, Hazy, and Strong Macroscopic Ribbon of Oriented Cellulose Nanofibrils Bearing Poly (ethylene glycol). *Adv. Mater.* **2015**, *27*, 2070−2076.
(360) Eichhorn, S. J. Cellulose Nanowhiskers: Promising Materials for Advanced Applications. *Soft Matter* **2011**, *7*, 303−315.
(361) Sharma, P. R.; Varma, A. J. Thermal Stability of Cellulose and Their Nanoparticles: Effect of Incremental Increases in Carboxyl and Aldehyde Groups. *Carbohydr. Polym.* **2014**, *114*, 339−343.
(362) Yano, H.; Sugiyama, J.; Nakagaito, A. N.; Nogi, M.; Matsuura, T.; Hikita, M.; Handa, K. Optically Transparent Composites Reinforced with Networks of Bacterial Nanofibers. *Adv. Mater.* **2005**, *17*, 153−155.
(363) Nishino, T.; Matsuda, I.; Hirao, K. All-Cellulose Composite. *Macromolecules* **2004**, *37*, 7683−7687.
(364) Tobjörk, D.; Österbacka, R. Paper Electronics. *Adv. Mater.* **2011**, *23*, 1935−1961.
(365) Simula, S.; Ikäläinen, S.; Niskanen, K.; Varpula, T.; Seppä, H.; Paukku, A. Measurement of the Dielectric Properties of Paper. *J. Imaging Sci. Technol.* **1999**, *43*, 472−477.
(366) Fahmy, T. Y. A.; Mobarak, F.; El-Meligy, M. G. Introducing Undeinked Old Newsprint as a New Resource of Electrical Purposes Paper. *Wood Sci. Technol.* **2008**, *42*, 691−698.
(367) Le Bras, D.; Stromme, M.; Mihranyan, A. Characterization of Dielectric Properties of Nanocellulose from Wood and Algae for Insulator Applications. *J. Phys. Chem. B* **2015**, *119*, 5911−5917.
(368) Lavoine, N.; Desloges, I.; Dufresne, A.; Bras, J. Microfibrillated Cellulose−Its Barrier Properties and Applications in Cellulosic Materials: A Review. *Carbohydr. Polym.* **2012**, *90*, 735−764.
(369) Spence, K. L.; Venditti, R. A.; Rojas, O. J.; Pawlak, J. J.; Hubbe, M. A. Water Vapor Barrier Properties of Coated and Filled Microfibrillated Cellulose Composite Films. *BioResources* **2011**, *6*, 4370−4388.
(370) Österberg, M.; Vartiainen, J.; Lucenius, J.; Hippi, U.; Seppälä, J.; Serimaa, R.; Laine, J. A Fast Method to Produce Strong NFC Films as a Platform for Barrier and Functional Materials. *ACS Appl. Mater. Interfaces* **2013**, *5*, 4640−4647.
(371) Robinson, B. H. E-waste: An Assessment of Global Production and Environmental Impacts. Science of the Total Environment. *Sci. Total Environ.* **2009**, *408*, 183−191.
(372) Geyer, R.; Blass, V. D. The Economics of Cell Phone Reuse and Recycling. *Int. J. Adv. Manuf. Technol.* **2010**, *47*, 515−525.
(373) Lorenzen, J. A. Green Consumption and Social Change: Debates over Responsibility, Private Action, and Access. *Sociology Compass.* **2014**, *8*, 1063−1081.
(374) Pramila, S.; Fulekar, M.; Bhawana, P. E-waste-A Challenge for Tomorrow. *Res. J. Recent Sci.* **2012**, *1*, 86−93.
(375) Irimia-Vladu, M.; Głowacki, E. D.; Voss, G.; Bauer, S.; Sariciftci, N. S. Green and Biodegradable Electronics. *Mater. Today* **2012**, *15*, 340−346.
(376) Jung, Y. H.; Chang, T.-H.; Zhang, H.; Yao, C.; Zheng, Q.; Yang, V. W.; Mi, H.; Kim, M.; Cho, S. J.; Park, D.-W. High-Performance Green Flexible Electronics Based on Biodegradable Cellulose Nanofibril Paper. *Nat. Commun.* **2015**, *6*, 7170.
(377) Hwang, S. W.; Song, J. K.; Huang, X.; Cheng, H.; Kang, S. K.; Kim, B. H.; Kim, J. H.; Yu, S.; Huang, Y.; Rogers, J. A. High-Performance Biodegradable/Transient Electronics on Biodegradable Polymers. *Adv. Mater.* **2014**, *26*, 3905−3911.

DOI: 10.1021/acs.chemrev.6b00225
Chem. Rev. XXXX, XXX, XXX−XXX

(378) Svagan, A. J.; Busko, D.; Avlasevich, Y.; Glasser, G.; Baluschev, S.; Landfester, K. Photon Energy Upconverting Nanopaper: A Bioinspired Oxygen Protection Strategy. *ACS Nano* **2014**, *8*, 8198−8207.
(379) Andersson, P.; Nilsson, D.; Svensson, P. O.; Chen, M.; Malmström, A.; Remonen, T.; Kugler, T.; Berggren, M. Active Matrix Displays Based on All-Organic Electrochemical Smart Pixels Printed on Paper. *Adv. Mater.* **2002**, *14*, 1460−1464.
(380) Martins, R.; Barquinha, P.; Pereira, L.; Correia, N.; Goncalves, G.; Ferreira, I.; Fortunato, E. Write-erase and Read Paper Memory Transistor. *Appl. Phys. Lett.* **2008**, *93*, 203501−3.
(381) Eder, F.; Klauk, H.; Halik, M.; Zschieschang, U.; Schmid, G.; Dehm, C. Organic Electronics on Paper. *Appl. Phys. Lett.* **2004**, *84*, 2673−2675.
(382) Kim, Y.-H.; Moon, D.-G.; Han, J.-I. Organic TFT Array on a Paper Substrate. *IEEE Electron Device Lett.* **2004**, *25*, 702−704.
(383) Yun, S.; Jang, S.-D.; Yun, G.-Y.; Kim, J.-H.; Kim, J. Paper Transistor Made with Covalently Bonded Multiwalled Carbon Nanotube and Cellulose. *Appl. Phys. Lett.* **2009**, *95*, 104102.
(384) Hu, L. B.; Hecht, D. S.; Gruner, G. Carbon Nanotube Thin Films: Fabrication, Properties, and Applications. *Chem. Rev.* **2010**, *110*, 5790−5844.
(385) Fujisaki, Y.; Koga, H.; Nakajima, Y.; Nakata, M.; Tsuji, H.; Yamamoto, T.; Kurita, T.; Nogi, M.; Shimidzu, N. Transparent Nanopaper-Based Flexible Organic Thin-Film Transistor Array. *Adv. Funct. Mater.* **2014**, *24*, 1657−1663.
(386) Ohno, Y.; Maehashi, K.; Yamashiro, Y.; Matsumoto, K. Electrolyte-gated Graphene Field-effect Transistors for Detecting pH and Protein Adsorption. *Nano Lett.* **2009**, *9*, 3318−3322.
(387) Purandare, S.; Gomez, E. F.; Steckl, A. J. High Brightness Phosphorescent Organic Light Emitting Diodes on Transparent and Flexible Cellulose Films. *Nanotechnology* **2014**, *25*, 094012.
(388) Graf, R. F. *Modern Dictionary of Electronics*; Newnes: 1999.
(389) Russo, A.; Ahn, B. Y.; Adams, J. J.; Duoss, E. B.; Bernhard, J. T.; Lewis, J. A. Pen-on-Paper Flexible Electronics. *Adv. Mater.* **2011**, *23*, 3426−3430.
(390) Nogi, M.; Komoda, N.; Otsuka, K.; Suganuma, K. Foldable Nanopaper Antennas for Origami Electronics. *Nanoscale* **2013**, *5*, 4395−4399.
(391) Wei, Y.; Lin, X.; Jiang, K.; Liu, P.; Li, Q.; Fan, S. Thermoacoustic Chips with Carbon Nanotube Thin Yarn Arrays. *Nano Lett.* **2013**, *13*, 4795−4801.
(392) Zhou, Q.; Zettl, A. Electrostatic Graphene Loudspeaker. *Appl. Phys. Lett.* **2013**, *102*, 223109.
(393) Chen, A. S.; Zhu, H.; Li, Y.; Hu, L.; Bergbreiter, S. In A Paper-Based Electrostatic Zipper Actuator for Printable Robots. *2014 IEEE International Conference on Robotics and Automation (ICRA)*; 2014; pp 5038−5043.
(394) Zhong, Q.; Zhong, J.; Hu, B.; Hu, Q.; Zhou, J.; Wang, Z. L. A Paper-based Nanogenerator as a Power Source and Active Sensor. *Energy Environ. Sci.* **2013**, *6*, 1779−1784.
(395) Zhong, J.; Zhu, H.; Zhong, Q.; Dai, J.; Li, W.; Jiang, S.-H.; Yao, Y.; Henderson, D.; Hu, Q.; Hu, L. Self-Powered Human Interactive Transparent Nanopaper Systems. *ACS Nano* **2015**, *9*, 7399−7406.
(396) Zhu, H.; Fang, Z.; Wang, Z.; Dai, J.; Yao, Y.; Shen, F.; Preston, C.; Wu, W.; Peng, P.; Jang, N.; Yu, Q.; Yu, Z.; Hu, L. Extreme Light Management in Mesoporous Wood Cellulose Paper for Optoelectronics. *ACS Nano* **2016**, *10*, 1369−1377.
(397) Ishikawa, M.; Maruyama, Y.; Ye, J.-Y.; Futamata, M. Single-molecule Imaging and Spectroscopy Using Fluorescence and Surface-enhanced Raman Scattering. *J. Biol. Phys.* **2002**, *28*, 573−585.
(398) Nie, S.; Emory, S. R. Probing Single Molecules and Single Nanoparticles by Surface-enhanced Raman Scattering. *Science* **1997**, *275*, 1102−1106.
(399) Wei, W. Y.; White, I. M. Chromatographic Separation and Detection of Target Analytes from Complex Samples Using Inkjet Printed SERS Substrates. *Analyst* **2013**, *138*, 3679−3686.
(400) Hoppmann, E. P.; Wei, W. Y.; White, I. M. Highly Sensitive and Flexible Inkjet Printed SERS Sensors on Paper. *Methods* **2013**, *63*, 219−224.
(401) Chen, Y.; Cheng, H.; Tram, K.; Zhang, S.; Zhao, Y.; Han, L.; Chen, Z.; Huan, S. A Paper-based Surface-enhanced Resonance Raman Spectroscopic (SERRS) Immunoassay Using Magnetic Separation and Enzyme-catalyzed Reaction. *Analyst* **2013**, *138*, 2624−2631.
(402) Tian, L.; Morrissey, J. J.; Kattumenu, R.; Gandra, N.; Kharasch, E. D.; Singamaneni, S. Bioplasmonic Paper as a Platform for Detection of Kidney Cancer Biomarkers. *Anal. Chem.* **2012**, *84*, 9928−9934.
(403) Ngo, Y. H.; Li, D.; Simon, G. P.; Garnier, G. Gold Nanoparticle−Paper as a Three-Dimensional Surface Enhanced Raman Scattering Substrate. *Langmuir* **2012**, *28*, 8782−8790.
(404) Pourreza, N.; Golmohammadi, H.; Naghdi, T.; Yousefi, H. Green In-situ Synthesized Silver Nanoparticles Embedded in Bacterial Cellulose Nanopaper as a Bionanocomposite Plasmonic Sensor. *Biosens. Bioelectron.* **2015**, *74*, 353−359.
(405) Yetisen, A. K.; Akram, M. S.; Lowe, C. R. Paper-based Microfluidic Point-of-care Diagnostic Devices. *Lab Chip* **2013**, *13*, 2210−2251.
(406) Li, X.; Ballerini, D. R.; Shen, W. A Perspective on Paper-based Microfluidics: Current Status and Future Trends. *Biomicrofluidics* **2012**, *6*, 011301.
(407) Martinez, A. W.; Phillips, S. T.; Butte, M. J.; Whitesides, G. M. Patterned Paper as a Platform for Inexpensive, Low Volume, Portable Bioassays. *Angew. Chem., Int. Ed.* **2007**, *46*, 1318−1320.
(408) Abe, K.; Suzuki, K.; Citterio, D. Inkjet-printed Microfluidic Multianalyte Chemical Sensing Paper. *Anal. Chem.* **2008**, *80*, 6928−6934.
(409) Li, X.; Tian, J.; Nguyen, T.; Shen, W. Paper-based Microfluidic Devices by Plasma Treatment. *Anal. Chem.* **2008**, *80*, 9131−9134.
(410) Carrilho, E.; Martinez, A. W.; Whitesides, G. M. Understanding Wax Printing: a Simple Micropatterning Process for Paper-based Microfluidics. *Anal. Chem.* **2009**, *81*, 7091−7095.
(411) Dungchai, W.; Chailapakul, O.; Henry, C. S. A Low-cost, Simple, and Rapid Fabrication Method for Paper-based Microfluidics Using Wax Screen-printing. *Analyst* **2011**, *136*, 77−82.
(412) Martinez, A. W.; Phillips, S. T.; Whitesides, G. M.; Carrilho, E. Diagnostics for the Developing World: Microfluidic Paper-based Analytical Devices. *Anal. Chem.* **2010**, *82*, 3−10.
(413) Nie, Z.; Nijhuis, C. A.; Gong, J.; Chen, X.; Kumachev, A.; Martinez, A. W.; Narovlyansky, M.; Whitesides, G. M. Electrochemical Sensing in Paper-based Microfluidic Devices. *Lab Chip* **2010**, *10*, 477−483.
(414) Cheng, C. M.; Martinez, A. W.; Gong, J.; Mace, C. R.; Phillips, S. T.; Carrilho, E.; Mirica, K. A.; Whitesides, G. M. Paper-Based ELISA. *Angew. Chem., Int. Ed.* **2010**, *49*, 4771−4774.
(415) Dungchai, W.; Chailapakul, O.; Henry, C. S. Electrochemical Detection for Paper-Based Microfluidics. *Anal. Chem.* **2009**, *81*, 5821−5826.
(416) Ali, M. M.; Aguirre, S. D.; Xu, Y.; Filipe, C. D.; Pelton, R.; Li, Y. Detection of DNA Using Bioactive Paper Strips. *Chem. Commun.* **2009**, 6640−6642.
(417) Khan, M. S.; Li, X.; Shen, W.; Garnier, G. Thermal Stability of Bioactive Enzymatic Papers. *Colloids Surf., B* **2010**, *75*, 239−246.
(418) Virtanen, H.; Orelma, H.; Erho, T.; Smolander, M. Development of Printable Bioactive Paper Containing Laccase. *Process Biochem.* **2012**, *47*, 1496−1502.
(419) Zhao, W.; Ali, M. M.; Aguirre, S. D.; Brook, M. A.; Li, Y. Paper-based Bioassays Using Gold Nanoparticle Colorimetric Probes. *Anal. Chem.* **2008**, *80*, 8431−8437.
(420) Warren, A. D.; Kwong, G. A.; Wood, D. K.; Lin, K. Y.; Bhatia, S. N. Point-of-care Diagnostics for Noncommunicable Diseases using Synthetic Urinary Biomarkers and Paper Microfluidics. *Proc. Natl. Acad. Sci. U. S. A.* **2014**, *111*, 3671−3676.
(421) Wang, J.; Yiu, B.; Obermeyer, J.; Filipe, C. D.; Brennan, J. D.; Pelton, R. Effects of Temperature and Relative Humidity on the Stability of Paper-immobilized Antibodies. *Biomacromolecules* **2012**, *13*, 559−564.

DOI: 10.1021/acs.chemrev.6b00225
Chem. Rev. XXXX, XXX, XXX−XXX

(422) Lamprecht, B.; Thünauer, R.; Ostermann, M.; Jakopic, G.; Leising, G. Organic Photodiodes on Newspaper. *Phys. Status Solidi A* **2005**, *202*, R50−R52.
(423) Wang, F.; Chen, Z.; Xiao, L.; Qu, B.; Gong, Q. Papery Solar Cells Based on Dielectric/Metal Hybrid Transparent Cathode. *Sol. Energy Mater. Sol. Cells* **2010**, *94*, 1270−1274.
(424) Kim, T. S.; Na, S. I.; Kim, S. S.; Yu, B. K.; Yeo, J. S.; Kim, D. Y. Solution Processible Polymer Solar Cells Fabricated on a Papery Substrate. *Phys. Status Solidi RRL* **2012**, *6*, 13−15.
(425) Barr, M. C.; Rowehl, J. A.; Lunt, R. R.; Xu, J.; Wang, A.; Boyce, C. M.; Im, S. G.; Bulović, V.; Gleason, K. K. Direct Monolithic Integration of Organic Photovoltaic Circuits on Unmodified Paper. *Adv. Mater.* **2011**, *23*, 3500−3505.
(426) Hübler, A.; Trnovec, B.; Zillger, T.; Ali, M.; Wetzold, N.; Mingebach, M.; Wagenpfahl, A.; Deibel, C.; Dyakonov, V. Printed Paper Photovoltaic Cells. *Adv. Energy Mater.* **2011**, *1*, 1018−1022.
(427) Águas, H.; Mateus, T.; Vicente, A.; Gaspar, D.; Mendes, M. J.; Schmidt, W. A.; Pereira, L.; Fortunato, E.; Martins, R. Thin Film Silicon Photovoltaic Cells on Paper for Flexible Indoor Applications. *Adv. Funct. Mater.* **2015**, *25*, 3592−3598.
(428) Hu, L. B.; Zheng, G. Y.; Yao, J.; Liu, N. A.; Weil, B.; Eskilsson, M.; Karabulut, E.; Ruan, Z. C.; Fan, S. H.; Bloking, J. T.; McGehee, M. D.; Wagberg, L.; Cui, Y. Transparent and Conductive Paper from Nanocellulose Fibers. *Energy Environ. Sci.* **2013**, *6*, 513−518.
(429) Ha, D.; Fang, Z.; Hu, L.; Munday, J. N. Paper-Based Anti-Reflection Coatings for Photovoltaics. *Adv. Energy Mater.* **2014**, *4*, 1301804.
(430) Solomon, B. D.; Barnes, J. R.; Halvorsen, K. E. Grain and Cellulosic Ethanol: History, Economics, and Energy Policy. *Biomass Bioenergy* **2007**, *31*, 416−425.
(431) Kamm, B.; Gruber, P. R.; Kamm, M. *Biorefineries−industrial processes and products*; Wiley Online Library, 2007.
(432) Saeman, J. F. Kinetics of Wood Saccharification-hydrolysis of Cellulose and Decomposition of Sugars in Dilute Acid at High Temperature. *Ind. Eng. Chem.* **1945**, *37*, 43−52.
(433) Himmel, M. E. Corn Stover Conversion to Biofuels: DOE's Preparation for Readiness in 2012. *Cellulose* **2009**, *16*, 531−534.
(434) Aden, A.; Foust, T. Technoeconomic Analysis of the Dilute Sulfuric Acid and Enzymatic Hydrolysis Process for the Conversion of Corn Stover to Ethanol. *Cellulose* **2009**, *16*, 535−545.
(435) Klein-Marcuschamer, D.; Oleskowicz-Popiel, P.; Simmons, B. A.; Blanch, H. W. The Challenge of Enzyme Cost in the Production of Lignocellulosic Biofuels. *Biotechnol. Bioeng.* **2012**, *109*, 1083−1087.
(436) Elander, R. T.; Dale, B. E.; Holtzapple, M.; Ladisch, M. R.; Lee, Y.; Mitchinson, C.; Saddler, J. N.; Wyman, C. E. Summary of Findings from the Biomass Refining Consortium for Applied Fundamentals and Innovation (CAFI): Corn Stover Pretreatment. *Cellulose* **2009**, *16*, 649−659.
(437) Wyman, C. E. What is (and is not) Vital to Advancing Cellulosic Ethanol. *Trends Biotechnol.* **2007**, *25*, 153−157.
(438) Ho, N. W.; Chen, Z.; Brainard, A. P. Genetically Engineered Saccharomycesyeast Capable of Effective Cofermentation of Glucose and Xylose. *Appl. Environ. Microbiol.* **1998**, *64*, 1852−1859.
(439) Zhang, M.; Chou, Y.-C.; Howe, W.; Eddy, C.; Evans, K.; Mohagheghi, A. Zymomonas Pentose-sugar Fermenting Strains and Uses Thereof. *Google Patents*, 2007.
(440) Humbird, D.; Davis, R.; Tao, L.; Kinchin, C.; Hsu, D.; Aden, A.; Schoen, P.; Lukas, J.; Olthof, B.; Worley, M. *Process Design and Economics for Biochemical Conversion of Lignocellulosic Biomass to Ethanol: Dilute-Acid Pretreatment and Enzymatic Hydrolysis of Corn Stover*; National Renewable Energy Laboratory: Golden, CO, 2011
(441) Fu, C.; Mielenz, J. R.; Xiao, X.; Ge, Y.; Hamilton, C. Y.; Rodriguez, M.; Chen, F.; Foston, M.; Ragauskas, A.; Bouton, J. Genetic Manipulation of Lignin Reduces Recalcitrance and Improves Ethanol Production from Switchgrass. *Proc. Natl. Acad. Sci. U. S. A.* **2011**, *108*, 3803−3808.
(442) Baxter, H. L.; Mazarei, M.; Labbe, N.; Kline, L. M.; Cheng, Q.; Windham, M. T.; Mann, D. G.; Fu, C.; Ziebell, A.; Sykes, R. W. Two Year Field Analysis of Reduced Recalcitrance Transgenic Switchgrass. *Plant Biotechnol. J.* **2014**, *12*, 914−924.
(443) Bonawitz, N. D.; Im Kim, J.; Tobimatsu, Y.; Ciesielski, P. N.; Anderson, N. A.; Ximenes, E.; Maeda, J.; Ralph, J.; Donohoe, B. S.; Ladisch, M. Disruption of Mediator Rescues the Stunted Growth of a Lignin-Deficient Arabidopsis Mutant. *Nature* **2014**, *509*, 376−380.
(444) Taylor, L. E.; Dai, Z.; Decker, S. R.; Brunecky, R.; Adney, W. S.; Ding, S.-Y.; Himmel, M. E. Heterologous Expression of Glycosyl Hydrolases in Planta: A New Departure for Biofuels. *Trends Biotechnol.* **2008**, *26*, 413−424.
(445) Wei, H.; Donohoe, B. S.; Vinzant, T. B.; Ciesielski, P. N.; Wang, W.; Gedvilas, L. M.; Zeng, Y.; Johnson, D. K.; Ding, S.-Y.; Himmel, M. E. Elucidating the Role of Ferrous Ion Co-catalyst in Enhancing Dilute Acid Pretreatment of Lignocellulosic Biomass. *Biotechnol. Biofuels* **2011**, *4*, 48.
(446) Wei, H.; Yang, H.; Ciesielski, P. N.; Donohoe, B. S.; McCann, M. C.; Murphy, A. S.; Peer, W. A.; Ding, S.-Y.; Himmel, M. E.; Tucker, M. P. Transgenic Ferritin Overproduction Enhances Thermochemical Pretreatments in Arabidopsis. *Biomass Bioenergy* **2015**, *72*, 55−64.
(447) Johnson, D. K.; Elander, R. T. Pretreatments for Enhanced Digestibility of Feedstocks. *Biomass recalcitrance: Deconstructing the plant cell wall for bioenergy* **2008**, 436−453.
(448) Ciesielski, P. N.; Wang, W.; Chen, X. W.; Vinzant, T. B.; Tucker, M. P.; Decker, S. R.; Himmel, M. E.; Johnson, D. K.; Donohoe, B. S. Effect of Mechanical Disruption on the Effectiveness of Three Reactors Used for Dilute Acid Pretreatment of Corn Stover Part 2: Morphological and Structural Substrate Analysis. *Biotechnol. Biofuels* **2014**, *7*, 47.
(449) Chen, X.; Shekiro, J.; Pschorn, T.; Sabourin, M.; Tao, L.; Elander, R.; Park, S.; Jennings, E.; Nelson, R.; Trass, O. A Highly Efficient Dilute Alkali Deacetylation and Mechanical (disc) Refining Process for the Conversion of Renewable Biomass to Lower Cost Sugars. *Biotechnol. Biofuels* **2014**, *7*, 98.
(450) Zhu, J.; Pan, X.; Wang, G.; Gleisner, R. Sulfite Pretreatment (SPORL) for Robust Enzymatic Saccharification of Spruce and Red Pine. *Bioresour. Technol.* **2009**, *100*, 2411−2418.
(451) Wang, Z.; Zhu, J.; Zalesny, R. S.; Chen, K. Ethanol Production from Poplar Wood through Enzymatic Saccharification and Fermentation by Dilute Acid and SPORL Pretreatments. *Fuel* **2012**, *95*, 606−614.
(452) Zhu, J.; Pan, X. Woody Biomass Pretreatment for Cellulosic Ethanol Production: Technology and Energy Consumption Evaluation. *Bioresour. Technol.* **2010**, *101*, 4992−5002.
(453) Himmel, M. E.; Xu, Q.; Luo, Y.; Ding, S.-Y.; Lamed, R.; Bayer, E. A. Microbial Enzyme Systems for Biomass Conversion: Emerging Paradigms. *Biofuels* **2010**, *1*, 323−341.
(454) Xu, Q.; Baker, J. O.; Himmel, M. E. Chimeric Enzymes with Improved Cellulase Activities. *Google Patents*, 2015.
(455) Brunecky, R.; Alahuhta, M.; Xu, Q.; Donohoe, B. S.; Crowley, M. F.; Kataeva, I. A.; Yang, S.-J.; Resch, M. G.; Adams, M. W.; Lunin, V. V. Revealing Nature's Cellulase Diversity: the Digestion Mechanism of Caldicellulosiruptor Bescii CelA. *Science* **2013**, *342*, 1513−1516.
(456) Brunecky, R.; Hobdey, S. E.; Taylor, L. E.; Tao, L.; Tucker, M. P.; Himmel, M. E.; Decker, S. R. High Temperature Pre-digestion of Corn Stover Biomass for Improved Product Yields. *Biotechnol. Biofuels* **2014**, *7*, 170.
(457) *DOE/EE 1193*; U.S. Department of Energy, Bioenergy Technologies Office (BETO), March 2015.
(458) Wang, C.; Yoon, S.-H.; Jang, H.-J.; Chung, Y.-R.; Kim, J.-Y.; Choi, E.-S.; Kim, S.-W. Metab. Eng. of Escherichia Coli for α-farnesene Production. *Metab. Eng.* **2011**, *13*, 648−655.
(459) Zhu, F.; Zhong, X.; Hu, M.; Lu, L.; Deng, Z.; Liu, T. In Vitro Reconstitution of Mevalonate Pathway and Targeted Engineering of Farnesene Overproduction in Escherichia Coli. *Biotechnol. Bioeng.* **2014**, *111*, 1396−1405.
(460) Blazeck, J.; Hill, A.; Liu, L.; Knight, R.; Miller, J.; Pan, A.; Otoupal, P.; Alper, H. S. Harnessing Yarrowia Lipolytica Lipogenesis to Create a Platform for Lipid and Biofuel Production. *Nat. Commun.* **2014**, *5*, 3131.

DOI: 10.1021/acs.chemrev.6b00225
Chem. Rev. XXXX, XXX, XXX−XXX

(461) Tapia, E.; Anschau, A.; Coradini, A. L.; Franco, T. T.; Deckmann, A. C. Optimization of Lipid Production by the Oleaginous Yeast Lipomyces Starkeyi by Random Mutagenesis Coupled to Cerulenin Screening. *AMB Express* **2012**, *2*, 1−8.
(462) Elliott, D. C. Historical Developments in Hydroprocessing Bio-oils. *Energy Fuels* **2007**, *21*, 1792−1815.
(463) Mukarakate, C.; Zhang, X. D.; Stanton, A. R.; Robichaud, D. J.; Ciesielski, P. N.; Malhotra, K.; Donohoe, B. S.; Gjersing, E.; Evans, R. J.; Heroux, D. S.; Richards, R.; Iisa, K.; Nimlos, M. R. Real-time Monitoring of the Deactivation of HZSM-5 During Upgrading of Pine Pyrolysis Vapors. *Green Chem.* **2014**, *16*, 1444−1461.
(464) Venkatakrishnan, V. K.; Degenstein, J. C.; Smeltz, A. D.; Delgass, W. N.; Agrawal, R.; Ribeiro, F. H. High-pressure Fast-pyrolysis, Fast-hydropyrolysis and Catalytic Hydrodeoxygenation of Cellulose: Production of Liquid Fuel from Biomass. *Green Chem.* **2014**, *16*, 792−802.
(465) Agrawal, R.; Singh, N. R. Solar Energy to Biofuels. *Annu. Rev. Chem. Biomol. Eng.* **2010**, *1*, 343−364.
(466) Minchener, A. J. Coal Gasification for Advanced Power Generation. *Fuel* **2005**, *84*, 2222−2235.
(467) Ruiz, J. A.; Juárez, M. C.; Morales, M. P.; Muñoz, P.; Mendívil, M. A. Biomass Gasification for Electricity Generation: Review of Current Technology Barriers. *Renewable Sustainable Energy Rev.* **2013**, *18*, 174−183.
(468) McKee, D. W. Mechanisms of the Alkali Metal Catalysed Gasification of Carbon. *Fuel* **1983**, *62*, 170−175.
(469) Ahrenfeldt, J.; Thomsen, T. P.; Henriksen, U.; Clausen, L. R. Biomass Gasification Cogeneration − A Review of State of the Art Technology and Near Future Perspectives. *Appl. Therm. Eng.* **2013**, *50*, 1407−1417.
(470) Behrendt, F.; Neubauer, Y.; Oevermann, M.; Wilmes, B.; Zobel, N. Direct Liquefaction of Biomass. *Chem. Eng. Technol.* **2008**, *31*, 667−677.
(471) Barreiro, D. L.; Prins, W.; Ronsse, F.; Brilman, W. Hydrothermal Liquefaction (HTL) of Microalgae for Biofuel Production: State of the Art Review and Future Prospects. *Biomass Bioenergy* **2013**, *53*, 113−127.
(472) Beckman, D.; Elliott, D. C. Comparisons of the Yields and Properties of the Oil Products from Direct Thermochemical Biomass Liquefaction Processes. *Can. J. Chem. Eng.* **1985**, *63*, 99−104.
(473) Yu, G.; Xie, X.; Pan, L.; Bao, Z.; Cui, Y. Hybrid Nanostructured Materials for High-performance Electrochemical Capacitors. *Nano Energy* **2013**, *2*, 213−234.
(474) Tarascon, J.-M.; Armand, M. Issues and Challenges Facing Rechargeable Lithium Batteries. *Nature* **2001**, *414*, 359−367.
(475) Pan, H.; Hu, Y.-S.; Chen, L. Room-temperature Stationary Sodium-ion Batteries for Large-scale Electric Energy Storage. *Energy Environ. Sci.* **2013**, *6*, 2338−2360.
(476) Chen, T.; Dai, L. Flexible Supercapacitors Based on Carbon Nanomaterials. *J. Mater. Chem. A* **2014**, *2*, 10756−10775.
(477) Dahn, J.; Zheng, T.; Liu, Y.; Xue, J. Mechanisms for Lithium Insertion in Carbonaceous Materials. *Science* **1995**, *270*, 590.
(478) Ellis, B. L.; Nazar, L. F. Sodium and Sodium-ion Energy Storage Batteries. *Curr. Opin. Solid State Mater. Sci.* **2012**, *16*, 168−177.
(479) Yabuuchi, N.; Kubota, K.; Dahbi, M.; Komaba, S. Research Development on Sodium-ion Batteries. *Chem. Rev.* **2014**, *114*, 11636−11682.
(480) Asher, R. C. A Lamellar Compound of Sodium and Graphite. *J. Inorg. Nucl. Chem.* **1959**, *10*, 238−249.
(481) Bommier, C.; Ji, X. Recent Development on Anodes for Na-Ion Batteries. *Isr. J. Chem.* **2015**, *55*, 486−507.
(482) Simon, P.; Gogotsi, Y. Materials for Electrochemical Capacitors. *Nat. Mater.* **2008**, *7*, 845−854.
(483) Zhang, L. L.; Zhao, X. S. Carbon-based Materials as Supercapacitor Electrodes. *Chem. Soc. Rev.* **2009**, *38*, 2520−2531.
(484) Frackowiak, E.; Beguin, F. Carbon Materials for the Electrochemical Storage of Energy in Capacitors. *Carbon* **2001**, *39*, 937−950.
(485) Whittingham, M. S. Lithium Batteries and Cathode Materials. *Chem. Rev.* **2004**, *104*, 4271−4302.
(486) Padhi, A. K.; Nanjundaswamy, K.; Goodenough, J. Phospho-olivines as Positive Electrode Materials for Rechargeable Lithium Batteries. *J. Electrochem. Soc.* **1997**, *144*, 1188−1194.
(487) Goodenough, J. B.; Kim, Y. Challenges for Rechargeable Li Batteries. *Chem. Mater.* **2010**, *22*, 587−603.
(488) Winter, M.; Besenhard, J. O.; Spahr, M. E.; Novák, P. Insertion Electrode Materials for Rechargeable Lithium Batteries. *Adv. Mater.* **1998**, *10*, 725−763.
(489) Xu, W.; Wang, J.; Ding, F.; Chen, X.; Nasybulin, E.; Zhang, Y.; Zhang, J.-G. Lithium Metal Anodes for Rechargeable Batteries. *Energy Environ. Sci.* **2014**, *7*, 513−537.
(490) Ding, F.; Xu, W.; Graff, G. L.; Zhang, J.; Sushko, M. L.; Chen, X.; Shao, Y.; Engelhard, M. H.; Nie, Z.; Xiao, J. Dendrite-free Lithium Deposition via Self-healing Electrostatic Shield Mechanism. *J. Am. Chem. Soc.* **2013**, *135*, 4450−4456.
(491) Zheng, G.; Lee, S. W.; Liang, Z.; Lee, H.-W.; Yan, K.; Yao, H.; Wang, H.; Li, W.; Chu, S.; Cui, Y. Interconnected Hollow Carbon Nanospheres for Stable Lithium Metal Anodes. *Nat. Nanotechnol.* **2014**, *9*, 618−623.
(492) Chan, C. K.; Peng, H.; Liu, G.; McIlwrath, K.; Zhang, X. F.; Huggins, R. A.; Cui, Y. High-performance Lithium battery Anodes Using Silicon Nanowires. *Nat. Nanotechnol.* **2008**, *3*, 31−35.
(493) Wu, H.; Chan, G.; Choi, J. W.; Yao, Y.; McDowell, M. T.; Lee, S. W.; Jackson, A.; Yang, Y.; Hu, L.; Cui, Y. Stable Cycling of Double-walled Silicon Nanotube Battery Anodes through Solid-electrolyte Interphase Control. *Nat. Nanotechnol.* **2012**, *7*, 310−315.
(494) Magasinski, A.; Dixon, P.; Hertzberg, B.; Kvit, A.; Ayala, J.; Yushin, G. High-performance Lithium-ion Anodes Using a Hierarchical Bottom-up Approach. *Nat. Mater.* **2010**, *9*, 353−358.
(495) Wu, Y.; Rahm, E.; Holze, R. Carbon Anode Materials for Lithium Ion Batteries. *J. Power Sources* **2003**, *114*, 228−236.
(496) Wang, Q.; Li, H.; Chen, L.; Huang, X. Novel Spherical Microporous Carbon as Anode Material for Li-ion Batteries. *Solid State Ionics* **2002**, *152*, 43−50.
(497) Stevens, D.; Dahn, J. High Capacity Anode Materials for Rechargeable Sodium-Ion Batteries. *J. Electrochem. Soc.* **2000**, *147*, 1271−1273.
(498) Cao, Y.; Xiao, L.; Sushko, M. L.; Wang, W.; Schwenzer, B.; Xiao, J.; Nie, Z.; Saraf, L. V.; Yang, Z.; Liu, J. Sodium Ion Insertion in Hollow Carbon Nanowires for Battery Applications. *Nano Lett.* **2012**, *12*, 3783−3787.
(499) Memarzadeh Lotfabad, E.; Kalisvaart, P.; Kohandehghan, A.; Karpuzov, D.; Mitlin, D. Origin of non-SEI Related Coulombic Efficiency Loss in Carbons Tested Against Na and Li. *J. Mater. Chem. A* **2014**, *2*, 19685−19695.
(500) Shen, F.; Zhu, H.; Luo, W.; Wan, J.; Zhou, L.; Dai, J.; Zhao, B.; Han, X.; Fu, K.; Hu, L. Chemically Crushed Wood Cellulose Fiber towards High-Performance Sodium-Ion Batteries. *ACS Appl. Mater. Interfaces* **2015**, *7*, 23291−23296.
(501) Jin, J.; Yu, B.-j.; Shi, Z.-q.; Wang, C.-y.; Chong, C.-b. Lignin-based Electrospun Carbon Nanofibrous Webs as Free-standing and Binder-free Electrodes for Sodium Ion Batteries. *J. Power Sources* **2014**, *272*, 800−807.
(502) Ding, J.; Wang, H.; Li, Z.; Kohandehghan, A.; Cui, K.; Xu, Z.; Zahiri, B.; Tan, X.; Lotfabad, E. M.; Olsen, B. C.; Mitlin, D. Carbon Nanosheet Frameworks Derived from Peat Moss as High Performance Sodium Ion Battery Anodes. *ACS Nano* **2013**, *7*, 11004−11015.
(503) Lotfabad, E. M.; Ding, J.; Cui, K.; Kohandehghan, A.; Kalisvaart, W. P.; Hazelton, M.; Mitlin, D. High-Density Sodium and Lithium Ion Battery Anodes from Banana Peels. *ACS Nano* **2014**, *8*, 7115−7129.
(504) Hong, K.-l.; Qie, L.; Zeng, R.; Yi, Z.-q.; Zhang, W.; Wang, D.; Yin, W.; Wu, C.; Fan, Q.-j.; Zhang, W.-x.; Huang, Y.-h. Biomass Derived Hard Carbon Ysed as a High Performance Anode Material for Sodium Ion Batteries. *J. Mater. Chem. A* **2014**, *2*, 12733−12738.
(505) Shen, F.; Luo, W.; Dai, J.; Yao, Y.; Zhu, M.; Hitz, E.; Tang, Y.; Chen, Y.; Sprenkle, V. L.; Li, X.; Hu, L. Ultra-Thick, Low-Tortuosity, and Mesoporous Wood Carbon Anode for High-Performance Sodium-Ion Batteries. *Adv. Energy Mater.* **2016**, DOI: 10.1002/aenm.201600377.

DOI: 10.1021/acs.chemrev.6b00225
Chem. Rev. XXXX, XXX, XXX−XXX

(506) Babel, K.; Jurewicz, K. KOH Activated Carbon Fabrics as Supercapacitor Material. *J. Phys. Chem. Solids* **2004**, *65*, 275−280.
(507) Wei, L.; Sevilla, M.; Fuertes, A. B.; Mokaya, R.; Yushin, G. Hydrothermal Carbonization of Abundant Renewable Natural Organic Chemicals for High-Performance Supercapacitor Electrodes. *Adv. Energy Mater.* **2011**, *1*, 356−361.
(508) Luo, W.; Wang, B.; Heron, C. G.; Allen, M. J.; Morre, J.; Maier, C. S.; Stickle, W. F.; Ji, X. Pyrolysis of Cellulose under Ammonia Leads to Nitrogen-Doped Nanoporous Carbon Generated through Methane Formation. *Nano Lett.* **2014**, *14*, 2225−2229.
(509) Bommier, C.; Xu, R.; Wang, W.; Wang, X.; Wen, D.; Lu, J.; Ji, X. Self-activation of Cellulose: A New Preparation Methodology for Activated Carbon Electrodes in Electrochemical Capacitors. *Nano Energy* **2015**, *13*, 709−717.
(510) Zhang, L.; Liu, Z.; Cui, G.; Chen, L. Biomass-derived Materials for Electrochemical Energy Storages. *Prog. Polym. Sci.* **2015**, *43*, 136−164.
(511) Ding, G.; Qin, B.; Liu, Z.; Zhang, J.; Zhang, B.; Hu, P.; Zhang, C.; Xu, G.; Yao, J.; Cui, G. A Polyborate Coated Cellulose Composite Separator for High Performance Lithium Ion Batteries. *J. Electrochem. Soc.* **2015**, *162*, A834−A838.
(512) Xu, Q.; Kong, Q.; Liu, Z.; Wang, X.; Liu, R.; Zhang, J.; Yue, L.; Duan, Y.; Cui, G. Cellulose/Polysulfonamide Composite Membrane as a High Performance Lithium-ion Battery Separator. *ACS Sustainable Chem. Eng.* **2014**, *2*, 194−199.
(513) Zhang, J.; Yue, L.; Kong, Q.; Liu, Z.; Zhou, X.; Zhang, C.; Xu, Q.; Zhang, B.; Ding, G.; Qin, B.; Duan, Y.; Wang, Q.; Yao, J.; Cui, G.; Chen, L. Sustainable, Heat-resistant and Flame-retardant Cellulose-based Composite Separator for High-performance Lithium Ion Battery. *Sci. Rep.* **2014**, *4*, 3935.
(514) Pushparaj, V. L.; Shaijumon, M. M.; Kumar, A.; Murugesan, S.; Ci, L.; Vajtai, R.; Linhardt, R. J.; Nalamasu, O.; Ajayan, P. M. Flexible Energy Storage Devices Based on Nanocomposite Paper. *Proc. Natl. Acad. Sci. U. S. A.* **2007**, *104*, 13574−13577.
(515) Zhang, Y.-Z.; Wang, Y.; Cheng, T.; Lai, W.-Y.; Pang, H.; Huang, W. Flexible Supercapacitors Based on Paper Substrates: A New Paradigm for Low-cost Energy Storage. *Chem. Soc. Rev.* **2015**, *44*, 5181−5199.
(516) Nyholm, L.; Nyström, G.; Mihranyan, A.; Strømme, M. Toward Flexible Polymer and Paper-Based Energy Storage Devices. *Adv. Mater.* **2011**, *23*, 3751−3769.
(517) Wang, Z.; Tammela, P.; Zhang, P.; Stromme, M.; Nyholm, L. High Areal and Volumetric Capacity Sustainable All-polymer Paper-based Supercapacitors. *J. Mater. Chem. A* **2014**, *2*, 16761−16769.
(518) Wang, Z.; Carlsson, D. O.; Tammela, P.; Hua, K.; Zhang, P.; Nyholm, L.; Strømme, M. Surface Modified Nanocellulose Fibers Yield Conducting Polymer-Based Flexible Supercapacitors with Enhanced Capacitances. *ACS Nano* **2015**, *9*, 7563−7571.
(519) Wang, Z.; Tammela, P.; Stromme, M.; Nyholm, L. Nanocellulose Coupled Flexible Polypyrrole@Graphene Oxide Composite Paper Electrodes with High Volumetric Capacitance. *Nanoscale* **2015**, *7*, 3418−3423.
(520) Milczarek, G.; Inganäs, O. Renewable Cathode Materials from Biopolymer/Conjugated Polymer Interpenetrating Networks. *Science* **2012**, *335*, 1468−1471.
(521) Norgren, M.; Edlund, H. Lignin: Recent Advances and Emerging Applications. *Curr. Opin. Colloid Interface Sci.* **2014**, *19*, 409−416.
(522) Nilsson, T. Y.; Wagner, M.; Inganäs, O. Lignin Modification for Biopolymer/Conjugated Polymer Hybrids as Renewable Energy Storage Materials. *ChemSusChem* **2015**, *8*, 4081−4085.
(523) Ajjan, F. N.; Jafari, M. J.; Rebis, T.; Ederth, T.; Inganas, O. Spectroelectrochemical Investigation of Redox States in a Polypyrrole/Lignin Composite Electrode Material. *J. Mater. Chem. A* **2015**, *3*, 12927−12937.
(524) Kim, S.-K.; Kim, Y. K.; Lee, H.; Lee, S. B.; Park, H. S. Superior Pseudocapacitive Behavior of Confined Lignin Nanocrystals for Renewable Energy-Storage Materials. *ChemSusChem* **2014**, *7*, 1094−1101.
(525) Milczarek, G.; Nowicki, M. Carbon Nanotubes/Kraft Lignin Composite: Characterization and Charge Storage Properties. *Mater. Res. Bull.* **2013**, *48*, 4032−4038.
(526) Leguizamon, S.; Diaz-Orellana, K. P.; Velez, J.; Thies, M. C.; Roberts, M. E. High Charge-capacity Polymer Electrodes Comprising Alkali Lignin from the Kraft Process. *J. Mater. Chem. A* **2015**, *3*, 11330−11339.
(527) Zhu, L.; Wu, L.; Sun, Y.; Li, M.; Xu, J.; Bai, Z.; Liang, G.; Liu, L.; Fang, D.; Xu, W. Cotton Fabrics Coated with Lignosulfonate-doped Polypyrrole for Flexible Supercapacitor Electrodes. *RSC Adv.* **2014**, *4*, 6261−6266.
(528) Xu, H.; Jiang, H.; Li, X.; Wang, G. Synthesis and Electrochemical Capacitance Performance of Polyaniline Doped with Lignosulfonate. *RSC Adv.* **2015**, *5*, 76116−76121.
(529) Admassie, S.; Elfwing, A.; Jager, E. W. H.; Bao, Q.; Inganas, O. A Renewable Biopolymer Cathode with Multivalent Metal Ions for Enhanced Charge Storage. *J. Mater. Chem. A* **2014**, *2*, 1974−1979.

DOI: 10.1021/acs.chemrev.6b00225
Chem. Rev. XXXX, XXX, XXX−XXX